THE UNIVERSITY OF CALGARY

NONLINEAR THEORY AND ANALYSIS OF LAMINATED SHALLOW SPHERICAL SHELLS

BY

CHANGSHI XU

A THESIS

SUBMITTED TO THE FACULTY OF GRADUATE STUDIES

IN PARTIAL FULFILLMENT OF THE REQUIREMENTS FOR THE

DEGREE OF DOCTOR OF PHILOSOPHY

DEPARTMENT OF CIVIL ENGINEERING

CALGARY, ALBERTA

APRIL, 1992

ISBN 0-315-75246-7

THE UNIVERSITY OF CALGARY

FACULTY OF GRADUATE STUDIES

The undersigned certify that they have read, and recommend to the Faculty of Graduate Studies for acceptance, a thesis entitled, "Nonlinear Theory and Analysis of Laminated Shallow Spherical Shells", submitted by Changshi Xu in partial fulfillment of the requirements for the degree of Doctor of Philosophy.

C. Y. Chia

Dr. C. Y. Chia, Supervisor
Department of Civil Engineering

A. Ghali

Dr. A. Ghali
Department of Civil Engineering

O. Vin

Dr. O. Vinogradov
Department of Mechanical Engineering

Mansa Singh

Dr. M. C. Singh
Department of Mechanical Engineering

K. S. Sivakumaran

Dr. K. S. Sivakumaran, External Examiner
Department of Civil Engineering and
Engineering Mechanics
McMaster University

Date: April 20, 1992

ABSTRACT

In this research, a generally dynamic nonlinear theory is developed for the axisymmetric deformation of moderately thick shallow spherical shells and circular plates comprising laminated cylindrically (or polar) orthotropic layers with flexible supports. The effects of transverse shear, rotatory inertia, geometrically initial imperfection and linear, nonlinear extension Winkler and shear Pasternak elastic foundations are included in the theory. The constitutive relations for a moderately thick laminated shell are established on the basis of the generalized Hooke's law and characterized by four independent engineering elastic constants. The extensional stiffness, the bending-stretching stiffness and flexural stiffness of the shell are presented for unsymmetrical laminate, symmetrical laminate, orthotropic and isotropic shell, respectively. The transverse shear stiffness is determined by employing a parabolic shear stress distribution across the shell thickness and the principle of complementary energy. Nonlinear equations of motion and the corresponding set of boundary conditions are derived through the dynamic principle of virtual work.

The governing equations composed of compatibility condition, equilibrium equation of inplane couples and equation of transverse motion are expressed in terms of transverse displacement, rotation of a normal to mid-surface and stress function. Those equations already reduce to Marguerre-

type equations for thin shallow spherical shells by neglecting the effects of transverse shear and rotatory inertia, and are simplified to those for the static case by treating the time functions as constants and neglecting the inertia terms.

A Fourier-Bessel series solution satisfying the required boundary conditions is formulated for the nonlinear free vibration, buckling and postbuckling behaviour of laminated shallow spherical shells. The Galerkin method is used to reduce the governing equations to a set of nonlinear ordinary differential equations which are solved by the principle of harmonic balance for the undamped vibration. The resulting equations are a set of nonlinear algebraic equations solved by the Newton-Raphson method. The nonliner bending and postbuckling behaviour of these laminates are treated as special cases.

Numerical results for nonlinear free vibration, buckling, postbuckling and static large deflection response of symmetrically and unsymmetrically laminated shallow spherical shells and circular plates are presented for various boundary conditions, initial rises of the shell, numbers of layers and material properties. The effects of transverse shear, rotatory inertia, geometrically initial imperfection, linear and nonlinear Winkler-Pasternak elastic foundations on the geometrically nonlinear behaviour of the shells and plates are investigated in some detail. In special cases, the present results are in good agreement with available results. Some significant conclusions are drawn on the basis of this study.

ACKNOWLEDGEMENTS

I would like to express my appreciation and gratitude to my supervisor Dr. C. Y. Chia for his financial support, reassuring encouragement and guidance throughout the course of this study.

I also feel indebted to Dr. A. Ghali, Dr. O. Vinogradov and Dr. M. C. Singh who readily offered their precious advice, expertise and criticism.

The financial support from the Department of Civil Engineering of the University of Calgary is gratefully acknowledged.

Finally, the completion of this thesis also owes to the devotion of my wife, whose understanding, patience and unreserved support made the study possible; and to my little son, who, without knowing it, has been giving me a kind of motivating urge from time to time during the course of this research.

THIS THESIS IS DEDICATED TO

MY FATHER ZHENSHENG XU

AND TO

THE MEMORY OF MY MOTHER YUELI YIN (1924-1989)

TABLE OF CONTENTS

LIST OF TABLES

LIST OF FIGURES

NOTATIONS

A_{ij}, B_{ij}, D_{ij} = Extensional, coupling and flexural rigidities of the laminated shallow spherical shell defined by Eqn. (2.32), i,j=1,2

A_{ij}^*, B_{ij}^*, D_{ij}^* = Constants for the laminated shallow spherical shell defined by Eqns. (2.58), i,j=1,2

$\bar{A}_{ij}$, $\bar{B}_{ij}$, $\bar{D}_{ij}$ = Diemnsionless constants for the laminated shallow spherical shell defined by Eqns. (2.64), i,j=1,2

a, h = Base radius and thickness of the shell

a_i, b_i, c_i, Q_n = Integration constants defined in Appendix B

E = Modulus of elasticity of an isotropic shell

E_r, E_θ = Principal moduli of elasticity of an orthotropic shell

E_L, E_T = Principal moduli of elasticity of an orthotropic layer or shell

F = Dimensionless stress function

F^* = Stress function

G^* = Constant for the shell

$\bar{G}$ = Dimensionless constant for the shell

G_{Lz}, G_{Tz} = Shear rigidities of the orthotropic layer in the shell

G_{rz} = Shear rigidity of an orthotropic shell

H = Initial rise of the shell

I, J = Inertia terms defined in Eqn. (2.50)

I_o, I_1 = Modified Bessel functions of first kind of order zero and order one, respectively

J_o, J_1 = Bessel functions of first kind of order zero and order one, respectively

K_b, K_i = Dimensionless rotational and inplane stiffness of the edge

K_f, K_n, G_f = Dimensionless extensional, nonlinear extensional and shear moduli of elastic foundations

k_b, k_i = Rotational and inplane stiffnesses of the edge

k_f, k_n, g_f = Extensional, nonlinear extensional and shear moduli of elastic foundation

M_r, M_θ = Stress couples per unit length in cylindrical polar coordinates

M_ρ = Dimensionless stress couple

N = Number of layers

N_r, N_θ = Stress resultants per unit length in cylindrical polar coodinates

N_ρ = Dimensionless stress resultant

Q = Dimensionless lateral distributed load

Q_r = Transverse shear stress resultant per unit length

q = Lateral distributed load per unit area

R = Radius of the curvature of the undeformed shell

R_I, T_S = Tracing constants for effects of transverse shear and rotatory inertia

r, θ, z = Cylindrically polar coordinates

S_{ij} = Inplane stiffnesses, i,j=1,2

t = Time

U = Dimensionless displacement component at the midsurface in the r direction

u = Displacement component at the midsurface in the r direction

u_r, u_θ, w = Displacement components at a point off the midsurface in r, θ, and z directions, respectively

W = Dimensionless displacement component in z direction

$\overline{W}$ = Dimensionless initial deflection

W_A = Dimensionless average deflection

$\overline{W}_i, W_i, R_i, S_r$ = Coefficients of Fourier-Bessel series

$W_i^{(k)}, R_i^{(k)}$ = Coefficients of Fourier series

$\overline{w}$ = Initial deflection

X_i, Y_i, Z_i = Fourier-Bessel series defined in Eqns. (3.15)

x, y, z = Rectangular cartesian coordinates

α_k, β_k = Eigenvalues of Bessel function defined in Eqns. (3.15)

γ = Mass per unit area of the shell

γ_o = Mass density

ε_{ij} = Total strain components in cylindrically polar coordinates ($i, j = r, \theta, z$)

$\varepsilon_{ij}{}^o$ = Midsurface strain components in cylindrically polar coordinates ($i, j = r, \theta, z$)

κ_r, κ_θ = Changes of curvatures of the midsurface

σ_{ij} = Total stess components in cylindrically polar coordinates ($i, j = r, \theta, z$)

ρ = Dimensionless coordinate (= r/a)

λ_i = Geometric parameters of the shell defined in Eqns. (2.64), $i = 1, 2$

τ = Dimensionless time defined in Eqns. (2.64)

υ = Poisson's ratio of an isotropic shell

$\upsilon_{r\theta}, \upsilon_{\theta r}$ = Poisson's ratios of an orthotropic shell

$\upsilon_{LT}, \upsilon_{TL}$ = Poisson's ratios of an orthotropic layer in the shell

ψ^* = Rotation of a normal to the midsuface

ψ = Dimensionless rotation of a normal to the midsuface

$\omega_o{}^*, \omega^*$ = Linear and nonlinear frequencies

ω_o, ω = Dimensionless linear and nonlinear frequencies

Other symbols are defined when they appear in the thesis.

CHAPTER 1

INTRODUCTION

1.1 THE NATURE AND SCOPE OF COMPOSITE MATERIALS

Modern composite materials have had a significant impact on the technology of design and construction of structural elements. By combining two or more materials together, it is now possible to tailor-make advanced composite materials which are lighter, stiffer and stronger than any other structural materials ever used. The history of man-made composite materials can be dated back to ancient Egyptians, Israelites and Chinese (Vinson and Chou, 1975). It is interesting to note that they all made bricks by mixing straw with clay. The pattern-welding of sabres developed in ancient China involved the forging together of wrought iron and steel. Laminated composites also were used by the ancient Egyptians. It was recognised that by gluing thin veneers together, the strength of wood was enhanced and the possibility of swelling and shrinkage minimized.

Composite materials can be found in numerous naturally occurring substances. Wood, for example, is an organic substance composed primarily of cellulose chains embedded in a lignin matrix at a ratio of about 2 to 1. The bundles of cellulose chains forming walls of the elongated cells are highly crystalline. The cells are held together by the amorphous lignin. The higher the lignin content, the softer and more resilient the combination is. The bond between the fibres and lignin is strong, as is made evident by the high strength and stiffness of wood.

The superior properties of man-made composite materials in structural applications can be best demonstrated by the example of a reinforced concrete beam. Concrete, a relatively inexpensive structural material, is excellent for supporting a compressive load. However, the low resistance of concrete to tension makes it an undesirable material for beam construction. One way to improve the situation is to strengthen its tensile properties by the use of steel bars. As a result, the tensile stress is borne chiefly by the reinforcing bars, and a heavier load can be applied to the beam without increasing its cross-sectional area. The combination of steel and concrete has not only made the best use of the strengths of the components but also resulted in properties that cannot be achieved by either component.

Technological progress has resulted in a continuous expansion of structural material types and in improvements of their properties. Generally, new materials emerge because of a natural desire to improve the efficiency of proposed structures. These materials in turn provide new possibilities of innovative designs and fabrication methods, while the subsequent development of structures and technology presents materials science with new tasks.

One of the clearest manifestations of such an interrelated process in the development of materials, structures and technology is closely associated with the development and application of reinforced composites. The emergence of glass-reinforced plastics, which have found extensive application because of their high strength and low density compared to conventional structural materials, has allowed the development of promising design concepts and efficient fabrication methods, followed in turn by new advanced materials based on organi, boron or graphite fibres dispersed in polymeric or metal matrices.

Modern composite materials not only have a wide range of properties superior to conventional materials, but these properties can be altered and improved according to the designation of the structures. These properties include (Jones, 1975): strength, fatigue life, stiffness, temperature-dependent behaviour, corrosion resistance, thermal insulation, wear resistance, thermal conductivity, attractiveness, acoustical insulation and weight. Naturally, not all the above properties are improved at the same time nor is there usually any requirement to do so.

In modern composites the components, which are combined to produce a material, are high-strength fibres providing mechanical properties of materials and a matrix realizing these properties in design. The resulting material has precisely oriented features which can be controlled by changing the structural parameters of the composites. There is no need to prove that such a special design will always be more effective compared to conventional all-purpose isotropic metals and alloys. The principle of specialized properties can be accurately traced, e.g. in all natural materials which have emerged as a result of a prolonged evolution after having been subjected to gravitational, wind and other static and dynamic loads.

The effective realization of merits of composite materials in specific designs calls for the solution of a series of problems including: selection of the matching initial components-- fibre and matrix, determination of the reasonable structure of materials adequate to the external load field and other influences, taking account of the specific properties of the material and processing limitation in the design.

There are three commonly accepted types of composite materials: (Jones, 1975)(i) Fibrous composite which consists of fibres in a matrix; (ii) Laminated composites which consist of layers of various materials; and (iii) Particulate composites which are composed of particles in a matrix. In recent years, one of the most commonly used composite is fibrous composites. Many commonly used fibres or wires are Aluminum, Titanium, Steel, Glass, Carbon, Boron and Graphite. Glass, Boron and Graphite fibres possess ultrahigh strength and stiffness. The matrix material can be either a plastic such as epoxy or polyimide or a metal such as aluminum. The purpose of the binder material, called matrix, is manifold: (i) binding together the fibres and protecting their surface from damage during handling fabrication and prolonging the service life of the composite; (ii) dispersing the fibres and separating them in order to avoid catastrophic propagation of cracks and subsequent failure of the composite; (iii) transferring stress to the fibres by adhesion and/or friction (when the composite is under load). For the remainder of this thesis, three composite materials--glass-epoxy, boron-epoxy and graphite-epoxy composites will be considered.

A lamina is a flat or curved (as in shells) arrangement of unidirectional fibres or woven fibres in a matrix. In a fibre-reinforced composite, fibres provide the majority of the strength and stiffness. The fibre-reinforced composites such as glass-epoxy, boron-epoxy and graphite-epoxy are usually treated as linearly elastic materials. Refinement of that approximation requires consideration of some form of plasticity, viscoelasticity or both (viscoplasticity).

In practice, composite materials rarely exist as a single lamina, but will be fabricated from a number of laminae bonded together. If the separate laminae possess orthotropic properties by virtue of the orientation of the fibres in the matrix, then the resulting composite will have properties depending upon thickness, principal material property , orientations and the final arrangement of each independent lamina within the composite. A major purpose of lamination is to tailor the directional dependence of strength and stiffness of a material to match the loading environment of the structural element. Laminates are uniquely suited to this objective since the principal material directions of each layer can be oriented according to the need. A generally laminated plate or shell comprises an arbitrary number of homogeneous orthotropic layers perfectly bonded together. Each layer has arbitrary elastic properties, thickness and orientation of orthotropic axes with respect to plate or shell axes. In the present analysis, the symmetrically cross-ply laminates, in which the cylindrically (or polar) orthotropic layers are so arranged that a mid-surface elastic symmetry exists, and the unsymmetrically ones, in which such elastic symmetry does not exist, are considered.

Composite materials are finding ever new applications in different engineering fields, especially in aerospace engineering. This is primarily owing to the excellent mechanical properties of these new materials at relatively low densities, and to their other merits offering advantages over conventional materials. Because of their great practical importance, the developments in composite materials have established a new area of scientific research -- the mechanics of composites, which has achieved a number of effective analytical methods and some significant results.

In recent years, almost every aerospace company is developing products composed of fiber-reinforced composite materials. The usage of composite materials has progressed through several stages. At present, for example, the fuselage section and horizontal tail on the General Dynamics F-111 airplane are made of boron-epoxy material. Graphite-epoxy horizontal and vertical stabilizers are in production for General Dynamics YF-16 airplane. This last goal has been approached in the deliberate, conservative, multistage fashion. A substantial composite materials technology has been built and awaits further challenge.

1.2 A REVIEW OF ADVANCES IN THE THEORY AND ANALYSIS OF LAMINATED SHELLS

In recent years, considerable attention has been given to the improvement of the classical theory of shells. By large, such efforts have been prompted by the necessity of designing structures which employ up-to-date composite materials. The correct and effective use of composite materials require more complex analysis in order to predict accurately the elastic response of these materials to external loadings. A great amount of research work, therefore, has been carried out on the elastic behaviour of laminated composites. As is well known, geometric nonlinearities stem from finite deformations of an elastic body. For composite plates and shells nonlinear strain-displacement relations are most commonly used in the literature for development of nonlinear theories. Many researchers have conducted studies in nonlinear vibration, buckling and postbuckling analyses of laminated plates and shells. A review of various studies on the geometrically nonlinear behaviour of composite plates may be found in references contributed by Chia (1980, 1988a), and the assessment of computational models for composite shells was given by Noor and Burton (1990). In this section, the developments of the nonlinear shell theory, analytical investigation into the nonlinear analysis of laminated shell structures, buckling, postbuckling and vibration of laminated shallow spherical shells are given for reference.

1.2.1 Shell Theories

The theory of plates and shells attempts, by using certain approximations, to reduce the essentially three-dimensional equations of solid mechanics to a set of two-dimensional, surface equations. In 1850 Kirchhoff applied geometric restrictions to obtain a linear theory of plates. Later, Love (1888) developed a corresponding theory for shells utilizing what is now known as the Kirchhoff-Love hypothesis (or the first approximation theory), which may be summarized as (i) normals to the undeformed midsurface are deformed into normals to the deformed midsurface, (ii) the effects of stress and strain in the direction of normal may be neglected, and (iii) the ratio of shell thickness to the radii of curvature is small compared with unity. Assumptions (i) and (ii) may not be consistent with the three-dimensional nature of even a thin shell and implies that the effect of transverse shear deformation is neglected but have been invoked purely for the purpose of sufficiently describing practical structures by means of midsurface strains and stress resultants when (i) the lateral dimension-to-thickness ratio is large; (ii) the dynamic excitations are within the low-frequency range; (iii) the material anisotropy is not severe. Therefore, it is true that the thinner the shell is, the more accurate the assumptions. Refinements to Love's "first approximation theory" have been made by several researchers using various assumptions.

Any relaxation of these restrictions prompts the necessity of improved theories in which the transverse shear deformation and/or transverse normal deformation are taken into account. As pointed out by Koiter (1959), refinement to Love's first approximation theory of elastic shells are meaningless, unless the effect of transverse shear deformation are included in the theory.

The simple and generalized theory (or the first-order shear deformation theory) which takes into account the effect of shear deformation is substantially due to Reissner (1945), where the displacements are assumed in the form:

$$\begin{aligned} u &= u_o(x,y,t) + z\alpha(x,y,t) \\ v &= v_o(x,y,t) + z\beta(x,y,t) \\ w &= w_o(x,y,t) \end{aligned} \tag{1.1}$$

in which u, v and w are the two inplane and transverse displacements in the x, y and z directions respectively, u_0, v_0 and w_0 are the values of u, v and w at the middle surface, and α and β, the slope functions, are averaged components of direction change of the normal to the undeformed middle surface. In 1951, Mindlin (1951) efficiently incorporated the influence of rotatory inertia on the flexural motions of linearly elastic, isotropic plates due to considering transverse shear deformation.

On the basis of the Kirchhoff-Love kinematic hypothesis, linear theories for laminated plates and shells have been well established by Reissner and Stavsky (1961), Dong et al. (1962) and Ambartsumyan (1964). This simple kinematic assumption stipulates the application of these theories to structural members with the large lateral dimension-to-thickness ratio and moderate variation of orthotropy of the materials across the thickness. It is expected that the transverse shear effect on the elastic behaviour of composite plates and shells, especially highly anisotropic materials, is greater than that on homogeneous isotropic ones. Application of laminated classical theories to layered anisotropic composite plates and shells could lead to as much as 30% or more errors in deflections, stresses and frequencies.

For moderately thick isotropic cylindrical shells, a refined shell theory including transverse shear deformation and rotatory inertia was developed by Naghdi and Cooper (1956) and Mirsky and Herrmann (1956, 1957). In the case of laminated composite cylindrical shells, several sets of equations have been derived, by Sinha and Rath (1975) using the Donnell-type shell theory (1933), by Dong and Tso (1972) and Rath and Das (1973) employing the Love's approximation. Since the derivation of all these sets of equations, except for those presented by Naghdi and Cooper (1956), guided by the work of Mindlin (1951) in the theory of homogeneous isotropic plates was based on the assumption of a uniform thickness shear deformation, it is not possible to satisfy the boundary conditions of zero thickness shear stresses at the inner and outer shell surfaces and, therefore, led to the introduction of shear correction factors in the transverse shear resultant-strain relations. By use of the higher-order approximation for transverse shear stresses and strains, the shear deformation theories of laminated shells were given by Reddy and Liu (1985), Soldatos (1986, 1987) and Fu and Chia (1989a,b). A significant common feature of these theories is that a parabolic distribution of the transverse shear stresses was obtained, whereby the need for using a shear correction factor was removed. Governing equations obtained in these theories include, entirely, the equations of the aforementioned classical Love-type theory. Further, for earlier works on the inclusion of higher-order effects, reference may be made to the higher-order theories proposed by Hsu and Wang (1970), Biricikoglu and Kalnins (1971), Dong (1972) and Whitney and Sun (1973, 1974). The developemnt of these higher-order theories is mostly based on a displacement field in which the inplane displacements in the surface of the shell are expanded as linear functions of the thickness coordinate and the transverse displacement is expanded as quadratic function of the thickness coordinate. These high-order shell theories are cumbersome and computationally more demanding, because, with each additional power of the thickness coordinate, an additional dependent unknown is introduced into the theory.

Nonlinearity in the behaviour of any structure is developed due to large deflections which substantially change the initial geometry of the structure or due to a nonlinear stress-strain relationship or both. Nonlinearity due to nonlinear constitutive relations is called material nonlinearity. Elastic-plastic constitutive relations should be considered when analyzing material nonlinearity. Nonlinearity caused by large deflection is called geometrical nonlinearity. In the present research, problems of geometric nonlinearity are examined. For the magnitude of the deflections beyond a certain level ($w \geq$

0.3h) (Sivakumaran, 1983), the lateral deflections are accompanied by stretching of the middle surface. In these instances the load carrying capacity of shells is increased considerably. Consequently, for such problems, the use of an extended shell theory, which accounts for the effect of geometric nonlinearity, requires the use of nonlinear strain-displacement relations, because displacement gradients can no longer be considered small compared to unity. The need for more accurate analysis for plates and shells has led to the appearance of a number of theories which are the formulation of von Karman's large deflection equations (1910), the Donnell type equations (1933), Marguerre-type equations (1938), Hildebrand configuration (1949), the Berger's linearlized equations (1955) and the others reviewed by Stein (1986). It is worth noting that Donnell's nonlinear theory, owing to its relative simplicity and practical accuracy, has been most widely used for analyzing the elastic behaviour of isotropic thin shells, especially for cylindrical shells and shallow shells, and for the basis of developing nonlinear laminated shell theories. This theory is based on the following assumptions: (i) the shell is sufficiently thin; (ii) the strains are sufficiently small compared to unity; (iii) straight lines normal to the undeformed middle surface remain straight, and the length of normal to the deformed middle surface stays unchanged; (iv) the normal stress acting in the direction normal to the middle surface may be neglected in comparison with the stresses acting in the direction parallel to the middle surface; (v) two inplane displacements are infinitesimal, while normal displacement is of the same order as the shell thickness; (vi) the derivatives of normal displacement are small, but their squares and products are of the same order; and (vii) curvature changes are small and the influences of two inplane displacements are negligible so that they can be represented by linear functions of normal displacement only. Assumptions (iii) and (iv) constitute the so-called Kirchhoff-Love hypotheses while those from (v) to (vii) correspond to the shallow shell approximations applicable for deformation dominated by the normal displacement. The Donnell's equations, in cases where the curvature radii of the shell become indefinitely large, reduce to the von Karman equations for large deflections of thin plates.

Attention has also been paid to geometrically nonlinear theories of laminated composite shells. Librescu (1987,1988) presented a refined geometrically nonlinear theory of anisotropic symmetrically laminated composite shallow shells by incorporating transverse shear deformation and transverse-normal stress effects. Lagrangian formulation was used to derive the theory, and the three-dimensional strain-displacement relations were modified to include the nonlinear terms. A rate theory for shells admitting anisotropic elastic-plastic behaviour was developed by Weichert(1988). The theory takes into account the shear effects using a first-order shear approximation theory and takes into account geometrically nonlinear effects by using consistent strain and relation-based approximations. Based on the Donnell-type assumptions and Mindlin hypothesis, Iu and Chia (1988a,b) derived a nonlinear theory for antisymmetric cross-ply circular cylindrical shells.

1.2.2 Analytical studies of Laminated shallow spherical shells

The geometrically nonlinear elastic behaviour of laminated circular cylindrical shells or panels was reported by several researchers (Knot, 1970; Hirano, 1979; Sheinman and Simitses, 1983; Zhang and Matthews, 1983, 1985; Bhattacharya, 1984; Hui, 1985; Chia, 1987a,b, Iu and Chia, 1988a,b and Hsu et al, 1991) using various analytical methods.

Based on the Donnell's shell approximations, the nonlinear axisymmetric response of cylindrically (or polar) orthotropic shallow spherical shells has been investigated in some detail. Making use of Hamilton's principle, Varadan and Pandalai (1978) utilized the one-term mode shape solution to solve the nonlinear flexural free vibration problem of clamped orthotropic shallow spherical shells. Using a two-term shape approximation associated with the Rayleigh-Ritz method, Varadan (1978) examined static buckling of clamped orthotropic shallow spherical shells. Alwar and Reddy (1979a) and Dumir et al. (1984a) analyzed the axisymmetric static and dynamic buckling behaviour of clamped orthotropic shallow spherical shells with a circular hole. The former used the Chebyshev series in the space domain and a Houbolt numerical integration scheme in the time domain while the latter adopted the orthogonal point collocation method in the space domain and Newmark-β scheme in the time domain. Ganapathi and Varadan (1982) presented a solution to the study of dynamic buckling of clamped orthotropic shallow spherical shells subjected to instantaneously uniform step-pressure load of infinite duration. With an assumed two-term mode shape for the lateral displacement, the governing equations were derived by using Lagrange's equations and the numerical results were obtained by the Runge-Kutta method. Dumir (1986) reported the nonlinear free vibration response and the response of orthotropic shallow spherical shells with immovable clamped and simply supported edges under uniformly distributed static load by using the spatial mode and Galerkin's method. For a flexible edge condition, Dumir et al (1984b) expanded deflection and stress function as polynomials and used the orthogonal collocation technique to examine the static and dynamic buckling of orthotropic shallow spherical shells with flexible supports and to investigate the influence of the edge stiffness parameters on the nonlinear behaviour.

The nonlinear analysis of orthotropic shallow spherical shells on elastic foundations have been carried out by several researchers. The study of interaction between deformable bodies is relevant to many engineering situations. The exact analysis of interaction is very complicated. Therefore, simplified mathematical models accounting for the structure interaction with the surroundings have been proposed by Winkler (1867), Pasternak (1954), Reissner (1958), Kerr (1964), Levinson and Bharatha (1978) and others. Nath et al (1985a,b, 1986, 1987, 1989) and Jain et al (1986) applied the Chebyshev series to analyzing the nonlinear behaviour of immovable simply-supported and clamped orthotropic shallow spherical shells on elastic foundations such as the transient response, the static and dynamic response and the effect of foundation on the transient response of these shells. In the first three and the last of these six papers, Winkler and Pasternak elastic foundation models were employed while in the others Winkler and nonlinear (cubic) Winkler models were used. Utilizing Winkler, nonlinear Winkler and Pasternak models of the elastic foundation, Dumir (1985) reported the nonlinear free vibration and static response of orthotropic shallow spherical shells with the flexible supports by a single-mode solution and the Galerkin's method.

The effect of geometrically initial imperfection on the nonlinear analysis of isotropic shallow spherical shells, however, has received some attention. Budiansky (1959) investigated the effect of the initial imperfection on the buckling of calmped isotropic shallow by use of the Bessel functions. Hui (1983a) reported the results of this effect on the nonlinear vibrations of isotropic shallow spherical shells. To simplify the theoretical analysis and provide useful information on the possible effects in a preliminary design, Budiansky proposed that the shape of the initial imperfection was the parabolic function and Hui suggested that the same mode shapes were assumed for the vibration mode and the geometric imperfection, although the shapes of the geometric imperfection are random in practical structures.

Recently, based on von Karman-Marguerre type nonlinear equations, nonlinear vibration and post-buckling of symmetrically-laminated shallow spherical shells of rectilinearly orthotropic material with rectangular planform were discussed by Chia (1988b) utilizing a generalized double-Fourier series.

All these analyese mentioned above, however, are confined to orthotropic and laminated thin shallow spherical shells, and the effects of transverse deformation and rotatory inertia are not taken into account.

As for the geometrically nonlinear analysis of laminated shallow spherical shells by use of the finite element method, some shell elements including the effects of transverse shear have been developed on the basis of the first-order assumption. Reddy and Chandrashekhara employed the displcement finite element model to study the large deflection (1985a) and the nonlinear transient response (1985b) of the laminated shallow spherical shells of rectilinearly orthotropic material with rectangular planform.

For the geometrically nonlinear analysis of circular plates, which is the special case of shallow spherical cap, some previous work are briefly reviewed as follows:

Nowinski (1963) employed a single-mode solution to discuss nonlinear vibrations of circular plates of rectilinearly orthotropic materials. Using the Chebyshev series, Alwar and Reddy (1979b) and Nath and Alwar (1980) considered the nonlinear static and dynamic response of orthotropic circular and annular plates. Ruei, Jiang and Chia (1984) studied static and dynamic problems of orthotropic circular plates with nonuniform edge constrains. The nonlinear vibration of isotropic layered circular plates were considered by Kunukkaseril and Venkatesan (1979). Employing a dynamic relaxation method, Turvey (1982) reported the large deflection of laminated circular plates. The nonlinear vibration and buckling of laminated anisotropic circular plates were investigated by Srinivasamurthy and Chia (1987). Based on von

Karman-Marguerre type equations, Nath et al (1987) discussed the nonlinear static response of orthotropic circular plates on Winkler and nonlinear Winkler elastic foundations by use of a Chebyshev series solution. Utilizing Winkler , nonlinear Winkler and Pasternak models of the elastic foundation, Dumir (1985) investigated the nonlinear axisymmetric response of orthotropic thin circular plates by a single mode solution. Including the effect of geometric imperfection in his investigation, Hui (1983b) studied the large amplitude vibration of isotropic circualr plates. In all the above studies, the effects of transverse shear and rotatory inertia have not been encompassed.

As for the effects of transverse shear and rotatory inertia, Sathyamoorthy and Chia discussed nonlinear vibrations of circular plates of rectilinearly orthotropic and isotropic materials for clamped boundary conditions by using the Galerkin method and the Runge-Kutta numerical procedure (1979, 1981) and by using the Berger's approach (1982). For laminated thick circular plates, Srinivasamurthy and Chia (1990) formulated a single-mode solution to study the nonlinear static and dynamic response of laminated thick circular plates of rectilinearly orthotropic material with a clamped edge.

Based on the works of Reissner (1945) and Fu and Chia (1989a,b), the writer developed a nonlinear theory for the elastic behaviour of laminated cross-ply moderately thick shallow spherical shells, which extended the Donnell-type shell theory to include transverse shear and rotatory inertia. A multi-mode solution in the Fourier-Bessel series is formulated for the nonlinear governing equations which are reduced to a set of nonlinear ordinary differential equations by making use of Galerkin's method. Analytical results were obtained for the buckling and postbuckling response of symmetrically laminated shallow spherical shells including the effect of transverse shear (Xu, 1991); for the nonlinear free vibration of these shells with the flexibly supported edge (Xu and Chia, 1991a); for the nonlinear static and dynamic analysis of these shells taking into account the effects of transverse shear, rotatory inertia, geometric imperfection and elastic foundations (Xu, 1992a); for the nonlinear analysis of unsymmetrically laminated moderately thick shallow spherical shells with considering the effects of the transverse shear and rotatory inertia (Xu and Chia, 1992a). Results were also obtained for the nonlinear vibration of symmetrically laminated moderately thick circular plates (Xu and Chia, 1991b); for the nonlinear static and dynamic responses of these plates including the effects of transverse shear, rotatory inertia, geometric imperfection and elastic foundations (Xu, 1992b); for the influence of the elastic foundation on the large amplitude vibration of unsymmetrically thick circular plates (Xu and Chia, 1992b).

1.3 SCOPE OF THE PRESENT THESIS

To the writer's knowledge there is no other literature available, except for the work conducted by the writer, on the buckling, postbuckling and nonlinear vibration response of laminated shallow spherical shells of cylindrically (or polar) orthotropic materials. A wide class of boundary conditions and the effects of transverse shear deformation, rotatory inertia, elastic foundation and geometrically initial imperfection are included in this study. The corresponding circular plate problems are treated as special cases.

The objective of the present thesis is

(i) to define a set of stress resultants and stress couples to incorporate the transverse shear for the laminated shallow spherical shell;

(ii) to establish a variational principle for the vibratory motion of laminated shallow spherical shells of cylindrically orthotropic materials including the effects of the transverse shear, rotatory inertia, geometric imperfection and elastic foundation;

(iii) to obtain a set of equations of motion, and the corresponding set of boundary conditions;

(iv) to simplify the equations of motion for the following cases:

(1) Unsymmetrically laminated cross-ply shallow spherical shells

(2) Symmetrically laminated cross-ply shallow spherical shells

(3) Orthotropic shallow spherical shells

(4) Isotropic shallow spherical shells

(5) Unsymmetrically laminated cross-ply circular plates

(6) Symmetrically lamianted cross-ply circular plates

(7) Orthotropic circular plates

(8) Isotropic circular plates

including transverse shear, rotatory inertia, geometric imperfection and elastic foundation;

(v) to obtain approximate solutions for buckling, postbuckling and nonlinear vibration of a laminated cross-ply shallow spherical cap and its special cases including the above-mentioned complicating effects with the following boundary conditions:

(1) The edge of a symmetrically laminated cross-ply shell is flexibly supported with its special cases:

(a) Movable simply-supported

(b) Movable clamped

(c) Immovable simply-supported

(d) Immovable clamped

(2) The edge of an unsymmetrically laminated cross-ply shell is movable and rotational restrained with the movable clamped edge as a special case.

(vi) to compare the present numerical results in special cases with available data;

(vii) to obtain relationships between the following with physical parameters for various boundary conditions, ratios of base radius to shell or plate thcikness, numbers of layers and elastic properties of materils:

(1) Frequency ratio (nonlinear frequency to the corresponding linear frequency) and maximum amplitude of

symmetrically and unsymmetrically laminated cross-ply shallow spherical shells;

(2) Frequency ratio (nonlinear frequency to the corresponding linear frequency) and maximum amplitude of symmetrically and unsymmetrically laminated cross-ply circular plates;

(3) Postbuckling load and maximum deflection of symmetrically and unsymmetrically laminated cross-ply shallow spherical shells;

(4) Load and maximum deflection of symmetrically and unsymmetrically laminated cross-ply circualr plates;

(viii) to draw conclusions and some recommendations for further research.

CHAPTER 2

NONLINEAR THEORY OF LAMINATED SHALLOW SPHERICAL SHELLS

A dynamic nonlinear theory for the axisymmetric deformation of a laminated elastic shallow spherical shell composed of cylindrically (or polar) orthotropic layers is developed with the aid of the variational principle of elasticity. The effects of transverse shear deformation, rotatory inertia, geometric imperfection and elastic foundation are included. The constitutive relations for the laminated shell are derived from the generalized Hooke's law. The equations of motion are expressed in terms of a transverse displacement, a rotation of a normal to mid-surface and a stress function. For special cases, the governing equations derived in this chapter agree with those given by the earlier theories.

In the derivation of the theory it is assumed that:

(1) The material of the shell is homogeneous, continuous and linear elastic and the stresses of the deformed shell at any time are less than the corresponding yield stress.

(2) The layers constituting the shallow spherical shell are perfectly bonded together and are of the same material.

(3) The type of elastic foundation is nonlinear Winkler-Pasternak

model and the bonding between the shell and foundation is perfect.

(4) The deformation of the shell is axisymmetric, namely, independent of the circumferential coordinate (say, θ).

(5) The shell is moderately thick and the products of inplane displacement derivatives in the nonlinear strain-displacement relations may be neglected in comparison with the other terms.

(6) The effect of transverse normal contraction or extension is neglected.

(7) The tangential inertia terms are neglected.

(8) The ratio of the shell rise to the base radius is less than 0.25 such that the tangential displacements and forces may be taken to be their projections on the base plane of the shell (Reissner, 1946).

2.1 GEOMETRY AND DISPLACEMENT FIELD

Consider a shallow spherical shell of constant thickness referred to a right-handed cylindrical coordinate system of r, θ and z (Fig. 2.1). The elevation of the undeformed middle surface of the shell above the base circular plane, f, is approximated by the paraboloid:

$$f=H[1-(r/a)^2] \tag{2.1}$$

where H is the initial rise of the spherical shell and a is the base radius. The radius of curvature of the undeformed shell is

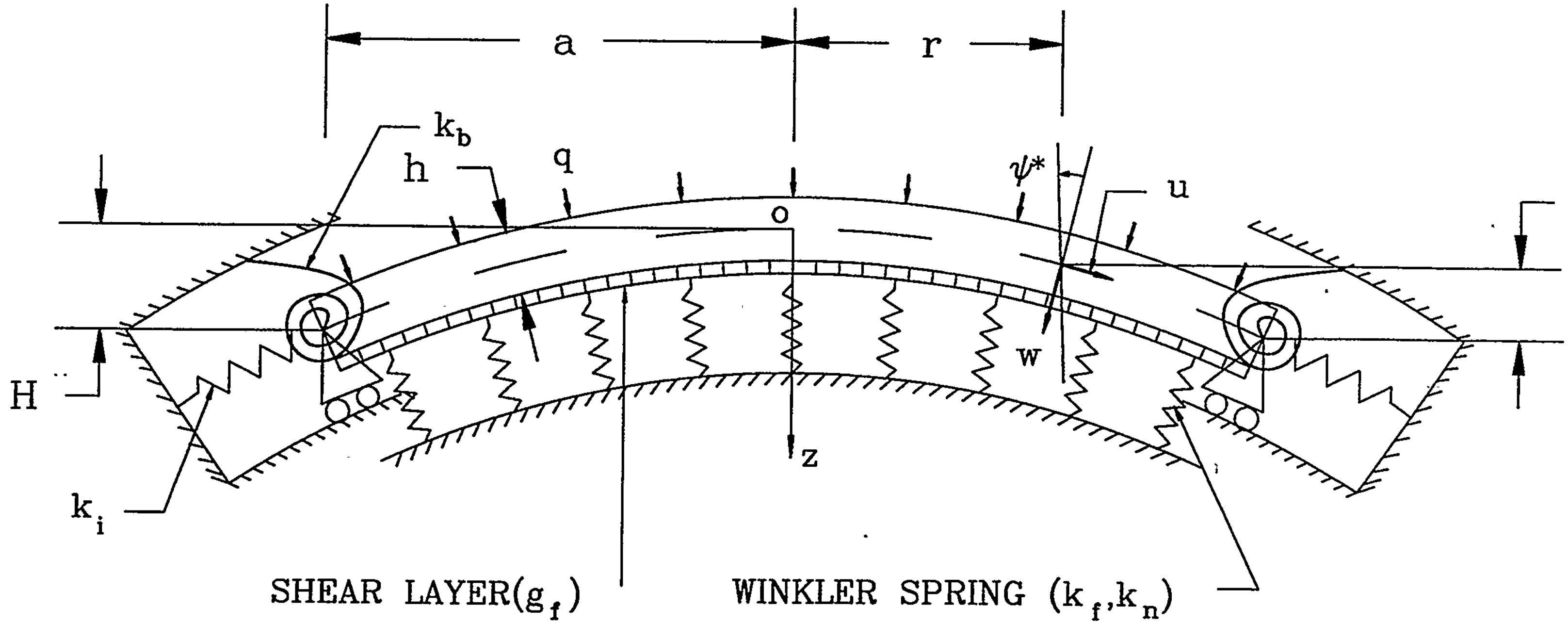

Figure 2.1: Geometry of a shallow spherical shell

$$R = a^2 / (2H) \tag{2.2}$$

The radial displacement at a distance z from the middle surface is assumed to vary linearly across the thickness of the shell and the transverse displacement is to remain constant. In the case of axisymmetric deformation of the shallow spherical shell, the displacement field may be written in the form:

$$\begin{aligned} u_r(r,z,t) &= u(r,t) + z\psi^*(r,t) \\ u_\theta(r,z,t) &= 0 \\ w(r,z,t) &= w(r,t) \end{aligned} \tag{2.3}$$

in which u_r, u_θ and w are the displacement components in the r, θ, and z directions, respectively and in which u is the value of u_r at the middle surface, ψ^* the rotation of a normal to the middle surface and t the time. With the transverse shear effect being taken into account, ψ^* is not equal to the derivative of w.

2.2 STRAIN-DISPLACEMENT RELATIONS

The nonlinear strain-displacement relations for axisymmetric deformation of a shallow spherical shell are derived from the three - dimensional nonlinear theory of elasticity by the classical method.

When a deformable body is under the action of external forces such as applied loads, body forces, and support reactions, the body will be deformed and the internal forces interacting between elemental portions of the body will be developed. The deformation of the body is characterized by the extension and distortion of line elements and the components of strain in engineering are defined as unit elongations of line elements and the changes in right angles between line elements, whereas those of a strain tensor are defined in terms of three displacement components. The deformation, however, may be either finite or infinitesimally small. In the theory of finite deformations or the nonlinear theory of elasticity, strain can be described by two different coordinate systems of reference, namely, the eulerian coordinates describing the material particles with respect to the deformed configuration, and the lagrangian coordinates describing these particles with respect to the original or undeformed configuration. In the following discussion, the lagrangian coordinate system is adopted. In the lagrangian description, all quantities are expressed in terms of the initial position coordinates of each particle and time during all subsequent motion. Thus the initial material lines and rectangular planes are deformed to curves and curved surface.

Consider a material particle $P(x_1, x_2, x_3)$ in an unstrained shallow spherical shell as shown in Fig.2.2. At a later instant of time the shell is deformed and the particle is deformed to a new location $P^*(x_1^*, x_2^*, x_3^*)$ by a displacement vector **u**. The deformation from the initial configuration to the deformed configuration is assumed to be continuous with one-to-one correspondence. From Fig. 2.2, the relation between x_i and x_i^* is given by

$$x_i^* = x_i + u_i \qquad (i = 1, 2, 3) \tag{2.4}$$

The square of length ds_o connecting the particle $P(x_1, x_2, x_3)$ to a

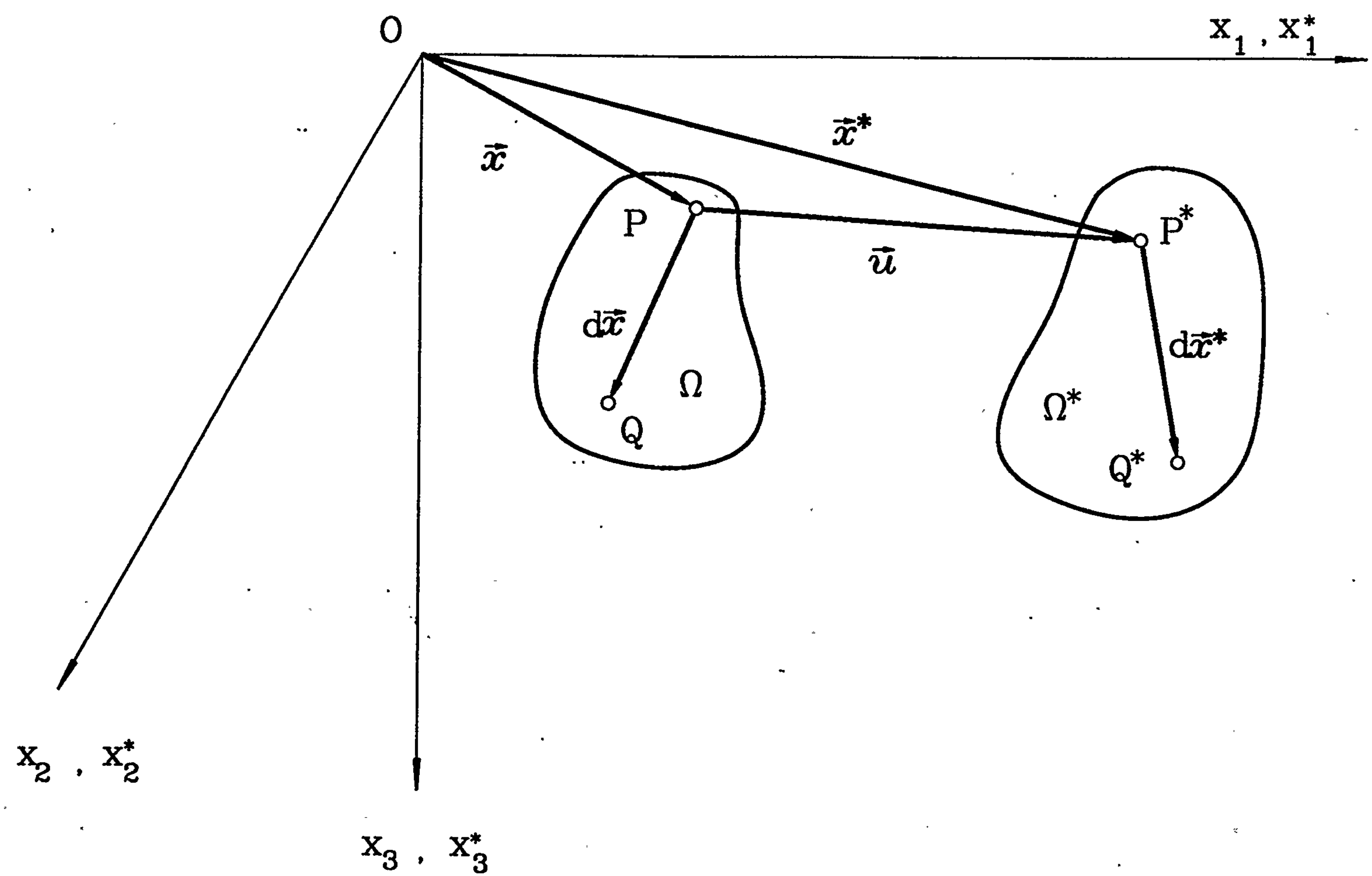

Figure 2.2: Deformation of a line element

neighbouring particle $Q(x_1+dx_1, x_2+dx_2, x_3+dx_3)$, both lying on a line element in the undeformed state, is

$$ds_o^2 = dx_i \, dx_i \tag{2.5}$$

in which the repeated index in a term indicates summation with respect to this index. During deformation the particle P and Q are displaced to $P^*(x_1^*, x_2^*, x_3^*)$ and $Q^*(x_1^*+dx_1^*, x_2^*+dx_2^*, x_3^*+dx_3^*)$, respectively. The square of the length ds of the new line element P^*Q^* is given by

$$ds^2 = dx_i^* \, dx_i^* \tag{2.6}$$

The difference $(ds^2 - ds_0^2)$ is a measure of strain. In the Lagrangian description the coordinate x_1, x_2, x_3 are regarded as independent variables such that $ds^2=(\partial x_i^*/\partial x_j)(\partial x_i^*/\partial x_k)dx_j dx_k$. Thus

$$ds^2 - ds_o^2 = dx_i^* \, dx_i^* - dx_i \, dx_i = 2\,\varepsilon_{ij}\, dx_i \, dx_j \tag{2.7}$$

where ε_{ij} is called the Green strain tensor or the lagrangian strain components and is symmetric.

Considering the cylindrical coordinate system used in this work and the axisymmetric deformation of the shell as assumed in (2.3), the following relations including the geometric imperfection exist (Fig. 2.3):

$$\begin{aligned}
x_1 &= r\cos\theta \qquad x_2 = r\sin\theta \qquad x_3 = z + \overline{w} \\
u_1 &= (\, u_r\cos\varphi - w\sin\varphi \,)\cos\theta \\
u_2 &= (\, u_r\cos\varphi - w\sin\varphi \,)\sin\theta \\
u_3 &= u_r\sin\varphi + w\cos\varphi
\end{aligned} \tag{2.8}$$

in which $\overline{w}$ is the initial deflection or geometric imperfection. Within the

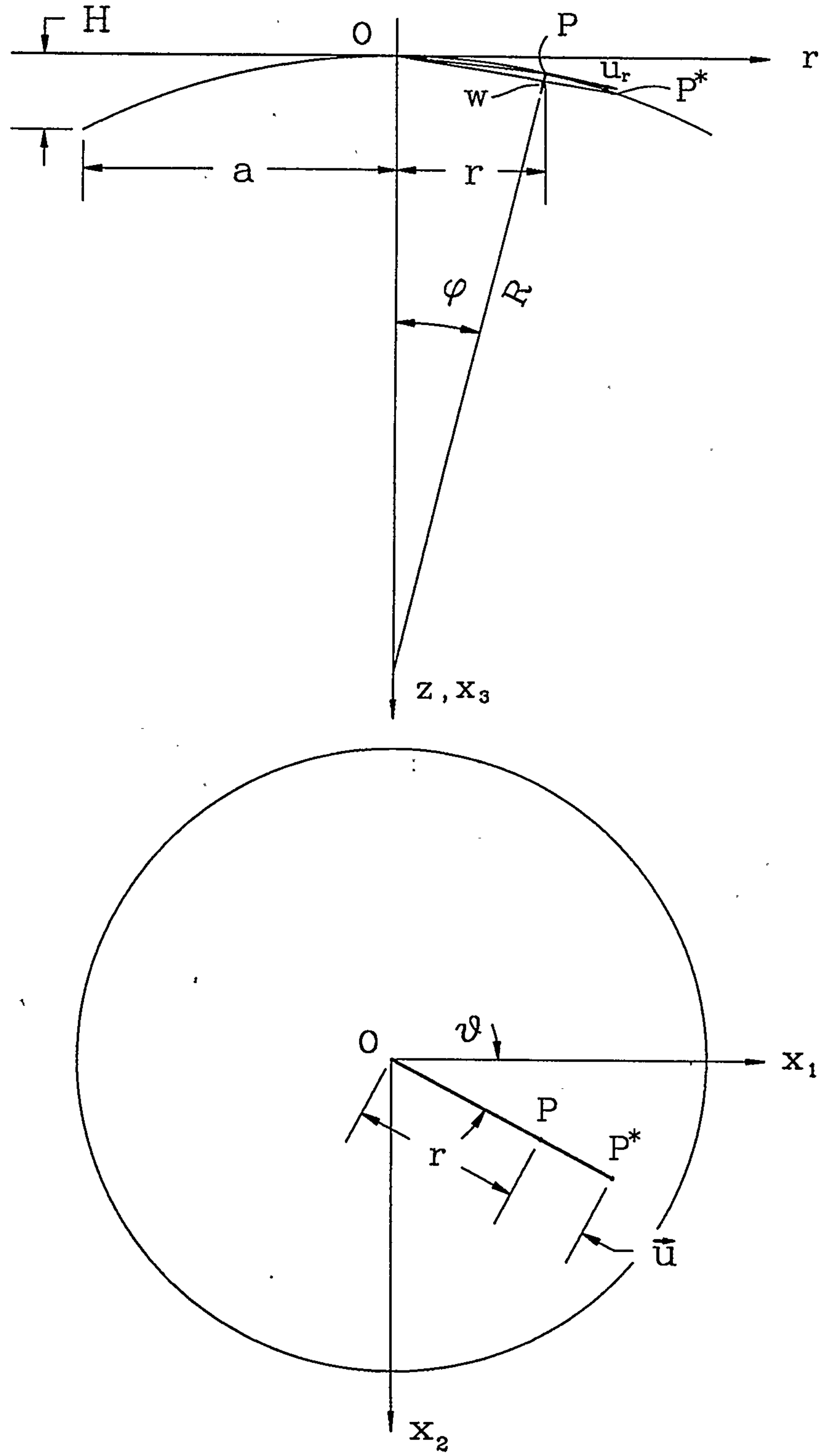

Figure 2.3: Displacement field of the shell

framework of the shallow shell theory (H/a < 0.25), the tangential displacements and forces can be taken to be their projections on the base plane of the shell, as proposed by Reissner (1946) and Donnell (1976). Due to the assumption of shell shallowness, some approximations are made,

$$\frac{d\varphi}{dr} \doteq \frac{1}{R}, \qquad \cos\varphi \doteq 1 \tag{2.9}$$

Substituting (2.8) and (2.9) into (2.5) and (2.6), the square of the length of the element before deformation is given by

$$ds_o^2 = dr^2 + r^2 d\theta^2 + dz^2 + d\overline{w}^2 + 2d\overline{w}dz \tag{2.10}$$

and after deformation by

$$\begin{aligned} ds^2 = & \left(dr + du_r - \frac{1}{R} w dr - \frac{r}{R} dw \right)^2 + \left(r + u_r - \frac{r}{R} w \right)^2 d\theta^2 \\ & + \left(dz + d\overline{w} + \frac{u_r}{R} dr + \frac{r}{R} du_r + dw \right)^2 \end{aligned} \tag{2.11}$$

With the products of inplane displacement derivatives and small quantities of other higher-order being neglected, the measure of strain in eqn. (2.7) can be written as

$$ds^2 - ds_o^2 = 2\varepsilon_r dr^2 + 2\varepsilon_\theta r^2 d\theta^2 + 2\varepsilon_{rz} dr dz \tag{2.12}$$

Thus, the strain-displacement relations are obtained:

$$\begin{aligned} \varepsilon_r &= u_{r,r} - w/R + \overline{w}_{,r} w_{,r} + w_{,r}^2/2 \\ \varepsilon_\theta &= u_r/r - w/R \\ \varepsilon_{rz} &= u_{r,z} + w_{,r} \\ \varepsilon_{r\theta} &= \varepsilon_{\theta z} = \varepsilon_z = 0 \end{aligned} \tag{2.13}$$

where a comma denotes differentiation with respect to the corresponding coordinates. By virtue of eqns. (2.3), the eqns. (2.13) can be rewritten as

$$\varepsilon_r = \varepsilon_r^o + z\,\kappa_r \quad , \quad \varepsilon_\theta = \varepsilon_\theta^o + z\,\kappa_\theta$$
$$\varepsilon_{rz} = \psi^* + w,_r \quad , \quad \varepsilon_{\theta z} = \varepsilon_{r\theta} = \varepsilon_z = 0 \tag{2.14}$$

in which $\varepsilon_r{}^o$ and $\varepsilon_\theta{}^o$ are the middle surface strains given by

$$\varepsilon_r^o = u,_r - w/R + \overline{w},_r w,_r + w,_r^2/2$$
$$\varepsilon_\theta^o = u/r - w/R \tag{2.15}$$

and κ_r and κ_θ are the changed values of shell curvatures given by

$$\kappa_r = \psi^*,_r$$
$$\kappa_\theta = \psi^*/r \tag{2.16}$$

When the transverse shear deformation and the geometric imperfection are neglected, i.e., $\varepsilon_{rz} = 0$ and $\overline{w} = 0$, the strain-displacement relations (2.14) are reduced to those given by Donnell (1933).

2.3 CONSTITUTIVE EQUATIONS

2.3.1 Stress

In discussing stress it is natural to employ the Lagrangian coordinate system since stress is related to strain. The components of a stress tensor per unit area of the deformed state are defined to be those of the Kirchhoff stress tensor which is measured with reference to the initial state. The stress tensor is symmetric in the system of orthogonal coordinates as the strain tensor. The normal components of the Kirchhoff stress tensor in the direction of cylindrical coordinate axes r, θ, z are denoted by σ_r, σ_θ, σ_z, respectively, and the shearing components by $\sigma_{r\theta}$, $\sigma_{\theta r}$, σ_{rz}, σ_{zr}, $\sigma_{\theta z}$, $\sigma_{z\theta}$. The first subscript in shearing stress components indicates the direction of the normal to the plane under consideration, and the second the direction of the stress component. The sense of stress components are depicted in Fig. 2.4.

2.3.2 Hooke's Law

Throughout this analysis the material of the shell is assumed to be linearly elastic. The stress then depends only on the deformation but not on the history of that deformation. A body whose elastic properties are different for different directions is called anisotropic. The generalized Hooke's law for a homogenous elastic body of general ansiotropy in the cylindrical coordinate system can be expressed in the matrix form as in Ref.(Chia, 1980).

$$\begin{Bmatrix} \varepsilon_r \\ \varepsilon_\theta \\ \varepsilon_z \\ \varepsilon_{rz} \\ \varepsilon_{\theta z} \\ \varepsilon_{r\theta} \end{Bmatrix} = \begin{bmatrix} r_{11} & r_{12} & r_{13} & r_{14} & r_{15} & r_{16} \\ r_{12} & r_{22} & r_{23} & r_{24} & r_{25} & r_{26} \\ r_{13} & r_{23} & r_{33} & r_{34} & r_{35} & r_{36} \\ r_{14} & r_{24} & r_{34} & r_{44} & r_{45} & r_{46} \\ r_{15} & r_{25} & r_{35} & r_{45} & r_{55} & r_{56} \\ r_{16} & r_{26} & r_{36} & r_{46} & r_{56} & r_{66} \end{bmatrix} \begin{Bmatrix} \sigma_r \\ \sigma_\theta \\ \sigma_z \\ \sigma_{rz} \\ \sigma_{\theta z} \\ \sigma_{r\theta} \end{Bmatrix} \tag{2.17}$$

where the coefficients r_{ij} are the elastic compliance and i, j = r, θ, z. The number of independent elastic constants is 21 in the general case. If,

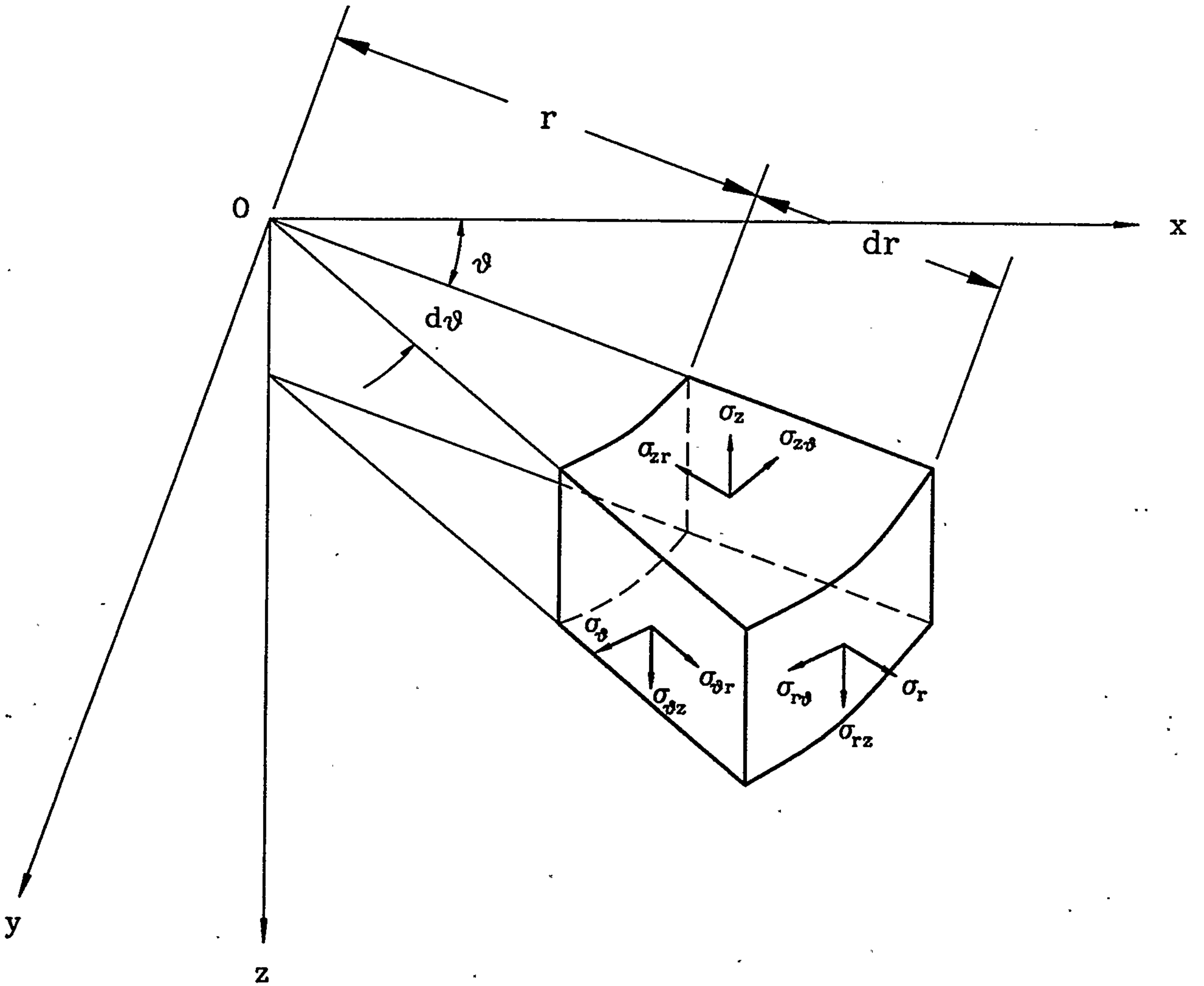

Figure 2.4: Sign convention for stresses in cylindrical coordinates

however, any plane of elastic symmetry is present in elastic properties, this number is reduced. In the case of an orthotropic body there are three mutually perpendicular planes of elastic symmetry. The matrix (2.17) then becomes

$$\begin{bmatrix} r_{11} & r_{12} & r_{13} & 0 & 0 & 0 \\ r_{12} & r_{22} & r_{23} & 0 & 0 & 0 \\ r_{13} & r_{23} & r_{33} & 0 & 0 & 0 \\ 0 & 0 & 0 & r_{44} & 0 & 0 \\ 0 & 0 & 0 & 0 & r_{55} & 0 \\ 0 & 0 & 0 & 0 & 0 & r_{66} \end{bmatrix} \tag{2.18}$$

where there are nine independent elastic constants. It can be shown that in the case of isotropic material, the elastic properties are independent of direction and the number of independent elastic constants is reduced to two.

It is evident from the symmetric matrix (2.18) that the constitutive relations for a cylindrically orthotropic material can be written in the so-called engineering constants as follows:

$$\begin{Bmatrix} \varepsilon_r \\ \varepsilon_\theta \\ \varepsilon_z \\ \varepsilon_{rz} \\ \varepsilon_{\theta z} \\ \varepsilon_{r\theta} \end{Bmatrix} = \begin{bmatrix} \frac{1}{E_r} & -\frac{\nu_{\theta r}}{E_\theta} & -\frac{\nu_{zr}}{E_z} & 0 & 0 & 0 \\ -\frac{\nu_{r\theta}}{E_r} & \frac{1}{E_\theta} & -\frac{\nu_{z\theta}}{E_z} & 0 & 0 & 0 \\ -\frac{\nu_{rz}}{E_r} & -\frac{\nu_{\theta z}}{E_\theta} & \frac{1}{E_z} & 0 & 0 & 0 \\ 0 & 0 & 0 & \frac{1}{G_{rz}} & 0 & 0 \\ 0 & 0 & 0 & 0 & \frac{1}{G_{\theta z}} & 0 \\ 0 & 0 & 0 & 0 & 0 & \frac{1}{G_{r\theta}} \end{bmatrix} \begin{Bmatrix} \sigma_r \\ \sigma_\theta \\ \sigma_z \\ \sigma_{rz} \\ \sigma_{\theta z} \\ \sigma_{r\theta} \end{Bmatrix} \tag{2.19}$$

in which E_i are Young's moduli along the i principal direction of elasticity, υ_{ij}

are the Poisson's ratios characterizing contraction in the j direction during tension applied in the i direction, and G_{ij} are the shear moduli characterizing changes of angles in the ij planes.

Due to the symmetric compliance matrix the elastic constants in equation(2.19) are related by

$$\begin{aligned} \nu_{zr} E_r &= \nu_{rz} E_z \\ \nu_{\theta z} E_z &= \nu_{z\theta} E_\theta \\ \nu_{\theta r} E_r &= \nu_{r\theta} E_\theta \end{aligned} \qquad (2.20)$$

The Hooke's law with the compliance matrix (2.18) can be written in the form

$$\begin{Bmatrix} \sigma_r \\ \sigma_\theta \\ \sigma_z \\ \sigma_{rz} \\ \sigma_{\theta z} \\ \sigma_{r\theta} \end{Bmatrix} = \begin{bmatrix} S_{11} & S_{12} & S_{13} & 0 & 0 & 0 \\ S_{12} & S_{22} & S_{23} & 0 & 0 & 0 \\ S_{13} & S_{23} & S_{33} & 0 & 0 & 0 \\ 0 & 0 & 0 & S_{44} & 0 & 0 \\ 0 & 0 & 0 & 0 & S_{55} & 0 \\ 0 & 0 & 0 & 0 & 0 & S_{66} \end{bmatrix} \begin{Bmatrix} \varepsilon_r \\ \varepsilon_\theta \\ \varepsilon_z \\ \varepsilon_{rz} \\ \varepsilon_{\theta z} \\ \varepsilon_{r\theta} \end{Bmatrix} \qquad (2.21)$$

in which S_{ij} are the elastic stiffness. Neglecting the influence of the transverse normal stress and considering the axisymmetric deformation (say, $\sigma_{r\theta} = \sigma_{\theta z} = 0$), the eqn. (2.21) is simplified to yield

$$\begin{Bmatrix} \sigma_r \\ \sigma_\theta \\ \sigma_{rz} \end{Bmatrix} = \begin{bmatrix} S_{11} & S_{12} & 0 \\ S_{12} & S_{22} & 0 \\ 0 & 0 & S_{44} \end{bmatrix} \begin{Bmatrix} \varepsilon_r \\ \varepsilon_\theta \\ \varepsilon_{rz} \end{Bmatrix} \qquad (2.22)$$

where S_{ij} are the reduced stiffness given by

$$S_{11} = \frac{E_r}{(1-\nu_{r\theta}\nu_{\theta r})} \quad , \quad S_{22} = \frac{E_\theta}{(1-\nu_{r\theta}\nu_{\theta r})}$$
$$S_{12} = \frac{\nu_{r\theta}E_\theta}{(1-\nu_{r\theta}\nu_{\theta r})} = \frac{\nu_{\theta r}E_r}{(1-\nu_{r\theta}\nu_{\theta r})} \quad , \quad S_{44} = G_{rz} \tag{2.23}$$

It is observed that eqn. (2.22) also represents the stress-strain relations for a cylindrically orthotropic shallow spherical shell which has principal directions of elasticity coinciding with the shell axes. Note that only four independent elastic constants for an orthotropic shallow spherical shell subject to axisymmetric deformation exist, that is, G_{rz} and any three of the four parameters E_r, E_θ, $\upsilon_{r\theta}$,$\upsilon_{\theta r}$.

In engineering applications, the elastic properties of an cylindrically orthotropic shallow spherical shell are usually known in the principal directions (L, T) of elasticity where L is the major direction and T the minor direction. The reduced stiffness are related to these material axes of symmetry by

$$S_L = \frac{E_L}{\mu} \quad , \quad S_{LT} = \frac{\nu_{LT}E_T}{\mu} \quad , \quad S_T = \frac{E_T}{\mu} \quad , \quad S_S = G_{LT}$$
$$S_{SL} = G_{Lz} \quad , \quad S_{ST} = G_{Tz} \tag{2.24}$$

in which E_L and E_T are major and minor Young's moduli, υ_{LT} and υ_{TL} the Poisson's ratios, G_{LT} the inplane shear modulus and G_{Lz} and G_{Tz} the transverse shear moduli, and in which

$$\mu = 1 - \nu_{LT}\nu_{TL}$$
$$\nu_{TL}E_L = \nu_{LT}E_T \tag{2.25}$$

The elastic constants of a composite material with reference to orthotropic directions (r, θ) can be found by the equations:

(1) when the major direction L coincides with the r axis

$$\begin{aligned} S_{11} &= S_L \;, \quad S_{12} = S_{LT} \\ S_{22} &= S_T \;, \quad S_{44} = S_{SL} \end{aligned} \tag{2.26}$$

(2) when the minor direction T coincides with the r axis

$$\begin{aligned} S_{11} &= S_T \;, \quad S_{12} = S_{LT} \\ S_{22} &= S_L \;, \quad S_{44} = S_{ST} \end{aligned} \tag{2.27}$$

2.3.3 Constitutive Equations of Laminated Shallow Spherical Shells

The type of the shell under consideration is constructed of an arbitrary number of homogeneous cylindrical orthotropic layers perfectly bonded together. Each layer has arbitrary thickness, elastic properties and orientation of orthotropic axes with respect to the shell axes. The geometry of the kth layer is defined by two surfaces $z = f_{k-1}(r)$ and $z = f_k(r)$ and the upper and lower boundary surfaces are defined by z = -h/2 and z = +h/2 from the middle surface (Fig. 2.5). The total thickness of the laminate is h. The shell materials are continuous everywhere and each layer obeys the generalized Hooke's law.

By the use of the constitutive equation (2.22), we have for the kth layer

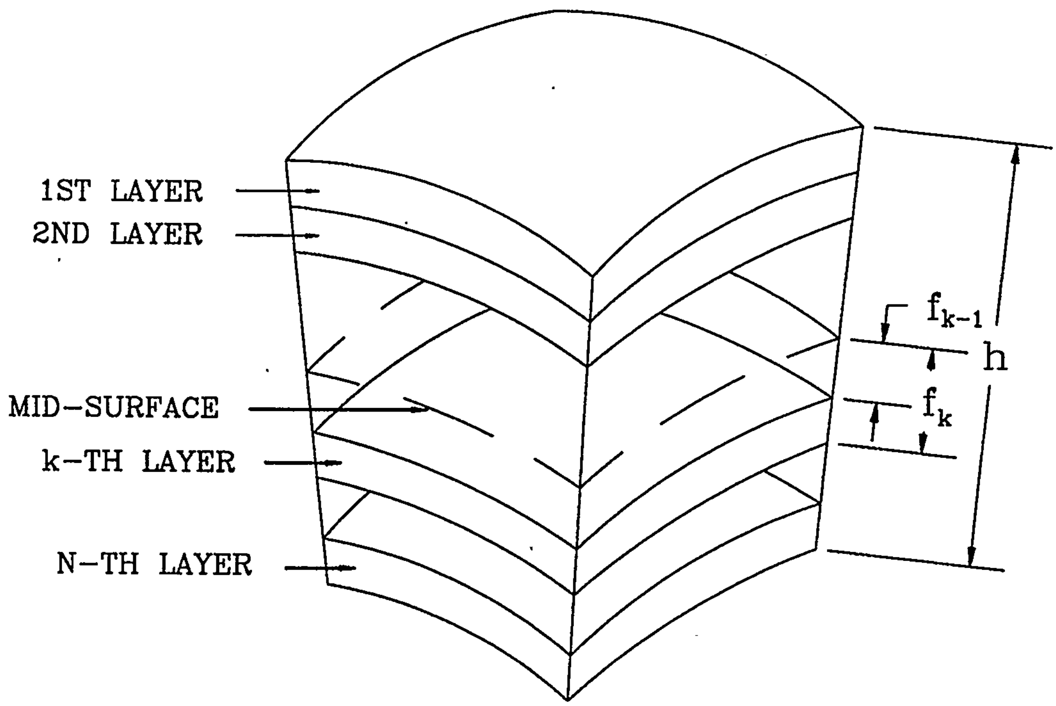

Figure 2.5: Structure of the laminated shell

$$\begin{Bmatrix} \sigma_r^{(k)} \\ \sigma_\theta^{(k)} \\ \sigma_{rz}^{(k)} \end{Bmatrix} = \begin{bmatrix} S_{11}^{(k)} & S_{12}^{(k)} & 0 \\ S_{12}^{(k)} & S_{22}^{(k)} & 0 \\ 0 & 0 & S_{44}^{(k)} \end{bmatrix} \begin{Bmatrix} \varepsilon_r^{(k)} \\ \varepsilon_\theta^{(k)} \\ \varepsilon_{rz}^{(k)} \end{Bmatrix} \tag{2.28}$$

in which $S_{ij}^{(k)}$ are the reduced stiffness of the *k*th layer.

As in the classical shell theory, the stress resultants and stress couples are defined by

$$\begin{aligned} [\, N_r \,,\, N_\theta \,] &= \int_{-h/2}^{+h/2} [\, \sigma_r^{(k)} \,,\, \sigma_\theta^{(k)} \,]\, dz \\ [\, M_r ,\, M_\theta \,] &= \int_{-h/2}^{+h/2} [\, \sigma_r^{(k)} \,,\, \sigma_\theta^{(k)} \,]\, z\, dz \end{aligned} \tag{2.29}$$

In which, N_r, N_θ are membrane forces and M_r, M_θ are bending moments, all per unit length. These forces and moments are shown in Fig. 2.6. Substituting eqn. (2.28) into eqns. (2.29) and taking eqns. (2.14) into account, yields the constitutive relations of the shell.

$$\begin{Bmatrix} [\, N \,] \\ [\, M \,] \end{Bmatrix} = \begin{bmatrix} [A] & [B] \\ [B] & [D] \end{bmatrix} \begin{Bmatrix} [\, \varepsilon^o \,] \\ [\, \kappa \,] \end{Bmatrix} \tag{2.30}$$

where

$$\begin{aligned} &[N] = \begin{Bmatrix} N_r \\ N_\theta \end{Bmatrix} , \quad [M] = \begin{Bmatrix} M_r \\ M_\theta \end{Bmatrix} \\ &[\varepsilon^o] = \begin{Bmatrix} \varepsilon_r^o \\ \varepsilon_\theta^o \end{Bmatrix} , \quad [\kappa] = \begin{Bmatrix} \kappa_r \\ \kappa_\theta \end{Bmatrix} \\ &[\, A \,] = \begin{bmatrix} A_{11} & A_{12} \\ A_{12} & A_{22} \end{bmatrix} , \quad [\, B \,] = \begin{bmatrix} B_{11} & B_{12} \\ B_{12} & B_{22} \end{bmatrix} , \quad [\, D \,] = \begin{bmatrix} D_{11} & D_{12} \\ D_{12} & D_{22} \end{bmatrix} \end{aligned} \tag{2.31}$$

and

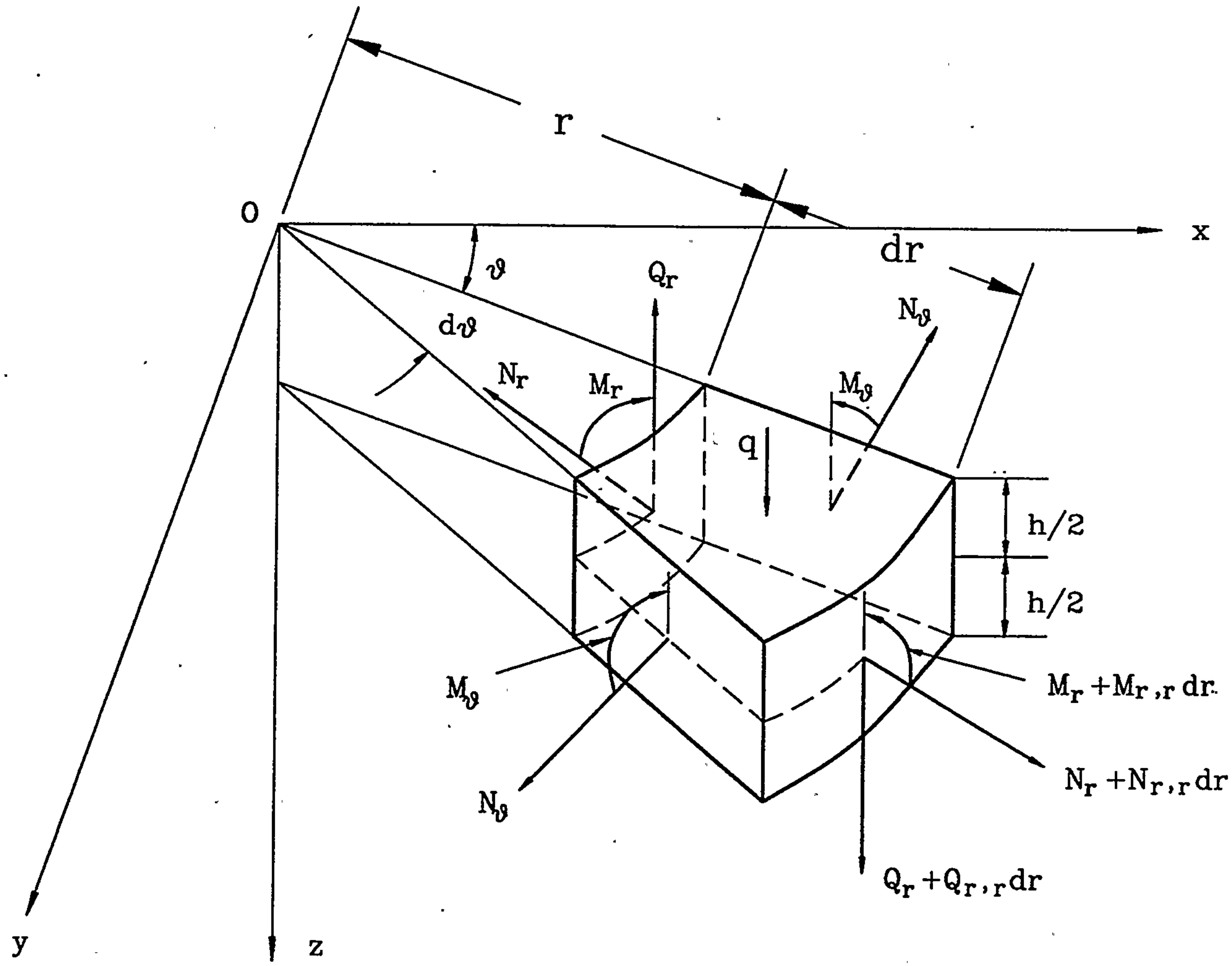

Figure 2.6: Shell element with stress resultants and couples

$$(A_{ij}, B_{ij}, D_{ij}) = \int_{-h/2}^{+h/2} S_{ij}^{(k)} (1, z, z^2)\, dz \quad (i, j=1, 2) \qquad (2.32)$$

The material constants A_{ij}, B_{ij} and D_{ij} (i, j = 1, 2) are, respectively, the extensional stiffnesses, the coupling stiffnesses and flexural stiffnesses of the shell. The B_{ij} display coupling between transverse bending and inplane stretching. It is noted that bending-stretching coupling exists even for a laminate constructed of isotropic layers of various materials. In fact, only when the shell is symmetric about its middle surface, the coupling B_{ij} will disappear. This requires symmetry in laminae properties, laminae orientation and distance from the middle surface.

For various types of shell construction in this study, the values of A_{ij}, B_{ij} and D_{ij} are presented as follows:

(1) Unsymmetric cross-ply laminate

Unsymmetric cross-ply laminates are constructed of an even number of cylindrically orthotropic layers all of the same thickness and identical mechanical properties, with orthotropic axes of symmetry in each layer alternately oriented at angles of 0° and 90° with the shell axes, namely, the base plane axes of the shell. The fiber direction of odd layers is assumed to be coincided with the θ axis and that of the even layers with the r axis. In this case, it can be shown that

$$(A_{11}, A_{12}, A_{22}) = h\left(\frac{S_L + S_T}{2}, S_{LT}, \frac{S_L + S_T}{2}\right)$$

$$B_{11} = -B_{22} = \frac{h^2}{4N}(S_T - S_L), \quad B_{12} = 0 \qquad (2.33)$$

$$D_{11} = D_{22} = \frac{h^3}{24}(S_L + S_T), \quad D_{12} = \frac{h^3}{12} S_{LT}$$

(2) Symmetric cross-ply laminate

Symmetric cross-ply laminates are constructed of an odd number of cylindrically orthotropic layers all of the same thickness and identical mechanical properties. The layers of a symmetric cross-ply laminate are so arranged that a mid-surface elastic symmetry exists. That is, for each layer above the mid-surface, there is a corresponding layer identical in thickness, elastic properties, and orientation of filaments located at the same distance below the mid-surface. Thus, it is assumed that the fiber direction of odd layers coincides with the θ axis, and that of the even layers with the r axis. In present case, the material coupling does not occur between bending and stretching and the shell stiffnesses are

$$
\begin{aligned}
A_{11} &= \frac{h}{2N}\left[\,(N+1)\,S_T + (N-1)\,S_L\,\right] \\
A_{22} &= \frac{h}{2N}\left[\,(N-1)\,S_T + (N+1)\,S_L\,\right] \\
A_{12} &= h\,S_{LT} \\
B_{ij} &= 0 \\
D_{11} &= \frac{h^3}{24N^3}\left[\,(N^3+3N^2-2)\,S_T + (N-1)\,(N^2-2N-2)\,S_L\,\right] \\
D_{22} &= \frac{h^3}{24N^3}\left[\,(N-1)\,(N^2-2N-2)\,S_T + (N^3+3N^2-2)\,S_L\,\right] \\
D_{12} &= \frac{h^3}{12}\,S_{LT}
\end{aligned}
\tag{2.34}
$$

(3) Orthotropic shell

For a cylindrically orthotropic shallow spherical shell its material axes of symmetry parallel to the coordinate axes of the shell and the fiber direction coinciding with θ axis, the stiffness are

$$
\begin{aligned}
&(A_{11} , A_{12} , A_{22}) = h (S_T , S_{LT} , S_L) \\
&B_{ij} = 0 \\
&(D_{11} , D_{12} , D_{22}) = \frac{h^3}{12} (S_T , S_{LT} , S_L)
\end{aligned}
\tag{2.35}
$$

(4) Isotropic shell

In the case of an isotropic shell

$$
\begin{aligned}
&A_{11} = A_{22} = \frac{Eh}{1-\nu^2} , \quad A_{12} = \nu A_{11} \\
&B_{ij} = 0 \\
&D_{11} = D_{22} = \frac{Eh^3}{12(1-\nu^2)} , \quad D_{12} = \nu D_{11}
\end{aligned}
\tag{2.36}
$$

where E is the modulus of elasticity and υ Poisson's ratio of the isotropic shell.

2.3.4 Transverse Shear Deformation

For the analysis of most plate or shell structures composed of composite materials, the transverse shear deformation should be taken into account. In the axisymmetric deformation of the shell, only one transverse stress exists. From eqn. (2.28), this shear stress is

$$
\sigma_{rz}^{(k)} = S_{44}^{(k)} \varepsilon_{rz}^{(k)} \tag{2.37}
$$

As in eqn. (2.29), the shear stress resultant is defined by

$$
Q_r = \int_{-h/2}^{+h/2} \sigma_{rz}^{(k)} dz \tag{2.38}
$$

The transverse shear strain in (2.14) represents the average shear strain across the thickness of the shell. As can be derived from (2.22), the transverse shear stress is a step distribution across the shell thickness and does not vanish on the bounding surface of the shell. To eliminate this discrepancy a parabolic shear stress distribution across the shell thickness is assumed in the form as in the work by Fu and Chia (1989a,b)

$$\sigma_{rz} = \frac{3Q_r}{2h}\left[1-\left(\frac{z}{h/2}\right)^2\right] \tag{2.39}$$

and the transverse shear stress resultant, Q_r, may be written as

$$Q_r = G^*\varepsilon_{rz} = G^*(\psi^* + w_{,r}) \tag{2.40}$$

in which G^* is the transverse shear stiffness.

By introducing the complementary energy, the shear stiffness G^* can be determined. The complementary energy due to σ_{rz}, given by expression (2.39) is

$$\begin{aligned} V &= \frac{1}{2}\int_{-h/2}^{+h/2}\left[(\sigma_{rz}^{(k)})^2/S_{44}^{(k)}\right]dz \\ &= \frac{9Q_r^2}{8h^2}\sum_{k=1}^{N}\frac{1}{S_{44}^{(k)}}\left[h_k-h_{k-1}-\frac{8}{3h^2}(h_k^3-h_{k-1}^3)+\frac{16}{5h^4}(h_k^5-h_{k-1}^5)\right] \end{aligned} \tag{2.41}$$

where N is the number of layers. On the other hand, the complementary energy from expression (2.40) is

$$V = \frac{1}{2}Q_r^2/G^* \tag{2.42}$$

Equating the shear complementary energies and hence coefficients of like terms yields

$$G^{*}=\frac{4h^{2}}{9\sum_{k=1}^{N}\{[(h_{k}-h_{k-1})-8(h_{k}^{3}-h_{k-1}^{3})/(3h^{2})+16(h_{k}^{5}-h_{k-1}^{5})/(5h^{4})]/S_{44}^{(k)}\}} \tag{2.43}$$

If the transverse shear effect is negligible, then $\varepsilon_{rz} = 0$ and consequently,

$$\psi^{*}+w,_{r}=0 \tag{2.44}$$

which is consistent with Kirchhoff's assumption that the straight line element of the shell which is perpendicular to the middle surface before deformation remains so after deformation.

2.4 NONLINEAR EQUATIONS OF MOTION

The principle of virtual work established by Lagrange is one of the variational principle in three dimensional continuum mechanics. It may be stated as follows: Assume that the mechanical system is in equilibrium under applied forces and prescribed geometrical constraints. Then, the sum of all the virtual work, denoted by δW, done by external and internal forces existing in the system in any arbitrary infinitesimal virtual displacements satisfying the prescribed geometrical constraints is zero:

$$\delta W=0 \tag{2.45}$$

This principle may be stated alternatively in the following manner: If the sum of all the virtual work vanishes for any arbitrary infinitesimal virtual displacements satisfying the prescribed geometrical constraints, then the mechanical system is in equilibrium. Thus, the principle of virtual work is equivalent to the equations of equilibrium of the system. The above formation may be extended to the dynamical problem of a mechanical system subjected to time-dependent applied forces and geometrical constraints. By the use of D'Alembert's principle which states that the system can be considered to be in equilibrium if inertial forces are taken into account, the principle of virtual work of the dynamical problem can be derived in a manner similar to the static problem case, except that terms representing the virtual work done by the inertial forces are now included. Based on the principle of virtual work, various variational principles have been derived by many researchers, such as, Reissner's principle (1950) which allows independent variation of both displacements and stresses and leads to equations of equilibrium, constitutive relations (assuming strain-displacement relations are satisfied) and natural boundary conditions, Washizu's principle(1968) which allows independent variation of stress, displacement and strain and results in all three sets of equilibrium equations, constitutive relations and the corresponding boundary conditions, and others.

In this work, making use of the principle of virtual work, the equilibrium equations of motion for laminated shallow spherical shells can be derived. Assuming that the strain-displacement and constitutive relations are satisfied, the sum of all the virtual work done by external and internal forces (including inertial forces) can be expressed in the form:

$$\underbrace{\delta W = \iiint_v \sigma_{ij}\,\delta\varepsilon_{ij}\,dv}_{\delta W_1} \;\underbrace{- \iiint_v \bar{B}_i\,\delta u_i\,dv}_{\delta W_2} \;\underbrace{- \iint_{S_1} \bar{T}_i\,\delta u_i\,dS}_{\delta W_3} \tag{2.46}$$

where: $\bar{B}_i$ = body force per unit volume of material acted on along the coordinate direction i.

$\bar{T}_i$ = surface traction per unit area acted on along the direction i.

S_1 = a part of the surface on which surface tractions.

S = surface of the shell.

v = space occupied by the shell.

For the present case, the first term of δW is

$$\delta W_1 = \int_0^a \int_0^{2\pi} \int_{-h/2}^{+h/2} [\,\sigma_r\delta\varepsilon_r + \sigma_\theta\delta\varepsilon_\theta + \sigma_{rz}\delta\varepsilon_{rz}\,]\; r\,dz\,d\theta\,dr \tag{2.47}$$

Using relations (2.14) and (2.29) and integrating with respect to z from -h/2 to +h/2 and to θ from 0 to 2π, expression (2.47) can be written as:

$$\begin{aligned}
\delta W_1 = 2\pi \int_0^a & [\,rN_r\delta\,(u,_r - w/R + \bar{w},_r w,_r + w,_r^2/2) + rM_r\delta\psi^*,_r \\
& + rN_\theta\delta\,(u/r - w/R) + rM_\theta\delta\,(\psi^*/r) + rQ_r\delta\,(\psi^* + w,_r)\,]\,dr \\
= 2\pi \int_0^a & \{\,[\,-(rN_r),_r + N_\theta]\delta u - [\,-(rM_r),_r + M_\theta + rQ_r]\,\delta\psi^* \\
& + [\,-(rN_r)/R - (rN_r\bar{w},_r + rN_r w,_r),_r - (rN_\theta)/R \\
& - (rQ_r),_r]\,\delta w\}\,dr + 2\pi\,(rN_r\delta u)\,\big|_0^a + 2\pi\,(rM_r\delta\psi^*)\,\big|_0^a \\
& + 2\pi\,[\,(rN_r\bar{w},_r + rN_r w,_r + rQ_r)\,\delta w]\,\big|_0^a
\end{aligned} \tag{2.48}$$

From D'Alember's principle, the effect due to acceleration of the shell in consideration, can be represented as a body force. Neglecting the mass body force effects and retaining only the acceleration terms, the second term of δW is given by

$$\begin{aligned}\delta W_2 &= -\int_0^a\int_0^{2\pi}\int_{-h/2}^{+h/2} \gamma_o^{(k)}\,(u_{r,tt}\delta u_r + u_{\theta,tt}\delta u_\theta + w_{,tt}\delta w)\,r\,dz\,d\theta\,dr \\ &= -\int_0^a\int_0^{2\pi}\int_{-h/2}^{+h/2} \gamma_o^{(k)}\,[(u_{,tt}+z\psi^*_{,tt})\,\delta(u+z\psi^*) + w_{,tt}\delta w]\,r\,dz\,d\theta\,dr \\ &= -2\pi\int_0^a [(\gamma u_{,tt}+I\psi^*_{,tt})\,\delta u + (Iu_{,tt}+J\psi^*_{,tt})\,\delta\psi^* \\ &\quad +\gamma w_{,tt}dw]\,r\,dr\end{aligned} \tag{2.49}$$

where $\gamma_0^{(k)}$ is the shell mass density per unit volume, and

$$(\gamma, I, J) = \int_{-h/2}^{h/2} \gamma_o^{(k)}\,(1, z, z^2)\,dz \tag{2.50}$$

The shell in this work is supported on a nonlinear Winkler-Pasternak elastic foundation and is subject to distributed transverse load q(r,t) on the upper face (Fig. 2.1). In this figure, K_f is the extensional modulus, k_n is the nonlinear extensional modulus and g_f is the shear modulus which assumes the existance of shear interaction between the foundation elements. On account of the elastic foundation, the total transverse load is to be replaced by $q-k_f w-k_n w^3+g_f(w_{,rr}+w_{,r}/r)$(Dumir, 1985). Also, the shell is rested on the flexible edge of inplane stiffness k_i and rotational stiffness k_b. Thus, the last term of δW is expressed as

$$\begin{aligned}\delta W_3 &= \int_0^a\int_0^{2\pi} [q-k_f w-k_n w^3+g_f(w_{,rr}+w_{,r}/r)]\,\delta w\,r\,d\theta\,dr \\ &\quad +2\pi a[-k_b\psi^*(a)\,\delta\psi^*(a) - k_i u(a)\,\delta u(a)]\end{aligned} \tag{2.51}$$

The sum of all virtual work is rewritten as

$$
\begin{aligned}
\delta W = 2\pi \int_0^a \{ & [-(rN_r)_{,r} + N_\theta + \gamma u_{,tt} + I\psi^*_{,tt}]\,\delta u \\
& - [-(rM_r)_{,r} + M_\theta + rQ_r + Iu_{,tt} + J\psi^*_{,tt}]\,\delta\psi^* \\
& + [-(rN_r + rN_\theta)/R - (rN_r\overline{w}_{,r} + rN_r w_{,r})_{,r} - (rQ_r)_{,r} \\
& - q + k_f w + k_n w^3 - g_f(w_{,rr} + w_{,r}/r) + \gamma w_{,tt}]\,\delta w\}\, dr \\
& + 2\pi\,(rN_r\delta u)\big|_0^a + 2\pi\,(rM_r\delta\psi^*)\big|_0^a \\
& + 2\pi\,[(rN_r\overline{w}_{,r} + rN_r w_{,r} + rQ_r)\,\delta w]\big|_0^a \\
& + 2\pi a\,[k_b\psi^*(a)\,\delta\psi^*(a) + k_i u(a)\,\delta u(a)]
\end{aligned} \tag{2.52}
$$

Employing the principle of virtual work, δW must vanish and hence the arbitrary and independent variations of displacements will lead to the following governing equations of motion and mixed boundary conditions:

(1) Governing Equations of Motion

$$(rN_r)_{,r} - N_\theta = \gamma u_{,tt} + rI\psi^*_{,tt} \tag{2.53a}$$

$$(rM_r)_{,r} - M_\theta - rQ_r = rIu_{,tt} + rJ\psi^*_{,tt} \tag{2.53b}$$

$$
\begin{aligned}
& r(N_r + N_\theta)/R + [rN_r(w_{,r} + w_{,r})]_{,r} + (rQ_r)_{,r} \\
& \quad + r[q - k_f w - k_n w^3 + g_f(w_{,rr} + w_{,r}/r)] = r\gamma w_{,tt}
\end{aligned} \tag{2.53c}
$$

(2) Mixed Boundary Conditions

$$N_r = -k_i u \qquad \text{or} \qquad u = u_o \qquad \text{at} \quad r = a \tag{2.54a}$$

$$M_r = -k_b\psi^* \qquad \text{or} \qquad \psi^* = \psi^*_o \qquad \text{at} \quad r = a \tag{2.54b}$$

$$Q_r = -N_r(\bar{w}_{,r} + w_{,r}) \quad or \quad w = w_o \qquad at \quad r = a \tag{2.54c}$$

where u_0, w_0 and ψ_0^* are the prescribed boundary displacement functions.

For axisymmetric deformation of a shallow spherical shell, the symmetry condition $\psi^* = 0$ at the apex should be satisfied. To ensure that membrane stress resultants do not increase indefinitely at apex, the condition of N_r being finite should be also imposed. In this work, since the shell edge is supported by elastic restraints and finite conditions are imposed at the apex, the boundary conditions may be rewritten as

$$\psi^* = 0 \quad and \quad N_r \quad is \quad finite \quad at \quad r=0. \tag{2.55a}$$

$$W=0 \ , \ N_r = -k_i\, u \ , \ M_r = -k_b\, \psi^* \quad at \ r=a \tag{2.55b}$$

Boundary conditions treat the specific values of k_b and k_i (i.e., k_b, $k_i = 0, \infty$) as special cases:

(a) Movable simply supported edge (SM), when $k_i = 0$ and $k_b = 0$;

(b) Immovable simply supported edge (SI), when $k_i = \infty$ and $k_b = 0$;

(c) Movable clamped edge (CM), when $k_i = 0$ and $k_b = \infty$;

(d) Immovable clamped edge (CI), when $k_i = \infty$ and $k_b = \infty$.

2.5 GOVERNING EQUATIONS IN TERMS OF TRANSVERSE DISPLACEMENT, ROTATION AND STRESS FUNCTION

As usual the tangential inertia terms are neglected and a stress function, F^*, is introduced as

$$N_r = F^*/r \quad , \quad N_\theta = F^*_{,r} \tag{2.56}$$

It is observed that I in eqn. (2.50) disappears when $\gamma_o^{(k)}$ is a constant as assumed. Thus the stress function satisfied the first governing eqn. (2.53a).

A partial inverse of eqn. (2.30) yields

$$\begin{Bmatrix} [\,\varepsilon^o\,] \\ [\,M\,] \end{Bmatrix} = \begin{bmatrix} [A^*] & [B^*] \\ -[B^*]^T & [D^*] \end{bmatrix} \begin{Bmatrix} [\,N\,] \\ [\,\kappa\,] \end{Bmatrix} \tag{2.57}$$

in which superscript T represents the matrix transpose and

$$\begin{gathered} [A^*] = [A]^{-1} \quad , \quad [B^*] = -[A]^{-1}[B] \\ [D^*] = [D] - [B]\,[A]^{-1}[B] \end{gathered} \tag{2.58}$$

In general $[A^*]$ and $[D^*]$ are symmetric but $[B^*]$ is not a symmetric matrix.

The equation obtained by eliminating u in strain-displacement relations (2.14) is called the compatibility condition:

$$-\varepsilon_r^o + (r\varepsilon_\theta^o)_{,r} + rw_{,r}/R + \overline{w}_{,r}w_{,r} + w_{,r}^2/2 = 0 \tag{2.59}$$

Making use of eqns. (2.56) and (2.57) , the compatibility condition in terms of w, ψ^* and F^* can be obtained,

$$\begin{aligned} &A_{22}^*(rF^*_{,rr} + F^*_{,r}) - A_{11}^*F^*/r + B_{21}^*r\psi^*_{,rr} + (B_{21}^* + B_{22}^* - B_{11}^*)\,\psi^*_{,r} \\ &-B_{12}^*\psi^*/r + rw_{,r}/R + \overline{w}_{,r}w_{,r} + w_{,r}^2/2 = 0 \end{aligned} \tag{2.60}$$

Employing the partial inversion of relation (2.57) for M_r, M_θ and eqn. (2.40) for Q_r respectively, eqn. (2.53b) is expressed in terms of w, ψ^* and F^* as

$$T_S[-B_{21}^{*}rF^{*},_{rr}-(B_{11}^{*}+B_{21}^{*}-B_{22}^{*})F^{*},_{r}+B_{12}^{*}F^{*}/r+D_{11}^{*}(\psi^{*},_{r}+r\psi^{*},_{rr}) \\ -D_{22}^{*}\psi^{*}/r-R_I rJ\psi^{*},_{tt}]-G^{*}r(\psi^{*}+w,_{r})=0 \tag{2.61}$$

In the above equation, tracing constants T_S and R_I are introduced to represent the influence of transverse shear and rotatory inertia when $T_S = 1$ and $R_I = 1$; when $T_S = 0$ and $R_I = 0$, these effects are neglected.

Using the governing equation (2.53b) for rQ_r, the partial inversion of the constitutive relation (2.57) for M_r, M_θ and eqn. (2.56), and integrating eqn. (2.53c) with respect to r from 0 to r, the governing equation of motion may be written in terms of w, ψ^* and F^* as

$$-B_{21}^{*}rF^{*},_{rr}-(B_{11}^{*}+B_{21}^{*}-B_{22}^{*})F^{*},_{r}+B_{12}^{*}F^{*}/r+D_{11}^{*}(\psi^{*},_{r}+r\psi^{*},_{rr}) \\ -D_{22}^{*}\psi^{*}/r-R_I[r\psi^{*},_{tt}]+(rF^{*})/R+F^{*}(r/R+\overline{w},_{r}+w,_{r}) \\ +\int_0^r r[q-k_f w-k_n w^3+g_f(w,_{rr}+w,_{r}/r)-w,_{tt}]\,dr=0 \tag{2.62}$$

To simplify the calculation for numerical results, equations (2.60) to (2.62) are expressed in the dimensionless form

$$\overline{A}_{22}(\rho F,_{\rho\rho}+F,_{\rho})-\overline{A}_{11}F/\rho+\overline{B}_{21}\rho\psi,_{\rho\rho}/\lambda_1+(\overline{B}_{21}+\overline{B}_{22}-\overline{B}_{11})\psi,_{\rho}/\lambda_1 \\ -\overline{B}_{12}\psi/(\lambda_1\rho)+2\lambda_2\rho W,_{\rho}+\overline{W},_{\rho}W,_{\rho}/\lambda_1+W,_{\rho}^{2}/(2\lambda_1)=0 \tag{2.63a}$$

$$T_S[-\lambda_1\overline{B}_{21}\rho F,_{\rho\rho}-\lambda_1(\overline{B}_{11}+\overline{B}_{21}-\overline{B}_{22})F,_{\rho}+\lambda_1\overline{B}_{12}F/\rho+\overline{D}_{11}(\psi,_{\rho}+\rho\psi,_{\rho\rho}) \\ -\overline{D}_{22}\psi/\rho-R_I\rho\psi,_{\tau\tau}/(12\lambda_1^2)]-\lambda_1^2\overline{G}\rho(\psi+W,_{\rho})=0 \tag{2.63b}$$

$$-\lambda_1\overline{B}_{21}\rho F,_{\rho\rho}-\lambda_1(\overline{B}_{11}+\overline{B}_{21}-\overline{B}_{22})F,_{\rho}+\lambda_1\overline{B}_{12}F/\rho+\overline{D}_{11}(\psi,_{\rho}+\rho\psi,_{\rho\rho}) \\ -\overline{D}_{22}\psi/\rho-R_I[\rho\psi,_{\tau\tau}/(12\lambda_1^2)]+2\lambda_1^2\lambda_2\rho F+\lambda_1 F(\overline{W},_{\rho}+W,_{\rho}) \\ +\int_0^\rho \rho[Q-K_f W-K_n W^3+G_f(W,_{\rho\rho}+W,_{\rho}/\rho)-W,_{\tau\tau}]\,d\rho=0 \tag{2.63c}$$

In which, the dimensionless parameters are defined as

$$\begin{aligned}
&\rho = r/a,\ W = w/h,\ \overline{W} = \overline{w}/h,\ \psi = (a/h)\psi^*,\ F = F^*/(E_T h^2) \\
&\lambda_1 = a/h,\ \lambda_2 = H/a,\ Q = qa^4/(E_T h^4),\ \tau = \frac{t}{a^2}\sqrt{E_T h^3/\gamma} \\
&\overline{A}_{ij} = A^*_{ij} E_T h,\ \overline{B}_{ij} = B^*_{ij}/h,\ \overline{D}_{ij} = D^*_{ij}/(E_T h^3)\quad (i,j = 1,2) \\
&\overline{G} = G^*/(E_T h) \\
&K_f = k_f a^4/(E_T h^3),\ K_n = k_n a^4/(E_T h),\ G_f = g_f a^2/(E_T h^3)
\end{aligned} \tag{2.64}$$

Also the boundary conditions (2.55) can be rewritten in terms of W, ψ and F dimensionlessly,

$$\psi = 0 \quad and \quad N_\rho \ (= F/\rho) \quad is\ finite \quad at\ \rho = 0. \tag{2.65a}$$

and

$$W = 0,\ M_\rho = -K_b\,\psi,\ N_\rho = -K_i\,U \quad at\ \rho = 1 \tag{2.65b}$$

where

$$\begin{aligned}
&M_\rho = -\overline{B}_{11} F/\rho - \overline{B}_{21} F,_\rho + \overline{D}_{11}\psi,_\rho + \overline{D}_{12}\psi/\rho \\
&U = \overline{A}_{12} F + \overline{A}_{22}\rho F,_\rho + \overline{B}_{21}\rho\psi,_\rho + \overline{B}_{22}\psi + 2\lambda_2\rho W
\end{aligned} \tag{2.66}$$

In the above expressions, M_ρ, N_ρ, U, K_b and K_i are defined as

$$\begin{aligned}
&M_\rho = M_r a^2/(E_T h^4),\ N_\rho = N_r a/(E_T h^2),\ U = u/h \\
&K_b = k_b a/(E_T h^3),\ K_i = k_i a/(E_T h)
\end{aligned} \tag{2.67}$$

Equations (2.63a,b,c) constitute a system of equations governing the nonlinear analysis of axisymmetric deformation of a laminated shallow spherical shell composed of cylindrically orthotropic layers. The effects of transverse shear, rotatory inertia, geometric imperfection and elastic foundation are included. It is to be noted that, with appropriate assumptions, equations (2.63) can be simplified for some particular cases:

(1) Marguerre-type equations of motion for laminated shallow spherical shells

Neglecting the effects of transverse shear and rotatory inertia, the second of governing equations in this case becomes

$$\psi = -W,_{\rho} \tag{2.68}$$

Substituting the above equation into the other two governing equations, a set of two governing equations are obtained.

$$\begin{aligned}&\bar{A}_{22}(\rho F,_{\rho\rho} + F,_{\rho}) - \bar{A}_{11}F/\rho - \bar{B}_{21}\rho W,_{\rho\rho\rho}/\lambda_1 + (\bar{B}_{21} + \bar{B}_{22} - \bar{B}_{11}) W,_{\rho\rho}/\lambda_1 \\ &\quad + \bar{B}_{12}W,_{\rho}/(\lambda_1\rho) + 2\lambda_2\rho W,_{\rho} + \bar{W},_{\rho}W,_{\rho}/\lambda_1 + W,_{\rho}^2/(2\lambda_1) = 0\end{aligned} \tag{2.69a}$$

$$\begin{aligned}&-\lambda_1\bar{B}_{21}\rho F,_{\rho\rho} - \lambda_1(\bar{B}_{11} + \bar{B}_{21} - \bar{B}_{22}) F,_{\rho} + \lambda_1\bar{B}_{12}F/\rho - \bar{D}_{11}(W,_{\rho\rho} + \rho W,_{\rho\rho\rho}) \\ &\quad + \bar{D}_{22}W,\rho/\rho + 2\lambda_1^2\lambda_2\rho F + \lambda_1 F(\bar{W},_{\rho} + W,_{\rho}) \\ &\quad + \int_0^{\rho} \rho\,[Q - K_f W - K_n W^3 + G_f(W,_{\rho\rho} + W,_{\rho}/\rho) - W,_{\tau\tau}]\,d\rho = 0\end{aligned} \tag{2.69b}$$

which are the so-called Marguerre-type equations for the dynamic analysis of a laminated thin shallow spherical shell.

(2) Mindlin and von Karman-type equations of motion for laminated circular Plates

Assuming that the curvature of the shell in eqns. (2.63) is zero (i.e., 1/R = 0), the governing equations are simplified to those for laminated circular plates. If the effects of transverse shear and rotatory inertia are neglected, these equations become those for laminated thin circular plates in the sense of von Karman.

(3) Equations of motion for symmetric laminated shallow spherical shells

In the case the material coupling does not occur between transverse bending and inplane stretching, namely, $B_{ij} = 0$. The governing equations (2.63) are simplified as

$$\overline{A}_{22}(\rho F,_{\rho\rho} + F,_{\rho}) - \overline{A}_{11}F/\rho + 2\lambda_2 \rho W,_{\rho} + \overline{W},_{\rho} W,_{\rho}/\lambda_1 + W,_{\rho}^{2}/(2\lambda_1) = 0 \quad (2.70a)$$

$$T_S[\overline{D}_{11}(\psi,_{\rho} + \rho\psi,_{\rho\rho}) - \overline{D}_{22}\psi/\rho - R_I \rho \psi,_{\tau\tau}/(12\lambda_1^2)] - \lambda_1^2 \overline{G}\rho(\psi + W,_{\rho}) = 0 \quad (2.70b)$$

$$\begin{aligned} &\overline{D}_{11}(\psi,_{\rho} + \rho\psi,_{\rho\rho}) - \overline{D}_{22}\psi/\rho - R_I[\rho\psi,_{\tau\tau}/(12\lambda_1^2)] + 2\lambda_1^2\lambda_2 \rho F \\ &\quad + \lambda_1 F(\overline{W},_{\rho} + W,_{\rho}) + \int_0^{\rho} \rho\,[Q - K_f W - K_n W^3 + G_f(W,_{\rho\rho} + W,_{\rho}/\rho) - W,_{\tau\tau}]\,d\rho = 0 \end{aligned} \quad (2.70c)$$

When eqns. (2.69) and (2.70) are specified for orthotropic and isotropic shells, the resulting equations agree with those given in the earlier theories or classical theories.

2.6 SUMMARY

In this chapter, the constitutive relation for a moderately thick shallow spherical shell composed of cylindrically orthotropic layers are established based on the generalized Hooke's law and are characterized by four independent engineering elastic constants. The extensional stiffness, the bending-stretching stiffness and flexural stiffness of the shell are presented for unsymmetric cross-ply laminate, symmetric cross-ply laminate, orthotropic and isotropic shell, respectively. The transverse shear stiffness is given by employing a parabolic shear stress distribution across the shell thickness and the principle of complementary energy.

The governing equations and corresponding boundary conditions are derived by the dynamic principle of virtual work and expressed in terms of a transverse displacement, a rotation of a normal to mid-surface and a stress function. The effects of transverse shear, rotatory inertia, geometric imperfection or initial deflection and elastic foundations are included. For specific cases, the governing equations are simplified to those given in the earlier theories. The governing equations agree with the dynamic Marguerre-type equations by neglecting the effects of transverse shear and rotatory inertia; become the dynamic Mindlin-von Karman-type equations for laminated circular plates by assuming zero curvature of the shell; reduce to those proposed in classical theories of orthotropic and isotropic shells; and are further simplified to those for static analysis by deleting the time-dependent terms. It is observed that the present governing equations are more general and accurate for studying the elastic behaviour of laminated shallow spherical shells than the existing theories.

CHAPTER 3

METHOD OF SOLUTION

3.1 INTRODUCTION

The equations derived in Chapter 2 constitute a system of equations for nonlinear analysis of axisymmetric deformation of a laminated shallow spherical shell composed of cylindrically (or polar) orthotropic layers. The effects of transverse shear deformation, rotatory inertia, geometric imperfection and elastic foundations are included. In some special cases, such as, neglecting the effects of transverse shear and rotatory inertia, assuming the zero curvature of the shell, and considering no bending-stretching coupling, etc., these equations may be reduced to the simplifying forms. An exact solution to this system of the nonlinear differential equations is in general very difficult to obtain. Therefore, in this chapter an approximate solution of the Fourier-Bessel series is sought in the analysis. And the Galerkin method is used to reduce the governing equations of motion to a set of nonlinear ordinary differential equations and these equations for time functions are expanded into Fourier cosine series in the time by the method of harmonic balance. The resulting equations are solved by the Newton-Raphson method.

The multi-mode solution has the advantage that an infinite set of nonlinear equations can be truncated to obtain any desired degree of accuracy, over the single-mode solution. In engineering, further, several terms taken in the truncated series may yield sufficient accuracy provided that the terms considered are close to the actual shape of vibration or the deformed configuration of the shell. Certainly, when an infinite series solution satisfying the governing equations and boundary conditions is presented, the solution can be said to be exact.

3.2 GALERKIN METHOD

A number of approximate methods have been developed by using the variational principle, numerical analysis and other mathematical theories. Those used extensively in solid mechanics are Double Fourier series by expressing the dependent variables and the loading function as double Fourier series; generalized double Fourier series by expressing these variables in terms of any orthogonal sets of functions; Ritz method (Ritz, 1908) by applying the principle of minimum potential energy and assuming that the desired extremal of a given problem can be approximated by linear combinations of suitably chosen functions; perturbation method or small parameter method (Poincare, 1892; Nowinski and Ismail, 1965) by generating the perturbation in the neighbourhood of the solution of the linearized equations such that the known properties of the linear system can be utilized for the solution to the perturbed system; and Galerkin's method (Galerkin,

1915) by minimizing the errors produced by the chosen spatial functions.

In this work, the Galerkin method is used to obtain an approximate solution. It is briefly reviewed as follows:

The Galerkin method which has been widely applied to both static and dynamic problems in the area of solid mechanics is the method of an approximate solution of the boundary-value problems. The idea of the method is minimization of error by orthogonalizing with respect to a set of given functions. Consider a system of differential equations

$$L_i\,(u, v, w) = 0 \qquad i = 1, 2, 3 \tag{3.1}$$

subjected to appropriate boundary conditions. In these equations L_i are nonlinear (or linear) differential operators. These equations physically represent the conditions of dynamic (or static) equilibrium of a differential element $d\Omega$ cut out from a structure under external forces. Let arbitrary virtual displacements δu, δv and δw be applied to the structural system. These displacements, however, are continuous function of x_i (i = 1, 2, 3) and t and satisfy the geometrical boundary conditions. The virtual work done on the element by these virtual displacements is

$$\{L_1\,(u, v, w)\,\delta u + L_2\,(u, v, w)\,\delta v + L_3\,(u, v, w)\,\delta w\}\,d\Omega \tag{3.2}$$

By the principle of virtual work the following is obtained

$$\begin{aligned}\iiint_V \{L_1\,(u, v, w)\,\delta u + L_2\,(u, v, w)\,\delta v \\ + L_3\,(u, v, w)\,\delta w\}\,d\Omega = 0\end{aligned} \tag{3.3}$$

in which the integration is carried out over the entire structural volume Ω.

An approximate solution of the problem is sought in the form

$$u = \sum_{k}^{\infty}\sum_{m}^{\infty}\sum_{n}^{\infty} A_{kmn}(t)\, a_{kmn}(x_1, x_2, x_3)$$
$$v = \sum_{k}^{\infty}\sum_{m}^{\infty}\sum_{n}^{\infty} B_{kmn}(t)\, b_{kmn}(x_1, x_2, x_3) \tag{3.4}$$
$$w = \sum_{k}^{\infty}\sum_{m}^{\infty}\sum_{n}^{\infty} C_{kmn}(t)\, c_{kmn}(x_1, x_2, x_3)$$

in which A's, B's, C's are undetermined variable coefficients of time and a's, b's, c's are suitably chosen spatial functions satisfying the prescribed boundary conditions and capable of representing the mode of deformation. The assumed solution (3.4) is not required to satisfy equations (3.1) but the functions a,b and c should have at least the same order of derivatives as those in these differential equations. The virtual displacements are taken to be of the form

$$\delta u = \sum_{k}^{\infty}\sum_{m}^{\infty}\sum_{n}^{\infty} a_{kmn}(x_1, x_2, x_3)\, \delta A_{kmn}(t)$$
$$\delta v = \sum_{k}^{\infty}\sum_{m}^{\infty}\sum_{n}^{\infty} b_{kmn}(x_1, x_2, x_3)\, \delta B_{kmn}(t) \tag{3.5}$$
$$\delta w = \sum_{k}^{\infty}\sum_{m}^{\infty}\sum_{n}^{\infty} c_{kmn}(x_1, x_2, x_3)\, \delta C_{kmn}(t)$$

and substituted into the variational equation (3.3). Since A's, B's and C's can be varied independently, the only way that the resulting variational equation can be zero is that the coefficients of δA_{kmn},δB_{kmn}, and δC_{kmn} must vanish identically in the domain, namely

$$\iiint_{\Omega} L_1(u, v, w)\, a_{mnk}(x_1, x_2, x_3)\, d\Omega = 0$$
$$\iiint_{\Omega} L_2(u, v, w)\, b_{mnk}(x_1, x_2, x_3)\, d\Omega = 0 \tag{3.6}$$
$$\iiint_{\Omega} L_3(u, v, w)\, c_{mnk}(x_1, x_2, x_3)\, d\Omega = 0$$

which provide the same number of equations for the number of A_{mnk}, B_{mnk}

and C_{mnk} taken. Introducing the approximate solution (3.4) into equations (3.6) and performing integration will lead either to a system of ordinary differential equations for $A_{mnk}(t)$, $B_{mnk}(t)$ and $C_{mnk}(t)$ in the dynamic problems or to a system of algebraic equations for constant coefficients A_{mnk}, B_{mnk} and C_{mnk} in the static problems. Unlike the Ritz method the Galerkin method does not require the formulation of an energy principle. This method yields good approximation only after taking a few terms for u, v, w in expressions (3.4). Evidently the accuracy of this procedure is very sensitive to the choice of the assumed solution.

3.3 FOURIER-BESSEL SERIES SOLUTION

3.3.1 Bessel Function

Bessel functions, like many other branches of mathematics, had their origin in the solution of physical problems. In 1824, F. W. Bessel studied a problem associated with elliptic planetary motion and made an attempt to deal with it in a systematic way. Thus, the terminology "Bessel Functions" were proposed.

Consider a differential equation

$$\frac{d^2y}{dz^2} + \frac{1}{z}\frac{dy}{dz} + \left(1 - \frac{n^2}{z^2}\right) y = 0 \tag{3.7}$$

which is known as Bessel's equation for functions of order n. It is a linear differential equation of the second order having variable coefficients, namely $1/z$ and $(1-n^2/z^2)$. By the theory of linear differential equations, it has two distinct or linearly independent solutions, i.e., one is not a constant multiple of the other. If we take $J_n(z)$ as the first solution to equation (3.7), we obtain Bessel's definition of the function which bears his name. $J_n(z)$ is sometimes called a Bessel coefficient, but it is regarded more generally as a Bessel function of the first kind of order n. It can be shown that $J_n(z)$ is expressed in the form (Mclachlom, 1955)

$$J_n(z) = \left(\frac{1}{2}z\right)^n \left\{ \frac{1}{n!} - \frac{(z/2)^2}{1!\,(n+1)!} + \frac{(z/2)^4}{2!\,(n+2)!} - \frac{(z/2)^6}{3!\,(n+3)!} + \dots \right\}$$
$$= \sum_{r=0}^{\infty} (-1)^r \frac{(z/2)^{n+2r}}{r!\,(n+r)!} \tag{3.8}$$

or

$$J_n(z) = \frac{1}{2\pi}\int_0^{2\pi} \cos(n\theta - z\sin\theta)\, d\theta \tag{3.9}$$

Series (3.8) and its derivatives are absolutely convergent for all finite values of z real or complex, and uniformly convergent in any boundary region of the z-plane, namely term by term differentiation and integration is permissible. In virtue of uniform convergence, $J_n(z)$, $J'_n(z)$ ..., the functions represented by the series and its derivatives, are continuous functions of z in the finite part of the z-plane. The function represented by the integrated series are continuous also.

Furthermore, we define the first solution to the differential equation

$$\frac{d^2y}{dz^2} + \frac{1}{z}\frac{dy}{dz} - (1 + \frac{n^2}{z^2})\, y = 0 \tag{3.10}$$

as a modified Bessel function of the first kind of order n, denoted $I_n(z)$. Similarly, it can be show that $I_n(z)$ is of the form

$$\begin{aligned} I_n(z) &= \frac{z^n}{2^n\Gamma(n+1)}\left\{1 + \frac{z^2}{2(2n+2)} + \frac{z^4}{2\cdot 4(2n+2)(2n+4)} + \ldots\right\} \\ &= \sum_{r=0}^{\infty} \frac{(z/2)^{n+2r}}{r!\,\Gamma(n+r+1)} \end{aligned} \tag{3.11}$$

or

$$I_n(z) = \frac{1}{2\pi}\int_0^{2\pi} e^{z\cos\theta}\cos n\theta\, d\theta \tag{3.12}$$

The properties on convergence and continuity of $J_n(z)$ apply to $I_n(z)$, namely the series (3.11) is absolutely and uniformly convergent in the finite part of the z-plane.

Some features of the Bessel function and modified Bessel function of the first kind used in this work are presented in Appendix A.

3.3.2 Solution

An approximate multi-mode solution to the system of equations (2.63) with the corresponding boundary conditions is assumed in the form of Fourier-Bessel series.

$$W(\rho,\tau) = \sum_{m=1}^{\infty} W_m(\tau)\, X_m(\rho)$$
$$\psi(\rho,\tau) = \sum_{m=1}^{\infty} R_m(\tau)\, Y_m(\rho) \tag{3.13}$$
$$F(\rho,\tau) = \sum_{r=1}^{\infty} S_r(\tau)\, Z_r(\rho)$$

To simplify the theoretical analysis, the geometric imperfection is also expanded into a Fourier-Bessel series as the transverse displacement although the shape of the geometric imperfection is random in practical structures.

$$\overline{W}(\rho) = \sum_{m=1}^{\infty} \overline{W}_m X_m(\rho) \tag{3.14}$$

In the above expressions, $\overline{W}_m$ are the constant coefficients, $W_m(\tau)$, $R_m(\tau)$ and $S_r(\tau)$ are time dependent coefficients to be determined and functions X_m, Y_m and Z_r are the combination of Bessel functions and modified Bessel functions given by

$$\begin{aligned} X_m(\rho) &= J_0(\alpha_m\rho) - I_0(\alpha_m\rho)J_0(\alpha_m)\,/\,I_0(\alpha_m) \\ Y_m(\rho) &= J_1(\alpha_m\rho) + I_1(\alpha_m\rho)J_0(\alpha_m)\,/\,I_0(\alpha_m) \\ Z_r(\rho) &= \rho J_0(\beta_r\rho) \end{aligned} \tag{3.15}$$

where J_0, J_1, I_0 and I_1 are the Bessel functions and modified Bessel functions of the first kind of order zero and order one. The condition W=0 at the edge, i.e., the first of eqns.(2.55b), and the finite conditions at the apex, i.e., eqns.(2.55a), are automatically satisfied by the assumed solution (3.13). The constants α_m and β_r in expressions (3.15) are determined by the last two of boundary conditions (2.55b) respectively.

(1) For a symmetrically laminated shallow spherical shell

In this case, $B_{ij} = 0$, the last two of edge boundary conditions (2.55b) are of the form:

$$M_\rho = -K_b \psi$$
$$N_\rho = -K_1 U \tag{3.16}$$

Using eqns. (2.66), the conditions (3.16) are rewritten as

$$\overline{D}_{11} \psi,_\rho + \overline{D}_{12} \psi / \rho + K_b \psi = 0$$
$$F/\rho + K_1 [\rho (\overline{A}_{12} F + \overline{A}_{22} \rho F,_\rho) + 2 \lambda_2 \rho w] = 0 \tag{3.17}$$

Substituting eqns. (3.13) into eqns. (3.17) and considering the values of W and ρ at the edge, the above equations become

$$\alpha_m \overline{D}_{11} [J_1'(\alpha_m) + I_1'(\alpha_m) J_0(\alpha_m) / I_0(\alpha_m)]$$
$$+ (\overline{D}_{12} + K_b) [J_1(\alpha_m) + I_1(\alpha_m) J_0(\alpha_m) / I_0(\alpha_m)] = 0 \tag{3.18}$$
$$(1 + K_1 \overline{A}_{12}) J_0(\beta_r) + K_1 \overline{A}_{22} [J_0(\beta_r) + \beta_r J_0'(\beta_r)] = 0$$

These equations are used for determining the coefficients α_m and β_r. Typical sets of values of these coefficients are given in Tables 3.1 and 3.2, respectively. The elastic constants of glass-epoxy (GL), boron-epoxy (BO), graphite-epoxy(GR) composite materials and isotropic material (ISO) used in this work are presented in Table 3.5.

(2) For an unsymmetrically laminated shallow spherical shell

In this work, the edge movable and rotationally restrained is considered for an unsymmetrically laminated shallow spherical shell. Thus, the last two of the edge boundary conditions (2.55b) are

$$N_\rho = 0$$
$$M_\rho = -K_b \psi \tag{3.19}$$

Similarly, introducing (3.13) into (3.19), we obtain

Table 3.1. Values of α_k in Eqns. (3.18)

B.C.	Material*	N	k=1	k=2	k=3
$K_b=0$	ISO		2.22151952	5.45160570	8.61139102
	GL BO GR	3	2.19856358 2.17409864 2.18432727	5.44445294 5.43713453 5.44015689	8.60711666 8.60277098 8.60456229
	GL BO GR	5	2.17837067 2.13993080 2.13840552	5.43839035 5.42741614 5.42699551	8.60351473 8.59704288 8.59679605
$K_b=1$	ISO		2.97361324	5.95335276	9.00131998
	GL BO GR	3	2.97287258 2.93546877 2.90560325	5.95242671 5.90741875 5.87383069	9.00038768 8.95624565 8.92474292
	GL BO GR	5	2.92092025 2.76153701 2.66983863	5.89080663 5.73674906 5.66712084	8.94051571 8.80767932 8.75449430
$K_b=2$	ISO		3.06978351	6.08634237	9.14610654
	GL BO GR	3	3.06964366 3.04557810 3.02506134	6.08612912 6.05035368 6.02122532	9.14585622 9.10470121 9.07242994
	GL BO GR	5	3.03570310 2.91896188 2.84083561	6.03618011 5.88860712 5.80745772	9.08886227 8.93845508 8.86586736
$K_b=5$	ISO		3.14114791	6.20354820	9.29345134
	GL BO GR	3	3.14117734 3.12974933 3.11954481	6.20360018 6.18365227 6.16623134	9.29352111 9.26704000 9.24439299
	GL BO GR	5	3.12488270 3.06307852 3.01557386	6.17529845 6.07619251 6.00816570	9.25612465 9.13425386 9.05831094
$K_b=\infty$			3.19622061	6.30643704	9.43949914

*The elastic constants of ISO, GL, BO and GR are given in Table 3.5.

Table 3.2. Values of β_k in Eqns. (3.18)

B.C.	Material	N	k=1	k=2	k=3
K_i=0			2.40482555	5.52007809	8.65372792
K_i=1	ISO		1.51935696	4.23172426	7.24963172
	GL	3	1.81599472	4.49277964	7.43261039
	BO	3	2.12760621	4.93652344	7.84428444
	GR	3	2.21464220	5.10259619	8.04352475
	GL	5	1.79910946	4.47446504	7.41863895
	BO	5	2.10770703	4.90129631	7.80554831
	GR	5	2.19857760	5.07050009	8.00283299
K_i=2	ISO		1.34557615	4.12495713	7.18305239
	GL	3	1.60486281	4.29522576	7.29123675
	BO	3	1.94887462	4.65556975	7.56606677
	GR	3	2.07165337	4.84007249	7.74100662
	GL	5	1.59127027	4.28457734	7.28414480
	BO	5	1.92339347	4.62160123	7.53674775
	GR	5	2.04793590	4.80159750	7.70218397
K_i=5	ISO		1.20484047	4.05616663	7.14205397
	GL	3	1.39265282	4.15126138	7.19909927
	BO	3	1.67685843	4.35545595	7.33229144
	GR	3	1.81121728	4.48754777	7.42859936
	GL	5	1.38673080	4.14785295	7.19700760
	BO	5	1.65340037	4.33509753	7.31823044
	GR	5	1.78361415	4.45808475	7.40630557
K_i=∞	ISO		1.08725429	4.00845193	7.11434701
	GL	3	1.17757340	4.04437232	7.13515350
	BO	3	1.22832799	4.06670280	7.14824868
	GR	3	1.23087936	4.06786886	7.14893604
	GL	5	1.18374410	4.04700118	7.13668850
	BO	5	1.23198514	4.06837554	7.14923482
	GR	5	1.23450466	4.06953302	7.14991765

$$F/\rho = 0$$
$$-\overline{B}_{11}\overline{F}/\rho - \overline{B}_{21}\overline{F}_{,\rho} + \overline{D}_{11}\overline{\Psi}_{,\rho} + \overline{D}_{12}\overline{\Psi}/\rho + K_b\psi = 0 \tag{3.20}$$

The constants β_r is determined by the first of (3.20) and as being the coupling boundary conditions, α_m is approximately taken to be the eigenvalue of the formula given by

$$\alpha_m\overline{D}_{11}\,[\,J_1'(\alpha_m) + I_1'(\alpha_m)\,J_0(\alpha_m)\,/\,I_0(\alpha_m)\,]$$
$$+\,(\overline{D}_{12}+K_b)\,\,[\,J_1(\alpha_m) + I_1(\alpha_m)\,J_0(\alpha_m)\,/\,I_0(\alpha_m)\,] = 0 \tag{3.21}$$

Some values of these coefficients α_m, β_r are listed in Tables 3.3 and 3.4, respectively.

To fulfil the rotational edge constraint, the following procedure is adopted (Chia, 1985). The moment at the edge of the shell is replaced by an equivalent lateral pressure near the edge (Fig. 3.1) denoted by Q_e, and this pressure is represented by a sine series. If the value of d shown in the figure approaches to zero, the Q_e may be expressed as

$$Q_e = 2\pi\sum_{i=1}^{\infty} -(-1)^i M_\rho|_{\rho=1}\sin(i\pi\rho) \tag{3.22}$$

The edge moment in this equation which can be evaluated by substituting eqns. (3.13) and (3.19) into (3.22) is written as

$$M_\rho|_{\rho=1} = -K_b\psi|_{\rho=1} = -K_b\sum_{m=1}^{\infty} R_m(\tau)\,Y_m(\alpha_m\rho)|_{\rho=1}$$
$$= -K_b\sum_{m=1}^{\infty} R_m(\tau)\,Y_m(\alpha_m) \tag{3.23}$$

Thus eqn. (3.22) is rewritten as

$$Q_e = 2\pi\sum_{i=1}^{\infty}\sum_{m=1}^{\infty}(-1)^i K_b R_m(\tau)\,Y_m(\alpha_m)\sin(i\pi\rho) \tag{3.24}$$

The total lateral load now is

Table 3.3. Values of α_k in Eqn. (3.21)

B.C.	Material	N	k=1	k=2	k=3
K_b=0	ISO		2.22151952	5.45160570	8.61139102
	GL BO GR	2	2.15897136 2.12495757 2.12299479	5.43276118 5.42333452 5.42280729	8.60018731 8.59465148 8.59434317
	GL BO GR	4	2.15897136 2.12495757 2.12299479	5.43276118 5.42333452 5.42280729	8.60018731 8.59465148 8.59434317
K_b=1	ISO		2.97361324	5.95335276	9.00131998
	GL BO GR	2	2.89227033 2.77160734 2.70634982	5.85946759 5.74514781 5.69343508	8.91163127 8.81436164 8.77414226
	GL BO GR	4	2.85705660 2.62730495 2.52338163	5.82329914 5.63860119 5.57744269	8.87952868 8.73378856 8.69132877
K_b=2	ISO		3.06978351	6.08634237	9.14610654
	GL BO GR	2	3.01644477 2.92787862 2.87423252	6.00935395 5.89869168 5.84062857	9.05958676 8.94794515 8.89474919
	GL BO GR	4	2.99135032 2.80312694 2.69928748	5.97595122 5.77249614 5.68820617	9.02438106 8.83654145 8.77019540
K_b=5	ISO		3.14114791	6.20354820	9.29345134
	GL BO GR	2	3.11540490 3.06845927 3.03699459	6.15926748 6.08432661 6.03801743	9.23546396 9.14374152 9.09090083
	GL BO GR	4	3.10250906 2.99128296 2.91562746	6.13795211 5.97586385 5.88488186	9.20856869 9.02429075 8.93497666
$K_b=\infty$			3.19622061	6.30643704	9.43949914

Table 3.4. Values of β_k in Eqns. (3.20)

B.C.	Material	N	k=1	k=2	k=3
K_i=0			2.40482555	5.52007809	8.65372792

Table 3.5. Numerical values of elastic constants

Material	E_L/E_T	υ_{LT}	G_{Lz}/E_T	G_{Tz}/E_T
Isotropic (ISO)	1	0.30	0.385	0.385
Glass-epoxy (GL)	3	0.25	0.5	0.333
Boron-epoxy (BO)	10	0.22	0.333	0.2
Graphite-epoxy (GR)	16	0.30	0.22	0.15

$$Q_T = Q + Q_e \tag{3.25}$$

The load in governing equations is to be replaced by Q_T.

With the equivalent lateral pressure and the values of α_m and β_r given by eqns. (3.17) and (3.18) or (3.20) and (3.21), all boundary conditions are satisfied by the assumed solution (3.13).

3.4 EQUATIONS FOR TIME-DEPENDENT COEFFICIENTS

3.4.1 Nonlinear Ordinary Differential Equations

Introducing the solution (3.13) in governing eqn. (2.63) and making use of the Galerkin method by multiplying the first by $Z_s(\rho)$, the second by $Y_n(\rho)$ and the third by $X_n(\rho)$, then integrating with respect to ρ from 0 to 1 and θ

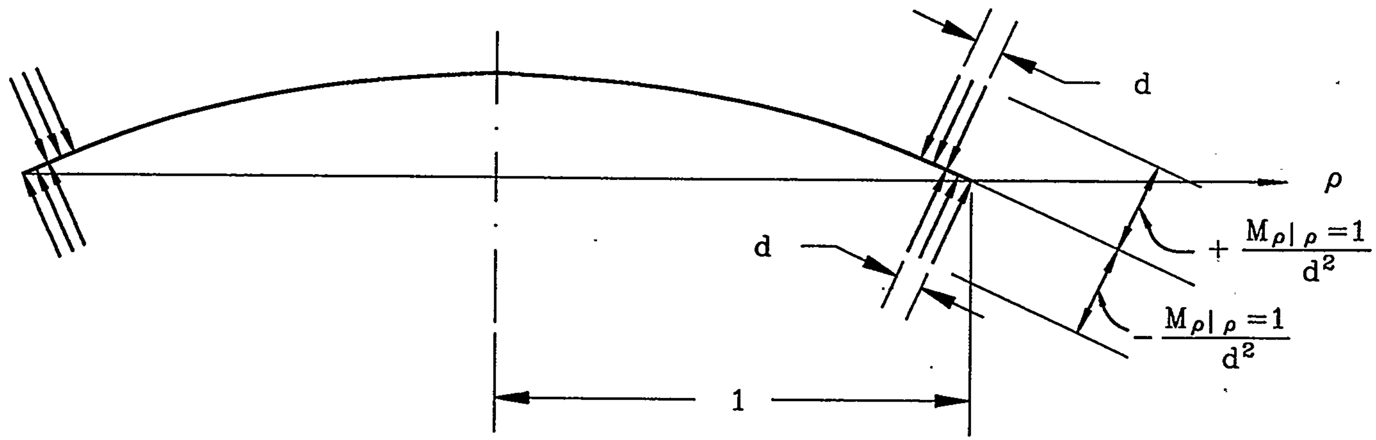

Figure 3.1: Equivalent pressure distribution ($d \rightarrow 0$) for edge moment

from 0 to 2π, the following three sets of nonlinear ordinary differential equations for $W_m(\tau)$, $R_m(\tau)$ and $S_r(\tau)$ are obtained:

$$
\begin{aligned}
&a_{1s}^{r} S_r + a_{2s}^{m} R_m + (a_{3s}^{m} + a_{4s}^{m}) W_m + a_{5s}^{mk} W_M W_k = 0 \\
&a_{6n}^{r} S_r + a_{7n}^{m} R_m + a_{8n}^{m} W_m + a_{9n}^{m} R_{m,\tau\tau} = 0 \qquad (3.26) \\
&(a_{10n}^{r} + a_{11n}^{r} + a_{12n}^{r}) S_r + (a_{13n}^{m} + a_{14n}^{m}) R_m + a_{15n}^{mr} W_m S_r + a_{16n}^{m} W_m + a_{17n}^{mkj} W_m W_k W_j \\
&\qquad + Q_n + a_{18n}^{m} R_{m,\tau\tau} + a_{19n}^{m} W_{m,\tau\tau} = 0
\end{aligned}
$$

where a_1 to a_{19} and Q_n are constant coefficients presented in Appendix B. In special cases, some coefficients disappear:

(1) For symmetrically laminated shells, $a_{10}=a_{14}=0$;

(2) For neglecting the geometric imperfection, $a_4=a_{12}=0$;

(3) For excluding the elastic foundations, $a_{16}=a_{17}=0$;

(4) For circular plates, $a_3=a_{11}=0$.

To simplify calculations, functions $S_r(\tau)$ can be expressed in terms of linear combinations of $R_m(\tau)$, $W_m(\tau)$ and $W_m(\tau)W_k(\tau)$ from the first of eqns. (3.26)

$$
S_r = -[a_{1s}^{r}]^{-1} a_{2s}^{m} R_m - [a_{1s}^{r}]^{-1} (a_{3s}^{m} + a_{4s}^{m}) W_m - [a_{1s}^{r}]^{-1} a_{5s}^{mk} W_m W_k \qquad (3.27)
$$

Substituting (3.27) into the last two of (3.26), the resulting equations for $W_m(\tau)$ and $R_m(\tau)$ are

$$
\begin{aligned}
&a_{20n}^{m} R_m + a_{21n}^{m} W_m + a_{22n}^{mk} W_m W_k + a_{9n}^{m} R_{m,\tau\tau} = 0 \\
&a_{23n}^{m} R_m + a_{24n}^{mk} W_m R_k + a_{25n}^{m} W_m + a_{26n}^{mk} W_m W_k + a_{27n}^{mkj} W_m W_k W_j \qquad (3.28) \\
&\qquad + Q_n + a_{18n}^{m} R_{m,\tau\tau} + a_{19n}^{m} W_{m,\tau\tau} = 0
\end{aligned}
$$

in which a_{20} to a_{27} are given in the Appendix B.

Making use of the properties of the Bessel-function and the Simpson integration method, all the coefficients a_1 to a_{27} can be calculated for a given set of shell parameters.

3.4.2 Resulting Equations for Nonlinear Free Vibration

In the case of the undamped nonlinear free vibration (Q_n=0), the method of harmonic balance is used to reduce eqns. (3.28) to a set of algebraic equations. This is a common method for obtaining a periodic solution of a nonlinear differential equations for time functions. The procedure has been fully explained by Hayashi (1964) or elsewhere. The idea is that the periodic solution is first expanded into M terms of a Fourier series with unknown coefficients. The assumed periodic solution is then inserted into the time equations. Equating the coefficient of each of harmonics to zero, a system of algebraic equations is obtained. In assuming the harmonic expansion, only terms of the harmonic frequency and a few additional terms of different frequencies (usually subharmonic or higher-harmonic frequencies) are considered because of their prime importance. Terms of frequency other than those are certain to be present also, but they may tolerably be omitted in most cases.

In this work, the unknowns $W_m(\tau)$ and $R_m(\tau)$ are expanded as Fourier cosine series in τ,

$$W_m(\tau)=\sum_{k=0}^{\infty} W_m^{(k)} \cos k\omega\tau$$
$$R_m(\tau)=\sum_{k=0}^{\infty} R_m^{(k)} \cos k\omega\tau \qquad (3.29)$$

where $W_m^{(k)}$ and $R_m^{(k)}$ are constant Fourier coefficients for the kth harmonic amplitude of $W_m(\tau)$ and $R_m(\tau)$ respectively, and in which ω is the dimensionless vibrating frequency related to the circular frequency ω^* by

$$(\omega,\ \omega_o)=a^2\sqrt{\gamma/(E_T h^3)}\ (\omega^*,\ \omega_o^*) \qquad (3.30)$$

in which the dimensional and dimensionless fundamental linear frequencies ω_0^* and ω_0 both neglecting the effects of transverse shear and rotatory inertia will be used for the presentation of numerical results.

The expressions (3.29) are inserted into equations (3.28) and each term is converted into the first power of cosine functions, a system of simultaneous nonlinear algebraic equations is obtained.

3.4.3 Resulting Equations for Static Response

In the case of buckling and postbuckling of laminated shallow spherical shells or static large deflections of laminated circular plates, the time parameter τ is treated as a constant. Deleting all inertia terms in (3.26), the unknowns S_r and R_m are expressed in terms of W_m and $W_m W_k$ from the first two of (3.26) as

$$S_r = b_{1r}^{m} W_m + b_{2r}^{mk} W_m W_k$$
$$R_j = b_{3j}^{m} W_m + b_{4j}^{mk} W_m W_k \tag{3.31}$$

where b's are constant coefficients presented in Appendix B. Substituting eqns. (3.31) into the last of eqns. (3.26), the relation between the load and the maximum transverse displacement is

$$c_{1n}^{m} W_m + c_{2n}^{mk} W_m W_k + c_{3n}^{mkj} W_m W_k W_j + Q_n = 0 \tag{3.32}$$

with the constants c's given in Appendix B.

3.5 NUMERICAL PROCEDURE

3.5.1 Newton-Raphson Method

Simultaneous nonlinear equations are in general much more difficult to be solved than a single equation. The iterations are involved and convergence is frequently very slow. Many really clever methods have been devised for speeding up a solution of these equations. The Newton-raphson method is widely accepted as one of the best methods for solving nonlinear algebraic equations. The excellent results that are generally obtained with the method and the simple computational routine justify its popularity. The method applies as well for complex roots as for real roots, and the iterations converge rapidly provided the initial estimate for roots is close enough. To briefly introduce this method (Hartee, 1958), consider a single nonlinear equation The algorithm for the Newton-raphson method is obtained from a Taylor-series

$$f(x) = 0 \tag{3.33}$$

expansion of f(x) about an approximation to a root. Let $x=x_0$ be an estimate to a root α. Then

$$f(x) = f(x_o+h) = f(x_o)+hf'(x_o)+\frac{h^2}{2!}f''(\xi) \tag{3.34}$$

where ξ is on the range x_0 to x_0+h. If x_0+h is set equal to α then

$$f(\alpha) = 0 = f(x_o)+hf'(x_o)+\frac{h^2}{2!}f''(\xi) \tag{3.35}$$

An estimate to the value of h can be made by using only the first two terms in eqn. (3.35). Let this estimate be designated by h_1

$$h_1 = -\frac{f(x_o)}{f'(x_o)} \tag{3.36}$$

The basic formula for the iterations in the Newton-Raphson method is obtained by adding h_1 to the estimate x_0. This new approximation is designated by x_1

$$x_1 = x_o+h_1 = x_o-\frac{f(x_o)}{f'(x_o)} \tag{3.37}$$

The (k+1)th approximation to the root is obtained by using the kth approximation in the right-hand side of the following

$$x_{k+1} = x_k-\frac{f(x_k)}{f'(x_k)} \tag{3.38}$$

The iteration defined by equation (3.38) usually gives fast convergence to a root of f(x)=0 provided the error in the initial approximation x_0 is small. Good results can even be obtained when the initial approximation is not close to a root, provided the slope on the interval between $x=x_0$ and $x=\alpha$ is not small. These statements are verified by the expression for the error in the first iterate

$$E(x_1) = \alpha - x_1 = \frac{f''(\xi)}{2f'(x_o)}(\alpha - x_o)^2 + o(\alpha - x_o)^3 \tag{3.39}$$

Equation (3.39) says the error in the first approximation from eqn. (3.38) (k=0) is $o(h^2)$, where $h=\alpha-x_0$. For this reason the method is said to be quadratically convergent and is a second-order method.

Figure 3.2 shows the geometric interpretation for the Newton-Raphson method when the root at α is real.

The Newton-Raphson method can obviously be applied to a system of n simultaneous nonlinear equations in n unknowns. At each step of the iteration, n^2 partial derivative functions and n functions should be evaluated. This represents a considerable amount of computational effort. However, the Newton-Raphson method is very fast and quite convenient for polynomials. In this work all simultaneous nonlinear equations are composed of polynomials of the third degree and this method used for solving these equations is suitable.

3.5.2 Numerical Procedure for Solving Simultaneous Nonlinear Equations

The numerical procedure for obtaining by solving the set of nonlinear algebraic equations (3.28) or (3.32) is briefly described. For nonlinear free

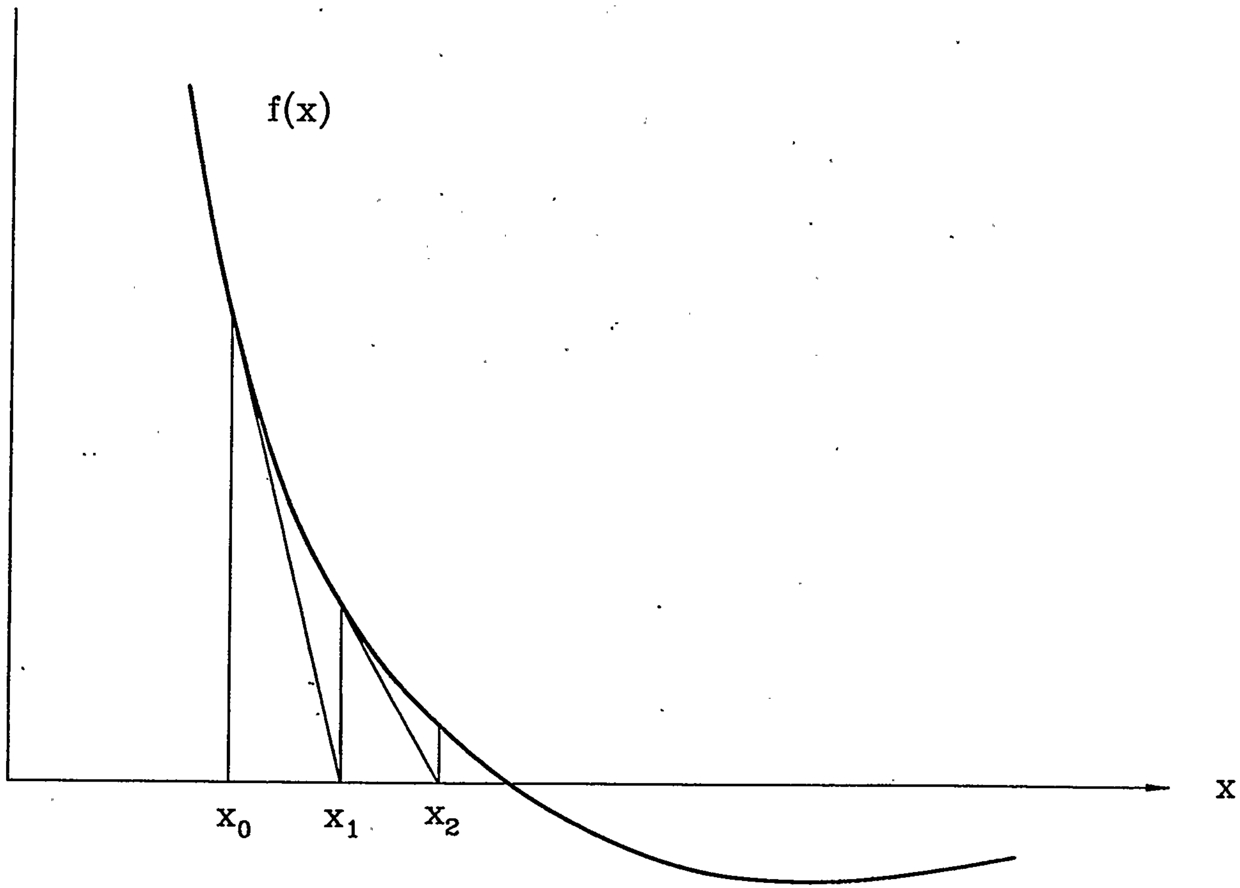

Figure 3.2: Newton–Raphson method

vibration, the number of nonlinear algebraic equations is equal to the product of the number of equations in eqns. (3.28) and the number of terms in the Fourier cosine expansion for each $W_m(\tau)$ and $R_m(\tau)$. By prescribing one of the unknowns among $W_m^{(k)}$, $R_m^{(k)}$ and ω, the resulting nonlinear algebraic equations can be solved by the Newton-Raphson method provided that a good initial estimate is given. By successively solving these nonlinear equations with a prescribed unknown and an initial approximation, the amplitude-frequency response curve can be traced. The prescribed unknown is chosen as one of the harmonic amplitudes and ω which has shown the greatest change in the last step of a solution while the initial estimate is approximated by the previous solution or an extrapolation from several of previous successive results. Usually, the prescribed value is one of the harmonic amplitudes as they change faster than ω, especially when the amplitude of vibration is small. However, the difference of the prescribed unknown and the corresponding unknown in the previous solution should be kept small to ensure proper convergence. Once a solution in terms of harmonic amplitudes and frequency ω is computed, the maximum amplitude W_{max} at the apex can then be determined from a plot of the dimensionless transverse displacement W at ρ=0 vs the dimensionless time τ over a period of 2π. Actually, the location of the maximum amplitude on the τ-axis can be easily pinpointed by inspection because the first few harmonic terms usually bear the greater contributions than higher ones.

For the static case, a similar procedure is implemented. The number of nonlinear algebraic equations is equal to the number of eqns. (3.32). The prescribed unknown is taken one of the unknowns W_m and Q. In general, the prescribed value is one of W_m.

3.5.3 Program NALSSS

The computer program NALSSS (Nonlinear Analysis of Laminated Shallow Spherical Shells) is designed to obtain the numerical results for a set of given shell parameters. This program is easily implemented only by inputting basic simple information. The program NALSSS is composed of the following:

(1) Processing the essential input data;

(2) Calculating the elastic coefficients of composite materials;

(3) Determining the eigenvalues of Bessel functions by boundary conditions;

(4) Forming the matrix for a set of nonlinear algebraic equations;

(5) Solving the nonlinear equations by the Newton-Raphson method;

(6) Giving the results of buckling load, postbuckling, static large deflection or amplitude-frequency response.

The flow chart of this program is listed in Fig. 3.3 and the copy of the program is given in Appendix C for reference.

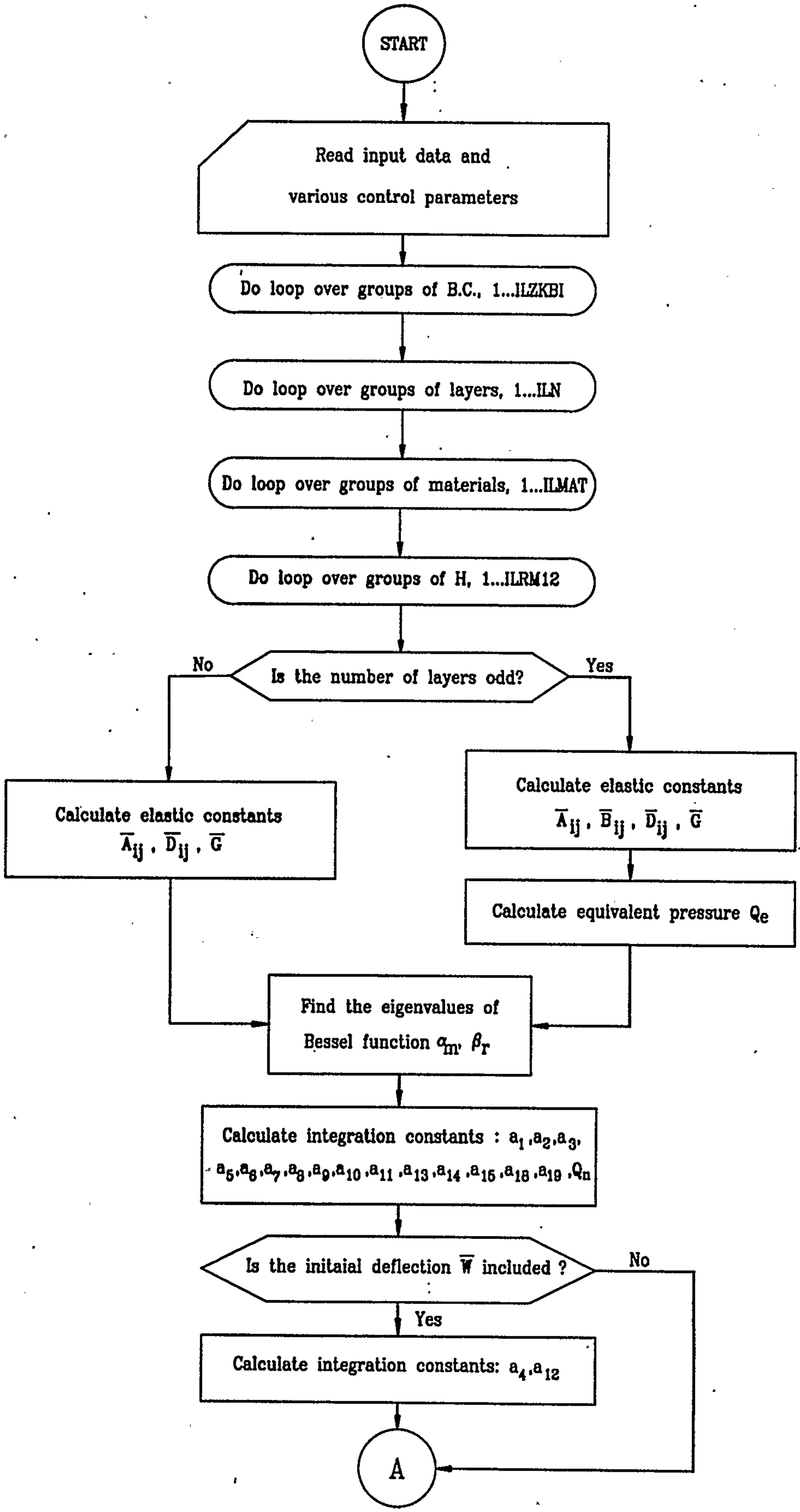

Figure 3.3: Flow chart for program NALSSS

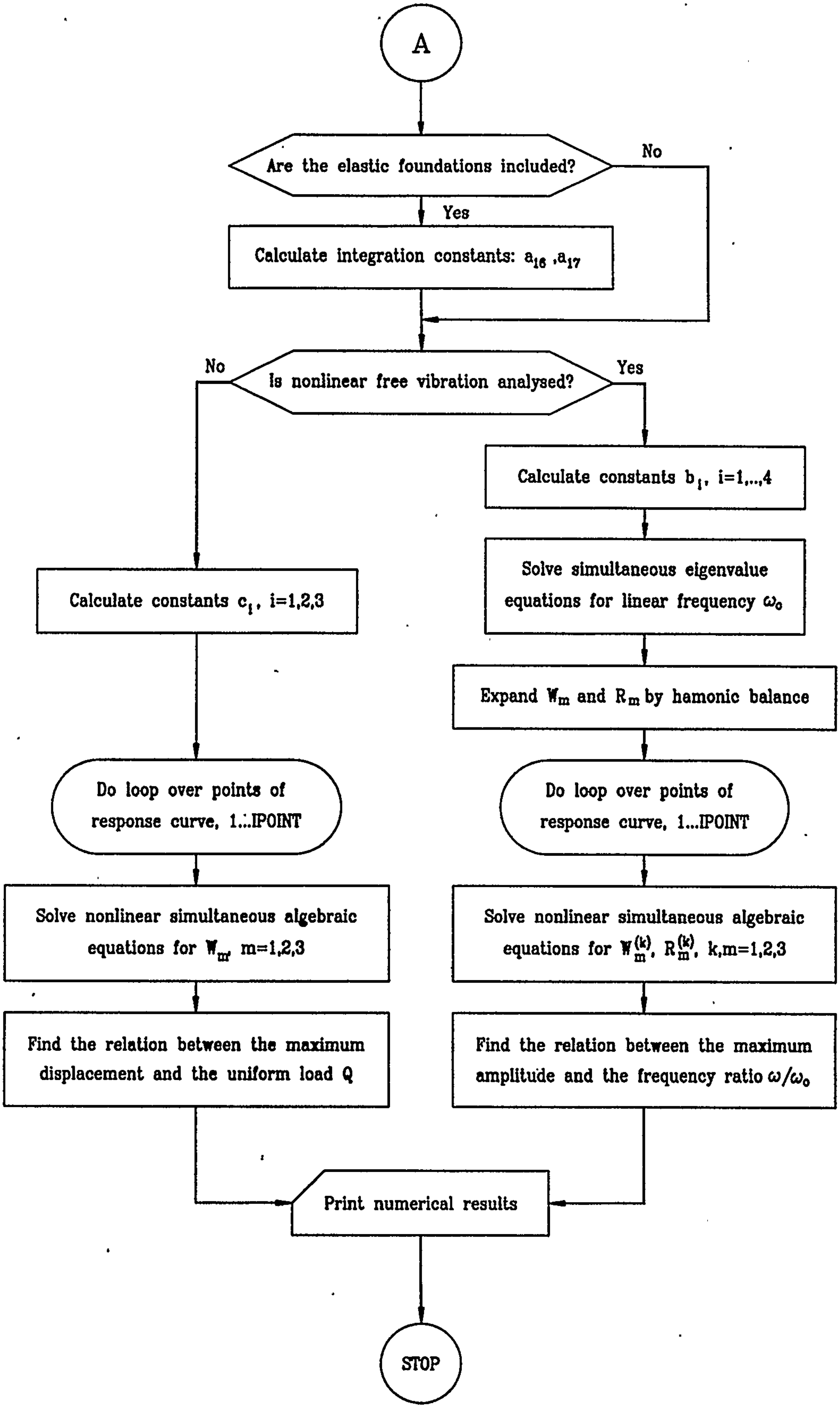

Figure 3.3: (Continued)

3.6 SUMMARY

In this chapter, a Fourier-Bessel series solution satisfying the prescribed boundary conditions is formulated for the governing equations of laminated shallow spherical shells. The eigenvalues of Bessel functions are listed in Tables for some typical cases. The Galerkin procedure furnishes three sets of nonlinear ordinary differential equations for time functions. For nonlinear free vibration, the time dependent coefficients of Fourier-Bessel series are expanded as Fourier cosine series and a system of simultaneous nonlinear algebraic equations is obtained and then solved by the method of harmonic balance. For the static response, the nonlinear ordinary differential equations become the nonlinear algebraic equations by treating the time as a constant and deleting the inertia terms. In some special cases, the simplified equations are presented. The Newton-Raphson method is used for solving the system of simultaneous nonlinear equations. Some features of computer programme NALSSS are briefly described. The numerical results can be obtained by implementing the programme NALSSS for a given set of shell parameters.

CHAPTER 4

NUMERICAL RESULTS AND DISCUSSIONS

4.1 INTRODUCTION

In Chapter 3, the solutions for nonlinear analysis of laminated shallow spherical shells satisfying the required boundary conditions have been obtained. The laminated circular plates are treated as a special case of the shell. In this chapter, numerical results for nonlinear free vibration, buckling, postbuckling and static large deflection responses of laminated shallow spherical shells and circular plates are presented. The effects of transverse shear, rotatory inertia, geometric imperfection and elastic foundation are investigated in detail.

Computations were performed for a laminated cross-ply moderately thick shallow spherical shell or circular plate which consists of a number of cylindrically (or polar) orthotropic layers. All of the laminae are of same thickness and material properties. Elastic constants used in calculation are listed in Table 3.5 for glass-epoxy (GL), boron-epoxy (BO) and graphite-epoxy (GR) composite materials and for an isotropic material (ISO). A uniformly distributed static loading normal to the undeformed middle surface in static problems is considered. In calculation, only the first three terms in each truncated series for W, ψ, F in solution (3.13) and the first three terms in cosine series (3.29) for the nonlinear free vibration are taken into account as the influence of the other terms have numerically demonstrated to be negligibly small. With geometric imperfection included, only the first term for $\overline{W}$ in eqn. (3.14) is considered in order to simplify the calculation. The results are presented in graphs and tables for dimensionless load, $Q / (H^2/h^2)$ (Q for circular plates), for buckling and postbuckling, and the frequency ratio, ω/ω_0, for nonlinear free vibration against the dimensionless maximum transverse displacement, w_{max}/h. In addition, the average dimensionless deflection, W_A, is introduced in Figs. 4.7 and 4.8 in order to be compared with the previous results obtained by Dumir et al(1984b) and Nath et al (1987):

$$W_A = 4 \int_0^1 \rho \, W d\rho \tag{4.1}$$

Unless otherwise stated, the present results obtained by neglecting effects of transverse shear and rotatory inertia are represented by solid curves ($T_S = R_I = 0$) and those taking these effects into account by dashed curves for nonlinear free vibration ($T_S = 1$, $R_I = 1$), or for buckling, postbuckling and large deflection response ($T_S = 1$, $R_I = 0$) in all figures. In this study, the least value of the geometric parameter, H/a, for which buckling occurs, is denoted by $(H/a)_{cr}$, and the corresponding buckling load denoted by Q_{cr}.

The convergence study of the solution is discussed in section 4.2 while a comparison with availably previous results is presented in section 4.3. The results are presented for nonlinear free vibrations of symmetrically and unsymmetrically laminated shallow spherical shells and circular plates with different parameters in section 4.4 and for buckling, postbuckling or static large-deflection response of these shells and plates with different parameters in section 4.5.

4.2 CONVERGENCE STUDY

To assess the reliability of the present multi-mode solution, a convergence study was made with different numbers of terms taken in each truncated series for W, ψ and F in the solution (3.13). The linear frequency parameter, ω_0, and the ratio, ω/ω_0, for the fundamental mode of an immovable clamped isotropic shallow spherical shell are presented in Table 4.1, while the static load parameter, Q, is given in Tables 4.2 and 4.3 for nonlinear bending of an elastically supported isotropic shallow spherical shell. The figures shown in Tables 4.1 and 4.2 are obtained by neglecting the effects of transverse shear and/or rotatory inertia and those in Table 4.3 are obtained by considering the effect of transverse shear. It can be seen from these tables that the difference between the results obtained by three terms and those obtained by four terms is very small. With an increase in the number of terms taken, this difference tends to decrease. Therefore the convergence is very good and a three term solution gives considerably accurate results.

4.3 COMPARISON WITH PREVIOUS RESULTS

As a partial check on the accuracy of the present solution for the

Table 4.1 Convergence study for an immovable clamped isotropic shallow spherical shell (H/h=1)

	ω / ω_0				
	Numbers of terms taken for W, ψ and F				
w_{max}/h	2 x 2 x 2 ω_0=4.167581	3 x 3 x 3 ω_0=4.169225	4 x 4 x 4 ω_0=4.175766	5 x 5 x 5 ω_0=4.176349	6 x 6 x 6 ω_0=4.177559
0.00	1.000000	1.000000	1.000000	1.000000	1.000000
0.25	0.992432	0.992584	0.992587	0.992610	0.992612
0.50	0.974748	0.975464	0.975483	0.975571	0.975578
0.75	0.953430	0.955310	0.955338	0.955525	0.955539
1.00	0.934167	0.937871	0.937831	0.938140	0.938150
1.25	0.922486	0.928298	0.928020	0.928452	0.928428
1.50	0.923136	0.930840	0.930044	0.930575	0.930463
1.75	0.939642	0.948160	0.946489	0.946345	0.946797
2.00	0.973496	0.981056	0.977376	0.978699	0.978187

Table 4.2 Convergence study for an elastically supported isotropic shallow spherical shell (K_b=5, K_i=5, H/h=1.5, T_s=0)

	Q				
	Numbers of terms taken for W, ψ and F				
w_{max}/h	2 x 2 x 2	3 x 3 x 3	4 x 4 x 4	5 x 5 x 5	6 x 6 x 6
0.00	0.000000	0.000000	0.000000	0.000000	0.000000
0.25	3.200569	3.157779	3.162981	3.157947	3.158763
0.50	5.180716	5.135711	5.140530	5.134824	5.135596
0.75	6.303466	6.276269	6.278049	6.274036	6.274316
1.00	6.884068	6.892340	6.890041	6.889167	6.888836
1.25	7.186695	7.252818	7.245803	7.249153	7.246719
1.50	7.430431	7.579849	7.566285	7.574929	7.573108
1.75	7.808203	8.069343	8.035509	8.050540	8.047001
2.00	8.515846	8.859200	8.823400	8.845903	8.838593

Table 4.3 Convergence study for an elastically supported isotropic shallow spherical shell (K_b=5, K_i=5, H/h=1.5, T_s=1)

	Q				
	Numbers of terms taken for W, ψ and F				
w_{max}/h	2 x 2 x 2	3 x 3 x 3	4 x 4 x 4	5 x 5 x 5	6 x 6 x 6
0.00	0.000000	0.000000	0.000000	0.000000	0.000000
0.25	3.189794	3.141400	3.152146	3.144479	3.148010
0.50	5.145913	5.096684	5.107294	5.099440	5.102940
0.75	6.239011	6.210338	6.216261	6.211214	6.213383
1.00	6.790282	6.798819	6.799172	6.797930	6.798759
1.25	7.066387	7.133220	7.128247	7.131274	7.131138
1.50	7.285434	7.434643	7.423661	7.431370	7.430500
1.75	7.637199	7.886080	7.865704	7.878329	7.876402
2.00	8.315154	8.657382	8.619799	8.636754	8.632536

nonlinear free vibration, buckling, postbuckling or large deflection response of shallow spherical shells and circular plates, some previous numerical results are presented for comparison with the corresponding present results. As indicated in Chapter 1, very few results exist on the nonlinear elastic behaviour of shallow spherical shells including effects of transverse shear and rotatory inertia. In this comparison, the effects of transverse shear and rotatory inertia for nonlinear free vibration and that of transverse shear for static response are not taken into account. Usually, in this section, thin shells or plates is considered.

4.3.1 Comparison of Fundamental Linear Frequency

The comparison of fundamental linear frequencies of an immovable clamped isotropic shallow spherical shell with those obtained by Reissner(1955) using an exact solution for different initial rises of the shell and Poisson's ratios is listed Table 4.4.

Table 4.4 Comparison of fundamental linear frequency of an isotropic shallow spherical shell

H/h	ω_0					
	$\upsilon = 0$		$\upsilon = 0.3$		$\upsilon = 0.5$	
	Present	Reissner (1955)	Present	Reissner (1955)	Present	Reissner (1955)
0.0	2.9490	2.9480	3.0914	3.0904	3.4053	3.4041
0.5	3.1958	3.1838	3.3940	3.3872	3.7619	3.7734
1.0	3.8413	3.8619	4.1692	4.1272	4.6656	4.6873
1.5	4.7226	4.7462	5.2031	5.1590	5.8547	5.8960
2.0	5.7285	5.7191	6.3606	6.3676	7.1672	7.1342
2.5	6.7999	6.8098	7.5711	7.5763	8.5168	8.4608
3.0	7.9051	7.8711	8.7950	8.8145	9.8499	9.7874
3.5	9.0255	9.0208	10.0058	10.0232	11.1269	10.9960
4.0	10.1490	10.1116	11.1831	11.1434	12.3194	12.1458
4.5	11.2666	11.2319	12.3121	12.2637	13.4166	13.2365
5.0	12.3711	12.3226	13.3859	13.2955	14.4272	14.4157
6.0	14.5203	14.4452	15.3846	15.2411	16.2767	16.0666
7.0	16.5772	16.4793	17.2597	17.0984	18.0280	17.7175
8.0	18.5584	18.3365	19.0921	18.8967	19.7674	19.4568
9.0	20.4981	20.2232	20.9256	20.6654	21.5281	21.2256
10.	22.4268	22.1100	22.7793	22.4638	23.3208	23.0534
11.	24.3654	23.9672	24.6622	24.3210	25.1486	24.8811
12.	26.3310	25.8245	26.5816	26.1782	27.0127	26.6794

It is observed that the two corresponding sets of the fundamental linear frequencies are very close and the difference is less than 2%. With elastic foundations, the fundamental linear frequencies of an orthotropic shallow spherical shell for four special cases of the elastically restrained edge are presented in Table 4.5 to compare with those given by Dumir (1985) using a single mode solution. It is found that these two sets of values are very consistent. The effect of geometric imperfection on the fundamental linear frequency of immovable clamped and movable simply supported isotropic circular plates is presented in Table 4.6 for comparison with those using Linstedt's perturbation solution (Hui, 1983b). A good agreement is observed between the corresponding two sets of values.

4.3.2 Comparison of the Frequency-Amplitude Response

The frequency ratios of an isotropic immovable clamped shallow spherical shell for $w_{max}/h=1$ are presented in Table 4.7 for comparison with those given by Grossman et al(1969) and Varadan and Pandalai(1978). A good agreement is found between the corresponding sets of values.

Figure 4.1 shows that present results for the movable clamped edge of a shallow spherical shell are in good agreement with those obtained by use of series solution (Ramachandran, 1976). The response curves for an immovable clamped edge are somewhat different from those given by Sinharay and Banerjee (1985) at large values of the amplitude.

Table 4.5 Comparison of fundamental linear frequency of an orthotropic shallow spherical shell with elastic foundations (K_f=4, K_n=0, H/h=1,$\upsilon_{\theta r}$=0.3)

K_b	K_i	G_f	E_θ/E_r=1		E_θ/E_r=3	
			ω_o(Present)	ω_o(Dumir, 1985)	ω_o(Present)	ω_o(Dumir, 1985)
∞	∞	0.0	4.6241	4.6784	5.1932	5.1792
		0.5	4.9938	5.0234	5.5518	5.4811
∞	0	0.0	3.9294	3.9430	4.6592	4.5754
		0.5	4.3504	4.3455	5.0143	4.9154
0	∞	0.0	3.9104	3.9461	4.4389	4.4024
		0.5	4.2620	4.2971	4.7557	4.7278
0	0	0.0	2.7333	2.7175	3.3890	3.2505
		0.5	3.2181	3.2077	3.8055	3.6814

Table 4.6 Comparison of fundamental linear frequency of an isotropic imperfect circular plate

	ω_o			
	Immovable clamped		Movable simply supported	
$\bar{W}_1$	Present	Hui(1983)	Present	Hui(1983)
0.0	3.0914	3.107	1.4934	1.498
0.2	3.1605	3.168	1.5092	1.513
0.4	3.3577	3.380	1.5555	1.567
0.6	3.6573	3.637	1.6291	1.648
0.8	4.0295	3.995	1.7258	1.740
1.0	4.4473	4.387	1.8410	1.858

Table 4.7 Comparison of the frequency ratio of an immovable clamped isotropic shallow spherical shell

	ω / ω_o for $w_{max}/h = 1$		
H/h	Present	Grossman et al (1969)	Varadan and Pandalai (1978)
0	1.1766	1.166	1.176
2	0.9122	0.898	0.895
5	0.9236	0.921	0.898

This difference arises from the fact that a single-mode solution is used in Sinharay and Banerjee(1985) and a multi-mode solution is used in present analysis. It is noted that the previous results in this figure are available in the range of values, $w_{max} \le h$. In Fig. 4.2, the present frequency-amplitude response curves are compared with those given in Varadan and Pandalai(1978) using a single mode solution. A slight difference is found from these four sets of curves for $w_{max} \le 1.3h$.

Considering the elastic foundations, the frequency-amplitude response curves of present results for an immovable clamped orthotropic shallow spherical shell resting on linear Winkler and Pasternak foundations shown in Fig. 4.3 are close to those obtained by use of a spatial mode solution(Dumir, 1985). In addition, the fundamental linear frequency is also compared with those (only E_θ/E_r=1,3 available) given by Dumir (1985) in Table 4.8.

Table 4.8 Comparison of fundamental linear frequency of an immovable clamped orthotropic shallow spherical shell in Fig. 4.3

	ω_o	
E_θ/E_r	Present	Dumir(1985)
1	4.9938	5.0234
3	5.5184	5.4810
10	6.5400	--

The effect of geometrically initial imperfection on the frequency ratio of an isotropic circular plate is illustrated in Fig. 4.4 for comparison with that given by Hui(1983b). The curves of frequency ratio are plotted at the value of vibration amplitude, $w_{max}/h=1$. A slight difference between these two sets of curves is observed, which arises from the fact that the assumed mode of geometric imperfection in Hui(1983b) is different that in this study. However, Figure 4.4 shows that the general behaviour reflected by these two sets of curves is similar.

For a circular plate, the frequency-amplitude response curves of isotropic immovable and movable clamped edges are depicted in Fig. 4.5. Previous results obtained by Huang and Sandman(1971) and Nowinski(1963) are also shown in the figure. A good agreement is observed between the corresponding sets of curves.

4.3.3 Comparison of the Buckling, Postbuckling and Load-Deflection Response

The values of $(H/a)_{cr}$ for which the buckling occurs and the associated buckling loads Q_{cr} for isotropic and orthotropic immovable clamped shallow spherical shells are presented in Table 4.9 for comparison with those given by Varadan(1978). The maximum difference between two sets of values is less than 3%.

Table 4.9 Comparison of values of $(H/a)_{cr}$ and Q_{cr} of an immovable clamped orthotropic shallow spherical shell

	Present		Varadan (1978)	
$\upsilon_{\theta r}=1/3$	$(H/a)_{cr}$	Q_{cr}	$(H/a)_{cr}$	Q_{cr}
$E_\theta/E_r=1$	0.08305	3.1802	0.08248	3.2152
$E_\theta/E_r=4$	0.09720	4.7172	0.10010	4.8170

A comparison of buckling loads is shown in Fig. 4.6 for an isotropic shallow spherical shell with immovable clamped and simply-supported edges. The present results are in good agreement with those given by Varadan(1978) for a clamped edge and those given by Dumir et al (1984b) for simply-supported edge, respectively. In Fig. 4.7, the present results for post-buckling behaviour of an immovable clamped orthotropic shallow spherical shell with different shell rises agree closely with those given by Dumir et al(1984b) using an orthogonal point collocation method.

Figure 4.8 shows the static large deflection of an immovable simply-supported orthotropic shallow spherical shell on elastic foundations. In this figure the present results are compared with those given by Nath et al (1987) employing the collocation method of the Chebyshev series. Good agreement is observed between the corresponding curves. In addition, the present results also agree very well with those given by Sinha(1963), Way(1934) and Chien and Yeh(1954) for the static large deflection of an isotropic clamped circular plate shown in Fig. 4.9.

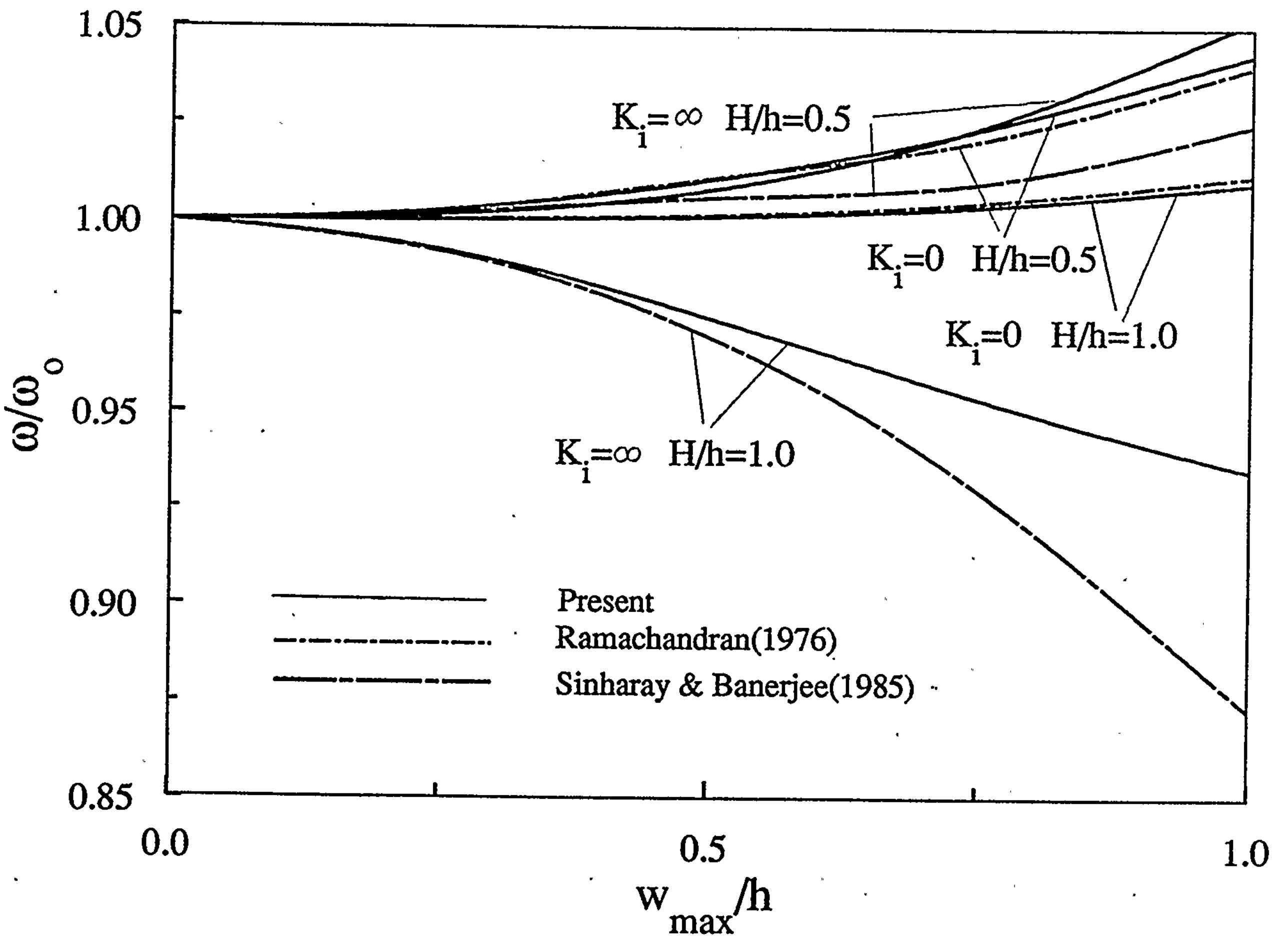

Figure 4.1: Comparison of the frequency-amplitude response for clamped immovable and movable isotropic shallow spherical shells with different shell rises ($\upsilon_{\theta r}$ = 0.3)

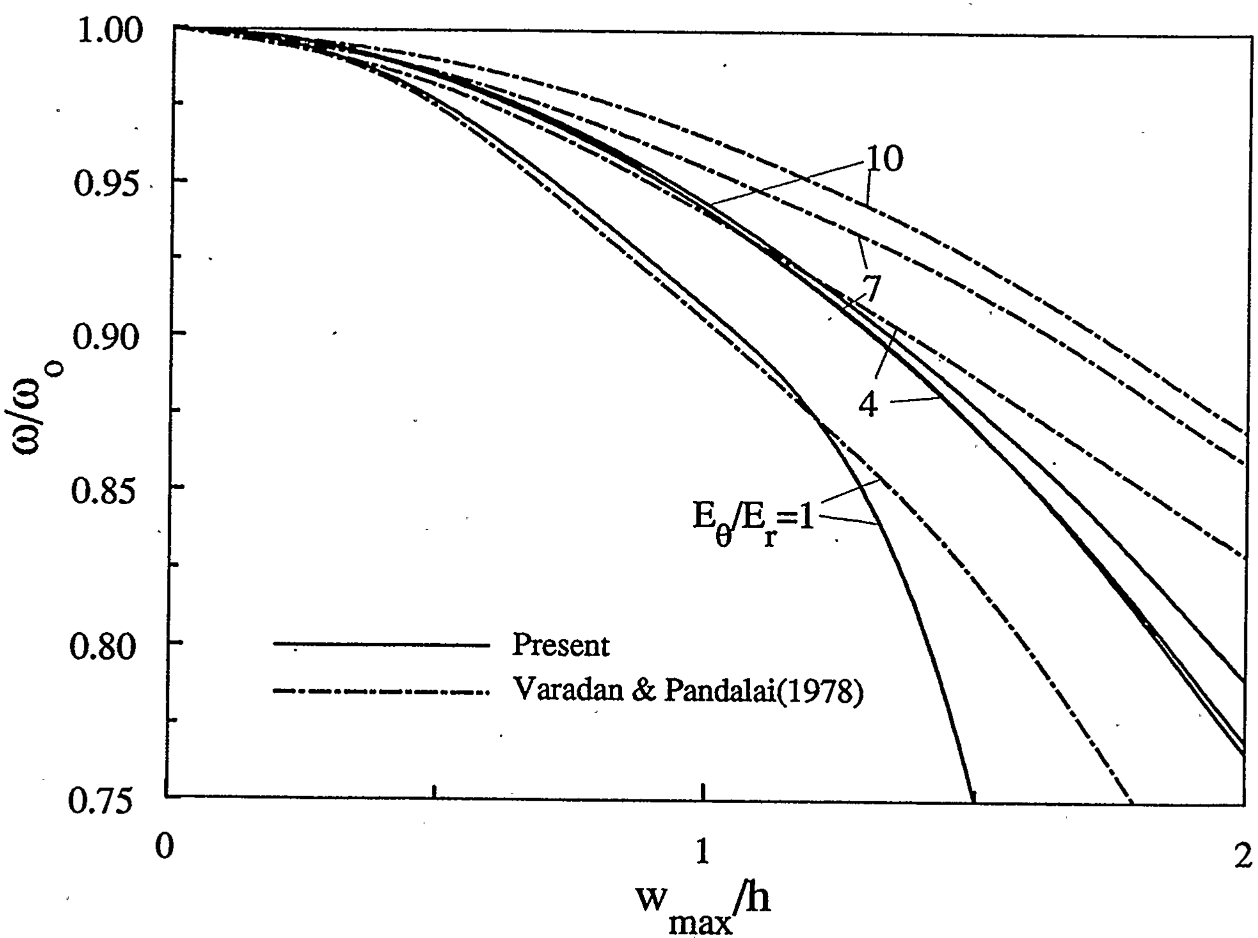

Figure 4.2: Comparison of the frequency-amplitude response for an immovable clamped orthotropic shallow spherical shell with different material properties (H/h = 3,$\upsilon_{\theta r}$=1/3)

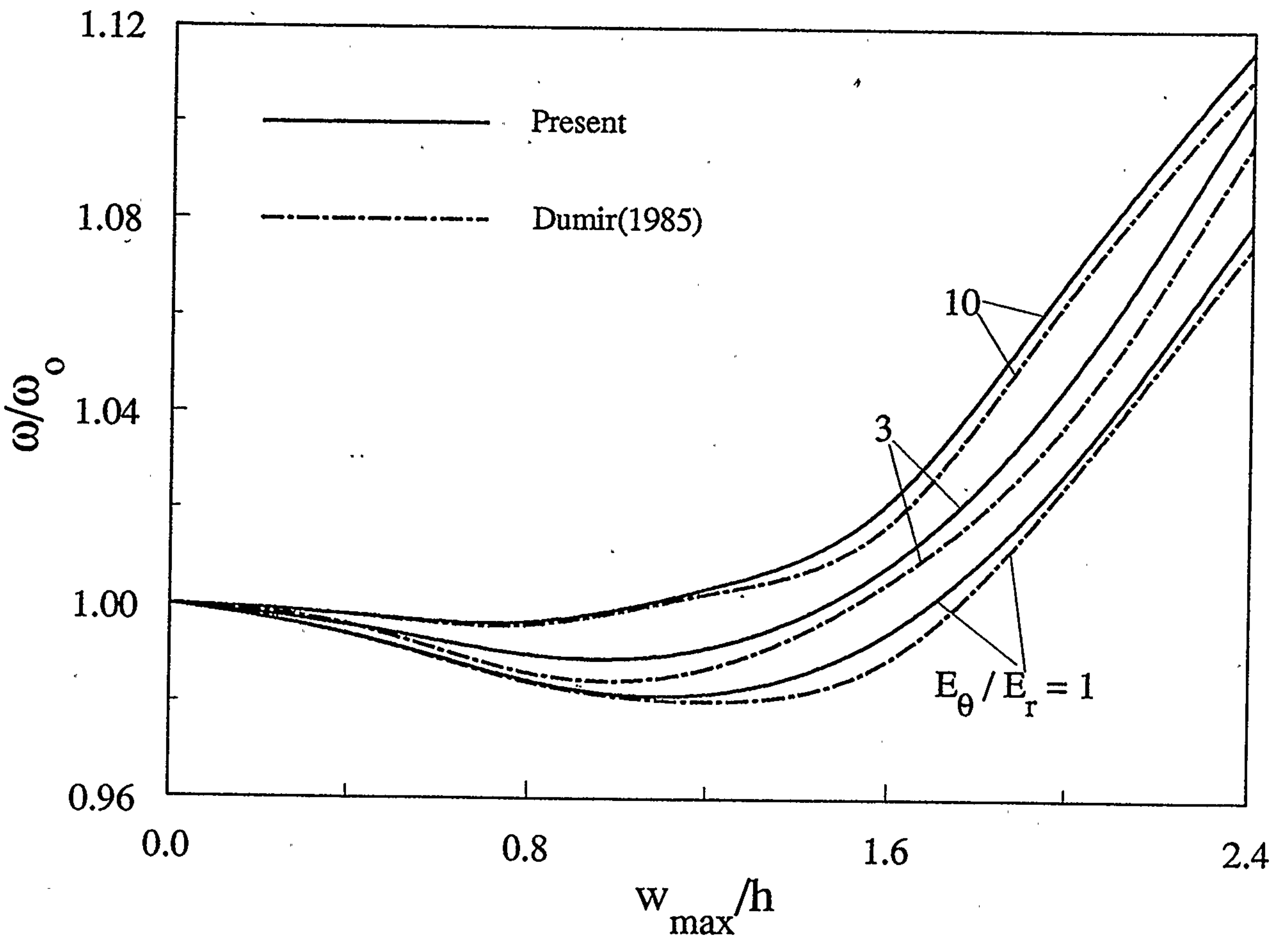

Figure 4.3: Comparison of the frequency-amplitude response for an immovable clamped orthotropic shallow spherical shell resting on elastic foundations ($\upsilon_{\theta r} = 0.3$, $K_f = 4$, $K_n = 0$, $G_f = 0.5$, $H/h = 1$)

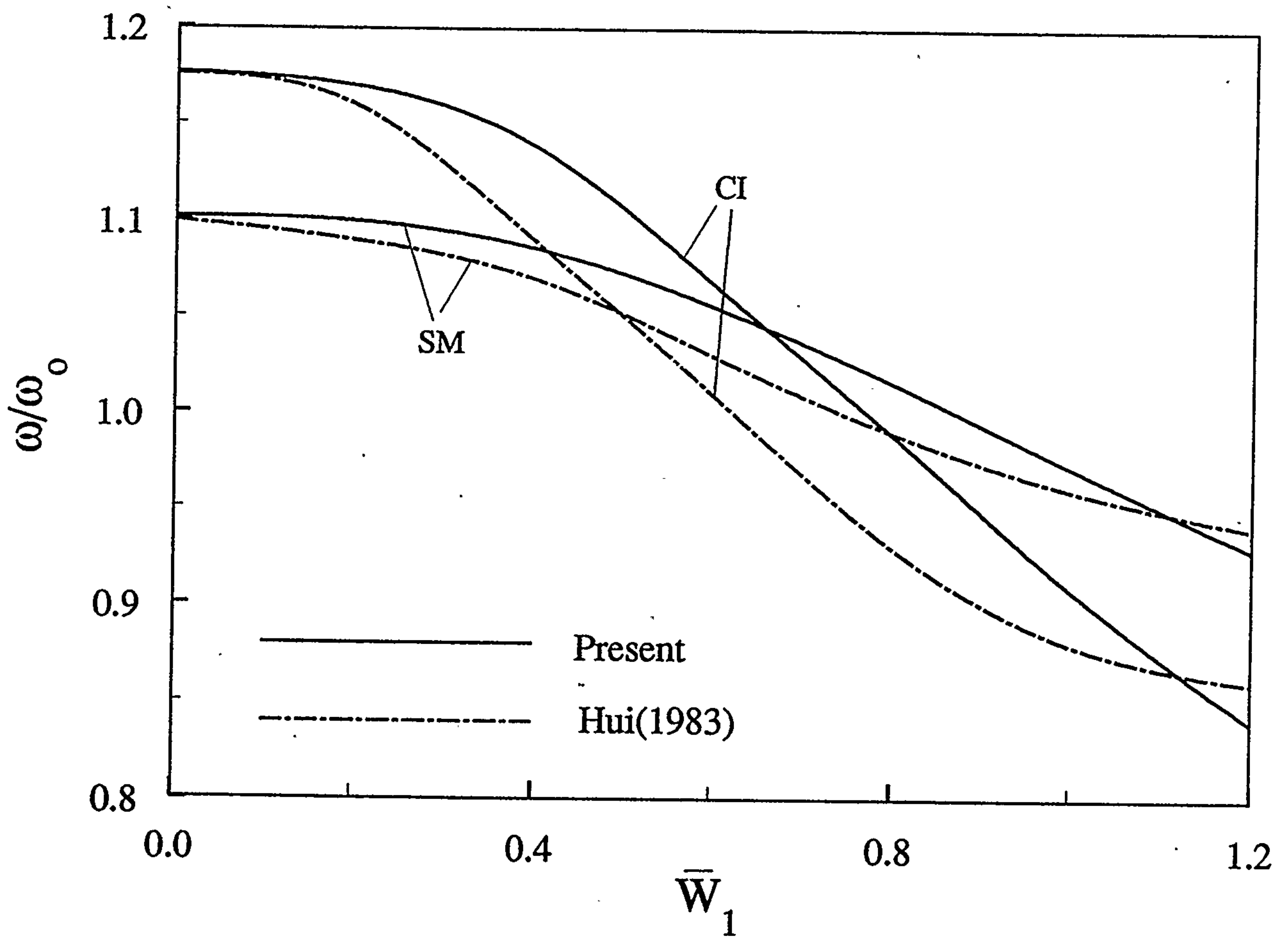

Figure 4.4: Comparison of the effect of geometric imperfections on the frequency ratio at $w_{max}/h=1$ of immovable clamped and movable simply-supported isotropic circular plates($\upsilon_{\theta r}=0.3$)

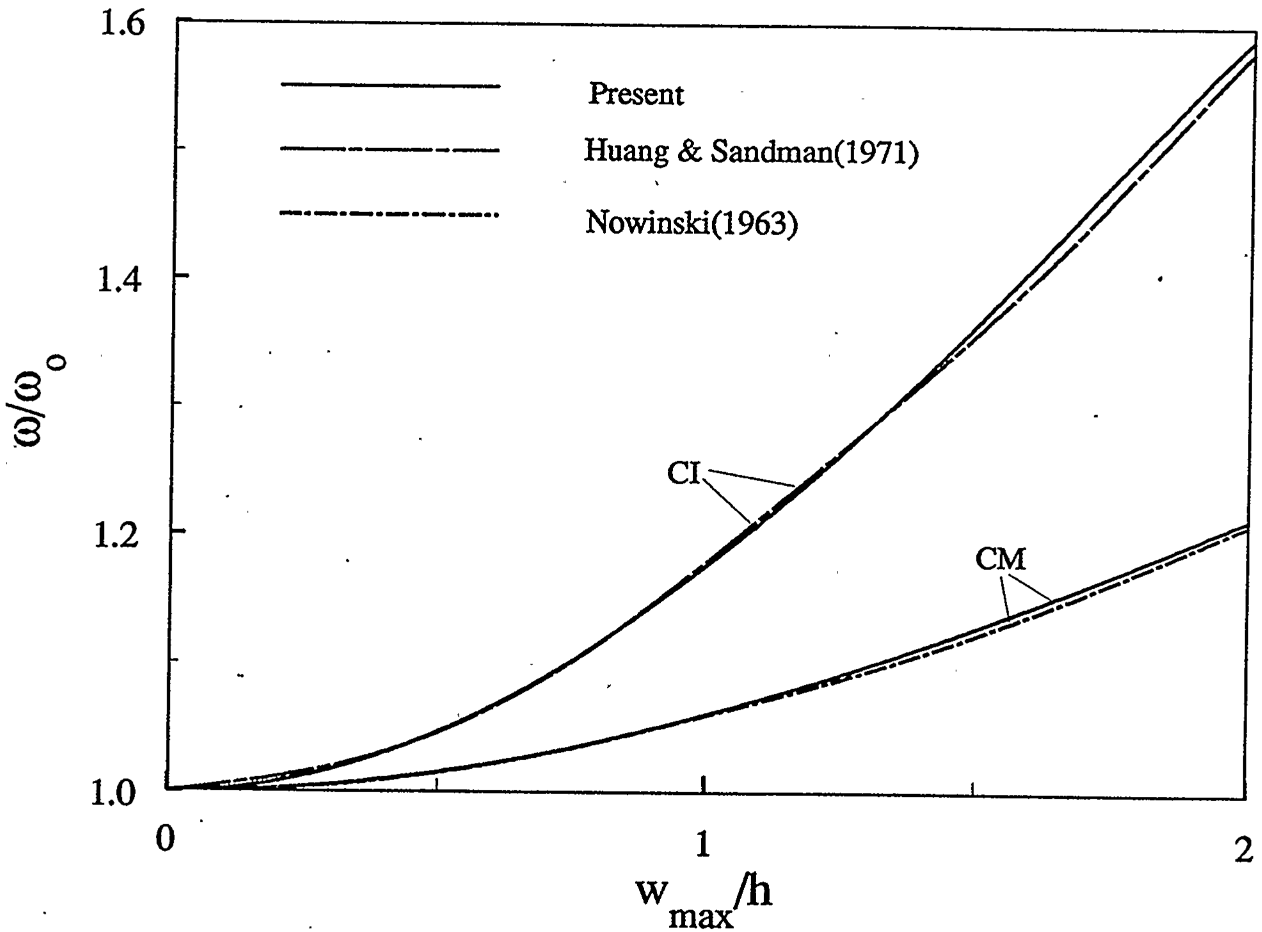

Figure 4.5: Comparison of the frequency-amplitude response for clamped immovable ($\upsilon_{\theta r}$=1/3) and movable ($\upsilon_{\theta r}$=0.3) isotropic circular plates

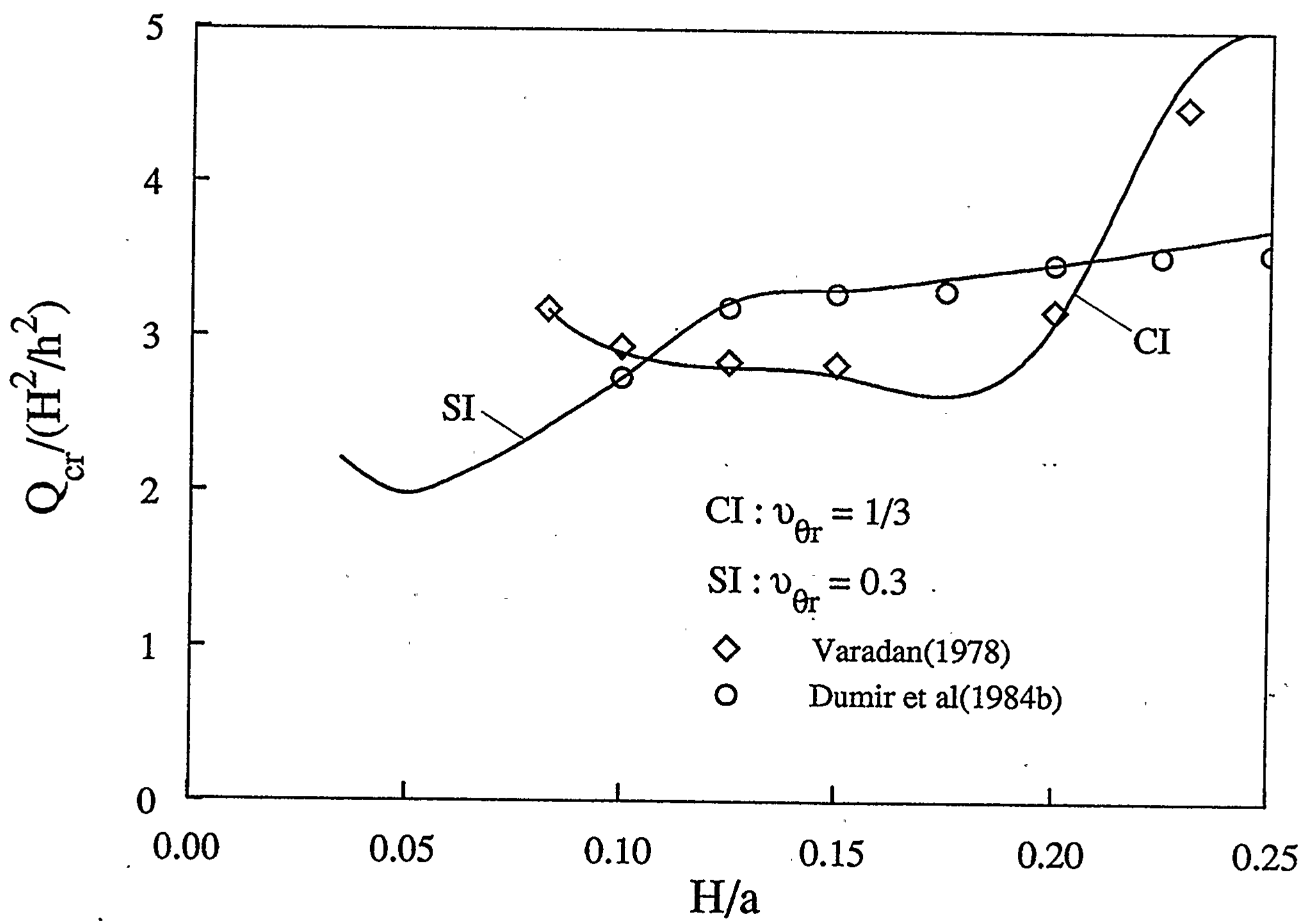

Figure 4.6: Comparison of buckling loads for immovable clamped(CI) and immovable simply-supported(SI) isotropic shallow spherical shells

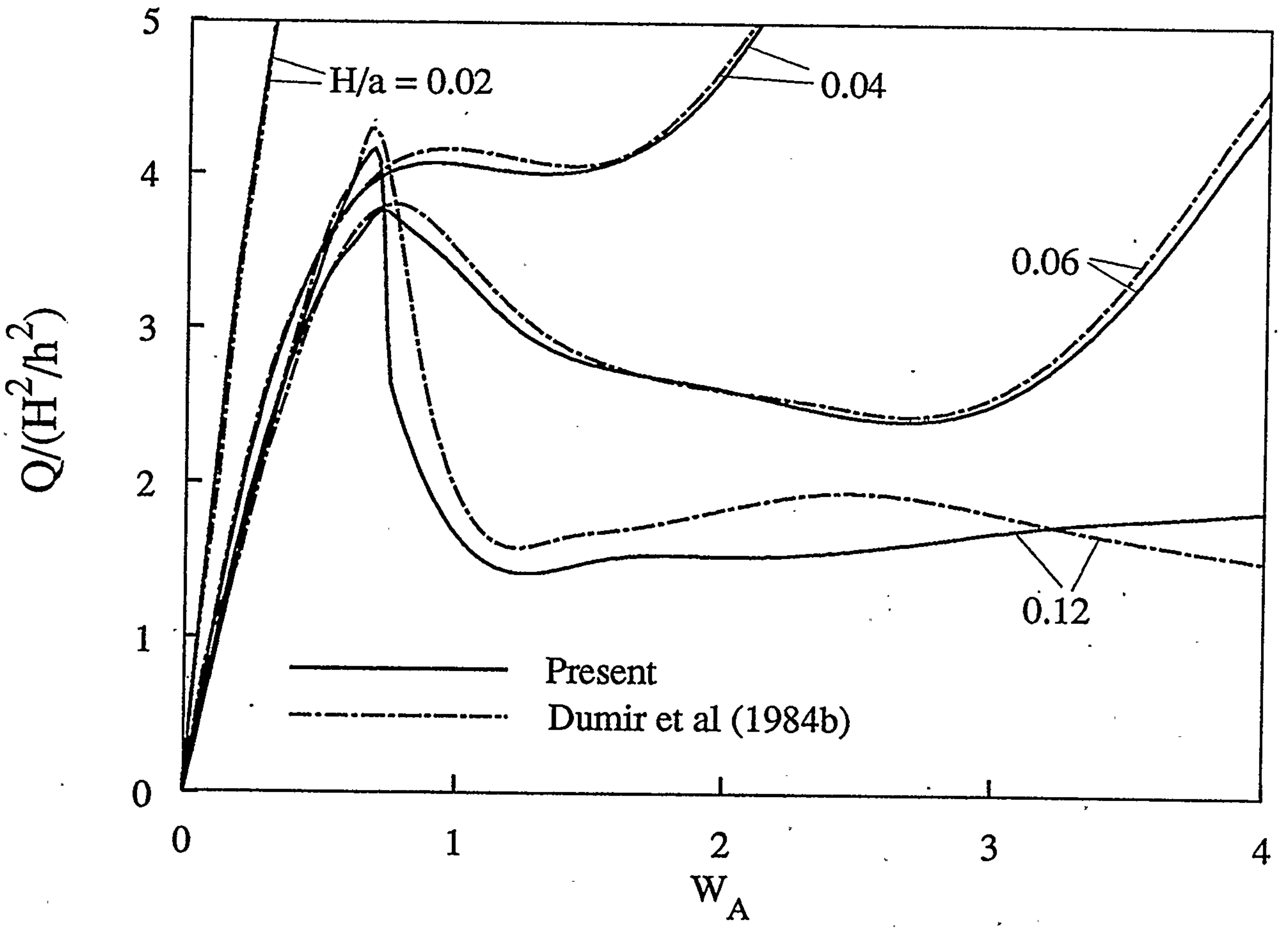

Figure 4.7: Comparison of buckling and postbuckling behaviour for an immovable clamped orthotropic shallow spherical shell with different shell rises (E_θ/E_r=3, $\upsilon_{\theta r}$=0.3)

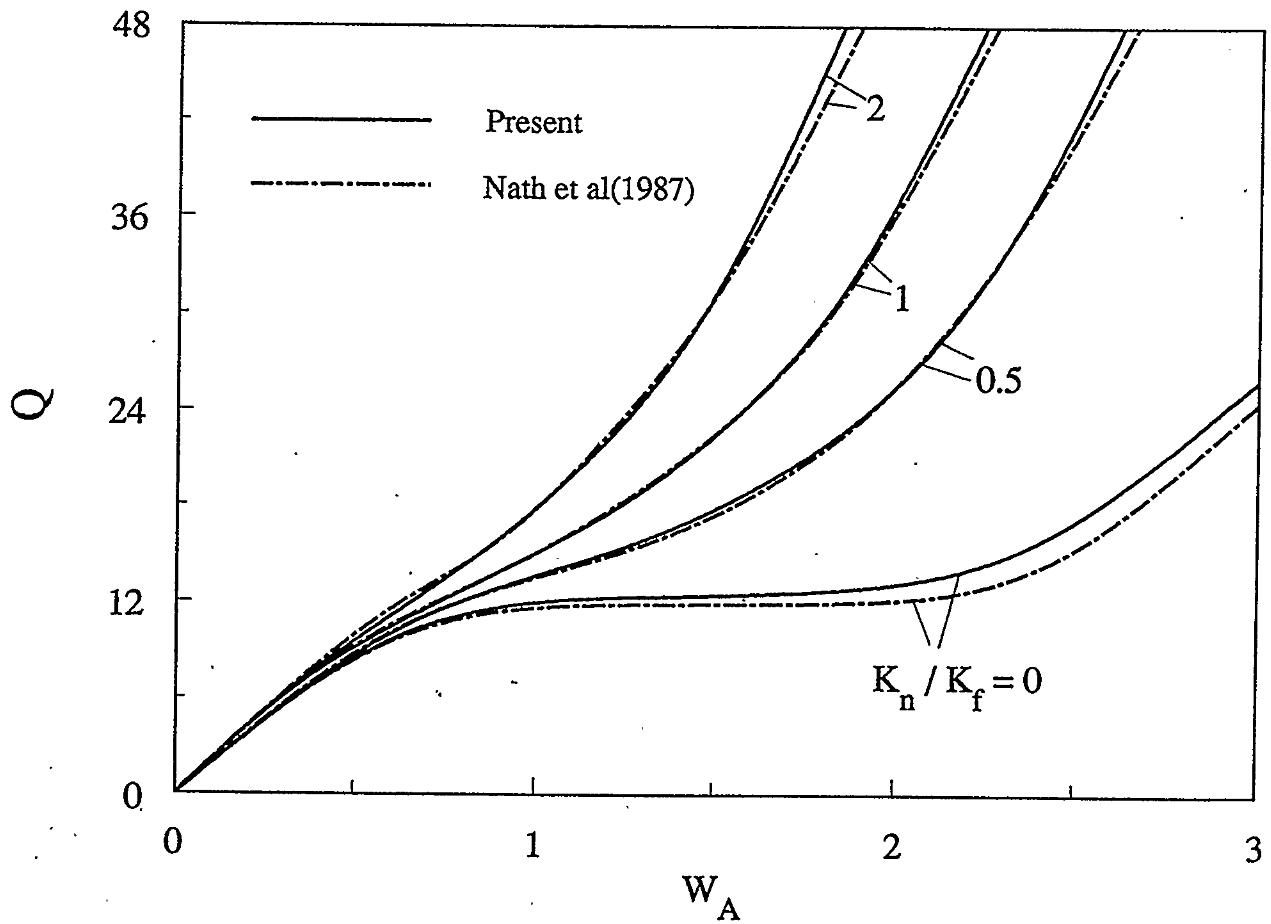

Figure 4.8: Comparison of the static large deflection of an immovable simply-supported orthotropic shallow spherical shell with different values of nonlinear Winkler foundation parameters (E_θ/E_r=1.5, $\upsilon_{\theta r}$=1/3, K_f=9, G_f=0, H/h=1.5)

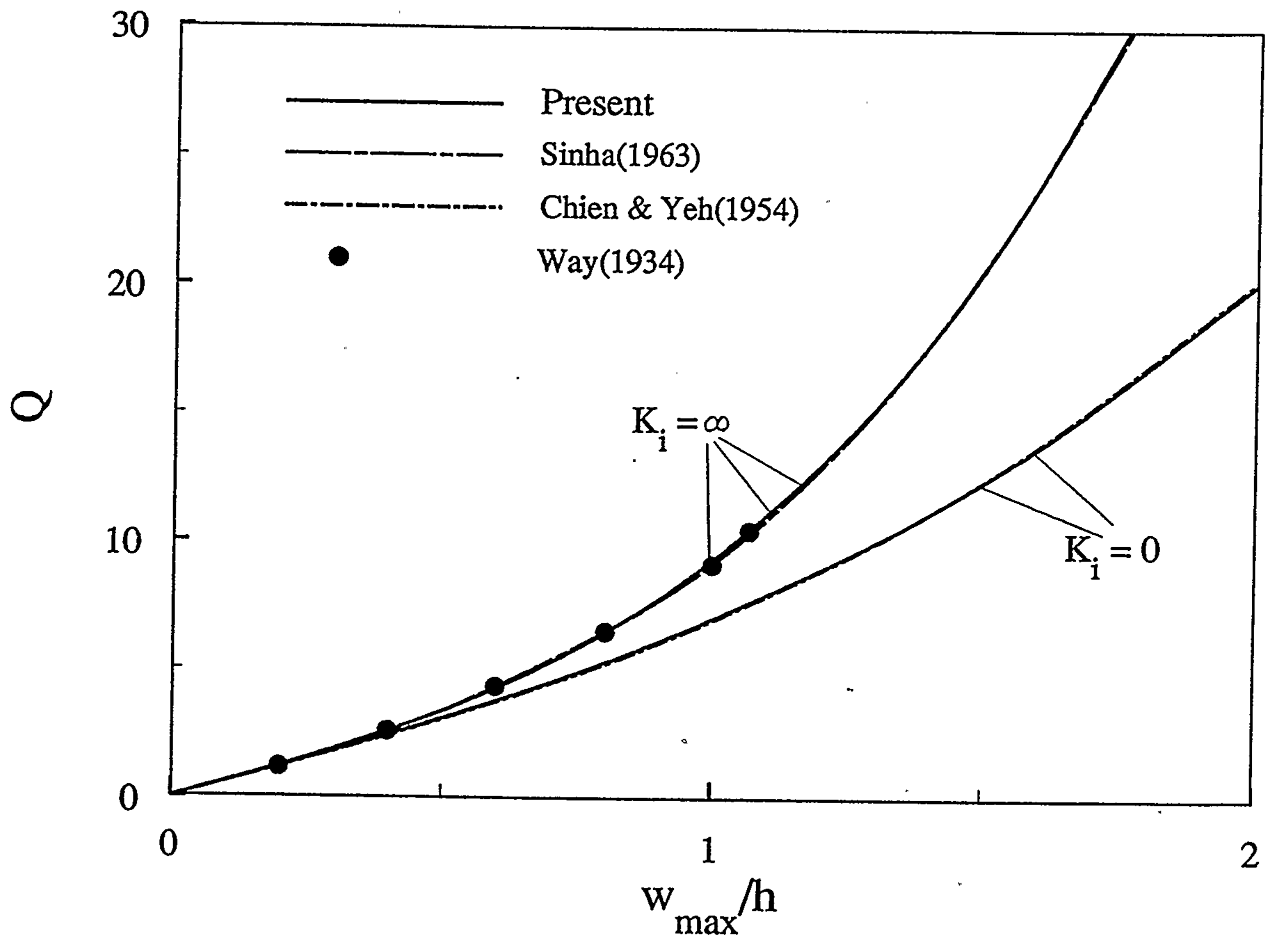

Figure 4.9: Comparison of the static large deflection of immovable and movable clamped isotropic circular plates($\upsilon_{\theta r}$=0.3)

4.4 NONLINEAR FREE VIBRATION

In this section, the numerical results as presented in the figures show the relationship between frequency ratio and dimensionless amplitude of vibration of a laminated cross-ply shallow spherical shell or circular plate having different edge conditions, shell rises, ratios of the base plane radius-to-thickness, numbers of layers, elastic properties of material, values of initial imperfection and moduli of linear, nonlinear Winkler and shear Pasternak elastic foundations. In the presentation, unless specified, the frequency ratio (ω/ω_0) is the ratio of the nonlinear frequency ω of vibration to the corresponding linear frequency ω_0, of a classical shallow spherical shell or circular plate. And the dimensionless amplitude (w_{max}/h) is the ratio of the maximum amplitude of vibration to the shell or plate thickness. The linear frequencies ω_0 are obtained by neglecting the nonlinear terms and the effects of transverse shear and rotatory inertia in eqns. (2.63a) and (2.63c).

4.4.1 Symmetrically Laminated Shallow Spherical Shells

4.4.1.1 The Effects of Transverse Shear and Rotatory Inertia on the Frequency-Amplitude Response

Figures 4.10 shows the individual effect of transverse shear and rotatory inertia on the frequency-amplitude response of a five-layer shallow spherical shell. And the effect of the ratio of base radius to thickness of the shell on the response is plotted in Figs. 4.11 and 4.12. The fundamental linear frequencies for these three figures are listed in Table 4.10. In Fig. 4.10, the effects of transverse shear and rotatory inertia reduce the frequency at infinitely small amplitude by approximately 2.7% and 3.5% for a movable simply-supported five-layer graphite-epoxy shallow spherical shell with a/h=10 and a/h=8, respectively, and these effects increase with decreasing ratio of base radius to shell thickness for given dimensionlessly initial rise of the shell, H/h, which, for instance, is equal to 2 in Fig. 4.10. These curves exhibit the softening type behaviour, and the frequency ratio, ω/ω_0, decreases as the amplitude of vibration increases. The nonlinear frequency is reduced approximately by 19%, 21%, and 25% at w_{max}=2h for the thin shell (i.e. T_S=R_I=0), the shell with a/h=10 and a/h=8, respectively. In these frequency-amplitude response curves shown in Figs. 4.10, as expected, the effect of transverse shear plays more important role than that of rotatory inertia. The effect of rotatory inertia generally reduces the nonlinear frequency including the effect of transverse shear (i.e., T_S=1, R_I=0) by only about 0.2% to 0.3%, and is very small compared with the effect of transverse shear. Therefore, the effect of rotatory inertia can be neglected in an analysis. Unless stated, for the rest of the study the individual effect of transverse shear and rotatory inertia is not separately investigated.

Table 4.10 Values of fundamental linear frequency parameter ω_0 in Figs. 4.10-4.12

ω_0		
Fig. 4.10	Fig. 4.11	Fig. 4.12
7.6407	9.8260	13.5535

The effect of the ratio of base radius to the shell thickness on the frequency-amplitude response is presented for a movable clamped three-layer graphite-epoxy shallow spherical shell in Fig. 4.11 and an immovable clamped five-layer boron-epoxy imperfect shallow spherical shell resting on elastic foundations in Fig. 4.12, both with the dimensionlessly initial rise , H/h, equating to 2. The effects of transverse shear and rotatory inertia reduce the frequency ratio at infinitely small amplitude of vibration by approximately 0.5%, 1.8%, 2.5%, 5.7% and 8.1% in Fig. 4.11 and 0.2%, 0.5%, 0.8%, 1.8% and 2.7% in Fig. 4.12 for a/h=50, 20, 16, 10 and 8, respectively. It is observed that theses effects increase with decreasing the ratio of base radius to shell thickness and increasing the ratio of major principal modulus to minor one. With the ratio of a/h=8, the frequency ratio reaches at 0.73 for a shell of graphite-epoxy material and 0.91 for one of boron-epoxy material. For the high ratio of a/h, for instance, which is larger than 50, these effects are very small and may be neglected in an analysis.

The curves behave the soften type of nonlinearity in Fig. 4.11, and initially hardening one, then softening one and finally hardening one in Fig. 4.12.

It is shown that the effects of transverse shear and rotatory inertia are pronounced especially for lower ratio of base radius to shell thickness and high modulus ratio, but generally do not change the behaviour of response. Also, it is noted that from these figures in this section, the frequency ratio response neglecting the effects of transverse shear and rotatory inertia only depends on the dimensionlessly initial rise of the shell, i.e., H/h, whatever the ratios of base radius to shell thickness and rise to the base radius are.

4.4.1.2 The Effect of the Number of Layers on the Frequency-Amplitude Response

The effect of number of layers on the frequency-amplitude is depicted for an elastically supported boron-epoxy shallow spherical shell in Fig. 4.13 and a movable clamped graphite-epoxy shallow spherical shell in Fig. 4.14. The fundamental linear frequencies in these two figures are listed in Table 4.11.

The frequency ratio in Fig. 4.13 increases with increasing the number of layers for given value of dimensionless maximum amplitude , w_{max}/h. The curves for number of layers larger than 7 (some not shown herein) are quite close. The effects of transverse shear and rotatory inertia reduce the

Table 4.11 Values of fundamental linear frequency parameter ω_0 in Figs. 4.13-4.14

	ω_0	
N	Fig. 4.13	Fig. 4.14
1	--	7.0882
3	7.4191	8.4514
5	7.9062	9.6448
7	8.0158	10.0019
9	--	10.1614
15	8.0694	--
21	--	10.3967
∞	--	10.4833

frequency ratio by 2.5%, 3.5%, 3.8% and 4.3% at infinitely small amplitude of vibration for N=3, 5, 7 and 15, respectively. It is shown that these effects increase slightly as the number of layers increases.

Figure 4.14 shows that the results for the number of layers 9, 21, and ∞ are close to that given by the one layer (i.e., orthotropic shell). These curves and Table 4.11 indicate that the nonlinear frequency increases with an increase in the number of layers although the frequency ratio for some curves decrease with this parameter. The results, including the effects of transverse shear and rotatory inertia (not shown herein), are similar to those neglecting these effects in Fig. 4.14 except for the frequency ratio being reduced. The curves in Fig. 4.13 exhibit softening type of nonlinearity while those in Fig. 4.14 exhibit initially softening one then changing to hardening one.

It is observed from these two figures that the effect of number of layers on the frequency-amplitude response is more significant for three and five layer shells. Therefore, three and five layer shells are typical for symmetrically laminated shell and the numerical results in this chapter are presented mainly for these shells.

4.4.1.3 The Effect of Material Properties on the Frequency-Amplitude Response

The frequency-amplitude response curves with different materials are plotted for an elastically supported five-layer shallow spherical shell in Fig. 4.15 and a movable simply-supported three-layer shallow spherical shell in Fig. 4.16. Table 4.12 lists the fundamental linear frequencies in Figs. 4.15 and 4.16. From these figures and Table 4.12, the nonlinear frequency neglecting the effects of transverse shear and rotatory inertia increase with increasing the ratio of major principal modulus of material to minor one, E_L/E_T, although the frequency ratio for some curves decreases with this parameter. The effects of transverse shear and rotatory inertia for materials of isotropic and glass-epoxy are small compared with those of boron-epoxy and graphite-epoxy with high modulus ratios. These effects reduce the frequency ratio by about 22% and 24.4% for material of BO and GR in Fig. 4.15, respectively. The results in Fig. 4.16 show that the effects of transverse shear and rotatory inertia reduce the frequency ratio by only 1.5% and 3% for material of BO and GR, respectively, due to lower edge restrained stiffnesses K_b and K_i (in this case K_b=K_i=0), which will be discussed in the section 4.4.1.4.

Table 4.12 Values of fundamental linear frequency parameter ω_o in Figs. 4.15-4.16

	ω_o	
Material	Fig. 4.15	Fig. 4.16
ISO	5.7248	2.2329
GL	7.1231	3.2006
BO	10.1658	5.0960
GR	11.8628	6.2858

4.4.1.4 <u>The Effect of Boundary Conditions on the Frequency-Amplitude Response</u>

In this study, the edge boundary conditions of the shell are characterized by the inplane and rotational restrained stiffnesses K_i and K_b and so called elastic supports. Individual effect of inplane and rotational stiffness on the frequency-amplitude response is illustrated for an elastically supported five-layer graphite-epoxy shell in Fig. 4.17 and three-layer boron-epoxy shell in Fig. 4.18, respectively. Figure 4.19 shows the results of a five-layer graphite-epoxy shallow spherical shell for four extreme cases of these stiffnesses. Table 4.13 lists the fundamental linear frequencies in these figures.

Table 4.13 Values of fundamental linear frequency parameter ω_o in Figs. 4.17-4.19

Fig. 4.17		Fig. 4.18		Fig. 4.19		
K_i	ω_o	K_b	ω_o	K_b	K_i	ω_o
0	9.6448	0	7.4986	∞	∞	9.9726
1	10.0477	0.3	7.7809	∞	0	7.5086
5	10.9988	0.5	7.8929	0	∞	8.2458
∞	12.9526	1	8.0597	0	0	5.8693
		5	8.3472			
		∞	8.4737			

In Fig. 4.17, all response curves for a clamped shell exhibit the softening type of nonlinearity. The values of K_i=0 and K_i=∞ correspond to movable and immovable edges, respectively. The frequency ratio neglecting the effects of transverse shear and rotatory inertia decreases with an increase of the amplitude of vibration and the inplane stiffness K_i. It is seen that the ratio at w_{max}=2h is reduced to 0.88 for K_i=5 and 0.77 for K_i=∞. The effects of transverse shear and rotatory inertia decrease with an increase of inplane stiffness K_i at infinitely small amplitude of vibration. These effects reduce the frequency ratio by approximately 6% for all curves in the figure.

The results for the shell with different stiffnesses of edge rotation show that the response curves behave the softening type of nonlinearity except for $K_b=0$, and the frequency ratio neglecting the effect of transverse shear and rotatory inertia increases with an increase of the rotational stiffness, K_b. The values of $K_b=0$ and $K_b=\infty$ correspond to simply-supported and clamped edges, respectively. It is shown in this figure that the frequency ratio reaches at $w_{max}=2h$ to 0.64 for $K_b=0.3$ and 0.55 for $K_b=0$, respectively. The curves for K_b larger than 5 are very close to that given for $K_b=\infty$.

It is observed form Fig. 4.19 that the response curves exhibit the hardening type of nonlinearity for immovable edge shells and initially softening one and then changing to hardening one for movable edge shells. For considering the effects of transverse shear and rotatory inertia, the effect of rotational edge conditions is much noticeable. The effects of transverse shear and rotatory inertia reduce the frequency ratio by 10% to 13% for clamped edge shells and 2% to 4% for simply supported edge shells.

4.4.1.5 The Effect of the Shell Rise on the Frequency-Amplitude Response

Figures 4.20 and 4.21 show the effect of dimensionlessly shell rise, H/h, on the frequency-amplitude response for an elastically supported five-layer graphite-epoxy shallow spherical shell and an immovable clamped three-layer glass-epoxy shallow spherical shell, respectively. The fundamental linear frequencies are listed in Table 4.14. It is seen that the response curves in Fig. 4.20 are the softening type of nonlinearity for dimensionless shell rise H/h=0 and 0.5, the hardening one for H/h=1.5 and 2.0, and the curve for H/h=1 is initially of the softening one and changes to the hardening one at large values of the amplitude. The frequency ratio neglecting the effects of transverse shear and rotatory inertia increases by 36.5% for the shell with H/h=0 (circular plate) and reduces by 15.2% for H/h=2. The frequency ratio including the effects of transverse shear and rotatory inertia is reduced by about 8-10% for all curves.

Table 4.14 Values of fundamental linear frequency parameter ω_o in Figs. 4.20-4.21

Fig. 4.20		Fig. 4.21	
H/h	ω_o	H/h	ω_o
0	7.0388	0	3.9995
0.5	7.4372	1	5.1803
1	8.5200	2	7.9589
1.5	10.0655	4	14.0810
2	11.8905	6	19.8237

It is observed that the response curve is the hardening type of nonlinearity for the value of H/h=0 (circular plate) and the other curves are initially of the softening type behaviour and change to the hardening one at large values of the amplitude for H/h=2,4,6. At w_{max}=2h, the frequency ratio neglecting the effects of transverse shear and rotatory inertia is increased by 63% for the circular plate but reduced by 38% for the shell with H/h=4. The response curves including the effects of transverse shear and rotatory inertia (not shown herein) are close those excluding these effects due to the glass-epoxy matérial with a lower ratio of E_L to E_T.

4.4.1.6 The Effect of Geometrically Initial Imperfections on the Frequency-Amplitude Response

The curves for the effect of the geometrically initial imperfection on the frequency-amplitude response are drawn for an elastically supported seven-layer graphite-epoxy shallow spherical shell in Fig. 4.22 and a movable simply-supported shallow spherical shell in Fig. 4.23. The result for $\bar{W}_1 = 0$ corresponds to that for a perfect laminate. The fundamental linear frequencies are given in Table 4.15. The frequency-amplitude response initially behaves the weak softening type then changes to the hardening type of nonlinearity for the values of $\bar{W}_1$=0 and 0.3 in Fig. 4.22 and $\bar{W}_1 \geq 0$ in Fig. 4.23, and exhibit the behaviours of the hardening type for those $\bar{W}_1$>0.3 in Fig. 4.22 and the softening type for those $\bar{W}_1 < 0$ in Fig. 4.23, respectively. This may arise from the fact that bent-outward type of imperfection increases the shell curvature in Fig. 4.23 while bent-inward type of imperfection reduces the shell curvature in Figs. 4.22 and 4.23. In Fig. 4.22 as the value of imperfection increases, the effects of transverse shear and rotatory inertia reduce the frequency ratio by approximately 10% to 17%, and decrease at infinitely small amplitude of vibration and increase at large amplitude of vibration. It is observed that these effects are noticeable due to the high ratio of material and the low ratio of base radius to shell thickness.

Table 4.15 Values of fundamental linear frequency parameter ω_o in Figs. 4.22-4.23

Fig. 4.22		Fig. 4.23	
$\overline{W}_1$	ω_o	$\overline{W}_1$	ω_o
0	10.7118	-0.6	3.1477
0.3	9.6708	-0.4	3.0638
0.5	9.0865	-0.2	2.9768
1.0	8.2125	0	2.8864
		0.2	2.7922
		0.4	2.6938
		0.6	2.5906
		0.8	2.4820

It is seen from Fig. 4.23 that the frequency ratio at $w_{max} = 2h$ is 0.82 for $\overline{W}_1 = -0.6$ and increases with an increase in the value of $\overline{W}_1$. The ratio reaches to 1.13 for $\overline{W}_1 = 0.8$. The results, including the effects of transverse shear and rotatory inertia (not shown herein), are quite close to those neglecting these effects to the glass-epoxy material with a lower ratio of E_L to E_T.

4.4.1.7 The Effect of Elastic Foundations on the Frequency-Amplitude Response

The results of frequency-amplitude response for the shell resting on elastic foundations are plotted in Figs. 4.24 to 4.26, and the fundamental linear frequencies in these figures are listed in Table 4.16.

Table 4.16 Values of fundamental linear frequency parameter ω_o in Figs. 4.24-4.26

Fig. 4.24		Fig. 4.25		Fig. 4.26
K_f	ω_o	G_f	ω_o	ω_o
0	11.7838	0	8.3418	8.7465
20	12.6039	5	10.1820	
40	13.3738	10	11.7295	
60	14.1017	20	14.3198	

Figure 4.24 shows the effect of linear Winkler elastic foundation on frequency-amplitude response of an immovable clamped graphite-epoxy shallow spherical shell. All response curves in the figure exhibit the hardening type of nonlinearity, and the nonlinear frequency increases with the linear Winkler parameter K_f. The frequency ratio for $T_S = 0$ and $R_I = 0$ is increased approximately by 24%, 21%, 19% and 18% at $w_{max} = 2h$ for $K_f = 0$, 20, 40 and 60 respectively. It is noted that the effects of transverse shear and rotatory inertia reduce the frequency ratio by approximately 6%

compared with the corresponding ratio with neglecting these effects. In Fig. 4.25, the frequency ratio for a movable clamped shallow spherical shell on an elastic foundation is plotted against the relative amplitude of vibration for different values of Pasternak foundation parameter G_f. The ratio in the figure decreases as the parameter G_f increases when $G_f > 0$. The ratio for $G_f = 0$ is lower in the range of value of $w_{max} < h$, and higher in the range of value of $h < w_{max} < 2h$, than that for $G_f > 0$ in the corresponding ranges of relative amplitude value. Actually, the nonlinear frequency for $G_f > 0$ is larger than those for $G_f = 0$ since the corresponding linear frequencies shown in Table 4.13 for $G_f > 0$ are much larger than that for $G_f = 0$. In addition, the effects of transverse shear and rotatory inertia reduce the frequency ratio by approximately 2% to 5% for different values of G_f. Figure 4.26 depicts the frequency-amplitude response curves of an elastically supported shallow spherical shell with different values of nonlinear Winkler foundation parameter K_n. The curves in the figure behave initially the softening type and then reverts to the hardening type of nonlinearity for $K_n \leq 10$ and behave the hardening type of nonlinearity for $K_n = 20$. For $K_n = 20$, the frequency ratio at $w_{max} = 2h$ reaches 1.34 when the effects of transverse shear and rotatory inertia are not taken into consideration, and 1.22 when these effects are taken into account. Similarly as mentioned above, the effects of transverse shear and rotatory inertia reduced the frequency ratio. It is worth noting from Table 4.13 that the linear frequency parameter, $\omega_{o,}$ for different nonlinear Winkler parameter, K_n, is the same since the ω_o is not affected by nonlinear terms in the governing equations.

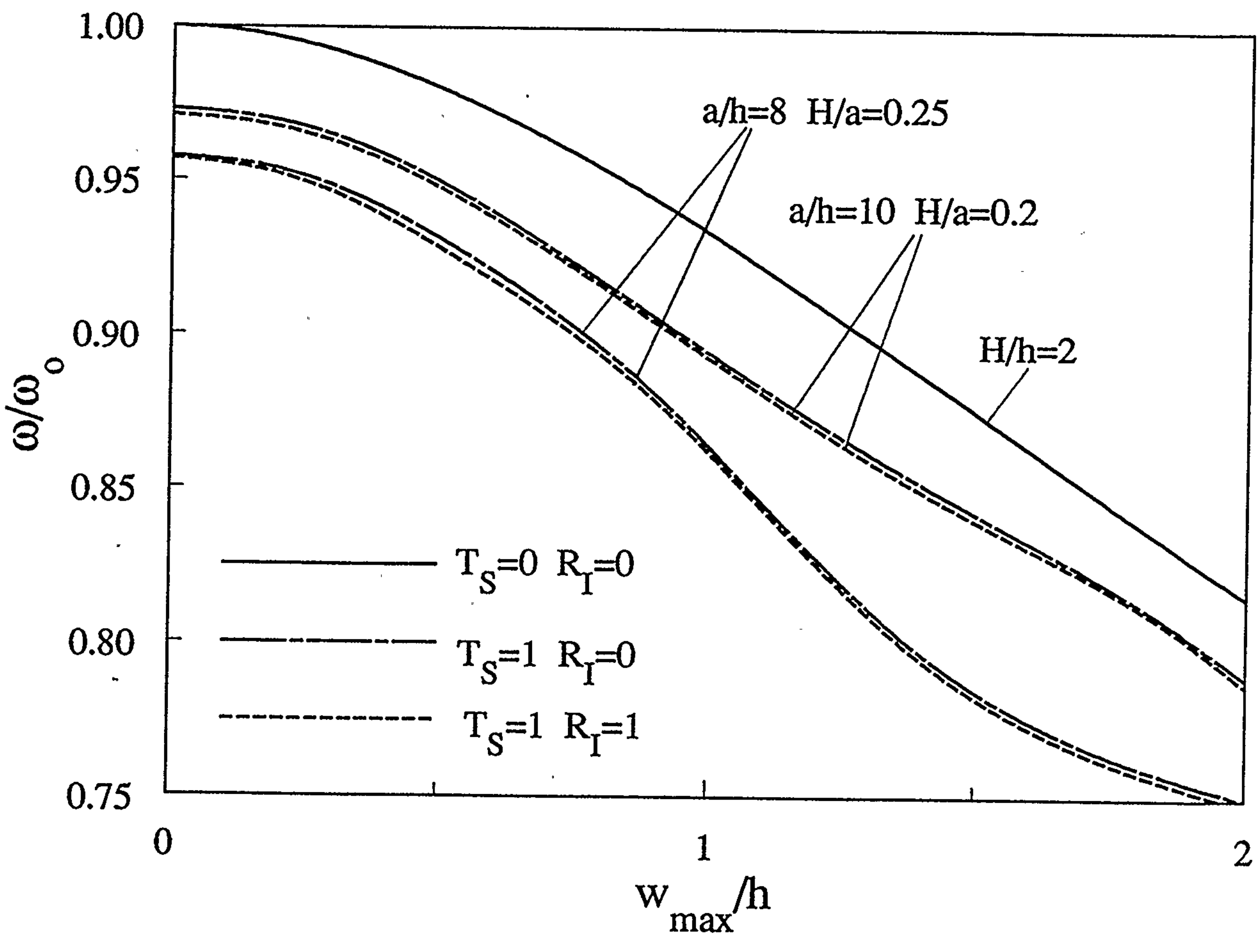

Figure 4.10: Individual effect of transverse shear and rotatory inertia on the frequency-amplitude response of a movable simply-supported five-layer graphite-epoxy shallow spherical shell

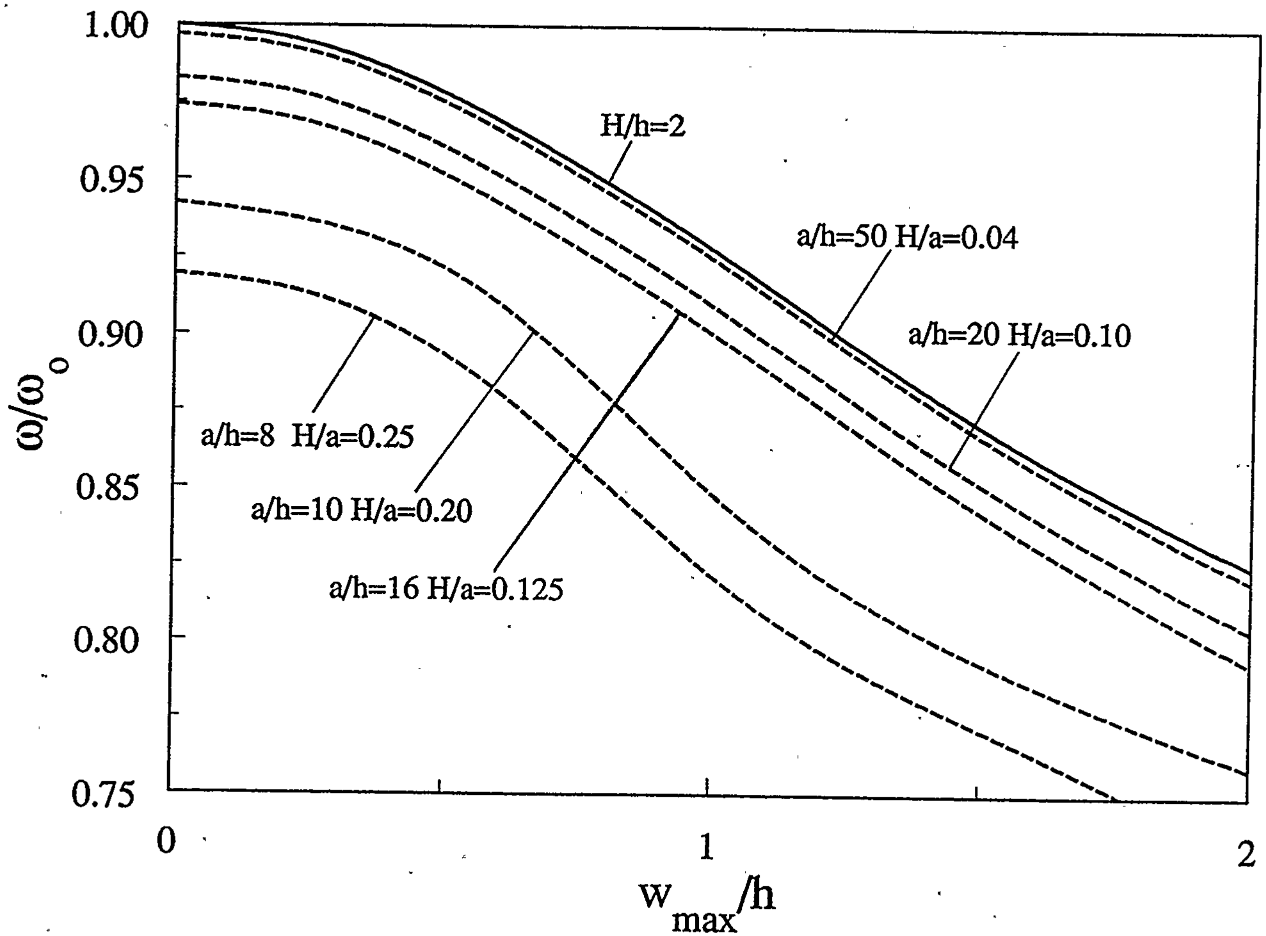

Figure 4.11: Effect of the base radius-to-thickness ratio on the frequency-amplitude response of a movable clamped three-layer graphite-epoxy shallow spherical shell

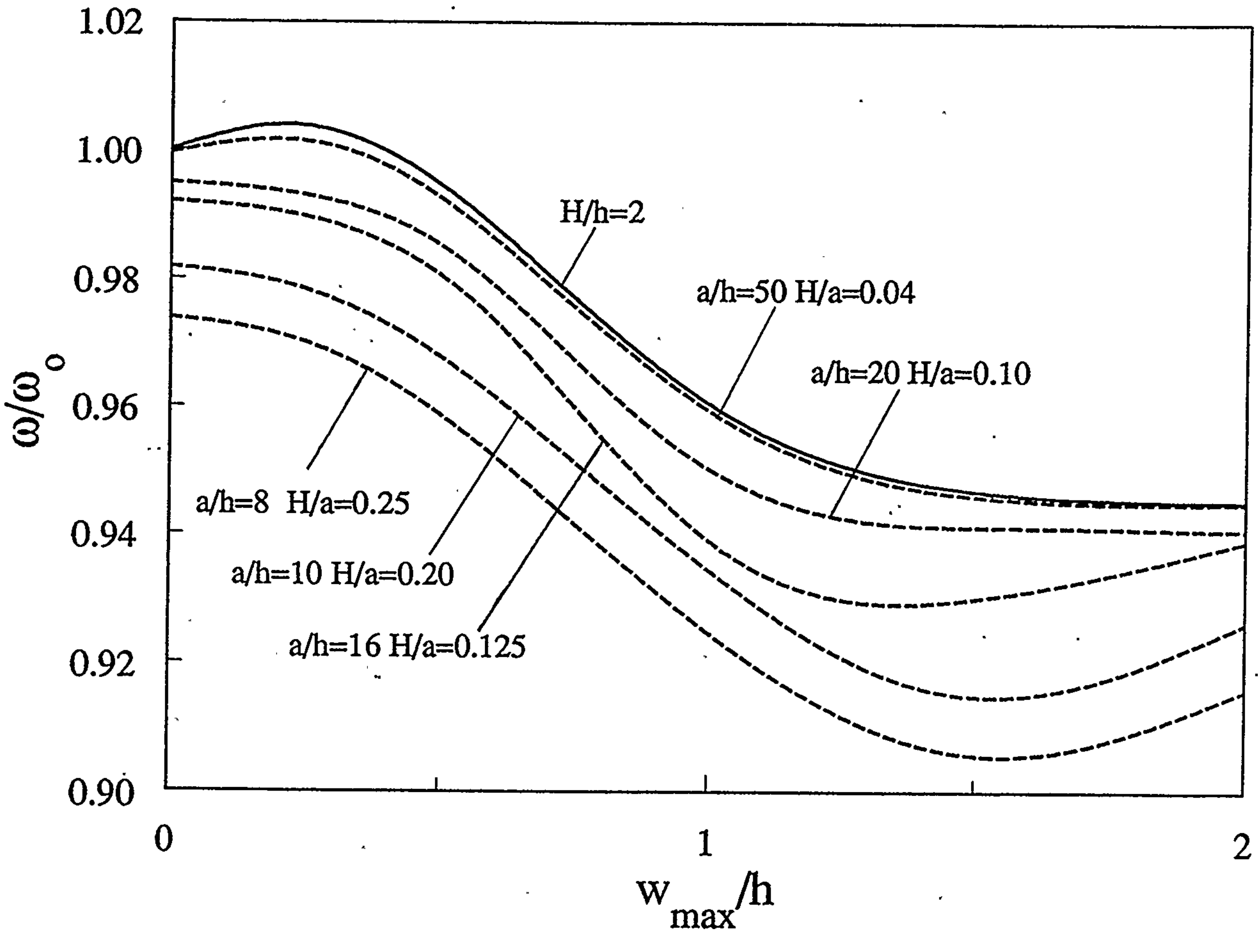

Figure 4.12: Effect of the base radius-to-thickness ratio on the frequency-amplitude response of an immovable clamped five-layer boron-epoxy shallow spherical shell resting on elastic foundation ($\bar{W}_1$=0.2, K_f=10, K_n=10, G_f=5)

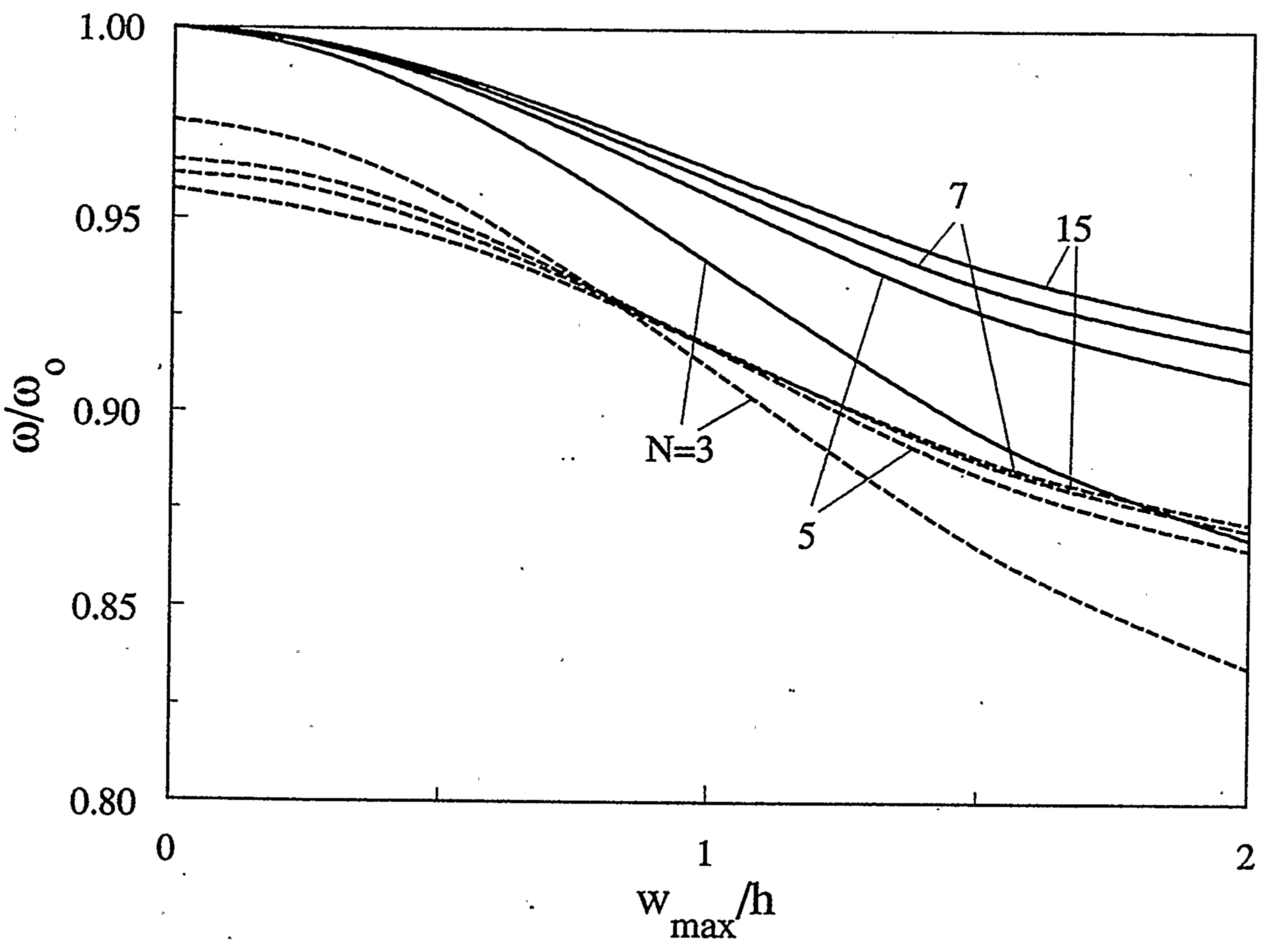

Figure 4.13: Effect of the number of layers on the frequency-amplitude response of an elastically supported boron-epoxy shallow spherical shell (K_b=5, K_i=0, a/h=12, H/a=0.15)

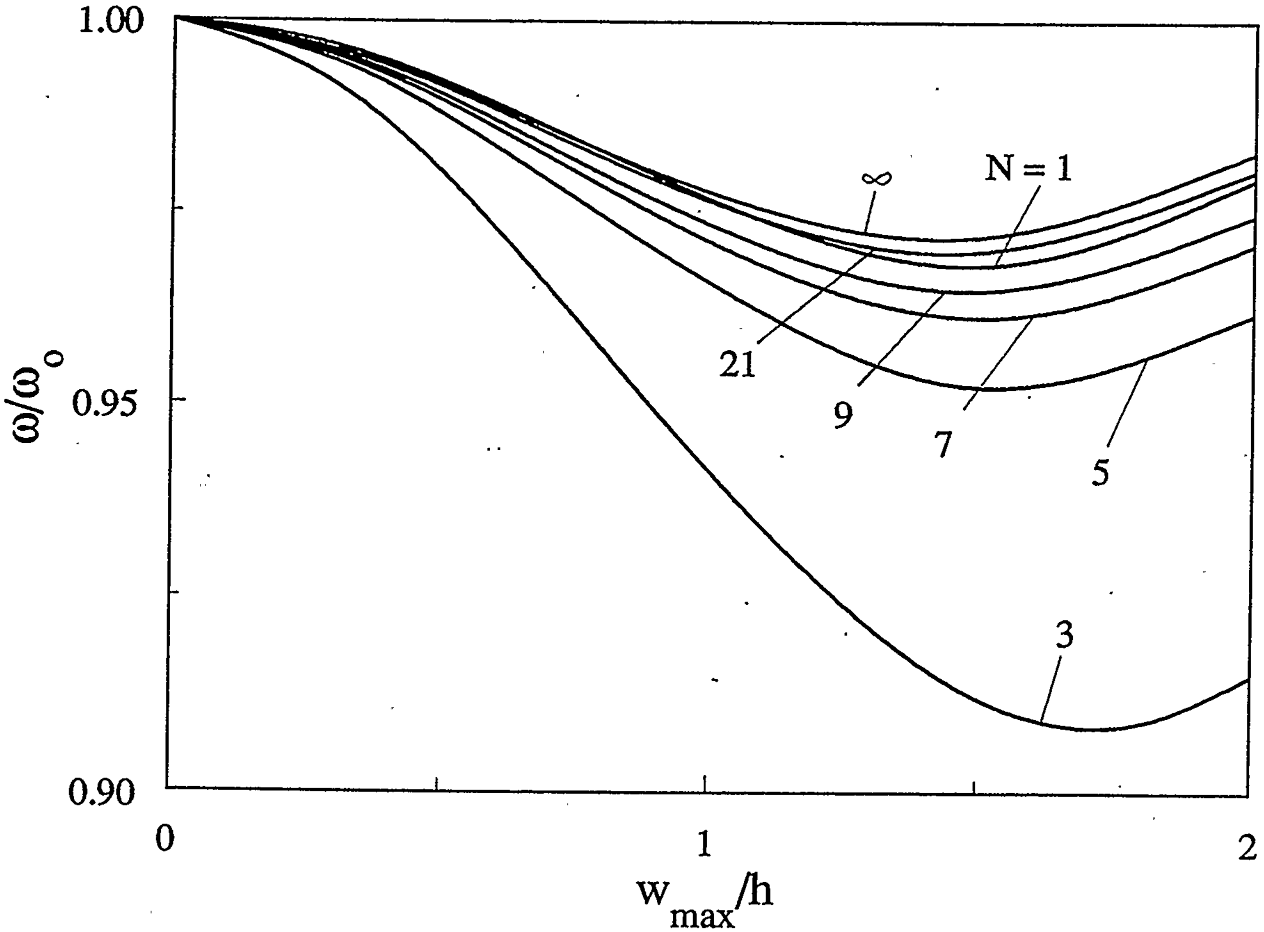

Figure 4.14: Effect of the number of layers on the frequency-amplitude response of a movable clamped graphite-epoxy shallow spherical shell (a/h=15, H/a=0.1)

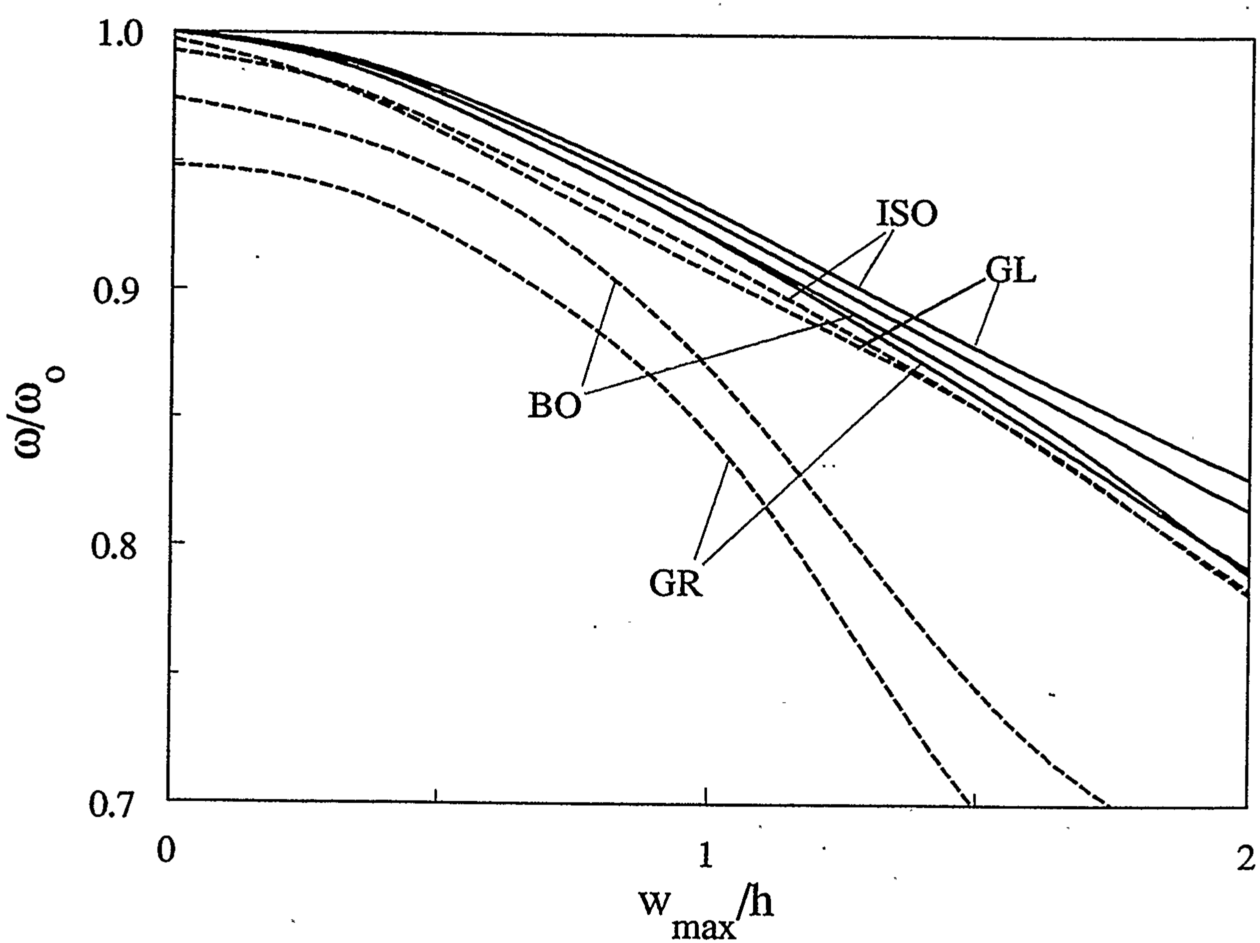

Figure 4.15: Effect of material properties on the frequency-amplitude response of an elastically supported five-layer shallow spherical shell (a/h=10, H/a=0.2)

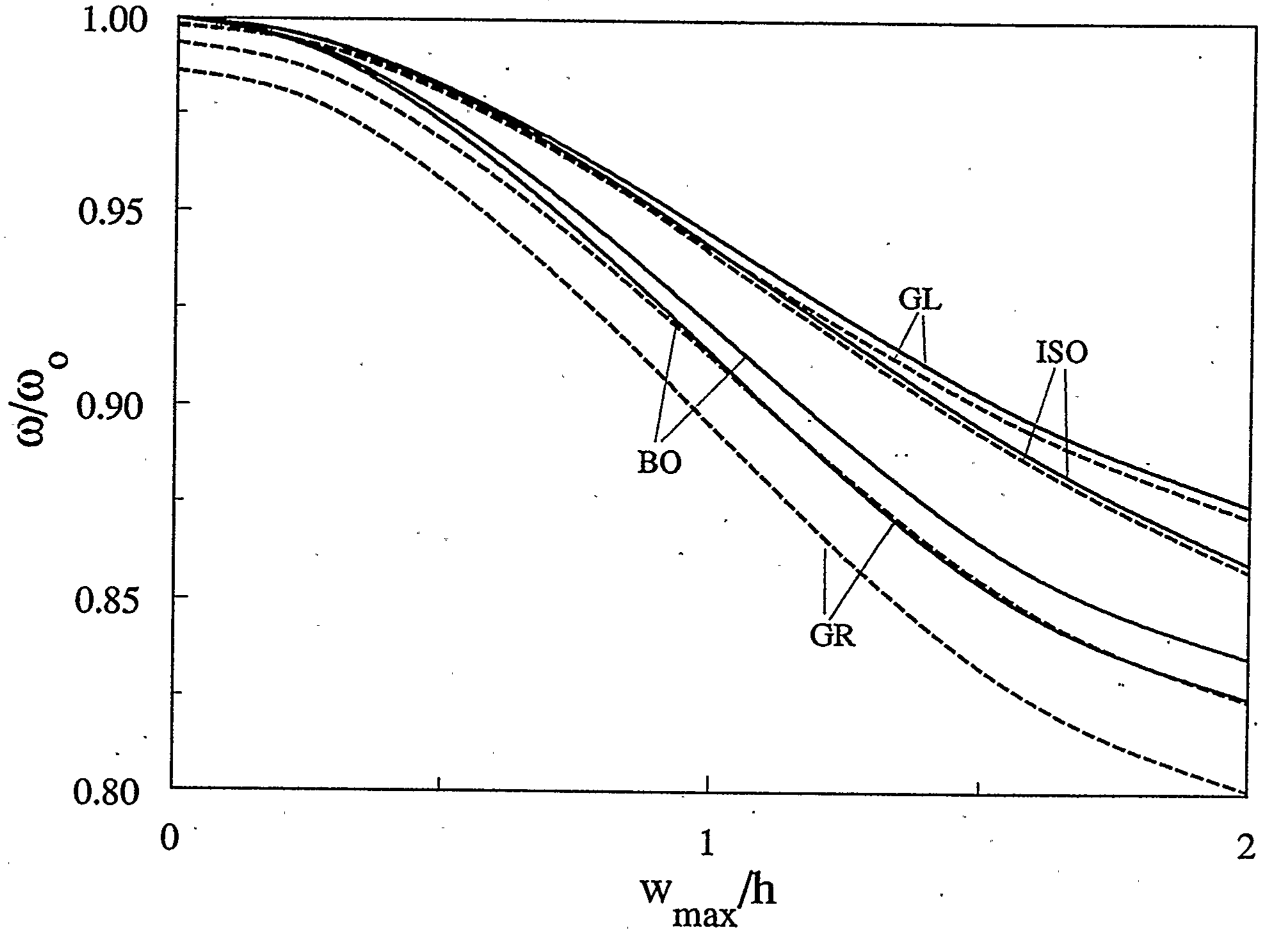

Figure 4.16: Effect of material properties on the frequency-amplitude response of a movable simply-supported three-layer shallow spherical shell (a/h=15, H/a=0.1)

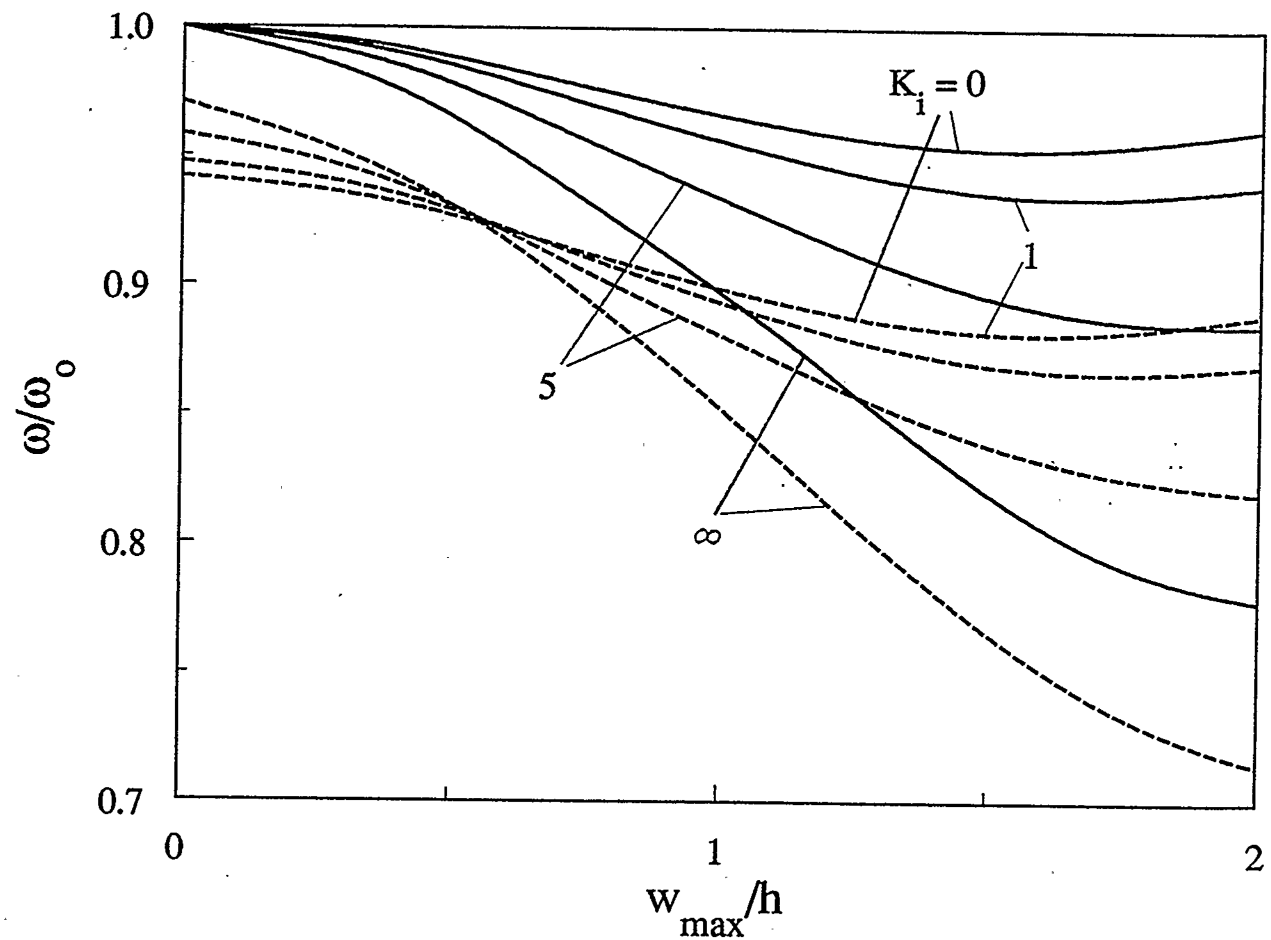

Figure 4.17: Effect of inplane edge stiffness on the frequency-amplitude response of a clamped five-layer graphite-epoxy shallow spherical shell (a/h=15, H/a=0.1)

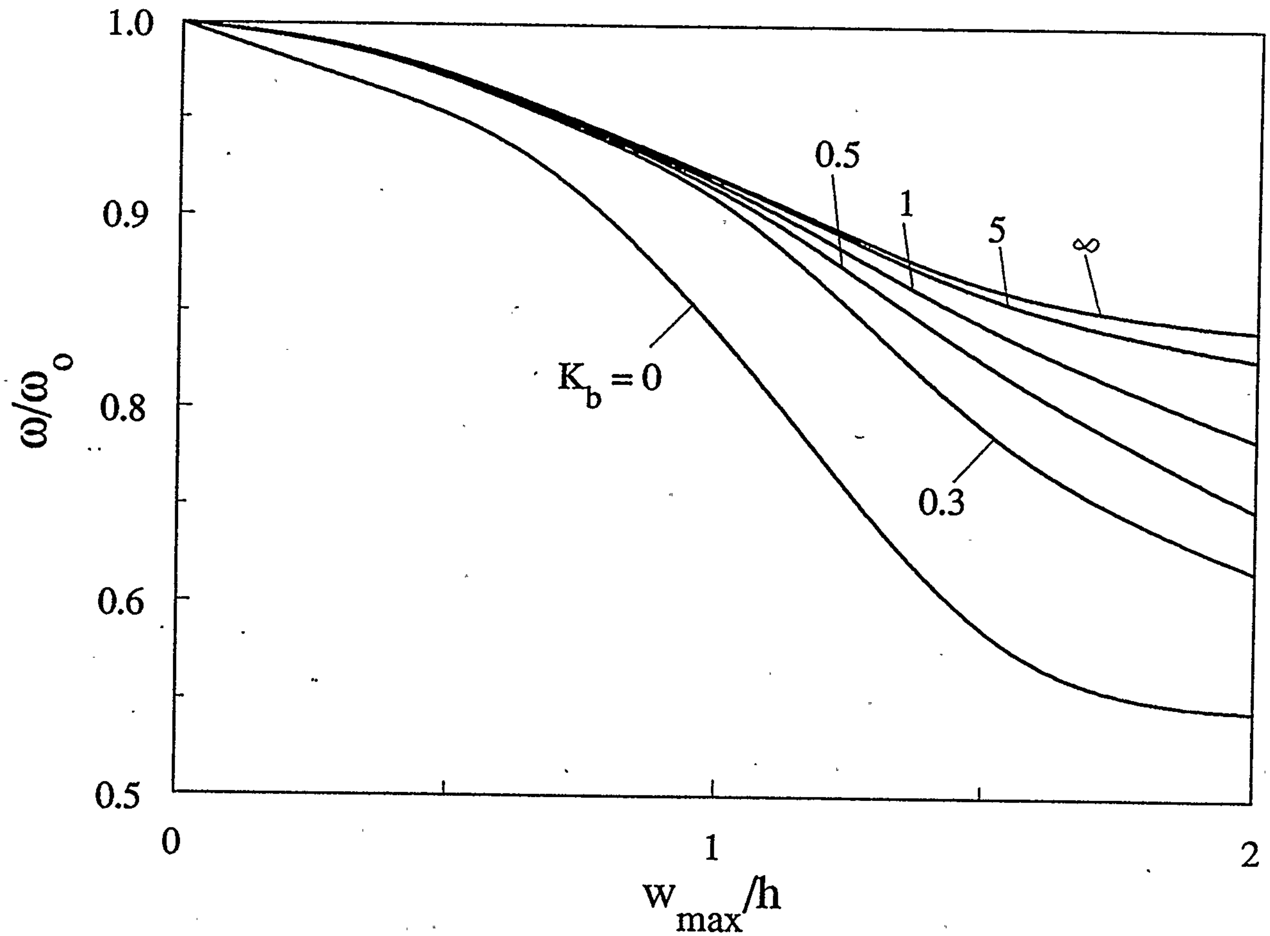

Figure 4.18: Effect of rotational edge stiffness on the frequency-amplitude response of an elastically supported three-layer boron-epoxy shallow spherical shell (K_i=5, a/h=10, H/a=0.15)

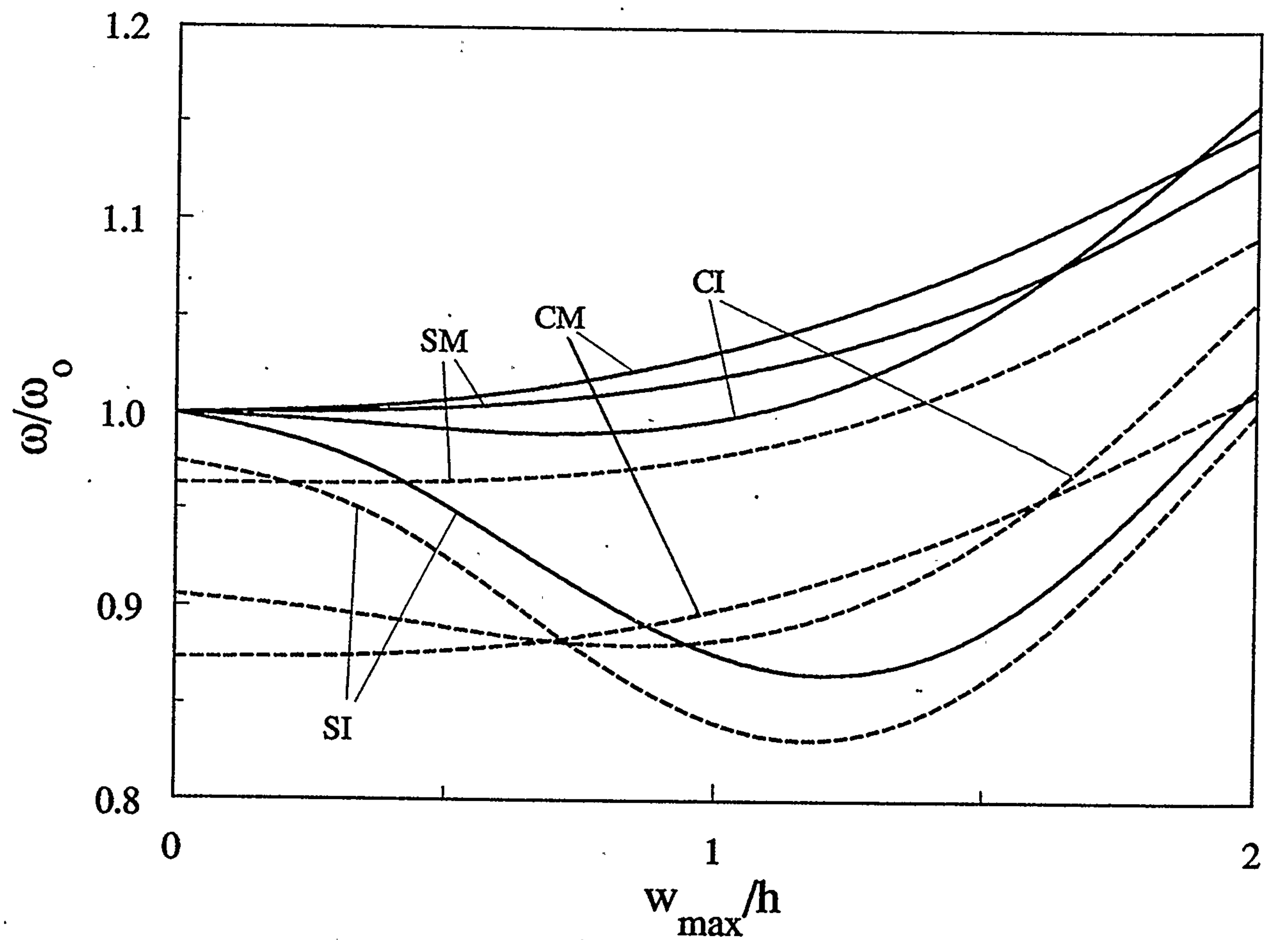

Figure 4.19: Effect of boundary conditions on the frequency-amplitude response of a five-layer graphite-epoxy imperfect shallow spherical shell resting on elastic foundations ($\overline{W}_1$=0.3, K_f=2, K_n=2, G_f=1, a/h=10, H/a=0.1)

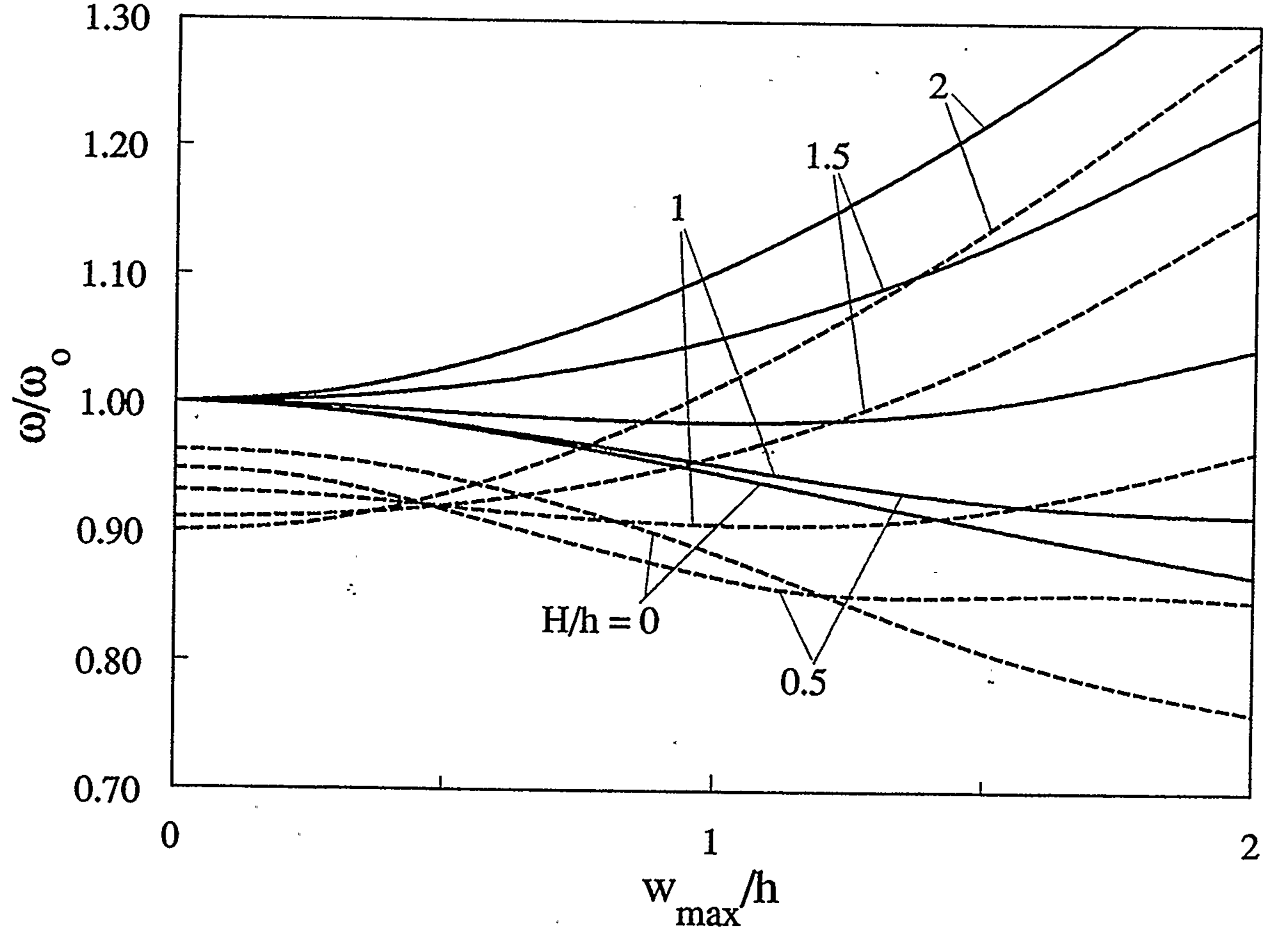

Figure 4.20: Effect of the shell rise on the frequency-amplitude response of an elastically supported five-layer graphite-epoxy shallow spherical shell resting on elastic foundations (K_b=2, K_i=3, K_f=2, K_n=2, G_f=1.5, a/h=10)

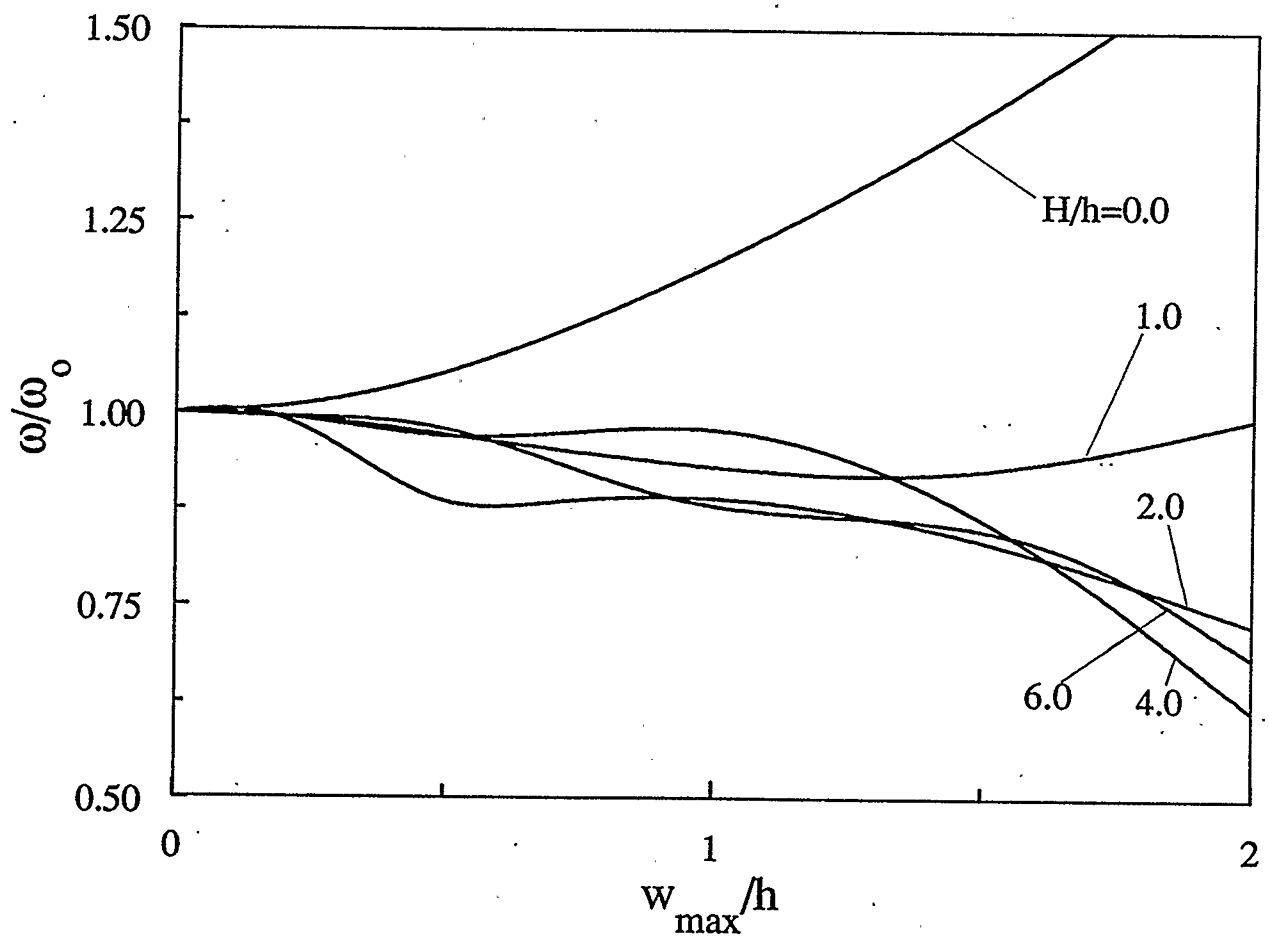

Figure 4.21: Effect of the shell rise on the frequency-amplitude response of an immovable clamped three-layer glass-epoxy shallow spherical shell (a/h=25)

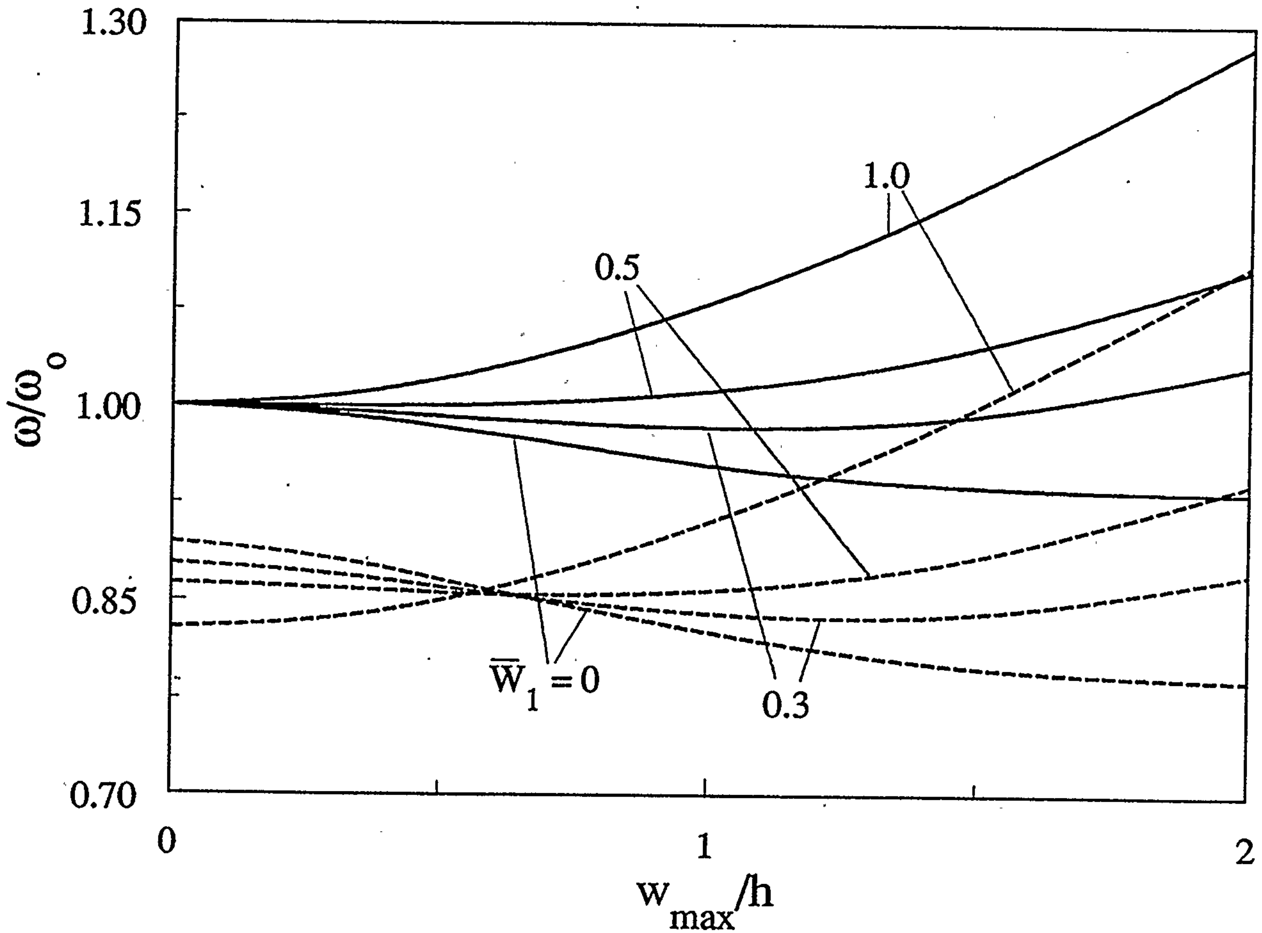

Figure 4.22: Effect of geometrically initial imperfection on the frequency-amplitude response of an elastically supported seven-layer graphite-epoxy shallow spherical shell ($K_b=\infty$, $K_i=2$, $a/h=10$, $H/a=0.15$)

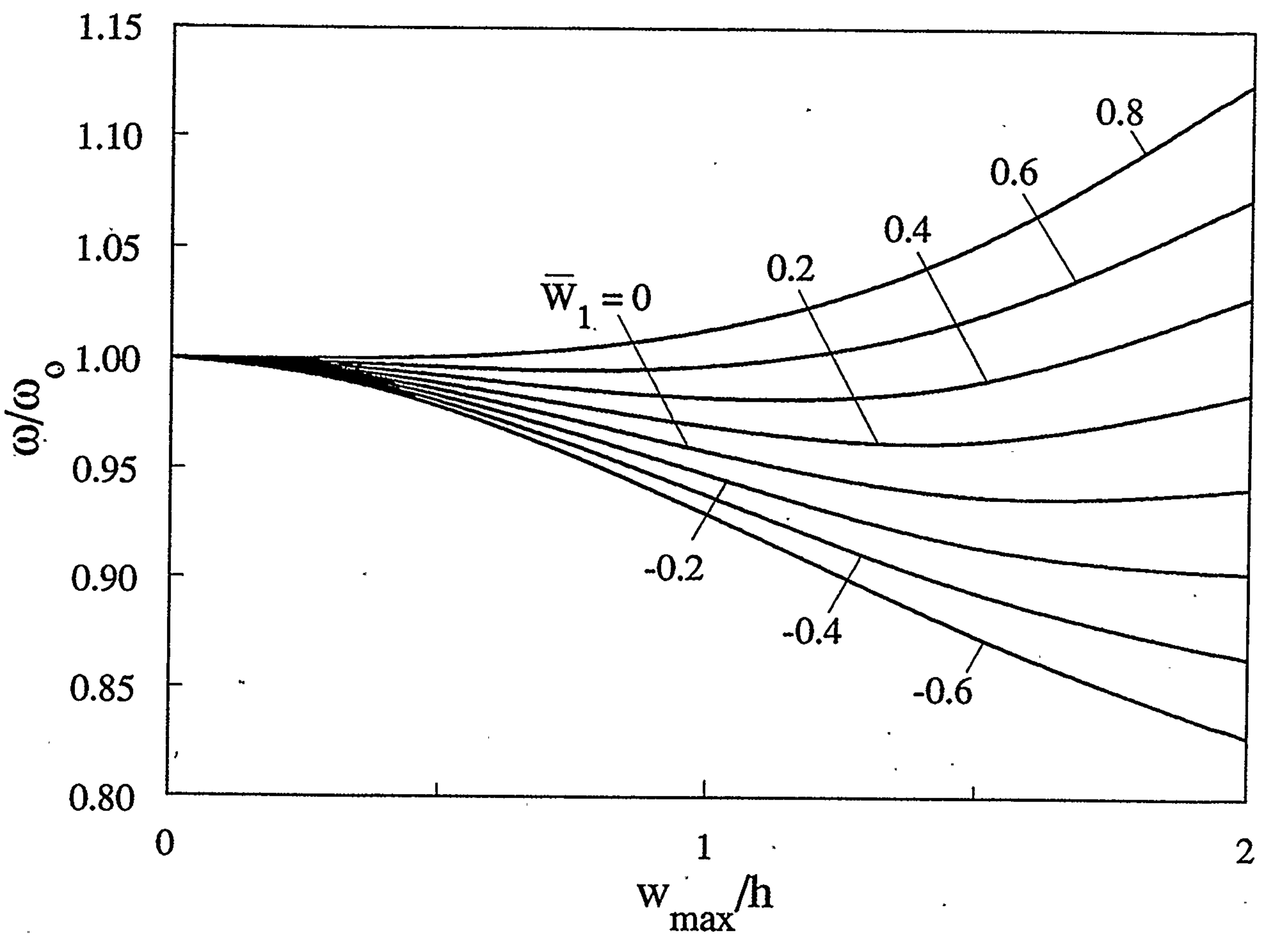

Figure 4.23: Effect of geometrically initial imperfection on the frequency-amplitude response of a movable simply-supported three-layer glass-epoxy shallow spherical shell (a/h=12, H/a=0.1)

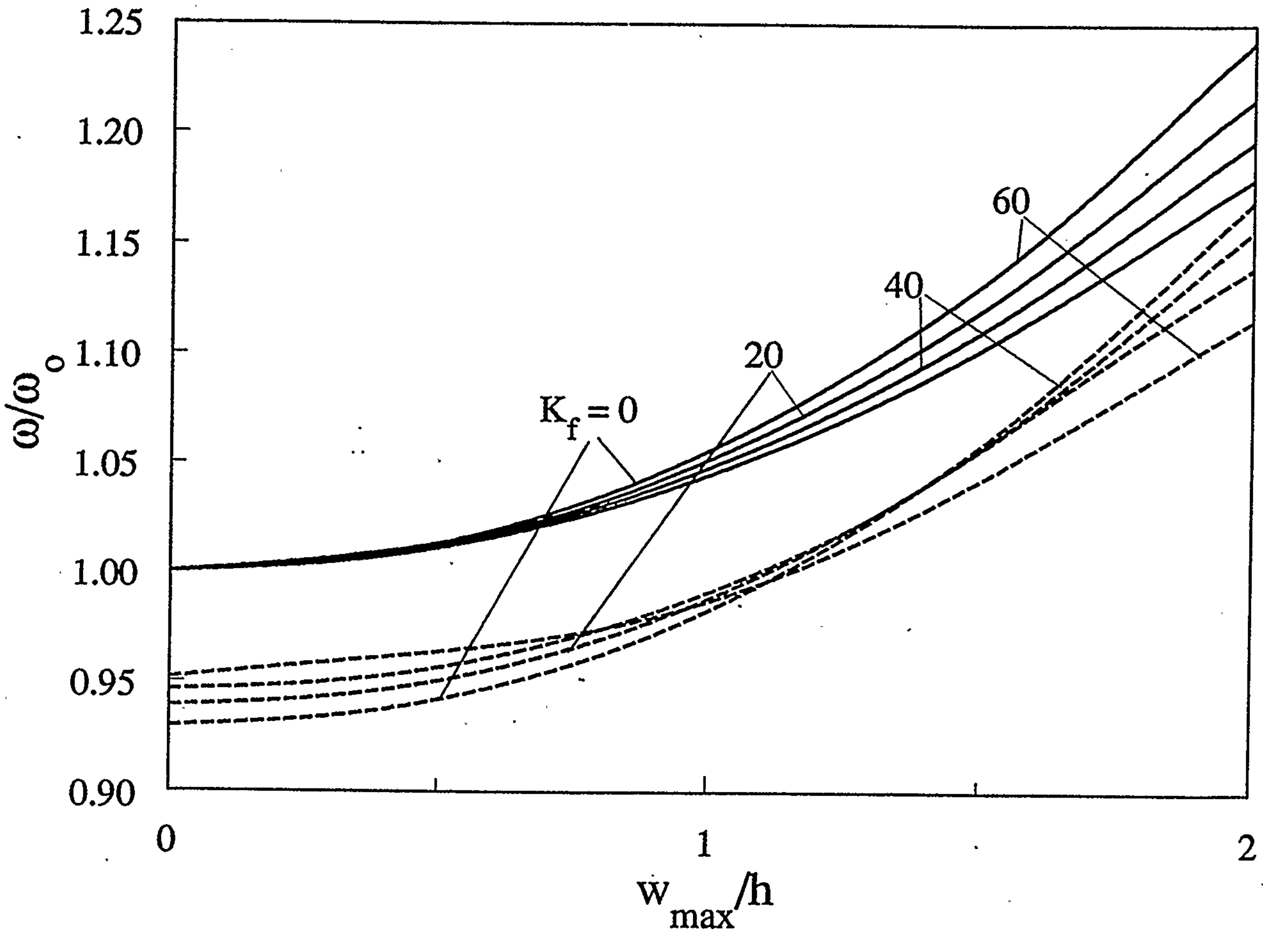

Figure 4.24: Effect of Winkler foundation parameter on the frequency-amplitude response of an immovable clamped five-layer graphite-epoxy shallow spherical shell (K_n=5, G_f=10, a/h=10, H/a=0.05)

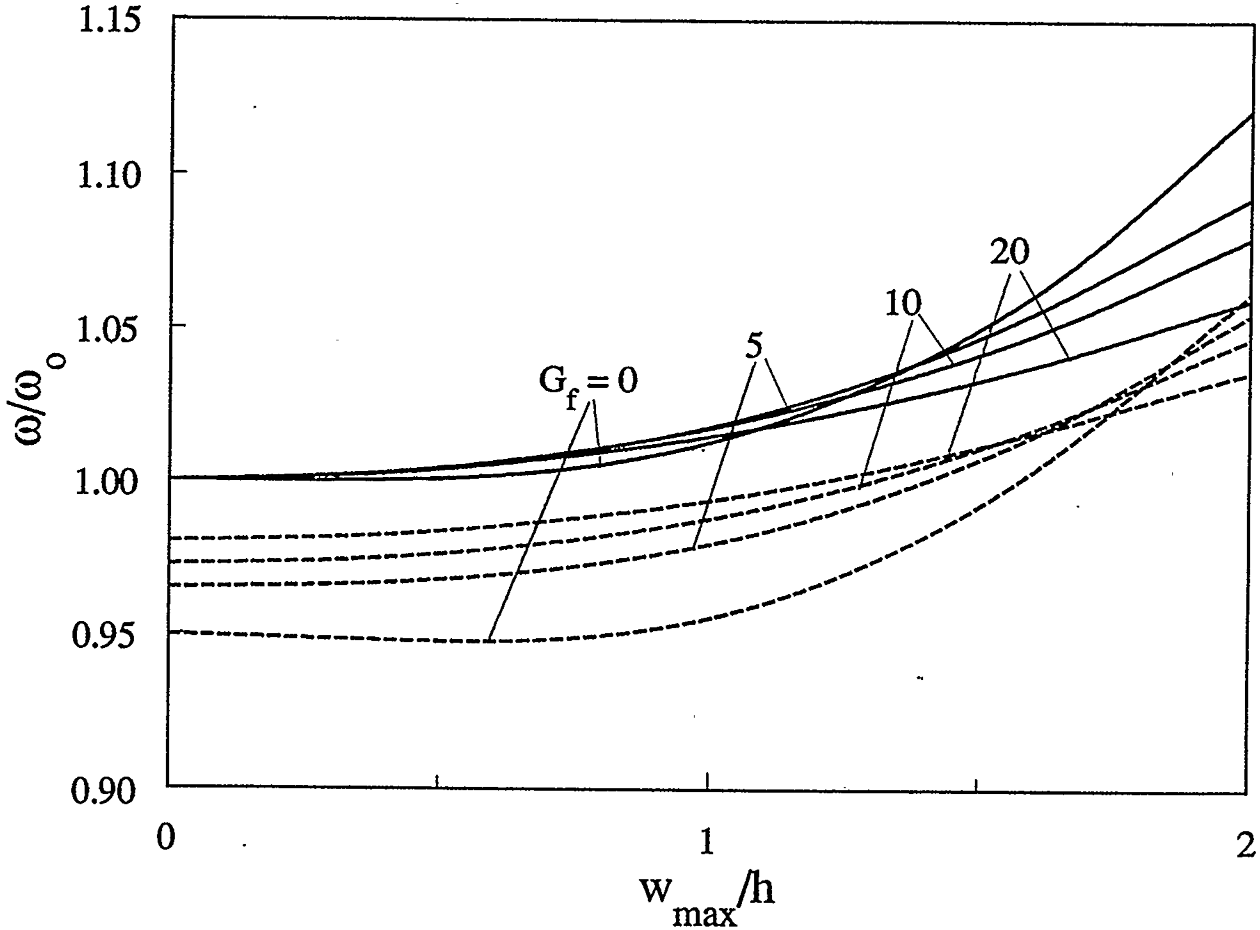

Figure 4.25: Effect of Pasternak foundation parameter on the frequency-amplitude response of a movable clamped five-layer boron-epoxy imperfect shallow spherical shell ($\bar{W}_1$=0.1, K_f=10, K_n=10, a/h=10, H/a=0.15)

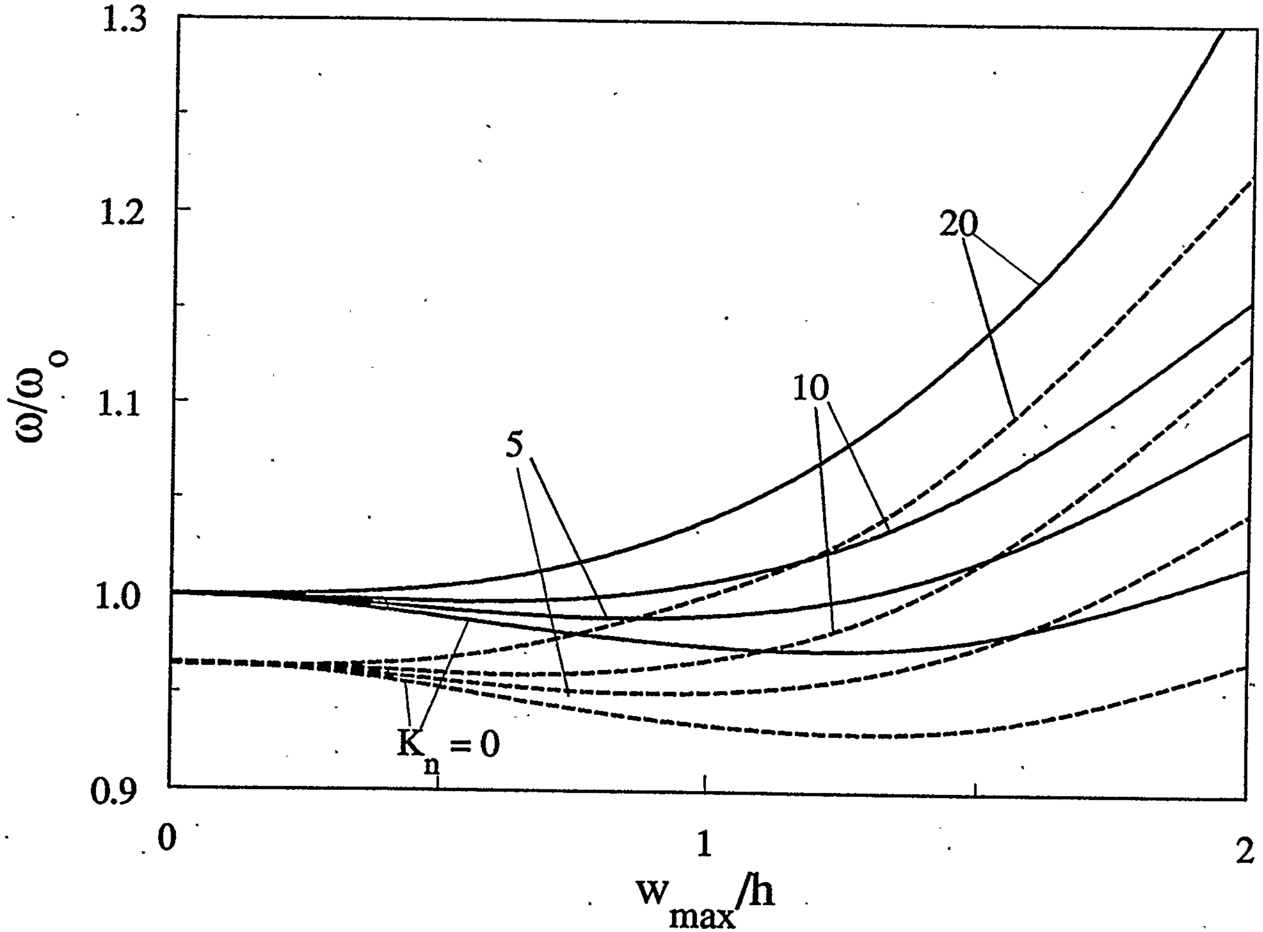

Figure 4.26: Effect of nonlinear Winkler foundation parameter on the frequency-amplitude response of an elastically supported three-layer graphite-epoxy imperfect shallow spherical shell (K_b=2, K_i=3, $\overline{W}_1$=0.2, K_f=5, G_f=2, a/h=12, H/a=0.1)

4.4.2 Symmetrically Laminated Circular Plates

In this section, numerical results are presented for the nonlinear vibration of symmetrically laminated circular plates which are the special cases of shallow spherical shells with the initial rise of the shell equal to zero. All curves of frequency-amplitude response, generally, behave the hardening type of nonlinearity. The fundamental linear frequencies in the figures of this section are listed in Tables 4.17 and 4.18.

4.4.2.1 The Effect of the Radius-to-Thickness Ratio on the Frequency-Amplitude Response

Figure 4.27 shows the effect of the ratio of radius-to-thickness on the frequency-amplitude response of an immovable clamped five-layer graphite-epoxy circular plate. It is observed from the figure that the effects of transverse shear and rotatory inertia are very dominant for thicker circular plates, i.e., low values of a/h. These effects reduce the nonlinear frequency at infinitely small amplitude of vibration as much as 40% for a/h=5. This reduction decreases with an increase in the ratio of radius-to-thickness and the amplitude of vibration. The response curves for the ratio of a/h larger than 20 and the amplitude larger than h are very close that given by neglecting these effects. Due to the nonlinearity, the frequency ratio in the range of value of amplitude 0 to 2h is raised by 65% from 1.0 to 1.65, 84%

from 0.83 to 1.53 and 133% from 0.6 to 1.40 for the thin shell(i.e., $T_S=R_I=0$), the shell with a/h=10 and 5, respectively.

Table 4.17 Values of fundamental linear frequency parameter ω_o in Figs. 4.27-4.31

Fig. 4.27	Fig. 4.28		Fig. 4.29		Fig. 4.30		Fig. 4.31		
ω_o	N	ω_o	Mat	ω_o	K_b	ω_o	K_b	K_i	ω_o
7.6030	1	2.1975	ISO	2.9858	0	4.1082	∞	∞	6.1781
	3	2.1989	GL	3.8951	2	5.6039	∞	0	6.1781
	5	2.1644	BO	5.9008	10	6.0293	0	∞	4.1082
	7	2.1226	GR	7.0248	∞	6.1781	0	0	4.1082
	9	2.0908							
	15	2.0348							
	21	2.0061							
	∞	1.9418							

Table 4.18 Values of fundamental linear frequency parameter ω_o in Figs. 4.32-4.35

Fig. 4.32		Fig. 4.33		Fig. 4.34		Fig. 4.35
W_1	ω_o	K_f	ω_o	G_f	ω_o	ω_o
0	2.1644	0	11.4470	0	7.9250	5.7599
0.2	2.1843	20	12.2896	5	9.8610	
0.4	2.2429	40	13.0780	10	11.4658	
0.6	2.3363	60	13.8215	20	14.1245	
0.8	2.4597					
1.0	2.6073					

4.4.2.2 The Effect of the Number of Layers on the Frequency-Amplitude Response

The effect of number of layers on the frequency-amplitude response is presented for an immovable clamped glass-epoxy circular plate in Fig. 4.28. The frequency ratio increases as the number of layers increases, and the ratio is smoothly raised as N larger than 3. It is shown that at w_{max}=2h, the ratio reaches to 2.02 for N=1(orthotropic), 2.31 for N=3 and 2.56 for N=∞, respectively. The effect of number of layers is not significant when N is value of range of 5 to 21. It is noted that from Table 4.17 that the fundamental linear frequency decreases with an increase in the number of layer except for N=3. The effects of transverse shear and rotatory inertia (not shown herein) are very small as the plate with low material ratio and high ratio of radius-to-thickness.

4.4.2.3 The Effect of Material Properties on the Frequency-Amplitude Response

The response curves for an elastically supported seven-layer circular plate with different material are depicted in Fig. 4.29. The frequency ratio for neglecting effects of transverse shear rotatory shows increasing slightly with an increase in modulus ratio, E_L/E_T, but no much difference among these curves although effect of material properties on the corresponding fundamental linear frequencies shown in Table 4.17 are pronounced. As expected, the effects of transverse shear and rotatory inertia increase when the modulus ratio is raised and reduce the frequency ratio by 3%, 4%, 12% and 22% for the material ISO, GL, BO and GR, respectively.

4.4.2.4 The Effect of Boundary Condition on the Frequency-Amplitude Response

The response of the frequency-amplitude for an elastically supported three-layer graphite-epoxy circular plate is illustrated in Fig. 4.30. In the figure the curves for K_b=0 and ∞ are those for simply supported and clamped edges respectively. The frequency ratio decreases as the rotational stiffness K_b increases. The curve for K_b=10 is very close to that for $K_b=\infty$, a clamped plate. The nonlinear frequency for T_s=0 and R_i=0 is increased approximately by 147 and 89 percent at w_{max}=2h for simply supported (K_b=0) and clamped ($K_b = \infty$) edges, respectively. In addition the effects of transverse shear and rotatory inertia reduce the frequency ratio by 4.0, 5.2, 6.1 and 6.4 percent at w_{max}=2h for K_b=0, 2, 10 and ∞ respectively.

Figure 4.31 shows the frequency-amplitude response curves of a three-layer graphite-epoxy circular plate for four extreme cases. It is noted that the nonlinear frequency increases more quickly for immovable edges than movable edges and that the effects of transverse shear and rotatory inertia are more significant for clamped edges than simply supported edges.

4.4.2.5 The Effect of Geometrically Initial Imperfections on the Frequency-Amplitude Response

The curves for the effect of the geometrically initial imperfection on the frequency-amplitude response of a movable simply-supported circular plate are shown in Fig. 4.32 The results for $\overline{W}_1 = 0$ corresponding to that for a perfect plate. The frequency-amplitude response behaves the hardening type of nonlinearity for $\overline{W}_1 = 0$, 0.2, 0.4 and 0.6, and initially the weak softening type then changing to the hardening type of nonlinearity for $\overline{W}_1 = 0.8$ and 1.0. This may arise from the fact that the larger values of initial imperfection increase the plate curvature. It is seen that the frequency ratio at $w_{max} = 2h$ is 1.35 for $\overline{W}_1 = 0$ and 1.27 for $\overline{W}_1 = 1.0$. Actually,the nonlinear frequency increases with increasing the value of $\overline{W}_1$ since the corresponding linear frequencies shown in Table 4.18 increase more quickly. The results, including the effects of transverse shear and rotatory inertia (not shown herein), are quite close to those neglecting these effects in Fig. 4.32 due to the glass-epoxy material with a lower ratio of E_L to E_T.

4.4.2.6 The Effect of Elastic Foundations on the Frequency-Amplitude Response

The ratio of nonlinear frequency ω to the corresponding linear frequency ω_o is illustrated in Figs. 33-35 against the relative amplitude w_{max}/h of the vibration of laminated plates for various foundation parameters. Figure 4.33 shows the effect of linear Winkler elastic foundation on frequency-amplitude response of an elastically supported circular plate. The frequency ratio for $T_S = 0$ and $R_I = 0$ is increased approximately by 24%, 21%, 19% and 17% at $w_{max} = 2h$ for $K_f = 0$, 20, 40 and 60, respectively. Referring to the linear frequency in Table 4.18, it is seen that the nonlinear frequency increases with the linear Winkler parameter K_f. The effects of transverse shear and rotatory inertia reduce the frequency ratio by approximately 3-4% compared with the corresponding ratio with neglecting these effects. In Fig. 4.34, the frequency ratio for a movable clamped circular plate on elastic foundation is given for different values of Pasternak foundation parameter G_f. The ratio neglecting the effects of transverse shear and rotatory inertia in the figure decreases as G_f increases. And the ratio considering these effects increases in the range of $0 < w_{max} < h$ and decreases in the range of $h < w_{max} < 2h$ with increasing G_f. In addition, the effects of transverse shear and rotatory inertia reduce the frequency ratio by 5-10% for different values of G_f. Figure 4.35 depicts the frequency-amplitude response curves of an elastically supported circular plate with different values of nonlinear Winkler foundation parameter K_n. The frequency ratio increases with an increase of K_n. At $w_{max} = 2h$, the ratio reaches to 1.41, 1.52, 1.62 and 1.71 ($T_S = 0$, $R_I = 0$) and to 1.35, 1.46, 1.56 and 1.66 ($T_S = 1$, $R_I = 1$) for $K_n = 0$, 5, 10 and 15, respectively. It is worth noting from Table 4.18 that the linear frequency parameter, ω_o, for different values of K_n is the same since the ω_o is not affected by the nonlinear terms in the governing equations.

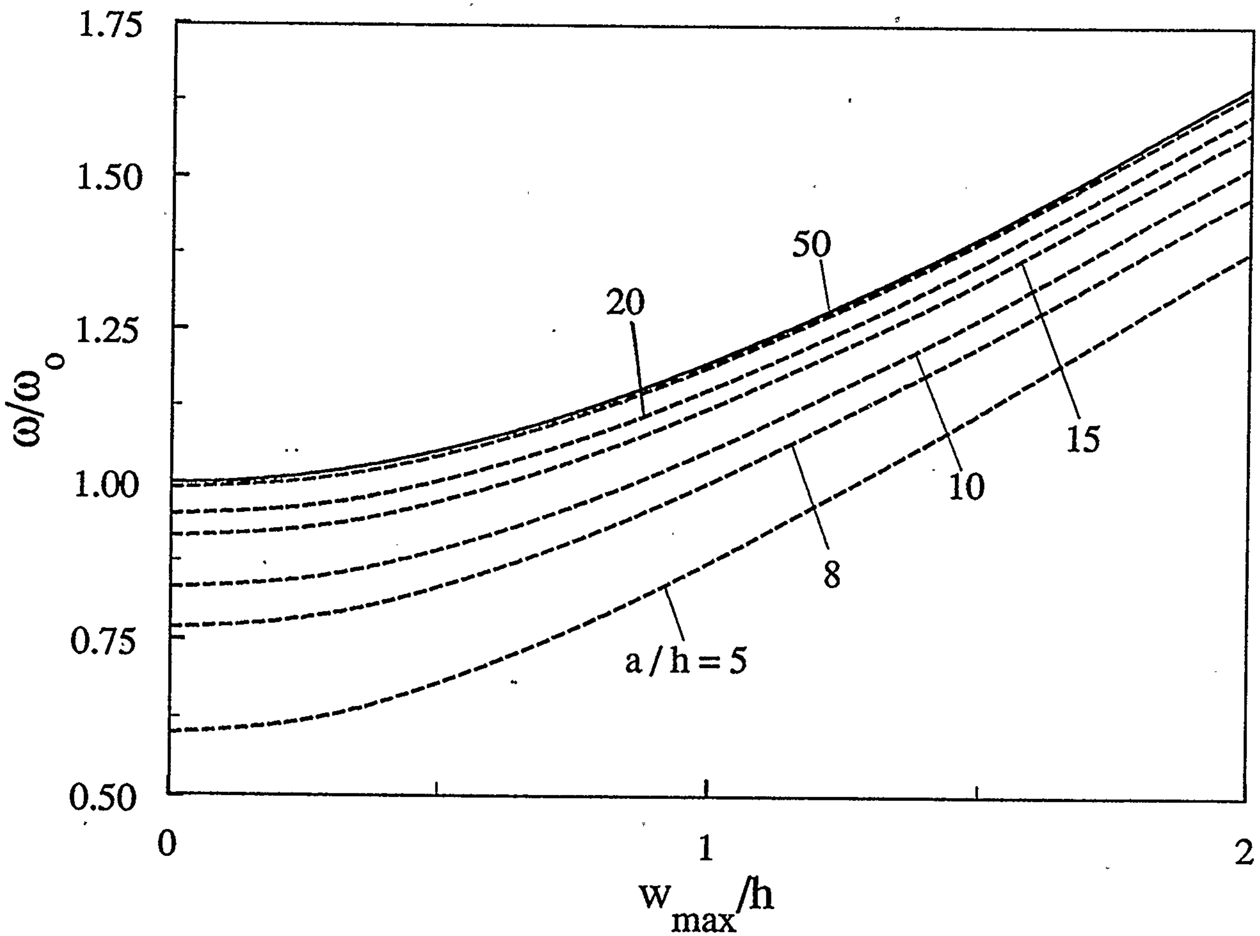

Figure 4.27: Effect of the base radius-to-thickness ratio on the frequency-amplitude response of an immovable clamped five-layer graphite-epoxy circualr plate

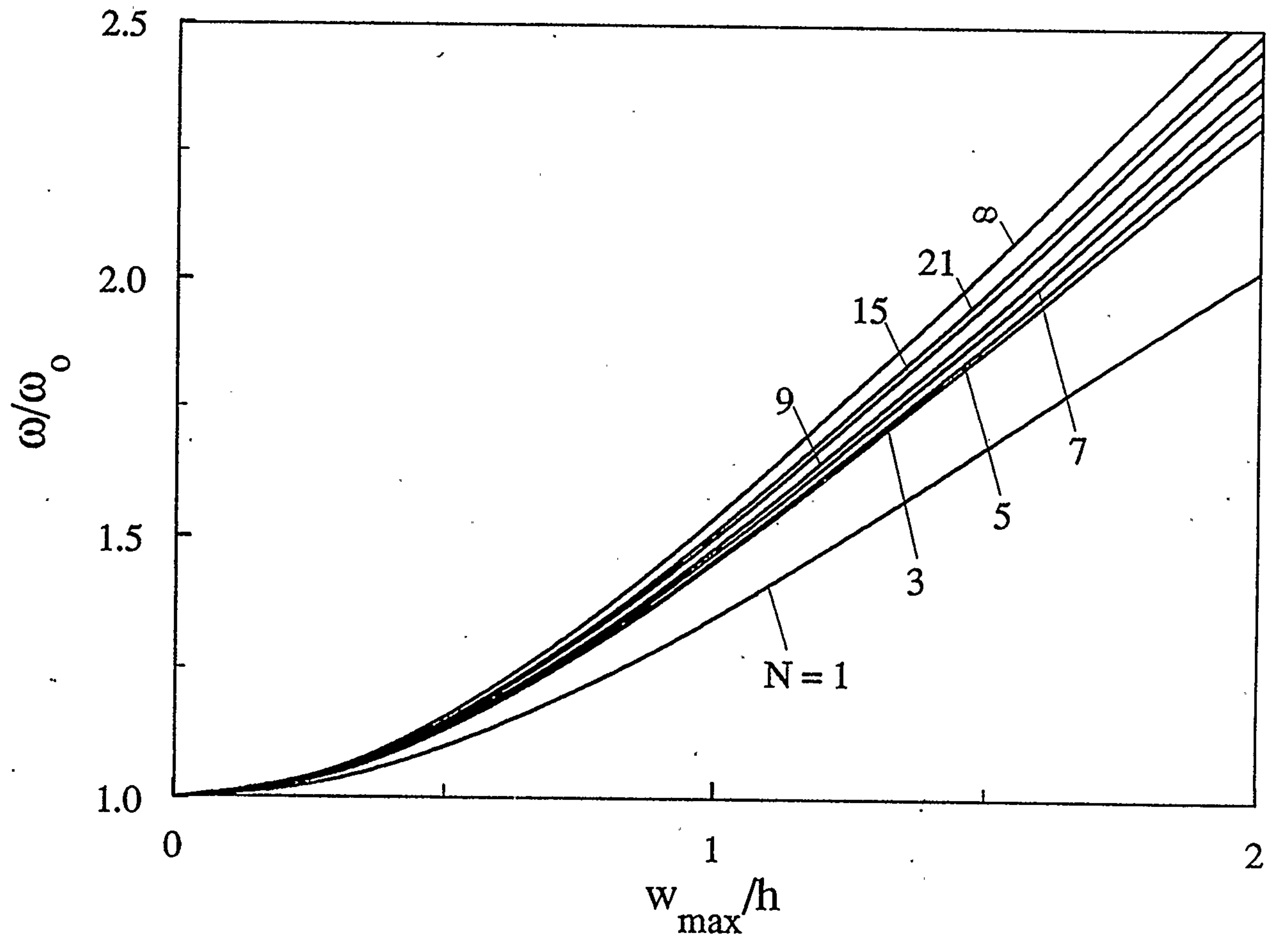

Figure 4.28: Effect of the number of layers on the frequency-amplitude response of an immovable simply-supported boron-epoxy circular plate (a/h=12)

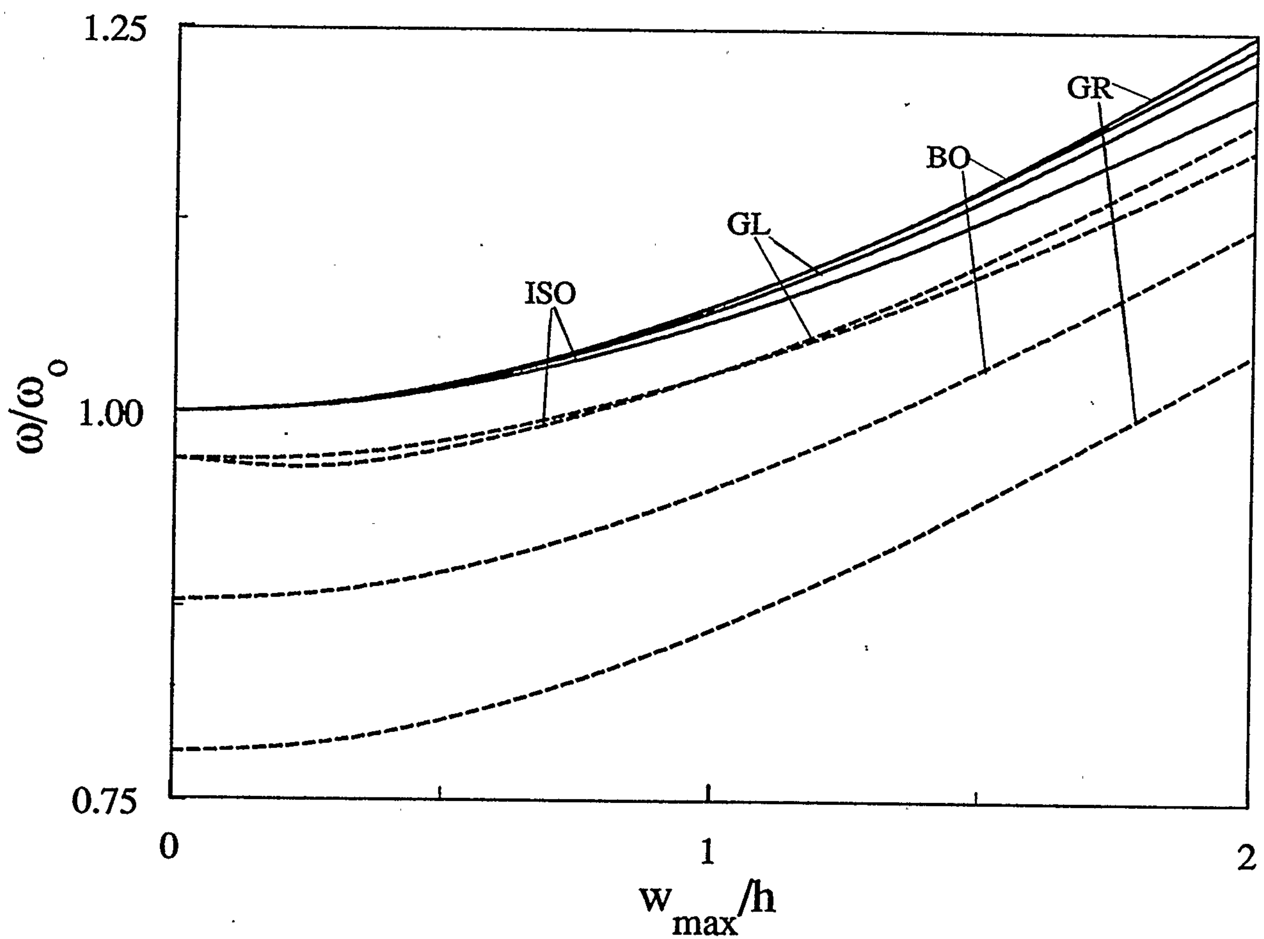

Figure 4.29: Effect of material properties on the frequency-amplitude response of an elastically supported seven-layer circular plate (a/h=8)

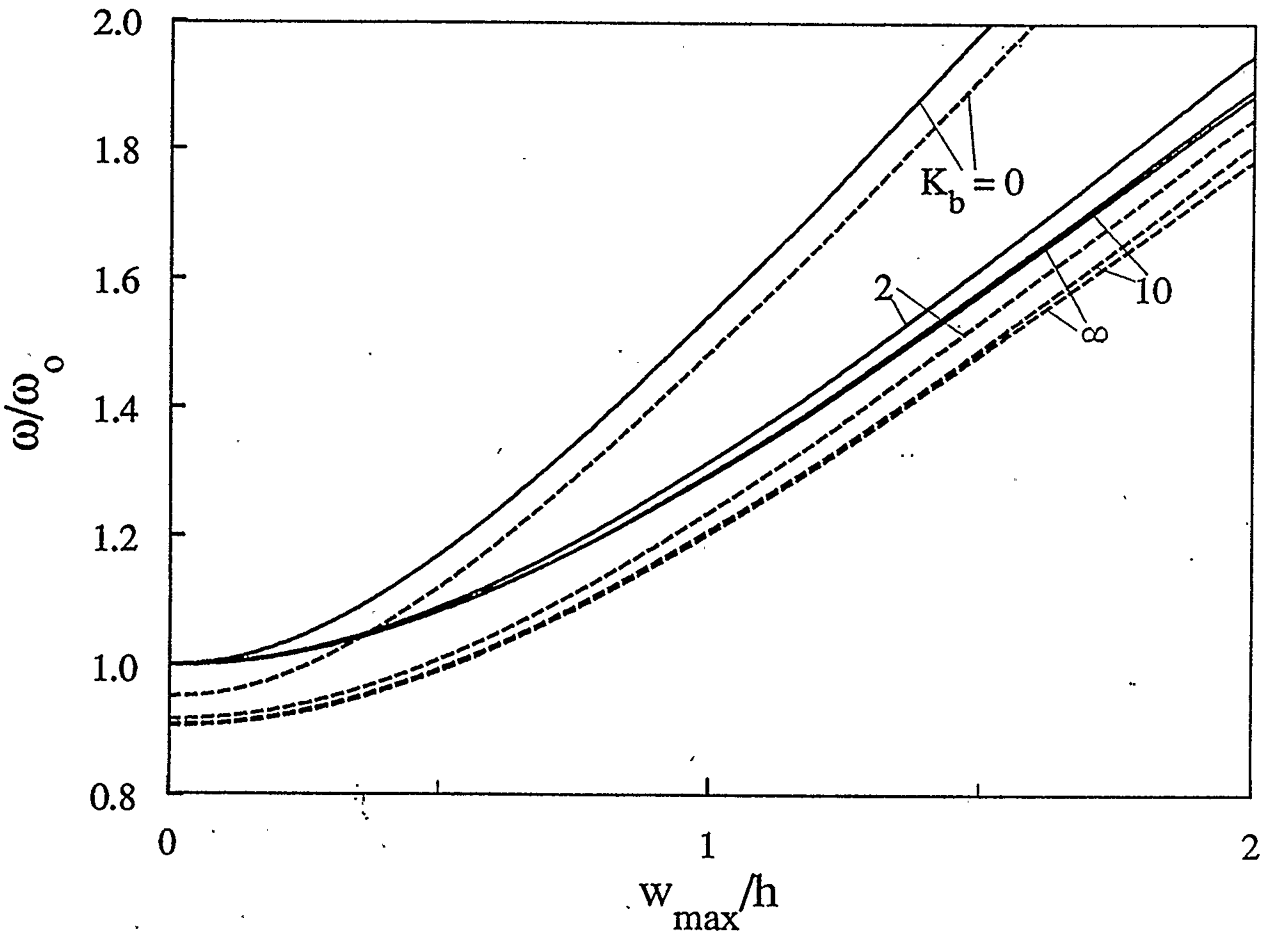

Figure 4.30: Effect of rotational edge stiffness on the frequency-amplitude response of a three-layer graphite-epoxy circular plate with an immovable edge (a/h=12)

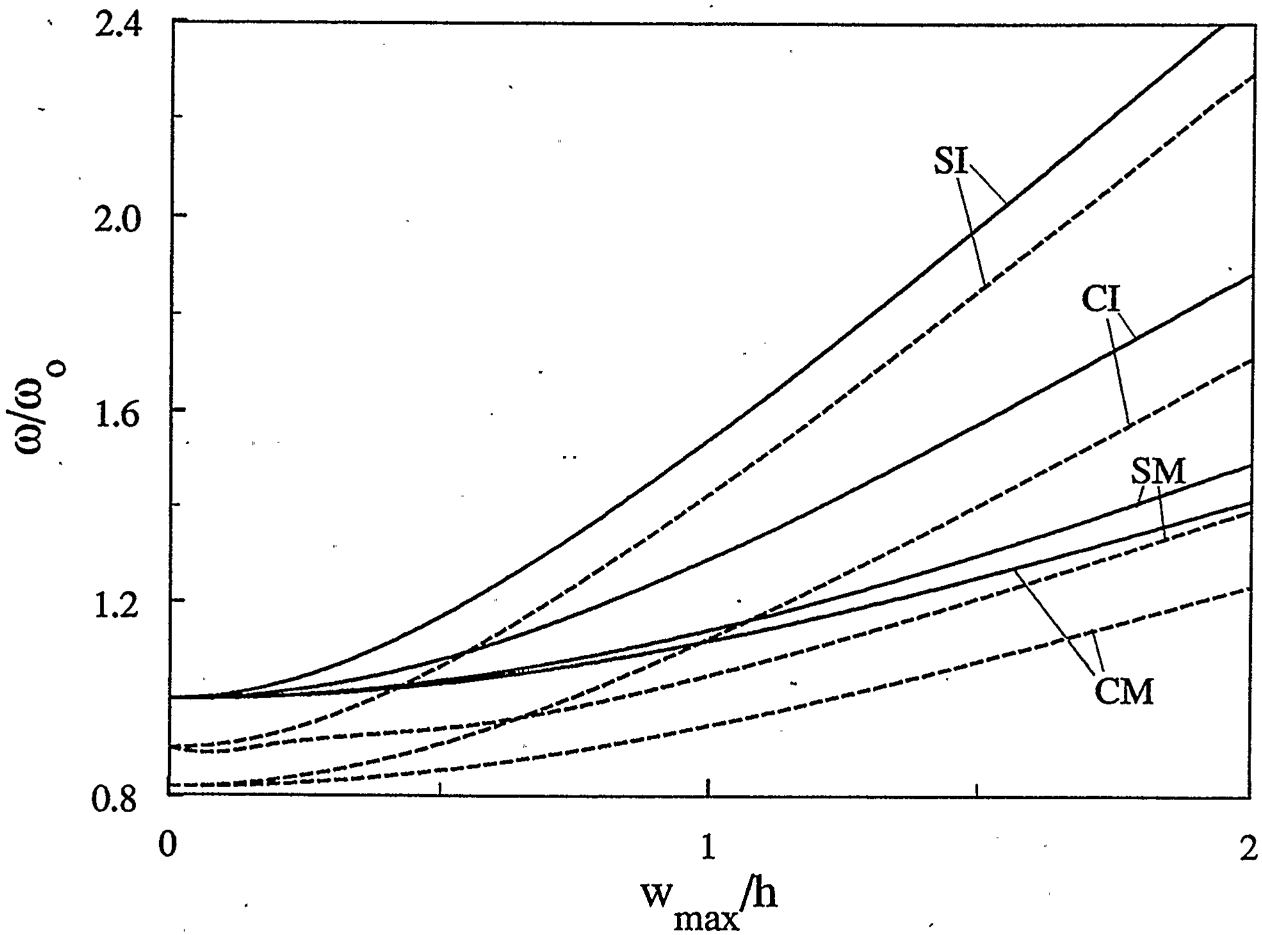

Figure 4.31: Effect of boundary conditions on the frequency-amplitude response of a three-layer graphite-epoxy circular plate (a/h=8)

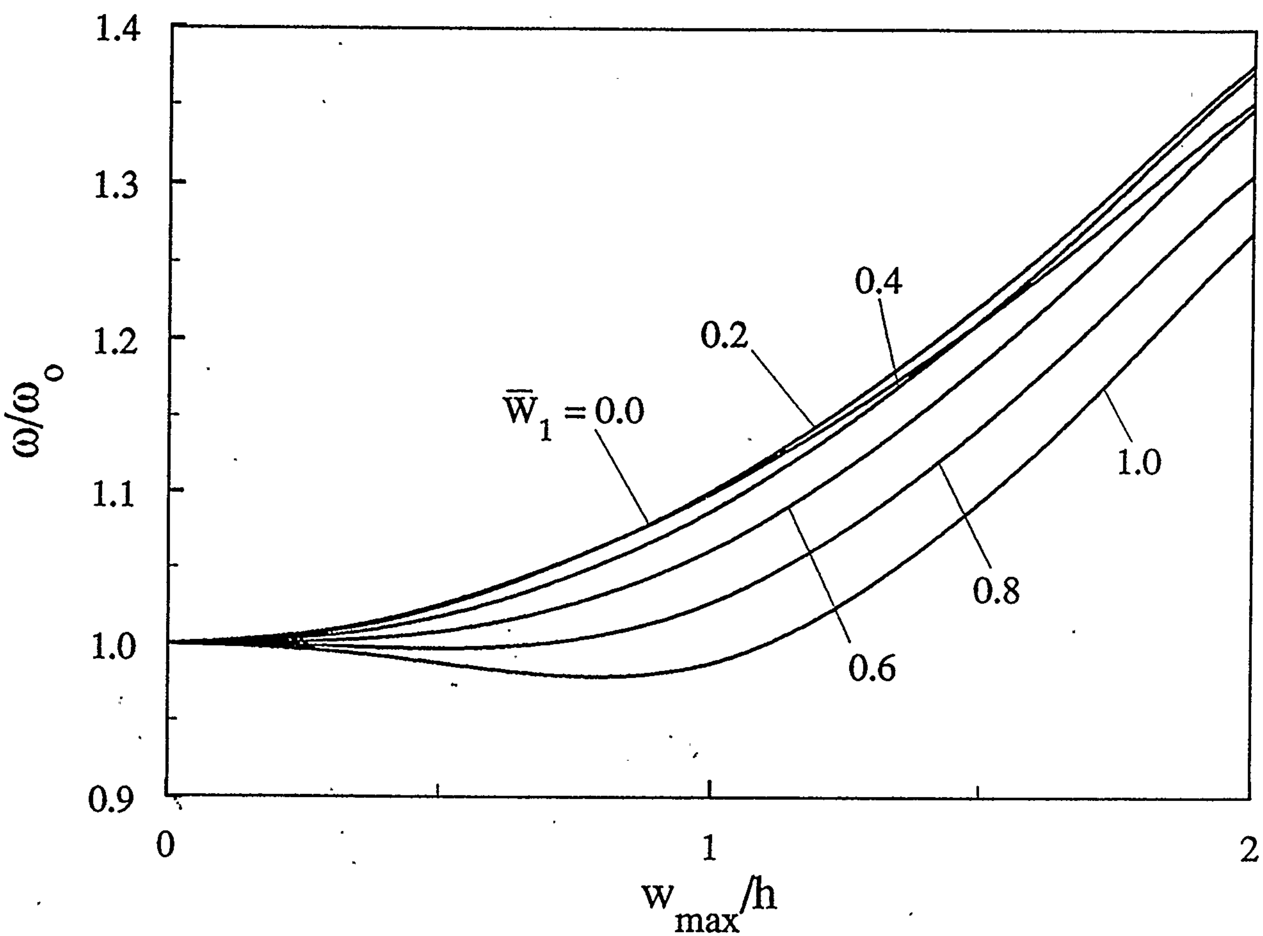

Figure 4.32: Effect of geometrically initial imperfections on the frequency-amplitude response of a movable simply-supported five-layer glass-epoxy circular plate (a/h=15)

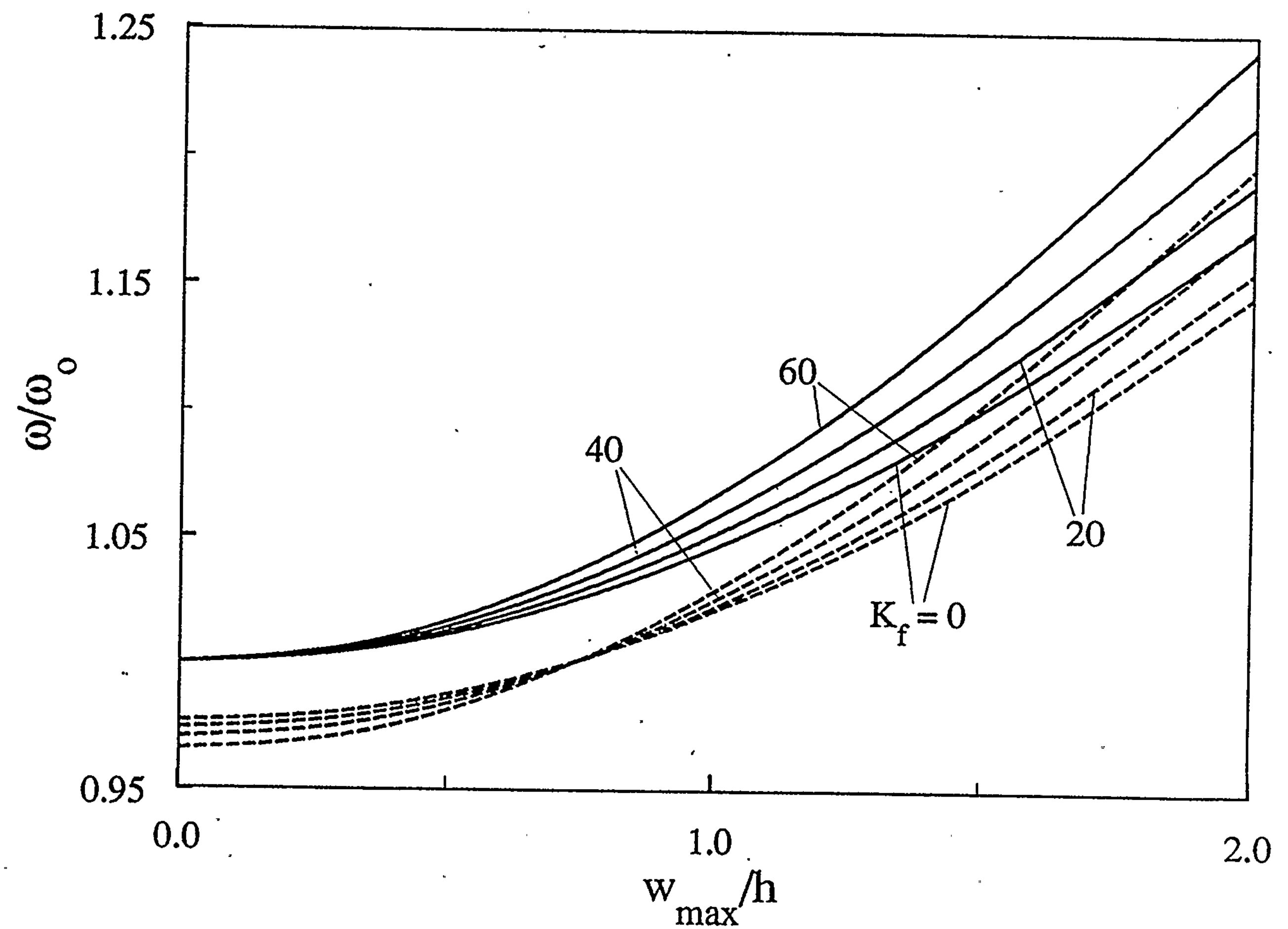

Figure 4.33: Effect of Winkler foundation parameter on the frequency-amplitude response of an elastically supported three-layer graphite-epoxy imperfect circular plate (K_b=3, K_i=5, $\bar{W}_1$=0.1, K_n=10, G_f=15, a/h=10)

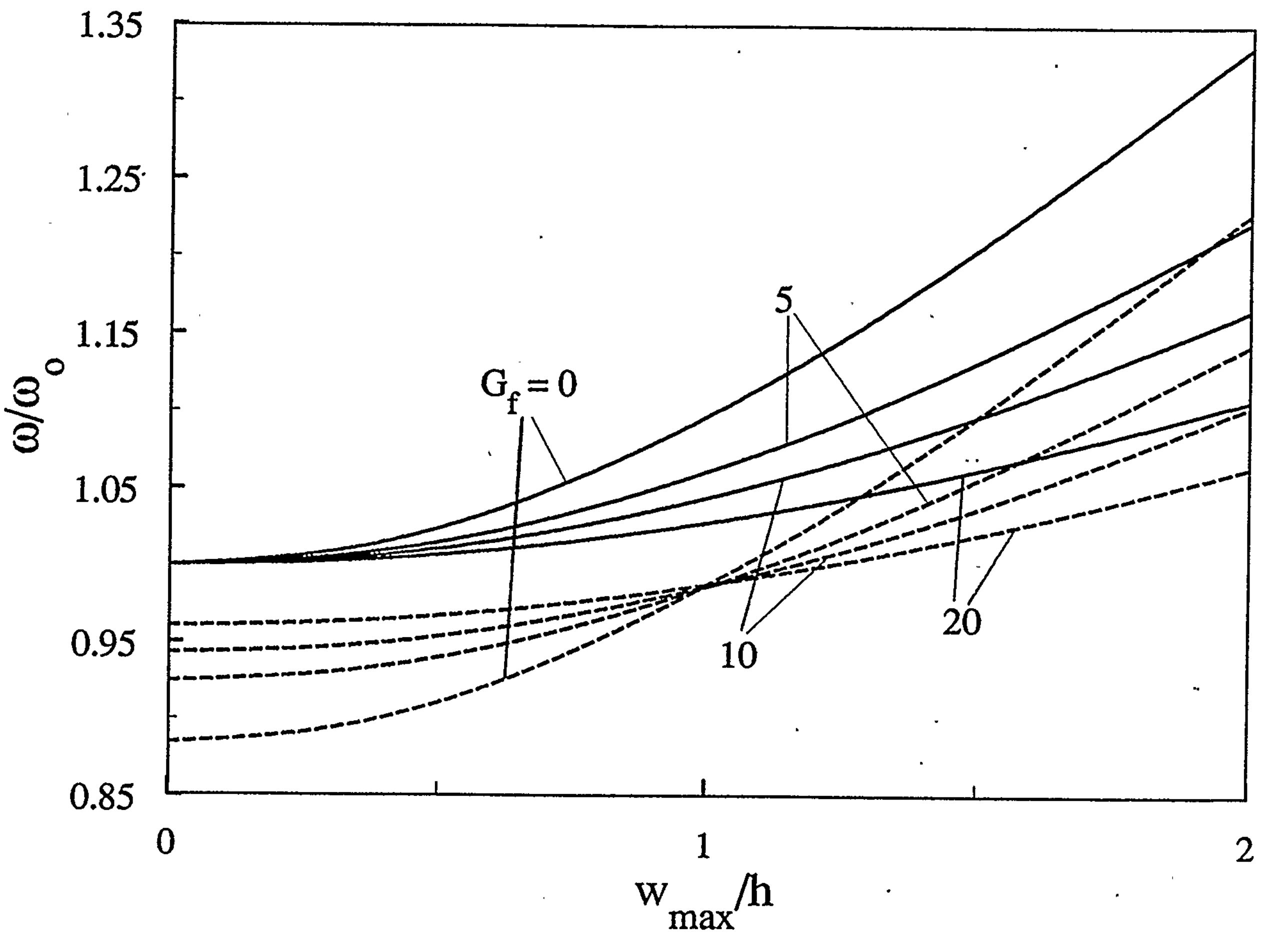

Figure 4.34: Effect of Pasternak foundation parameter on the frequency-amplitude response of a movable clamped five-layer graphite-epoxy imperfect circular plate shell ($\overline{W}_1$=0.2, K_f=5, K_n=5, a/h=12)

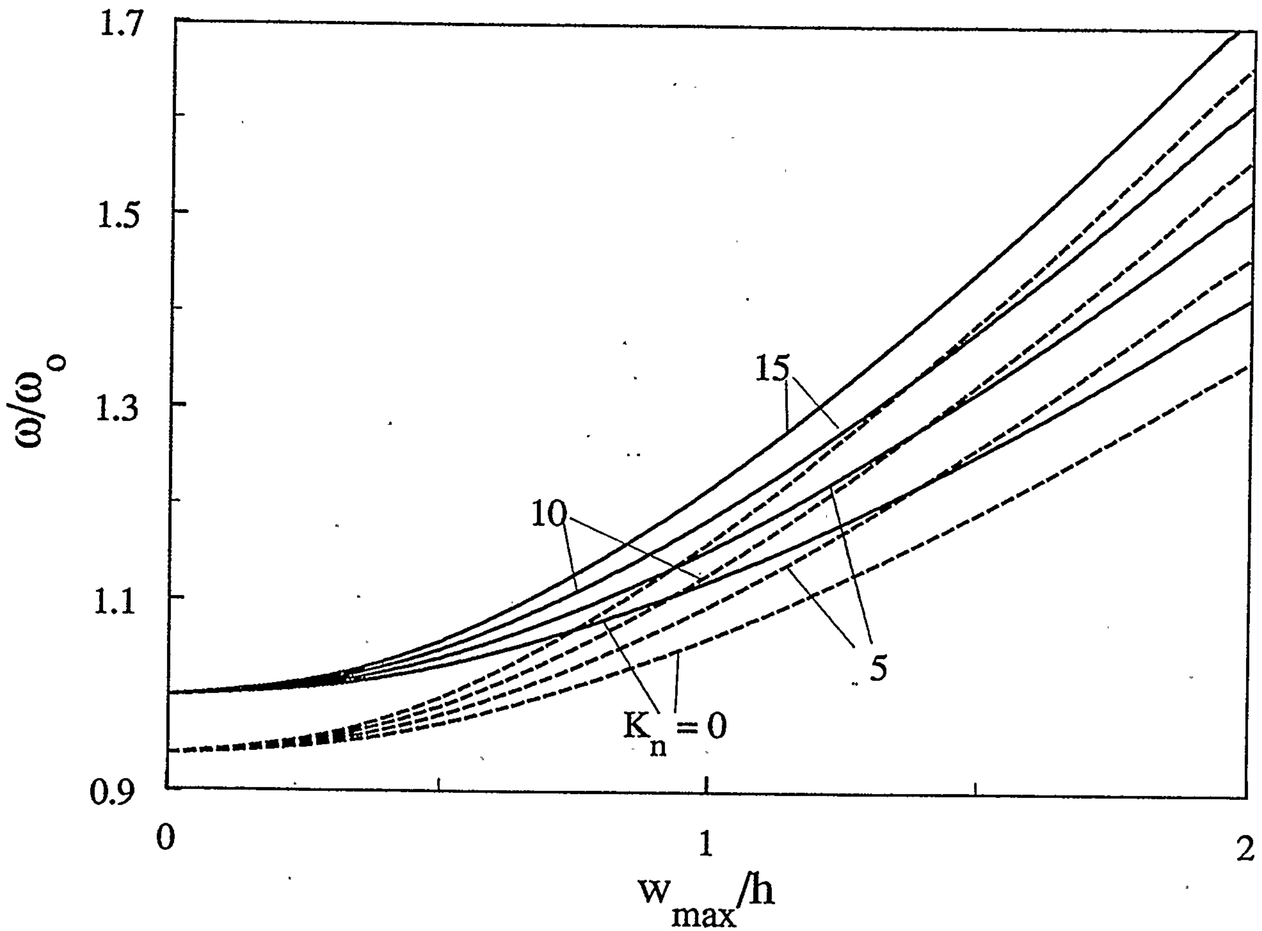

Figure 4.35: Effect of nonlinear Winkler foundation parameter on the frequency-amplitude response of an elastically supported three-layer boron-epoxy circular plate (K_b=2, K_i=3, K_f=10, G_f=0, a/h=8)

4.4.3 Unsymmetrically Laminated Shallow Spherical Shells and Circular Plates

The nonlinear free vibration response of unsymmetrically shallow spherical shells and circular plates is presented in this section. The shells and plates consist of even number of orthotropic layers. The edge boundary conditions under consideration are movable in radial direction and elastically restrained in rotational direction which are given in eqns. (3.19). Due to the coupling terms exist in boundary conditions, the technique of the equivalent lateral pressure has been introduced in Chapter 3 in order to fulfil the rotational edge constraint condition. In calculations, the terms of sine series in (3.22) for expansion of the equivalent lateral pressure, Q_e, are taken 10, as other terms have demonstrated numerically to be negligibly small. It may be noted that the movable clamped edge condition is exactly satisfied by the assumed solution. The corresponding fundamental linear frequencies in this section are given in Tables 4.19 and 4.20. The presentation in Figs 4.37, 4.39 and 4.41 is only given the response neglecting the effects of transverse shear and rotatory inertia for clarity.

Table 4.19 Values of fundamental linear frequency parameter ω_o in Figs. 4.36-4.39

Fig. 4.36	Fig. 4.37		Fig. 4.38		Fig. 4.39	
ω_o	N	ω_o	Mat.	ω_o	K_b	ω_o
9.5172	2	8.2421	ISO	3.0134	0	1.8872
	4	10.1047	GL	4.0142	0.5	3.1689
	6	10.3712	BO	6.1154	1.0	3.6823
	8	10.4524	GR	7.3331	2.0	4.1061
	10	10.4852			5.0	4.4548
	20	10.5155			∞	4.7121
	∞	10.5063				

Table 4.20 Values of fundamental linear frequency parameter ω_o in Figs. 4.40-4.42

Fig. 4.40		Fig. 4.41		Fig. 4.42	
H/h	ω_o	$\bar{W}_1$	ω_o	K_f,K_n,G_f	ω_o
0.5	6.7537	0	4.1148	$K_f=K_n=G_f=0$	8.2421
1.0	7.3452	0.2	4.1417	$K_f=10$, $K_n=G_f=0$	8.8280
1.5	8.1847	0.4	4.2339	$K_n=10$, $K_f=G_f=0$	8.2421
2.0	9.1909	0.6	4.3885	$G_f=10$, $K_f=K_n=0$	11.6372
		0.8	4.5951		
		1.0	4.8415		

4.4.3.1 <u>The Effect of the Radius-to-Thickness Ratio on the Frequency-Amplitude Response</u>

The effect of the ratio of base radius-to-thickness on the frequency-amplitude response is shown in Fig. 4.36 for a movable clamped two-layer graphite-epoxy shallow spherical shell of initial rise equal to 2h. This effect increases with decreasing the values of the ratio, a/h. The effects of transverse shear and rotatory inertia are much pronounced for the shell with ratio, a/h, equal to 16, 10 and 8. The frequency ratio compared that excluding these effects is reduced by 0.3%, 1.7%, 5.7% and 8% for a/h=50, 20, 10 and 8, respectively. Like the symmetrically laminated shell, the effects of transverse shear and rotatory inertia do not change the general behaviour of vibration response. The curves in the figure exhibit the softening type of nonlinearity.

4.4.3.2 The Effect of the Number of Layers on the Frequency-Amplitude Response

Figure 4.37 shows the response curves of a movable clamped graphite-epoxy shallow spherical shell with different number of layers. It is observed that the curves for shells with the number larger than 6 and the linear frequencies for these shells in Table 4.19 are very close. The behaviour of the shell with numbers 2, 4 and 6 is typical. The frequency ratio increases with an increase in the number. For the two-layer shell, the frequency ratio is reduced to 0.923 at w_{max}=2h. All curves behave initially softening type of nonlinearity and then invert to hardening one at the amplitude w_{max}>1.5h.

4.4.3.3 The Effect of Material Properties on the Frequency-Amplitude Response

The effect of the material properties on the frequency-amplitude response of a six-layer circular plate with elastically rotational edge is presented in Fig. 4.38. It is noted that when the modulus ratio, E_L/E_T, is raised the frequency ratio for neglecting effects of transverse shear and rotatory inertia increases very slightly although the corresponding linear frequency shown in Table 4.19 increases significantly. The effects of transverse shear and rotatory inertia on the frequency ratio are pronounced for material with the high modulus ratio. In this figure, these effects reduce the frequency ratio by approximately 10% and 16% for boron-epoxy and graphite-epoxy material, respectively.

4.4.3.4 The Effect of Rotational Edge Stiffness on the Frequency-Amplitude Response

The results for the effects of rotational edge stiffness on the frequency-amplitude response of a movable six-layer glass-epoxy circular plate are plotted in Fig. 4.39. The curves exhibit the hardening type of nonlinearity. When the rotational stiffness, K_b, is raised, the frequency ratio decreases for $K_b<2$ and slightly increases for $K_b\geq2$, but the nonlinear frequency increases referring the corresponding linear frequency in Table 4.19. And the response curves for $K_b>2$ are close that for $K_b=\infty$, i.e., clamped edge. It is noted that the frequency ratio reaches 1.42 at w_{max}=2h for K_b=0, i.e., simply-supported edge.

4.4.3.5 The Effect of the Shell Rise on the Frequency-Amplitude Response

The nonlinear free vibration response of a movable clamped four-layer boron-epoxy shallow spherical shell with different initial rise is presented in Fig. 4.40. The response curves are hardening type of nonlinearity for the dimensionless shell rise H/h=0.5 and 1 and softening one for H/h=1.5 and 2. At w_{max}=2h, the frequency ratio neglecting the effects of transverse shear and rotatory inertia is 1.167, 1.066, 0.976 and 0.913 for H/h=0.5, 1, 1.5 and 2, respectively. The effects of transverse shear and rotatory inertia reduce the frequency ratio at infinitely small amplitude of vibration by 10%, 8%, 6.5% and 5.7% for H/h=0.5, 1, 1.5 and 2, respectively, and at larger values of amplitude by approximately 9% for all cases.

4.4.3.6 The Effect of Geometrically Initial Imperfections on the Frequency-Amplitude Response

Figure 4.41 fives the frequency-amplitude response of a movable clamped four-layer glass-epoxy circular plate with different values of initial imperfection. The curves behave the hardening type of nonlinearity for $\overline{W}_1 \leq 0.6$, and initially softening one and then changing to hardening one for

$\bar{W}_1$>0.6. The frequency ratio decreases with an increase in the value of initial imperfection as the increase of the plate curvature resulting from the initial imperfection.

4.4.3.7 The Effect of Elastic Foundations on the Frequency-Amplitude Response

The curves of frequency-amplitude response for a movable clamped two-layer graphite-epoxy shallow spherical shell resting on elastic foundations are depicted in Fig. 4.42. These curves show the softening behaviour for the shell without elastic foundation and with linear Winkler elastic foundation, and initially softening one and then inverting to hardening one for with nonlinear Winkler and Pasternak elastic foundations, respectively. The effects of transverse shear and rotatory inertia are more significant for the shell without elastic foundation that for the shell with one. These effects reduce the frequency ratio by approximately 9%, 8%, 6% and 4% for the shell without elastic foundation, with nonlinear Winkler one, with linear Winkler one and with Pasternak one, respectively.

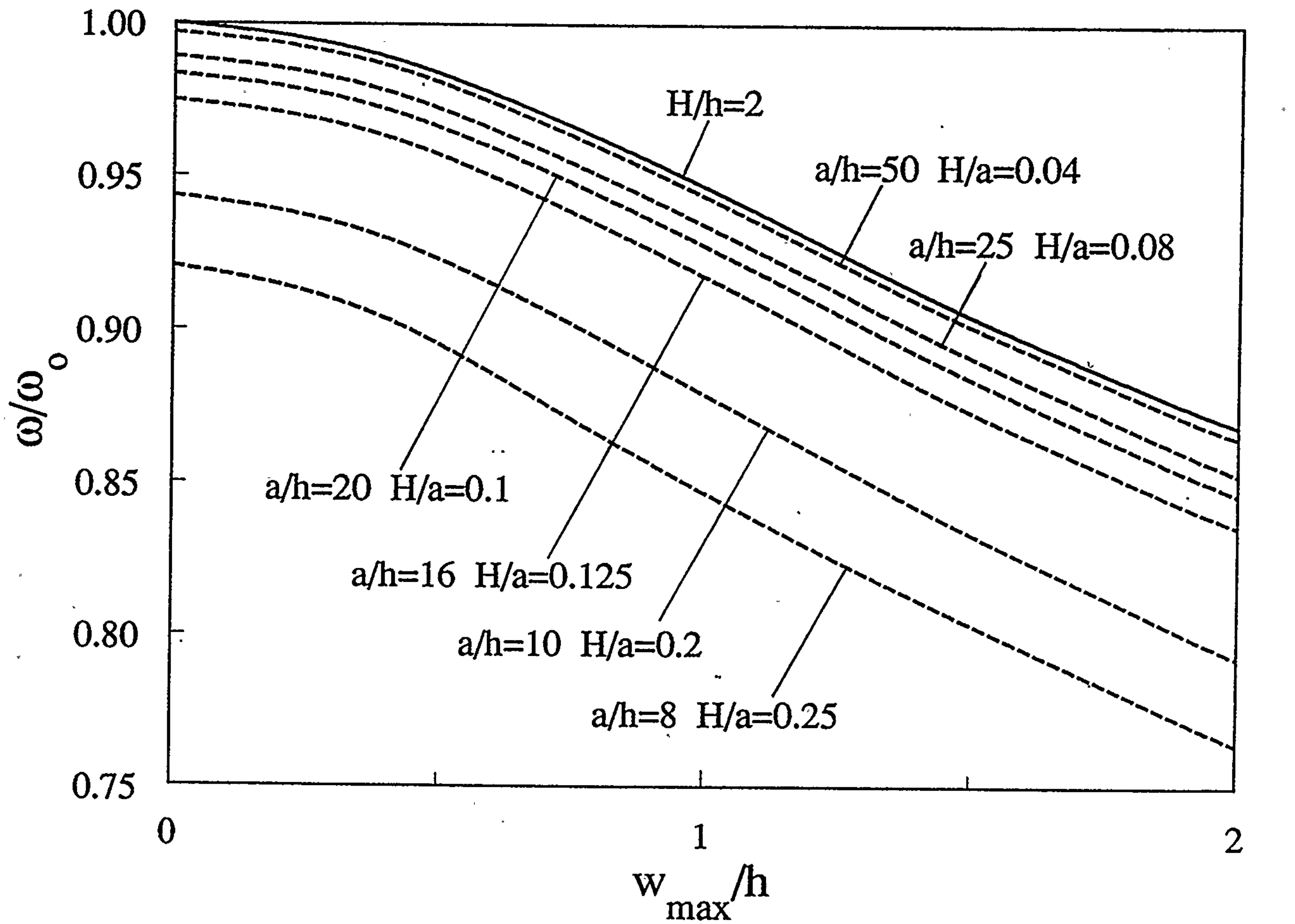

Figure 4.36: Effect of the base radius-to-thickness ratio on the frequency-amplitude response of a movable clamped two-layer graphite-epoxy shallow spherical shell

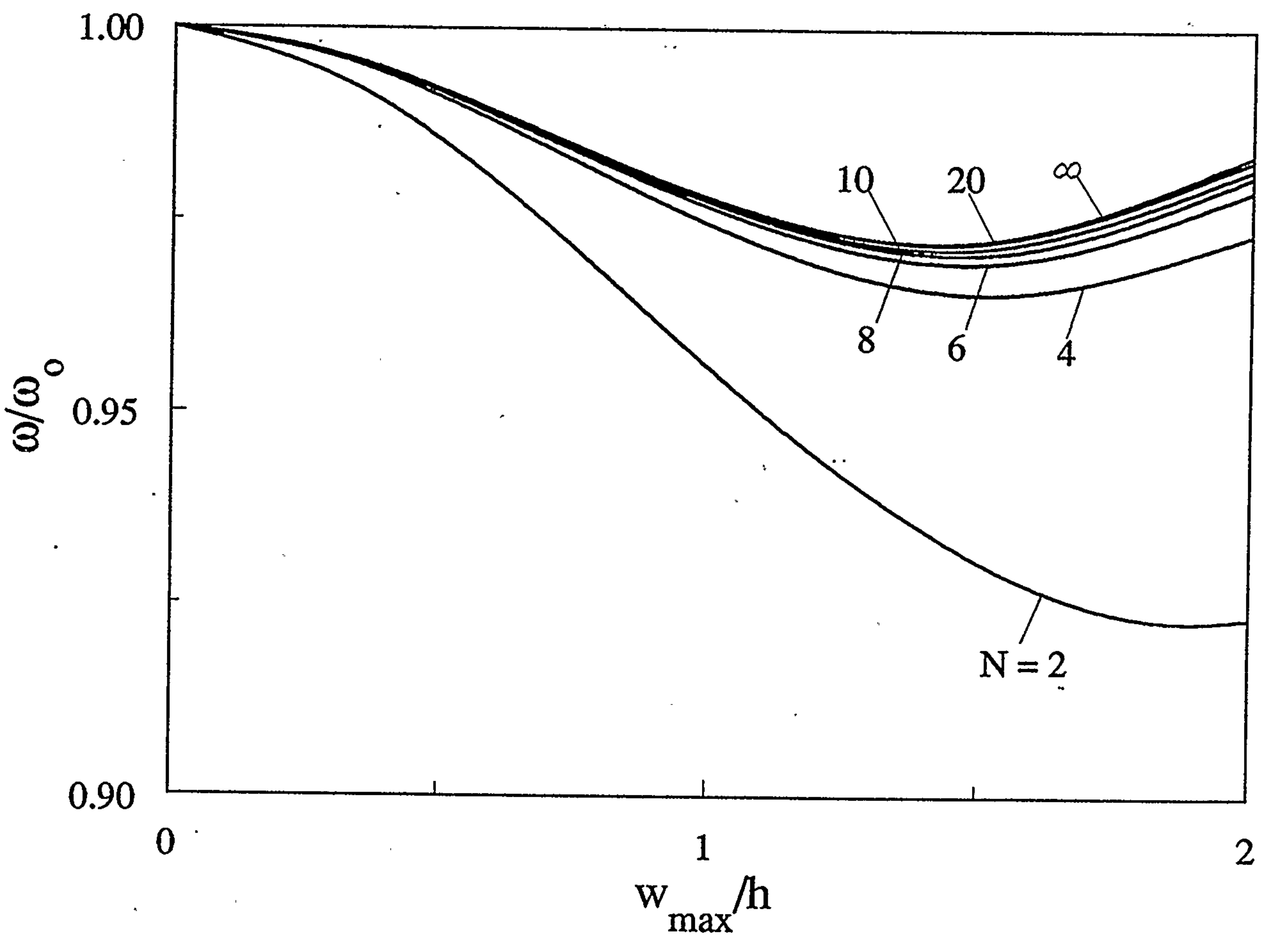

Figure 4.37: Effect of the number of layers on the frequency-amplitude response of a movable clamped glass-epoxy shallow spherical shell (a/h=15, H/a=0.1)

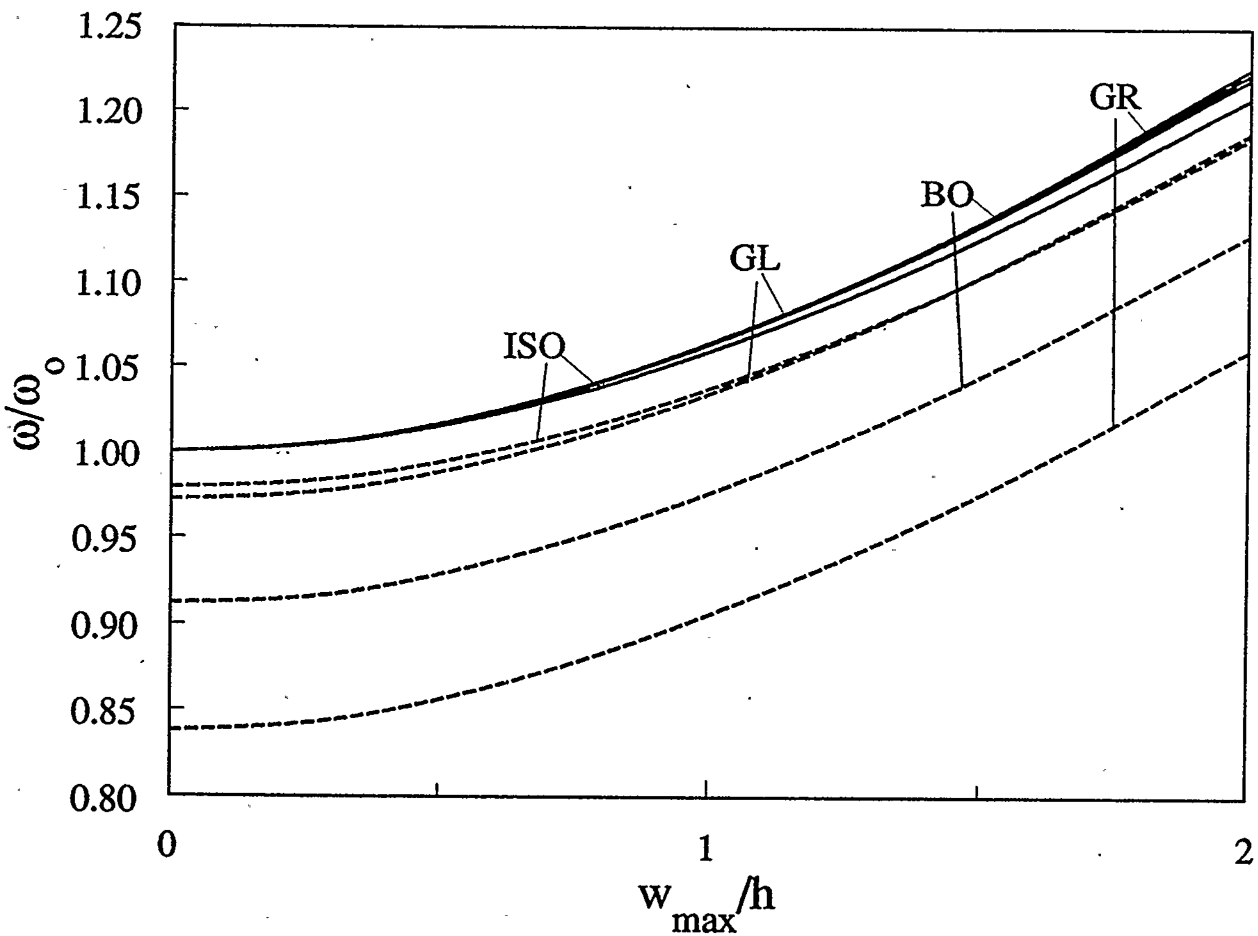

Figure 4.38: Effect of material properties on the frequency-amplitude response of an elastically supported six-layer circular plate (a/h=10)

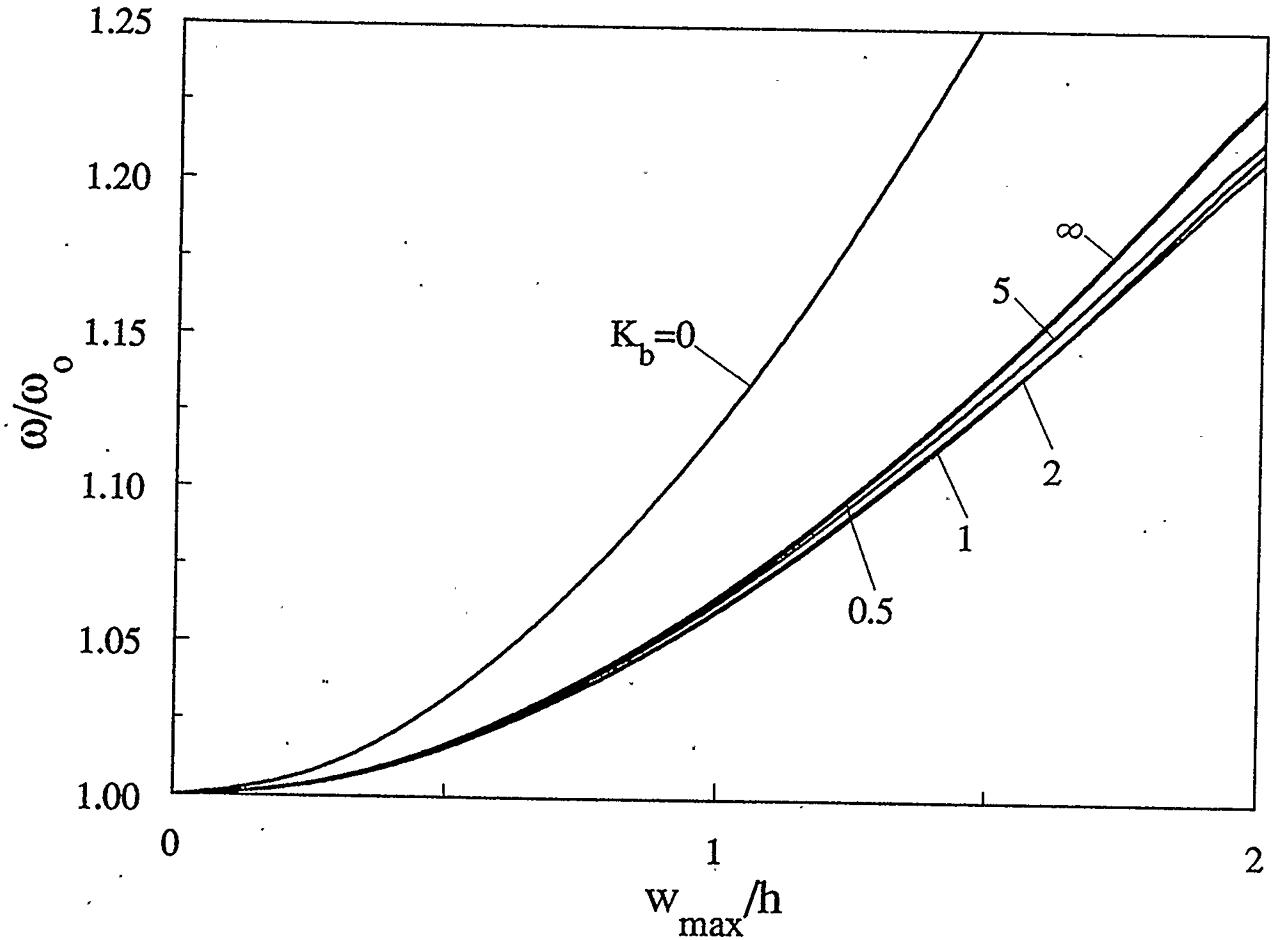

Figure 4.39: Effect of rotational edge stiffness on the frequency-amplitude response of a six-layer glass-epoxy circular plate with a movable edge (a/h=15)

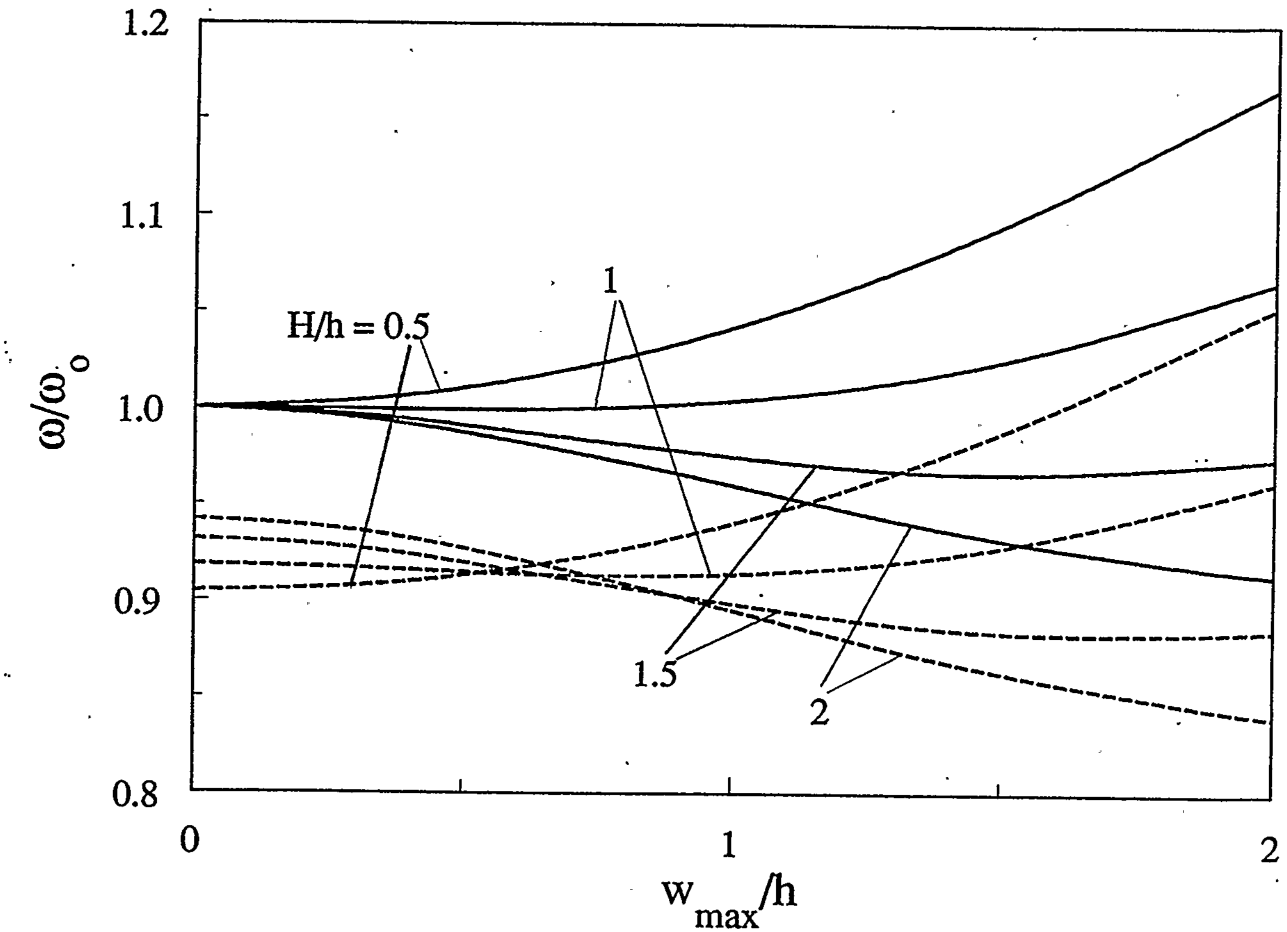

Figure 4.40: Effect of the shell rise on the frequency-amplitude response of a movable clamped four-layer boron-epoxy shallow spherical shell (a/h=10)

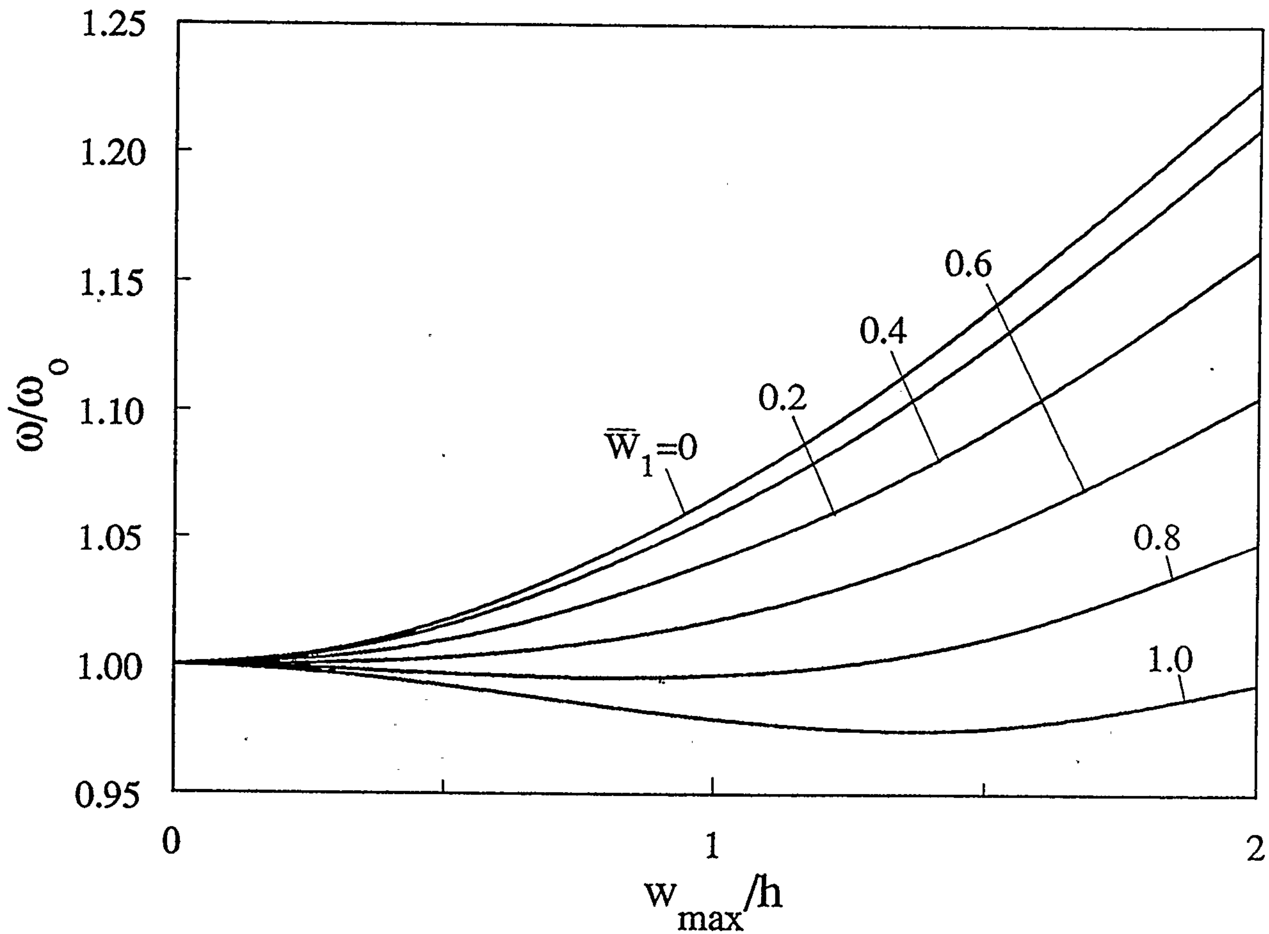

Figure 4.41: Effect of geometrically initial imperfections on the frequency-amplitude response of a movable clamped four-layer glass-epoxy circular plate (a/h=15)

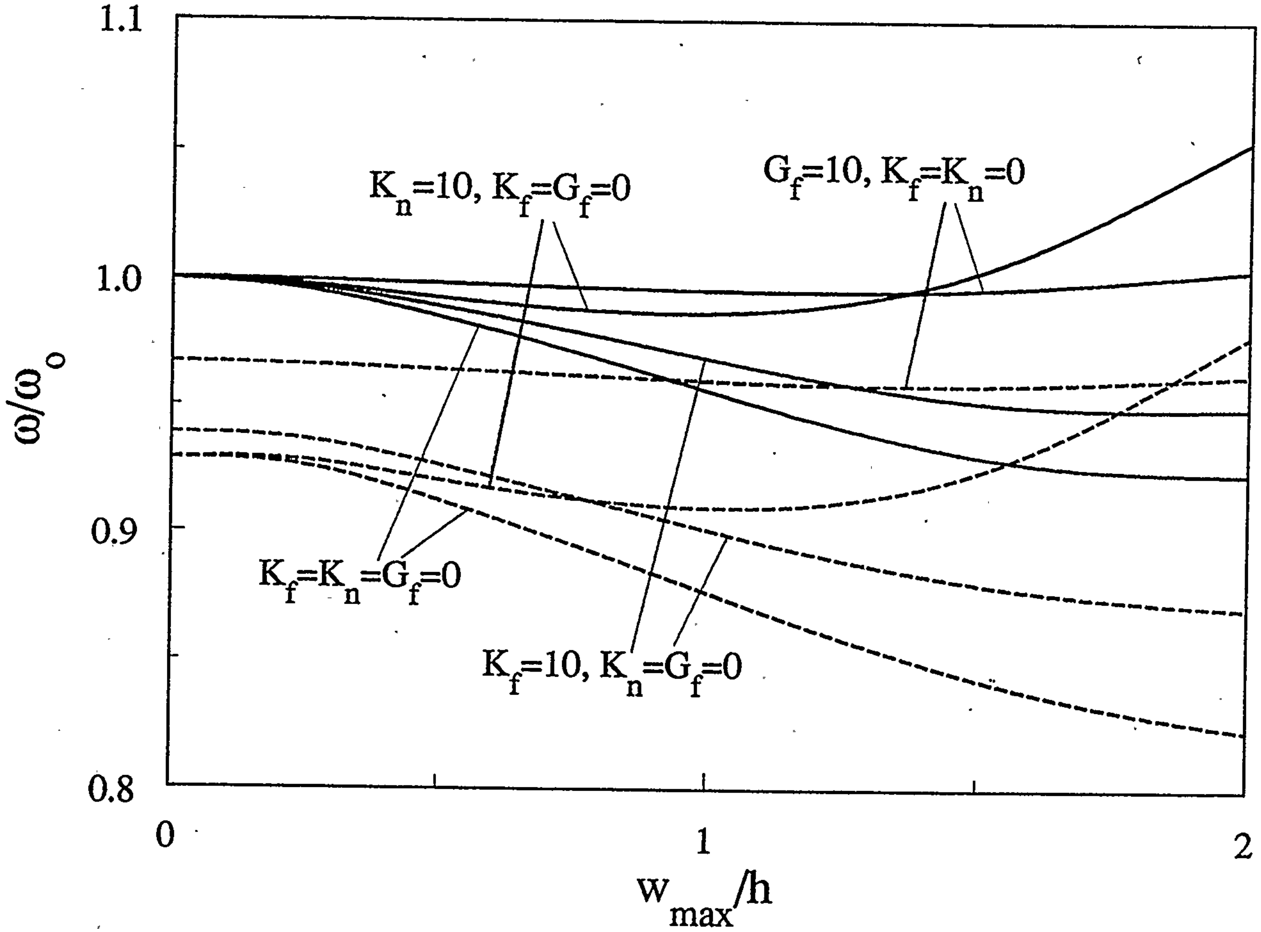

Figure 4.42: Effect of elastic foundations on the frequency-amplitude response of a movable clamped two-layer graphite-epoxy shallow spherical shell (a/h=10, H/a=0.15)

4.5 BUCKLING, POSTBUCKLING AND STATIC LARGE DEFLECTION

In this section, the numerical results are presented for the relation between the load and deflection of a laminated cross-ply shallow spherical shell. The buckling and postbuckling behaviour is investigated for the shell. In the calculation, the uniformly-distributed static load normal to the undeformed middle surface is assumed. In the presentation, the load is specified by dimensionless load, Q, for a circular plate, and the ratio of dimensionless load to square of dimensionless rise, $Q/(H/h)^2$, for a shallow spherical shell, and the deflection is specified by the dimensionless maximum deflection w_{max}/h.

For large deflections, deformation of a shallow spherical shell is not proportional to the external loading. The load-deflection relation may be represented by a curve. After reaching the first maximum value of uniformly distributed lateral load, q_{cr}, the load tends to have a reduction. The value q_{cr} is called the buckling load for axisymmetrical snapping. Tests indicate that buckling generally starts as a small circular dimple and tends to occur where the shell is weakest (Donnell, 1976). To study this phenomenon, many researchers (von Karman and Tsien, 1939; Kaplan and Fung, 1954; Budiansky, 1959; Weinitschke, 1960; Stephens and Fulton, 1969; Hyman, 1971;) proposed various methods. Most of them included nonlinear finite deflections in their analysis instead of just considering stability with respect to infinitesimal deflection from the prebuckled condition. Their calculations also show that the stiffness of the shell decreases with the deflection. A comprehensive survey of the state-of-the-art for buckling of a shallow spherical shell is given by Hutchinson and Koiter (1970).

4.5.1 Symmetrically Laminated Shallow Spherical Shells

4.5.1.1 The Effect of Material Properties on Buckling Load

Figures 4.43 and 4.44 show the effect of material properties on the buckling load of an immovable clamped five-layer and immovable simply-supported shallow spherical shell, respectively. In this study, the least value of the geometric parameter, H/a, denoted by $(H/a)_{cr}$, for which buckling occurs is obtained by use of iterative procedure. The value of the ratio H/a for which buckling does not occur is increased by a small increment and the eqn. (3.32) is solved by the Newton-Raphson method. The process is repeated until buckling just occurs and vice versa until buckling just disappears. The values of $(H/a)_{cr}$ and the associated buckling Q_{cr} in these figures are given in Table 4.21. The effect of transverse shear is also presented in the table. The value of $(H/a)_{cr}$ is roughly 0.08 for an immovable clamped five-layer shallow spherical shell with a/h=20 in Fig. 4.43 and 0.05 for an immovable simply-supported three-layer shallow spherical shell with a/h=15 in Fig. 4.44. It may be noted from these figures that once the critical value $(H/a)_{cr}$ occurs, the buckling load Q_{cr} initially decreases and then increases with an increase in the ratio H/a. These figures also indicate that the buckling load Q_{cr} increase with increasing the modulus ratio, E_L/E_T, but the critical value $(H/a)_{cr}$ decreases for a laminated cross-ply shallow spherical shell. Evidently the transverse shear deformation reduces the buckling load. This effect is more pronounced for the composite of high modulus ratio.

Table 4.21 Values of $(H/a)_{cr}$ and $[Q/(H^2/h^2)]_{cr}$ in Figs. 4.43 and 4.44

	Mat.	N	a/h	$T_S=0$		$T_S=1$	
				$(H/a)_{cr}$	$[Q/(H^2/h^2)]_{cr}$	$(H/a)_{cr}$	$[Q/(H^2/h^2)]_{cr}$
Fig. 4.43	GL	5	20	0.08484	5.2143	0.08441	5.1709
	BO	5	20	0.08221	13.0095	0.08013	12.6998
	GR	5	20	0.08037	19.9635	0.07666	18.8221
Fig. 4.44	GL	3	15	0.05414	3.9635	0.05393	3.9478
	BO	3	15	0.05246	9.1398	0.05168	9.0142
	GR	3	15	0.05197	13.6390	0.05037	13.2362

4.5.1.2 The Effect of the Radius-to-Thickness Ratio on the Postbuckling Response

The postbuckling response of movable simply -supported and clamped three-layer graphite-epoxy shallow spherical shells with different ratios of radius-to-thickness are given in Figs. 4.45 and 4.46. The effect of transverse reduces the buckling load and the load-carrying capacity in the postbuckling range especially for moderately thick shells. This can be found in Figs. 4.45 and 4.46 which demonstrate the response curves for movable simply-supported and clamped three-layer graphite-epoxy shallow spherical shells with different ratios of radius-to-thickness. The buckling load generally increases with this ratio. The effect of transverse shear reduces the buckling load by 10.3% for simply supported shell with a/h=10, and by 8.2% for the clamped shell with a/h=15. This effect, however, is not significant for large values of this ratio.

4.5.1.3 The Effect of the Number of Layers on the Postbuckling Response

In Fig. 4.47, the effect of the number of layers, N, on the buckling load are illustrated for a movable clamped boron-epoxy shallow spherical shell. These curves indicate that the buckling load increases with increasing the number of layers. For the values $N \leq 5$ the influence of the number of layers on the buckling load is much pronounced. The buckling load increases by 60% for N=15 than for N=1 (orthotropic shell). This increase is considerably significant for the load-carrying capacity. Figure 4.48 shows that the effects of the number of layers and the transverse shear on the load-deflection response of a movable simply-supported graphite-epoxy shallow spherical shell. A similar behaviour as in Fig. 4.47 is observed for the effect of the number of layers. The effect of transverse shear on the load-carrying capacity generally increases more rapidly than that of the number of layers.

4.5.1.4 The Effect of Material Properties on the Postbuckling Response

The response curves of an immovable clamped five-layer shallow spherical shell are plotted in Fig. 4.49 for different material properties. Neglecting the transverse shear effect the snap-through buckling of all shells of different materials approximately occurs at the maximum deflection equal to the shell thickness. The effect of transverse shear reduces the buckling load by 4%, 11% and 18% for glass-epoxy, boron-epoxy and graphite-epoxy materials, respectively. For a given deflection the reduction in the transverse load caused by the effect of transverse shear is evidently greater for the high modulus ratio than for low one. In the case of graphite-epoxy composite material the postbuckling load is reduced by 35% at w_{max}=1.2. A similar behaviour is also observed in Fig. 4.50 for a movable simply-supported five-layer shallow spherical shell. The effect of transverse shear, however, is much reduced in this example.

4.5.1.5 The Effect of Boundary Condition on the Postbuckling Response

The postbuckling response for different boundary conditions are illustrated in Figs. 4.51-4.53. Figure 4.51 shows that the effect of rotational stiffness of edge on the postbuckling response of a movable edge three-layer boron-poxy shallow spherical shell. The K_b=0 and ∞ correspond the simply-supported and clamped edges, respectively. All shells with different values of K_b undergo the snap-through buckling and have a slight reduction after buckling and then a little increase at large value of deflection in the load. The buckling load and postbuckling load carrying capacity increase as the rotational stiffness, K_b, increases. The buckling load for K_b=5 is only less than that for K_b=∞ by approximately 3.5%. The effect of transverse shear reduces the buckling load and postbuckling load carrying capacity. This effect increases with an increase in K_b and the maximum deflection. At w_{max}=2h, the effect of transverse shear reduces the postbuckling load by approximately

5%, 6.3%, 10%, 12% and 13% for K_b=0, 0.4, 1, 5 and ∞, respectively.

The response curves excluding the effect of transverse shear for a clamped five-layer boron-epoxy shallow spherical shell are depicted in Fig. 4.52 for different inplane stiffness of edge, K_i. The values of K_i=0 and ∞ correspond the immovable and movable edges. The buckling occurs in all different values of K_i. The buckling load increases with an increase in K_i. The reduction of the postbuckling load is increased by raising K_i and the load are largest for K_i=0 and the smallest for $K_i=\infty$ in the range of deflection $2.5h \leq w_{max} < 3h$.

The load-deflection curves shown in Fig. 4.53 illustrate the effect of edge conditions on the buckling load of a five-layer graphite shell. It is noted that the effect of inplane edge condition is much noticeable. The buckling load is increased by 80% for an immovable edge than a movable edge for the clamped shell, and by 240% for simply-supported shell. It is also shown from this figure that the effect of edge rotation on an immovable edge is less than a movable edge. The buckling load of the shell with an immovable edge is nearly the same for the clamped and simply-supported shells and that with a movable edge is increased by 90% for a clamped edge than for a simply-supported edge. For these four types of boundary conditions the effect of transverse shear generally reduces the buckling load. The reduction in the postbuckling load caused by this effect is much more significant for an immovable clamped and movable simply-supported shells. In the case of a movable simply-supported shell the effect of transverse shear generally increases the postbuckling load rather than reduces.

4.5.1.6 The Effect of the Shell Rise on the Postbuckling Response

The postbuckling response curves are shown for an elastically supported three-layer boron-epoxy shallow spherical shell in Fig.4.54 and a movable simply-supported seven-layer graphite-epoxy shallow spherical shell in Fig. 4.55. It can be seen from Fig. 4.54 that the shell undergoes snap-through buckling, and have a reduction in the load after the first maxima for H/h=2.4 and no buckling occurs for H/h=1.2 and 1.8. It is noted that for the shell with H/h=2.4, the load after reduction from buckling inverts to increase with an increase in deflection. In Fig. 4.55, all response curves demonstrate the buckling phenomenon and the buckling load increases as H/h is raised. The effect of transverse shear reduce the load. This effect generally increases with the deflection and is considerably pronounced for a moderately thickness shell at large values of the deflection.

4.5.1.7 The Effect of Geometrically Initial Imperfections on the Postbuckling Response

The postbuckling load-deflection curves for a movable clamped spherical cap on elastic foundation are plotted in Fig. 4.56 for various values of the initial imperfection, $\overline{W}_1$. It may be seen from these response curves that all caps undergo buckling and have a reduction in load after buckling. The buckling load decreases as the value $\overline{W}_1$ increases. The postbuckling load decreases with the amplitude of initial imperfection in the range of the values of $0 < w_{max} < 2.2h$ due to the neglecting of the effect of transverse shear (T_S=0) and of $0 < w_{max} < 2.1h$ for including these effects (T_S=1), and increases in the range of values of $2.2h < w_{max} < 3h$ for $T_S=0$ and of $2.1h < w_{max} < 3h$ for $T_S=1$, respectively.

4.5.1.8 The Effect of Elastic Foundations on the Postbuckling Response

In Fig. 4.57, the postbuckling response curves for an imperfect spherical cap are shown for different values of the linear Winkler foundation parameter, K_f. It is found that the buckling load increases with this value. The buckling phenomenon occurs in the range of values of $1.09h < w_{max} < 1.35h$ for all values of K_f indicated in the figure and the buckling load is 53% greater for $K_f = 20$ than for $K_f = 0$. The effect of Pasternak elastic foundation parameter, G_f, on postbuckling of a movable simply supported cap is illustrated in Fig. 4.58. The response curves exhibit the buckling phenomenon except for the values of $G_f = 5$ and 10 without considering the effect of transverse shear and except for the value of $G_f = 10$ with this effect. The load increases with an increase of the value of the Pasternak foundation parameter, G_f. The effect of transverse shear reduces the buckling and postbuckling load as expected. This reduction is pronounced at high values of the deflection. The load-deflection curves shown in Fig. 4.59 depict the effect of nonlinear Winkler foundation parameter, K_n, on the buckling and postbuckling load of an elastically supported spherical cap. It is observed that there is a reduction in load after buckling for $K_n = 0$ and 2. The load for a given deflection increases with the values of K_n. The effect of transverse shear reduces the load slightly due to the shell with large ratio of base radius to the cap thickness, i.e., $a/h = 20$.

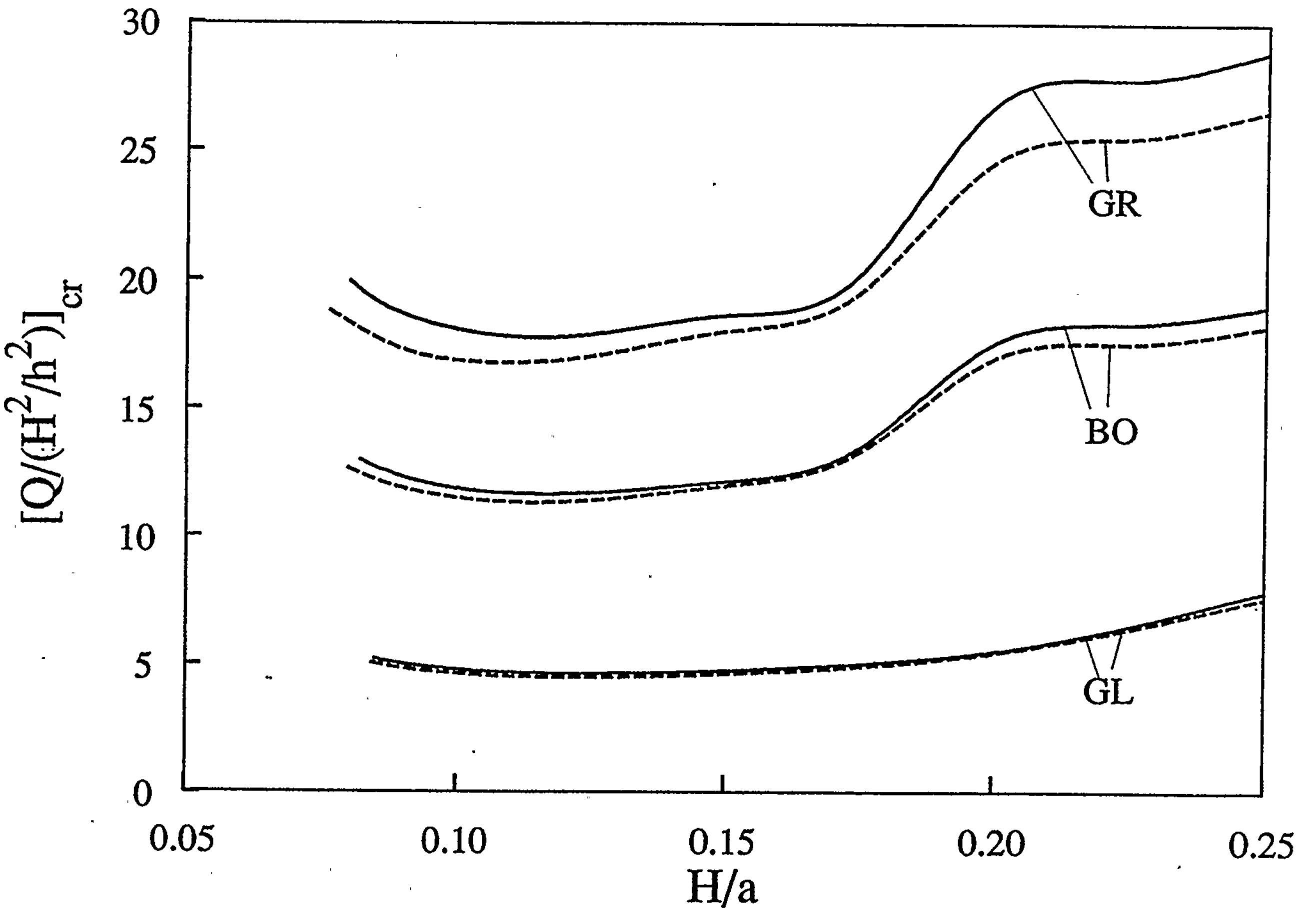

Figure 4.43: Effect of material properties on buckling load of an immovable clamped five-layer shallow spherical shell (a/h=20)

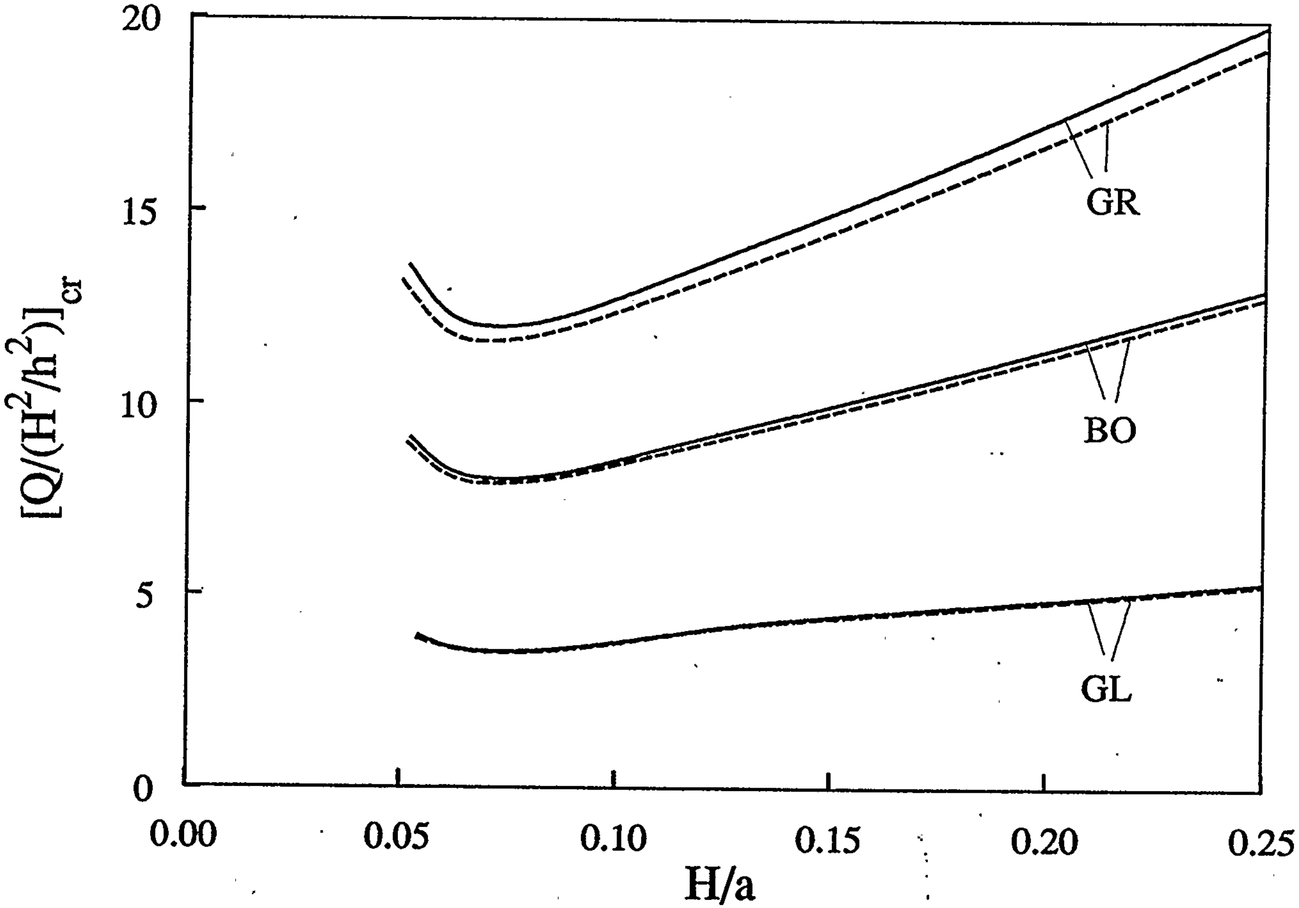

Figure 4.44: Effect of material properties on buckling load of an immovable simply-supported three-layer shallow spherical shell (a/h=15)

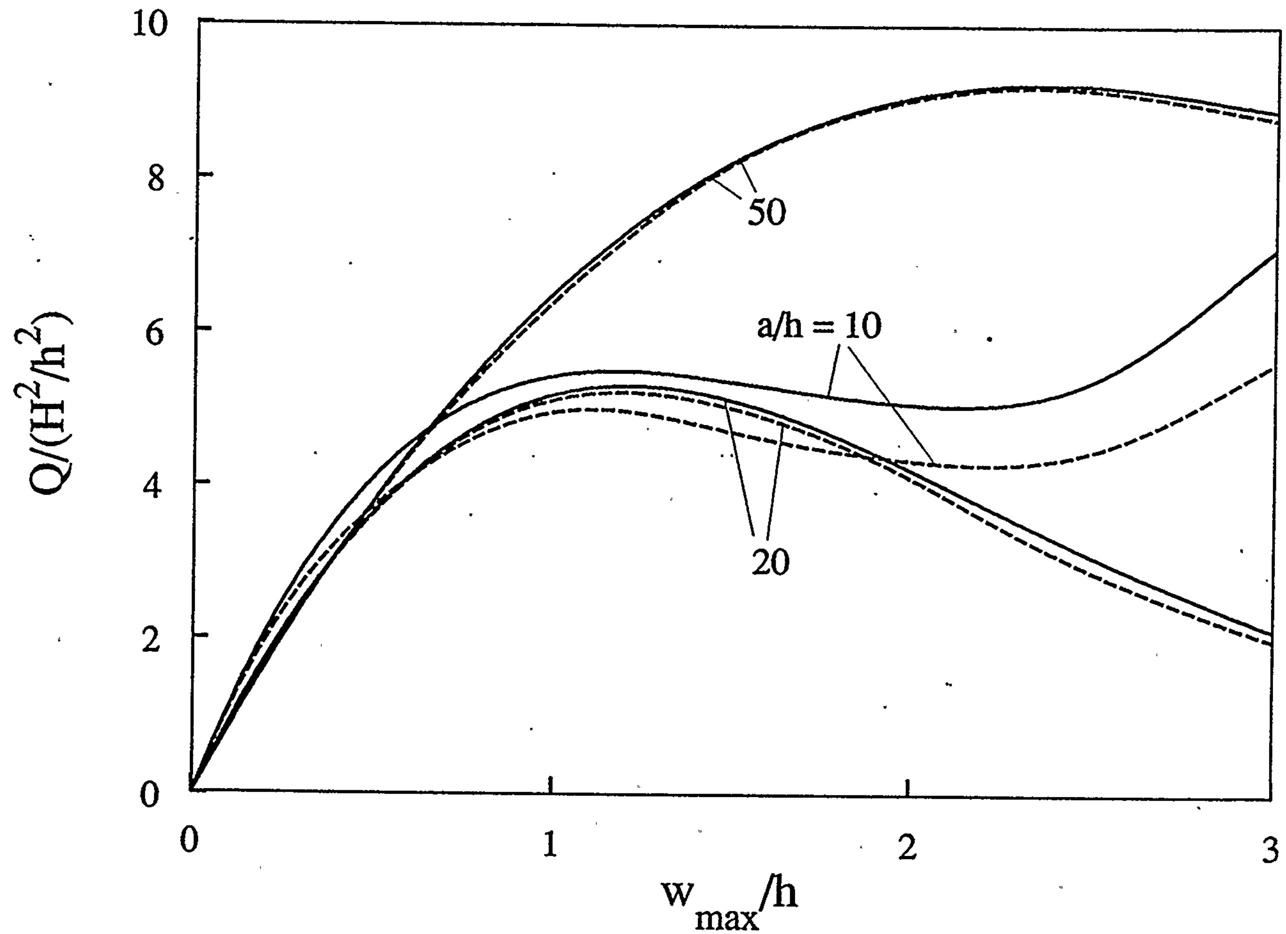

Figure 4.45: Effect of the base radius-to-thickness ratio on the postbuckling response of a movable simply-supported three-layer graphite-epoxy shallow spherical shell (H/a=0.2)

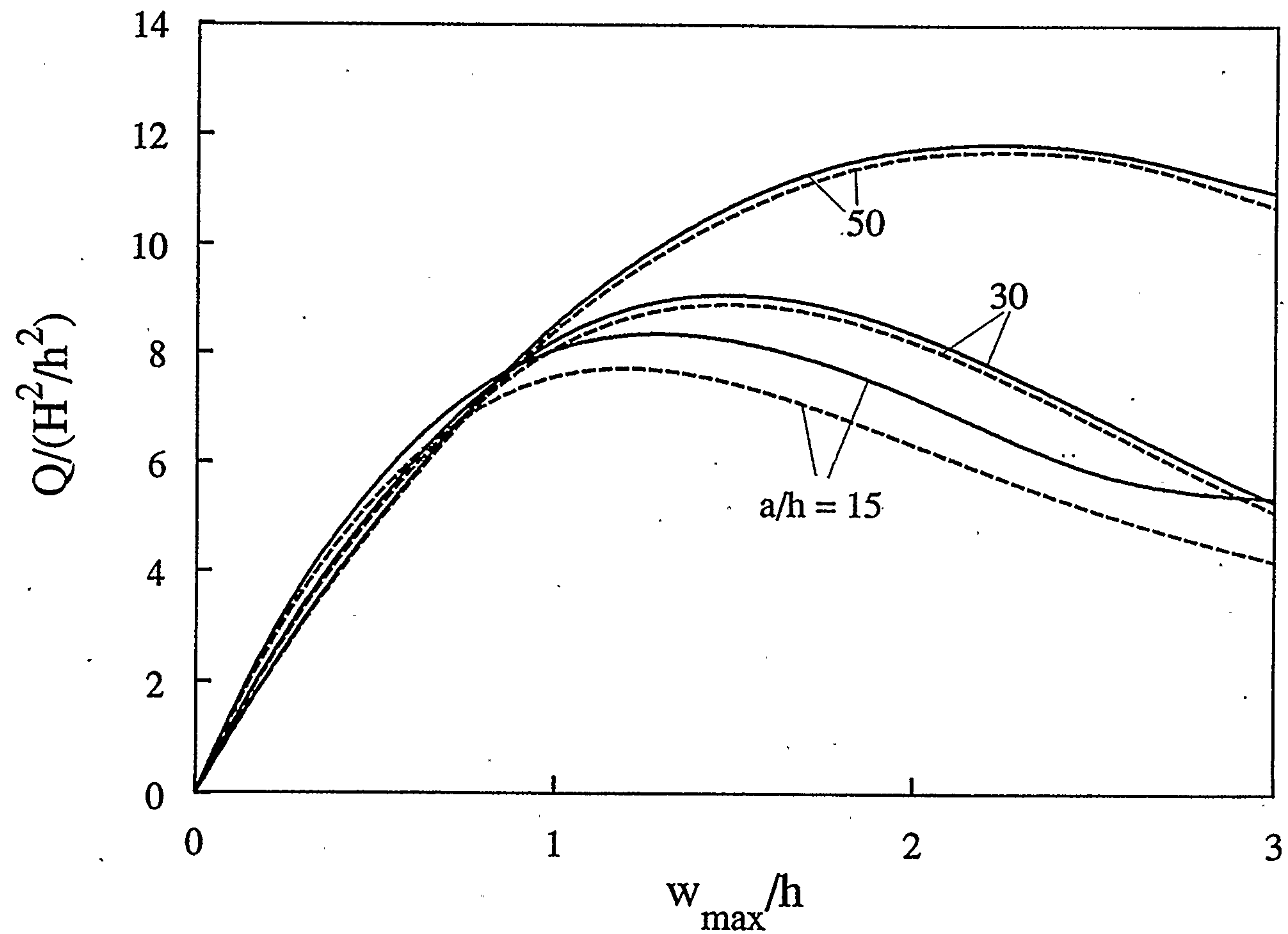

Figure 4.46: Effect of the base radius-to-thickness ratio on the postbuckling response of a movable clamped three-layer graphite-epoxy shallow spherical shell (H/a=0.2)

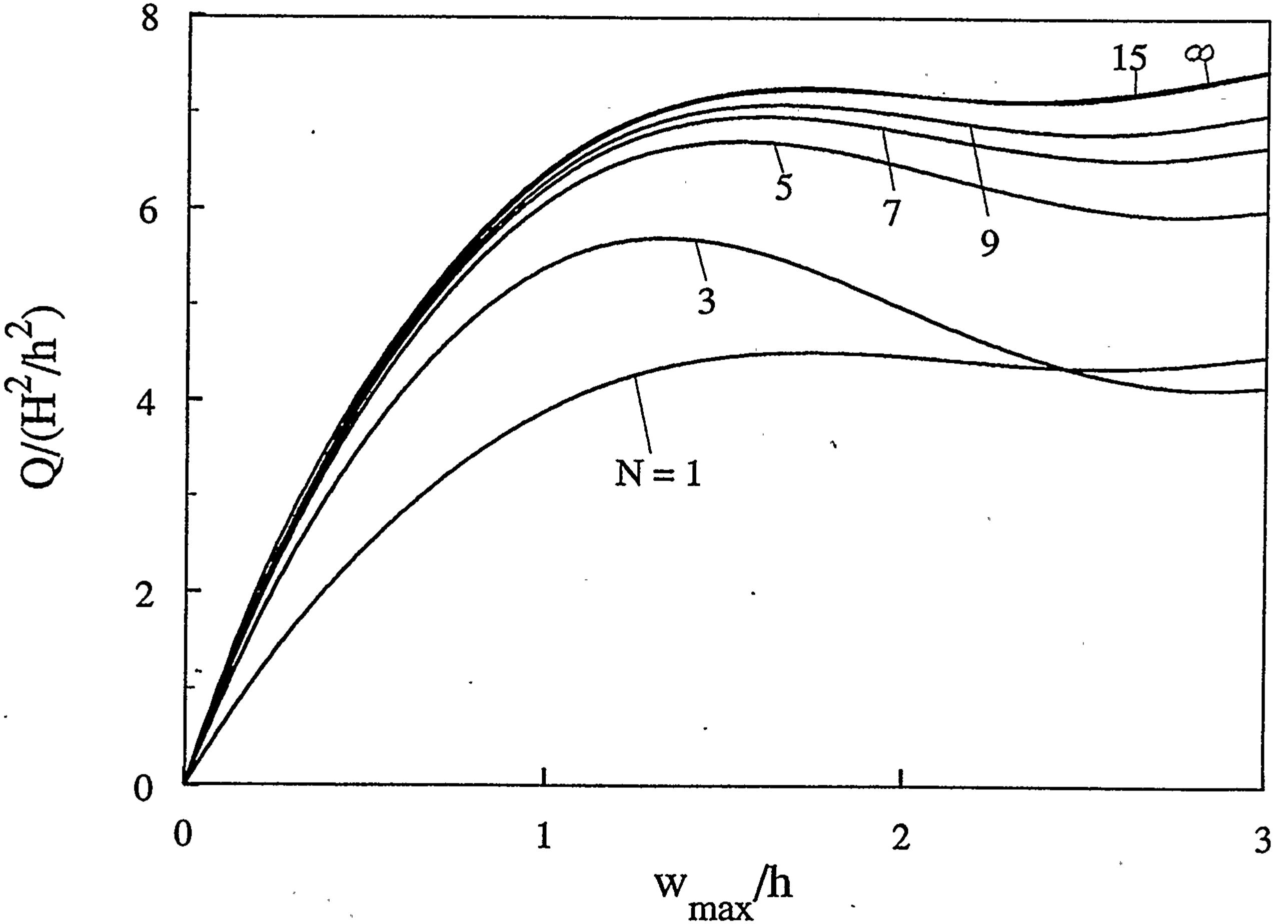

Figure 4.47: Effect of the number of layers on the postbuckling response of a movable clamped boron-epoxy shallow spherical shell (a/h=30, H/a=0.1)

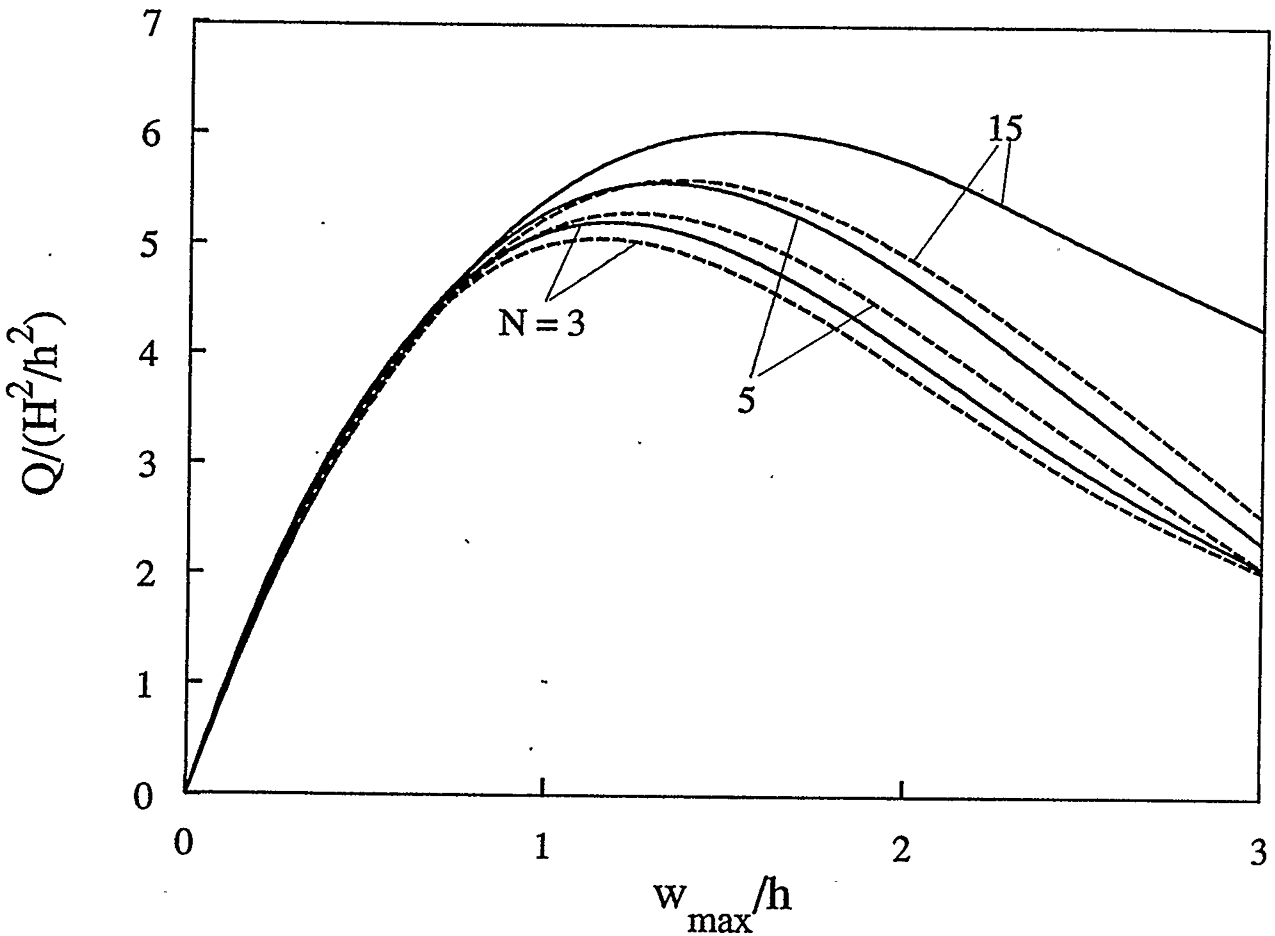

Figure 4.48: Effect of the number of layers on the postbuckling response of a movable simply-supported graphite-epoxy shallow spherical shell (a/h=15, H/a=0.25)

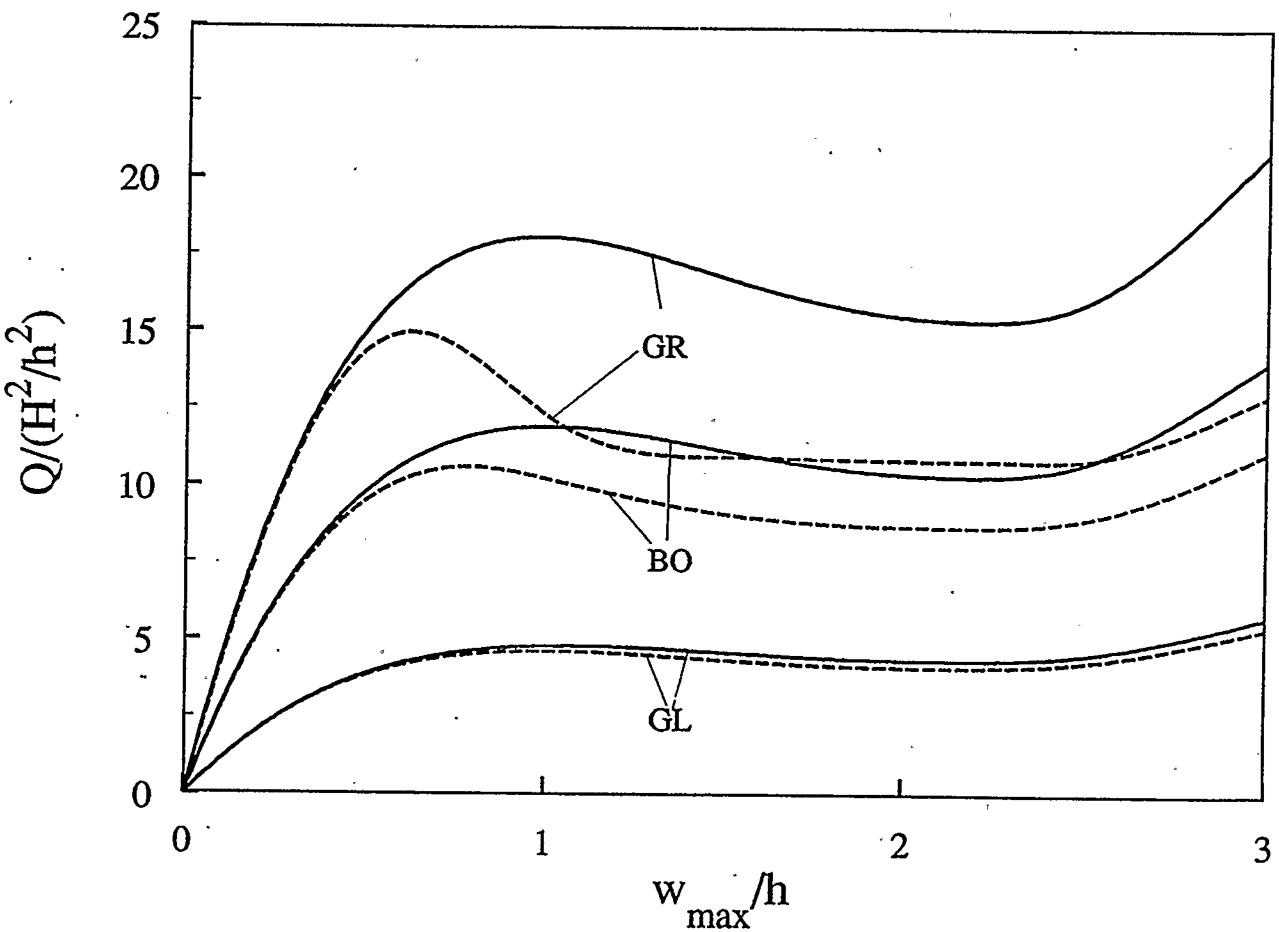

Figure 4.49: Effect of material properties on the postbuckling response of an immovable clamped five-layer shallow spherical shell (a/h=10, H/a=0.2)

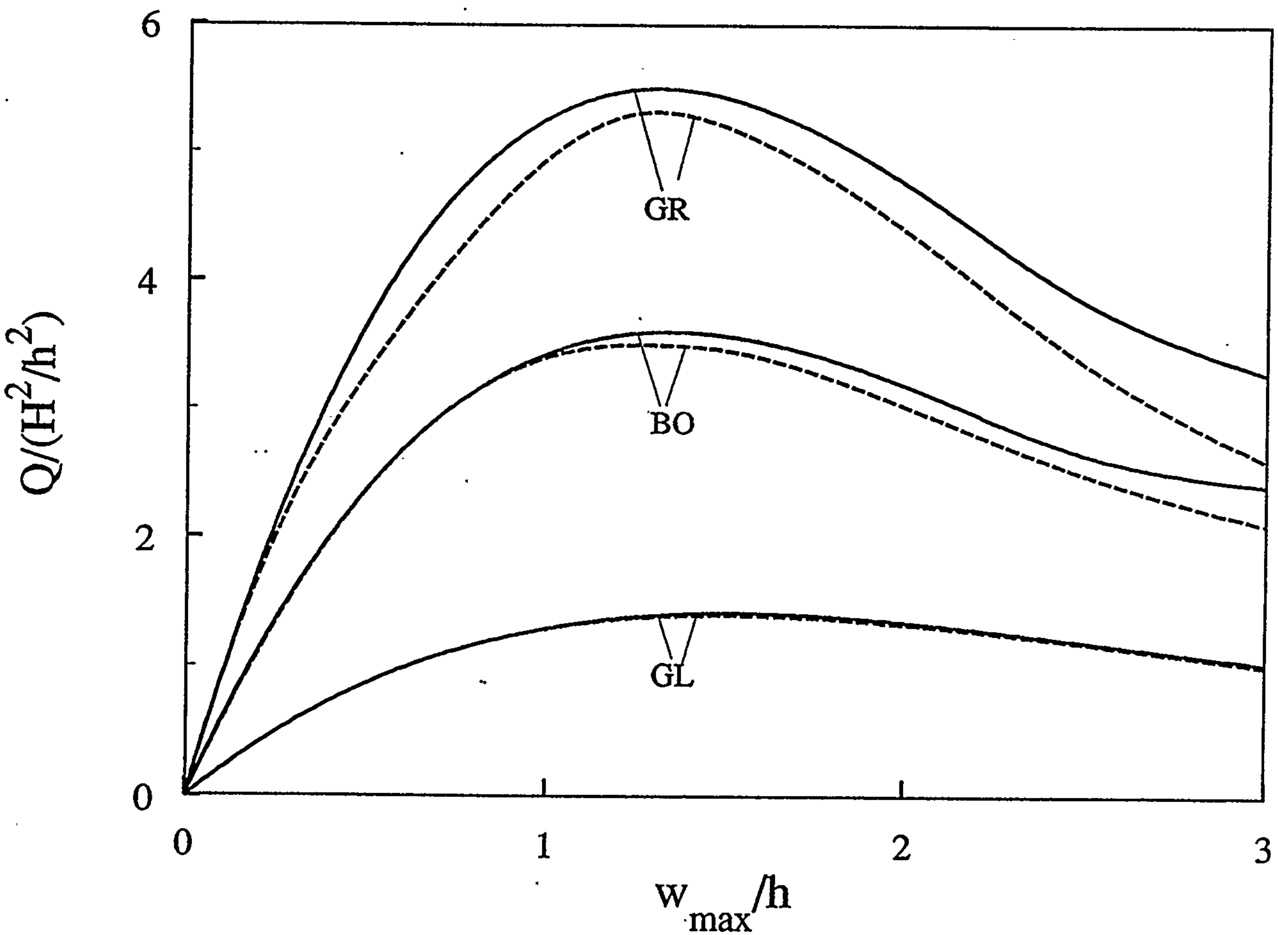

Figure 4.50: Effect of material properties on the postbuckling response of a movable simply-supported five-layer shallow spherical shell (a/h=20, H/a=0.15)

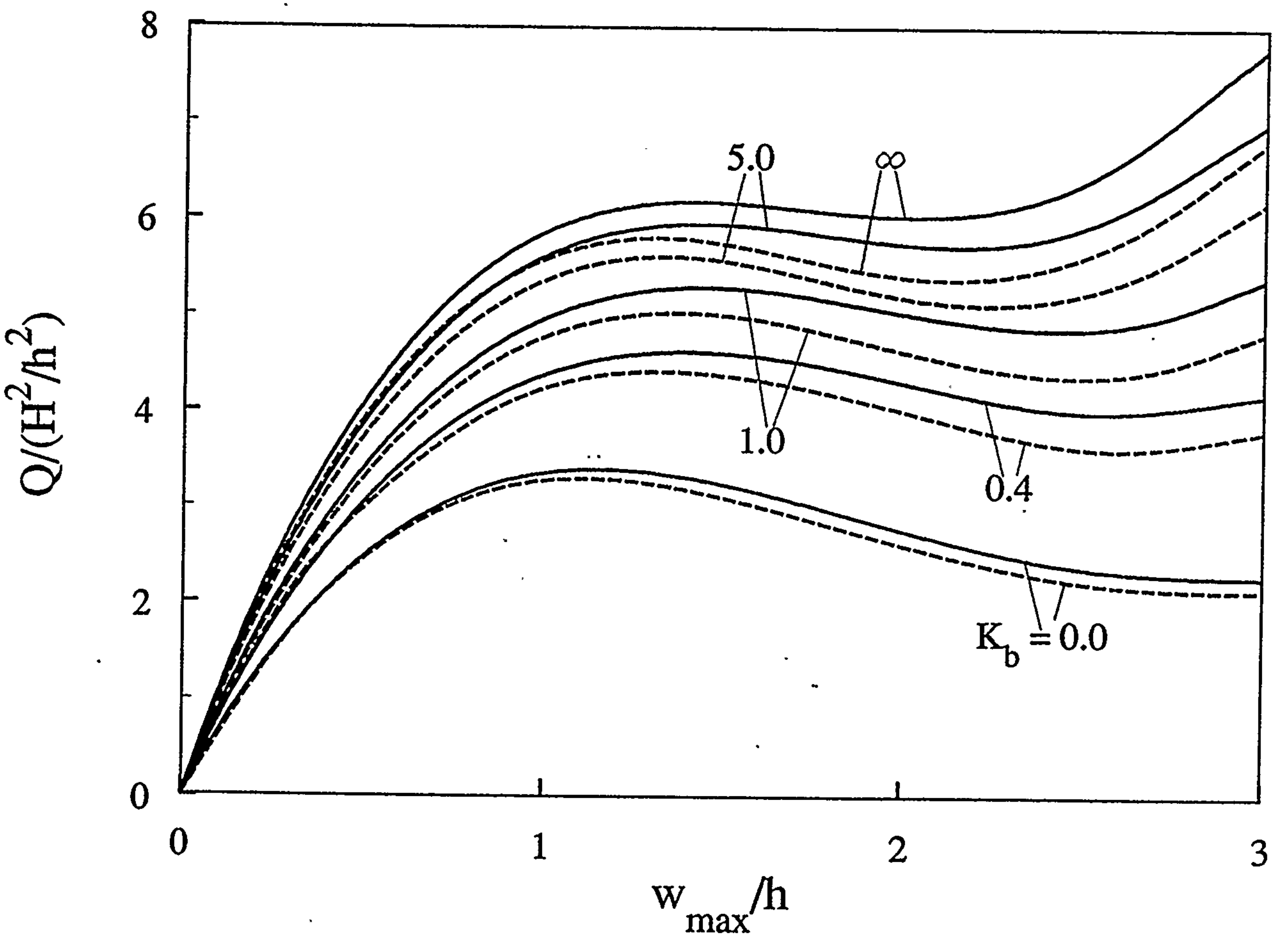

Figure 4.51: Effect of rotational edge stiffness on the postbuckling response of a three-layer boron-epoxy shallow spherical shell with a movable edge (a/h=12, H/a=0.2)

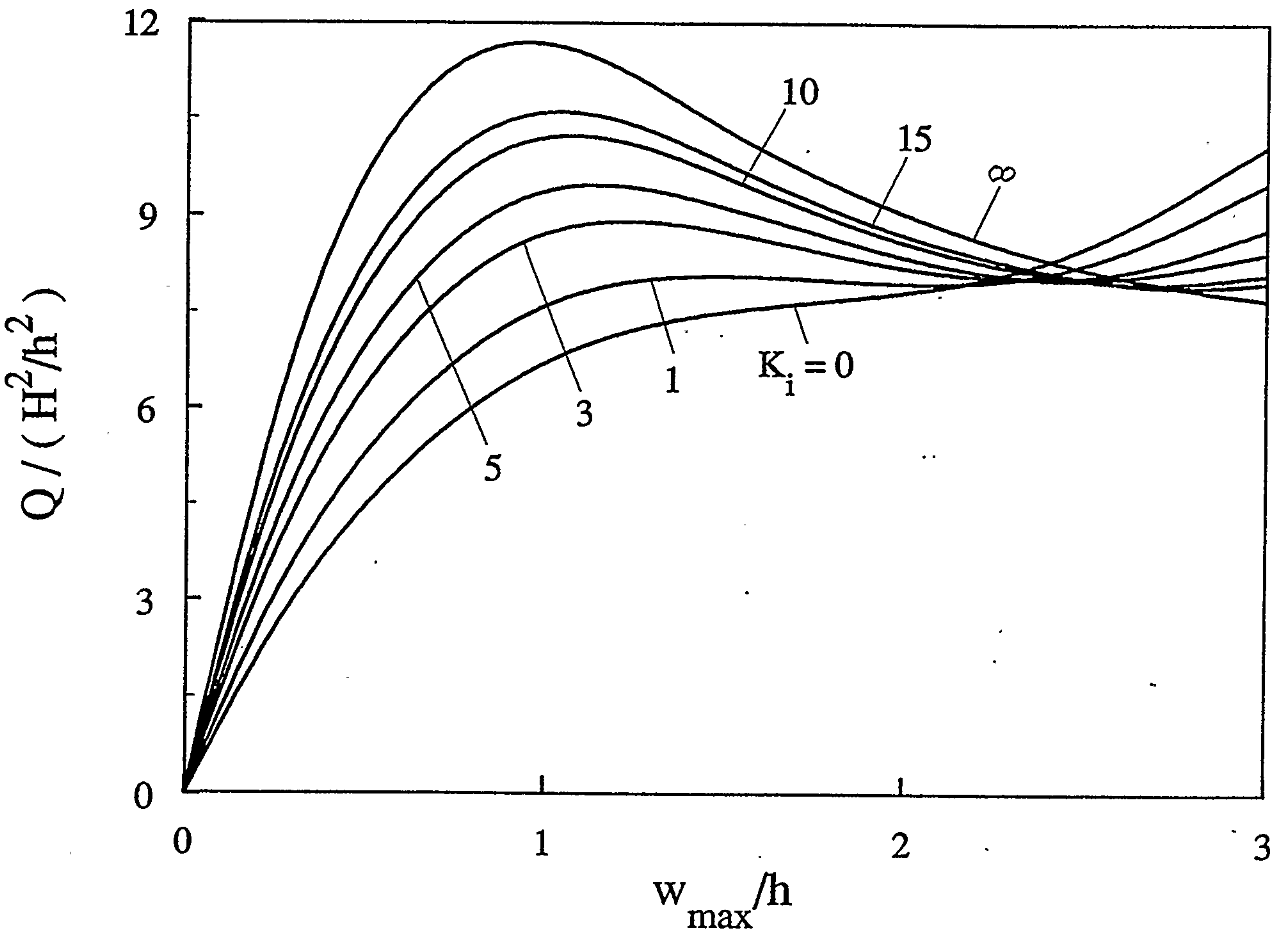

Figure 4.52: Effect of inplane edge stiffness on the postbuckling response of a five-layer boron-epoxy shallow spherical shell with a clamped edge (a/h=20, H/a=0.125)

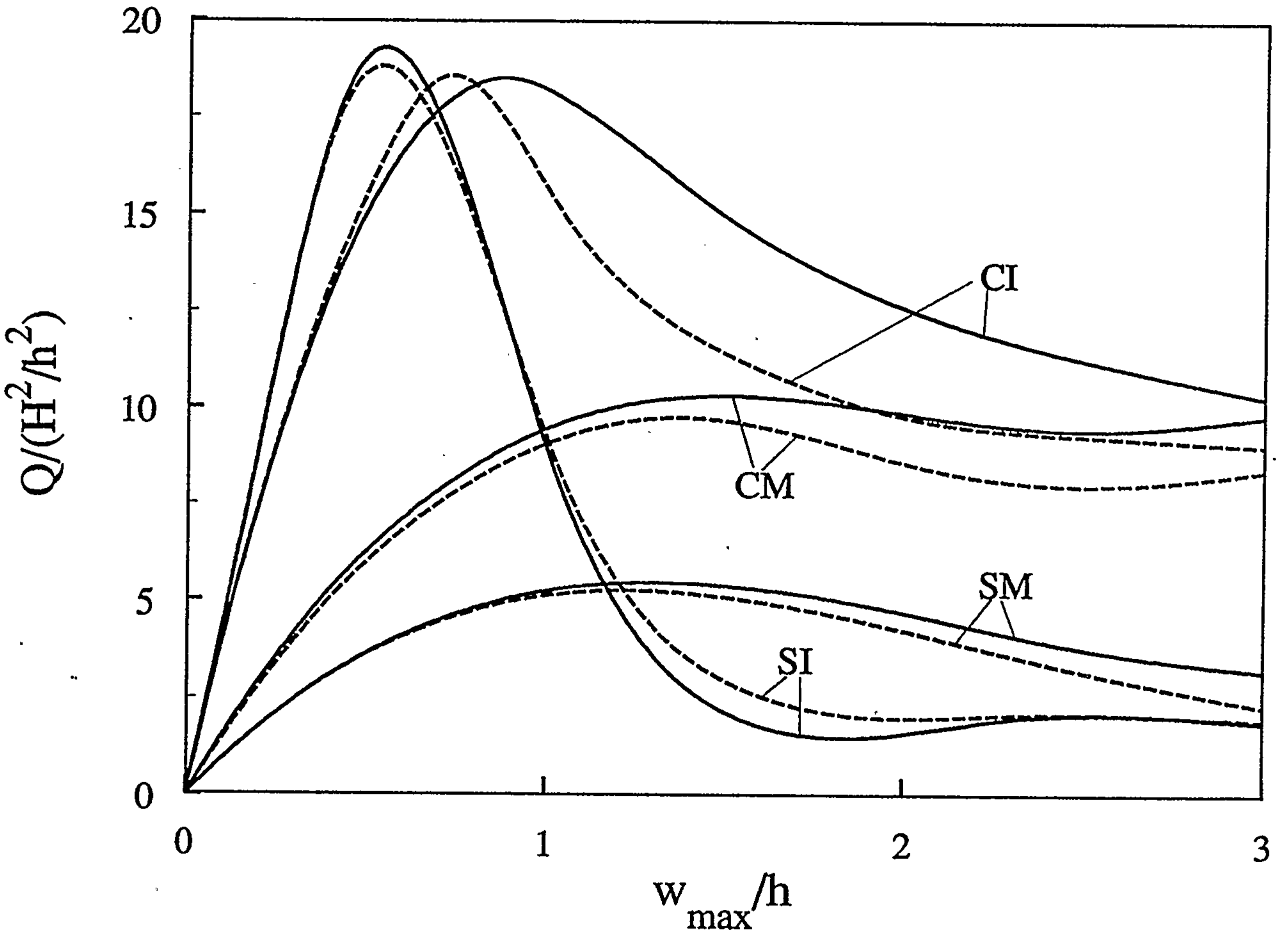

Figure 4.53: Effect of boundary conditions on the postbuckling response of a five-layer graphite-epoxy shallow spherical shell (a/h=15, H/a=0.2)

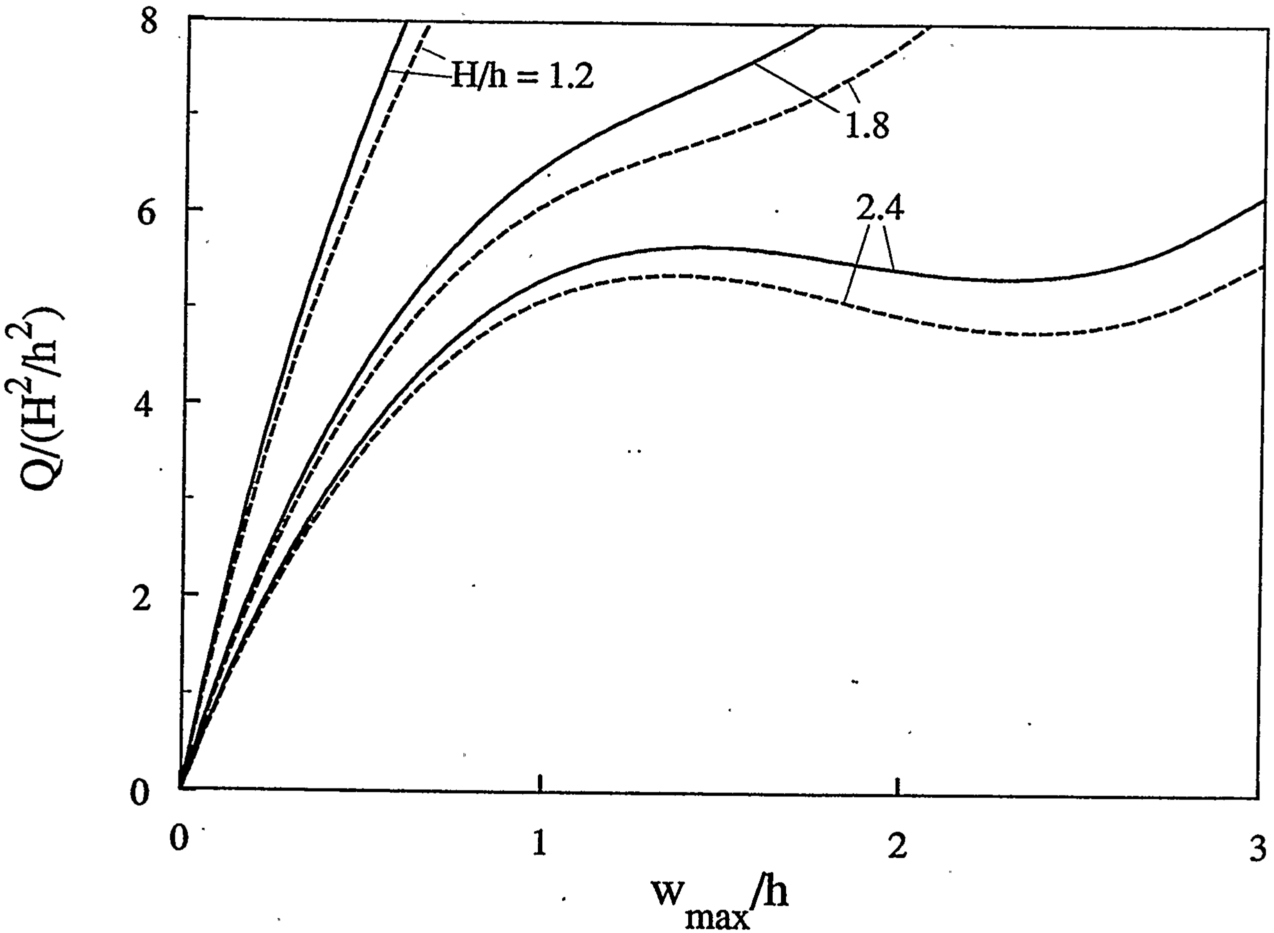

Figure 4.54: Effect of the shell rise on the postbuckling response of an elastically supported three-layer boron-epoxy shallow spherical shell (K_b=2, K_i=0, a/h=12)

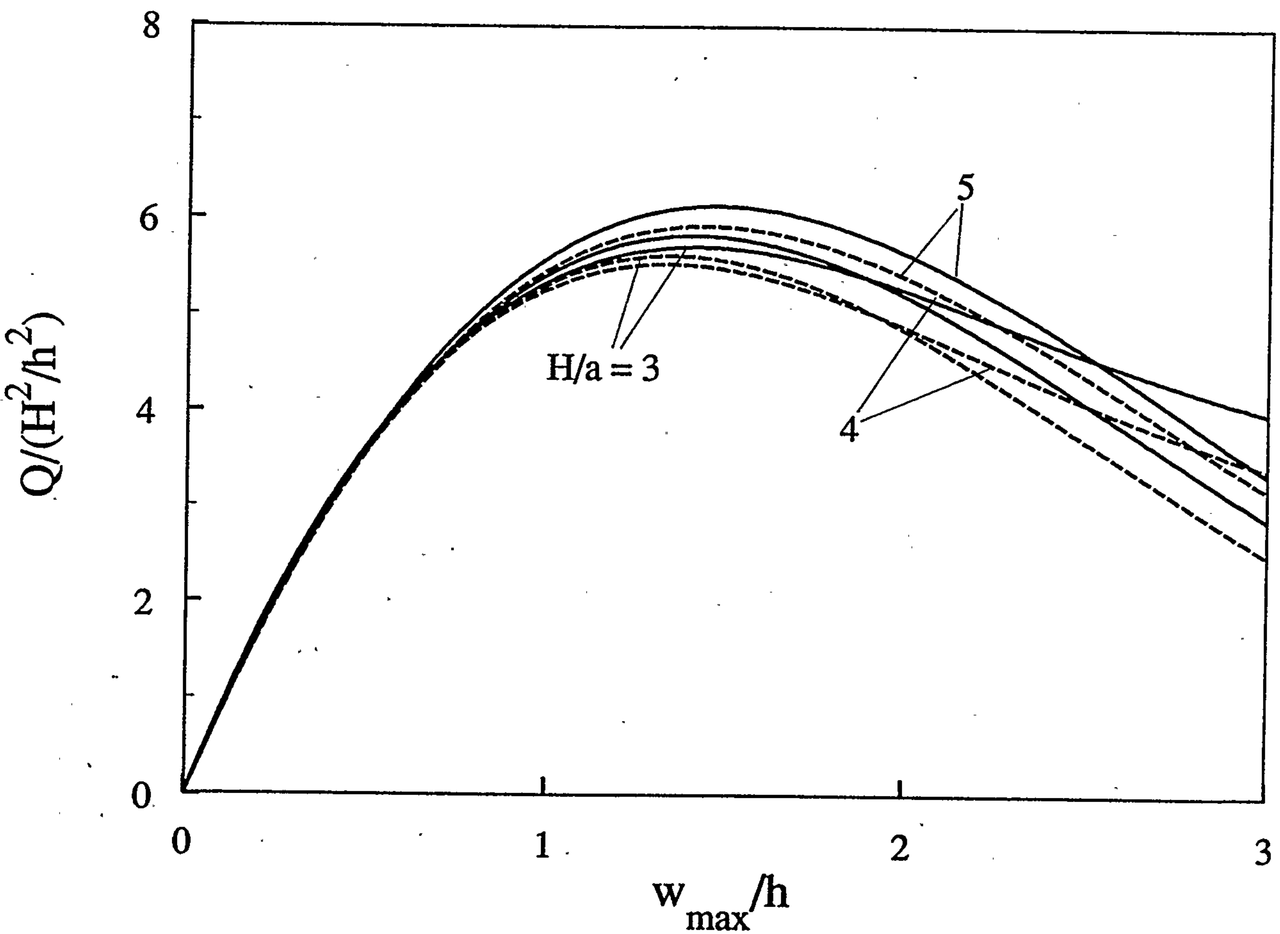

Figure 4.55: Effect of the shell rise on the postbuckling response of a movable simply-supported seven-layer graphite-epoxy shallow spherical shell (a/h=20)

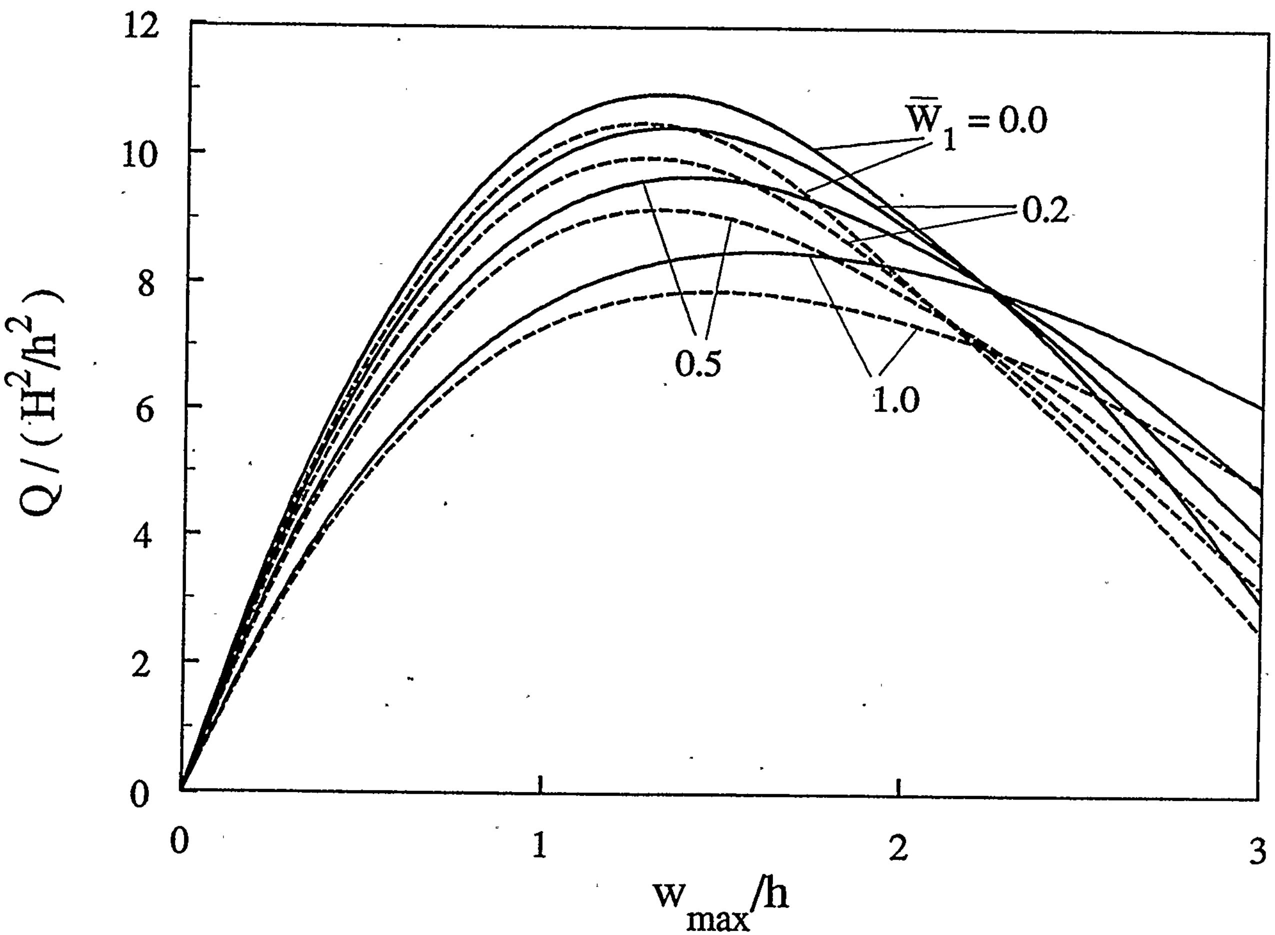

Figure 4.56: Effect of geometrically initial imperfection on the postbuckling response of a movable clamped five-layer graphite-epoxy shallow spherical shell resting on elastic foundations (K_f=5, K_n=10, G_f=0, a/h=20, H/a=0.2)

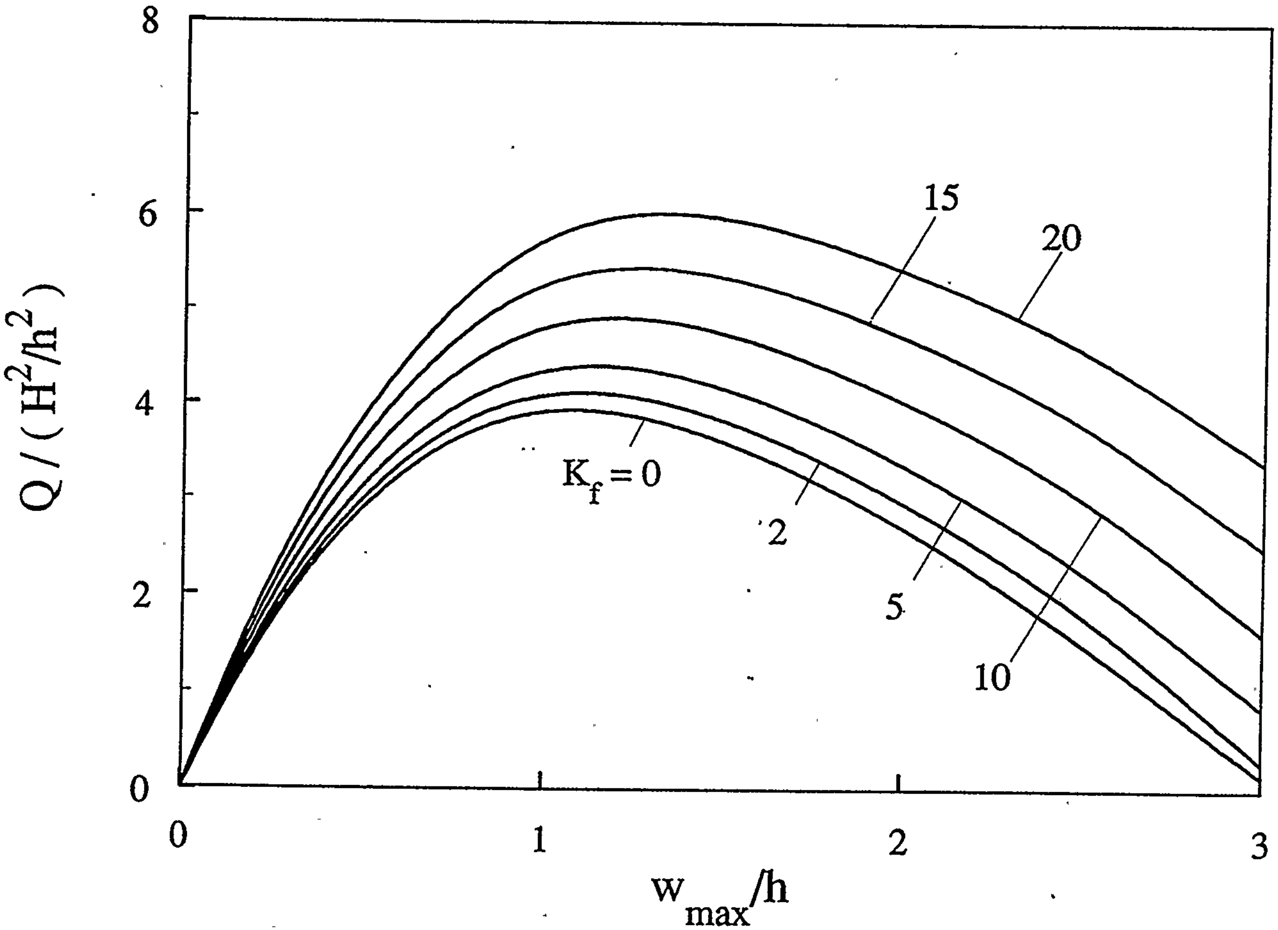

Figure 4.57: Effect of Winkler foundation parameter on the postbuckling response of an elastically supported five-layer glass-epoxy imperfect shallow spherical shell (K_b=2, K_i=5, $\overline{W}_1$=0.5, K_n=5, G_f=1, a/h=15, H/a=0.2)

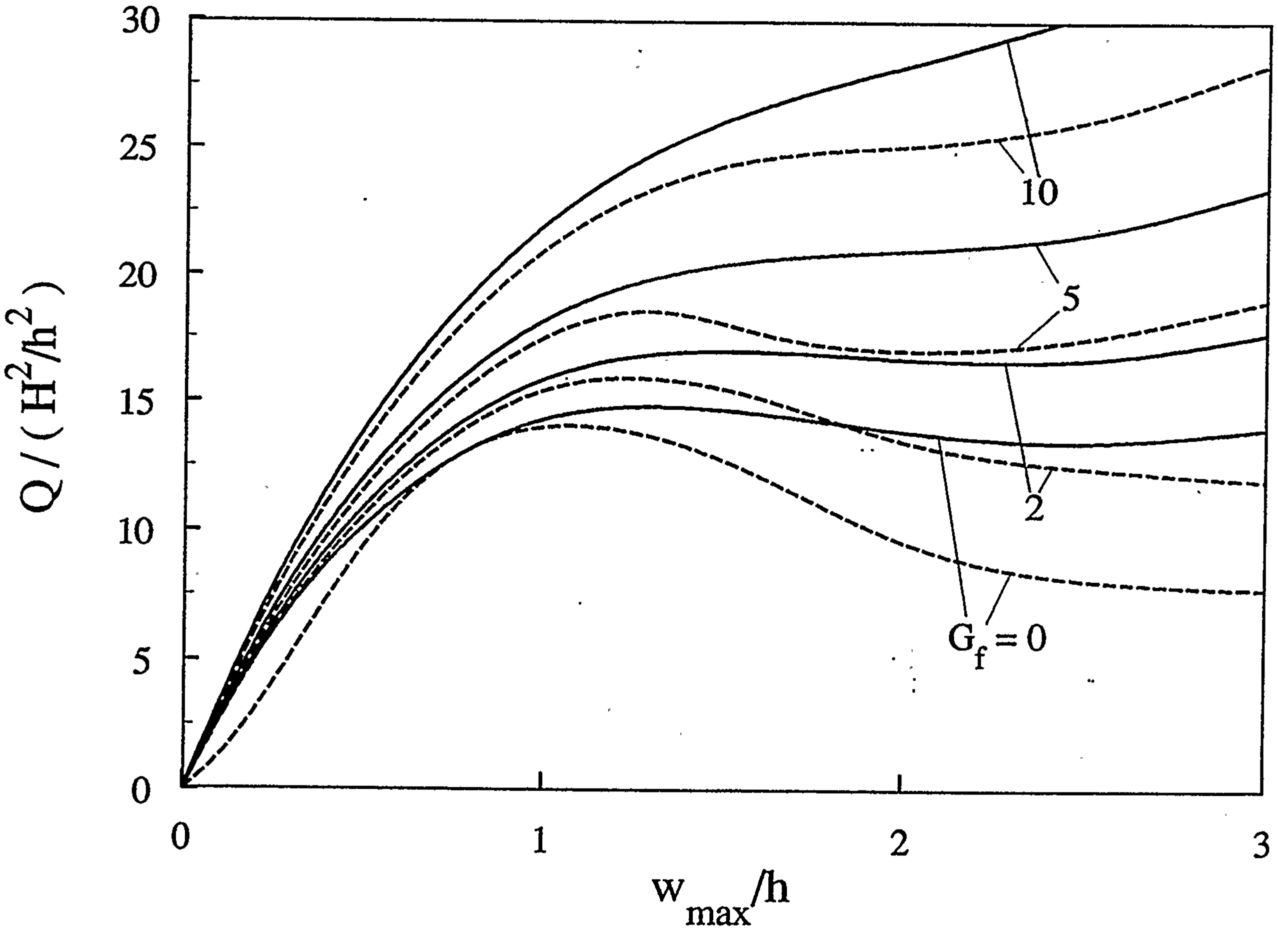

Figure 4.58: Effect of Pasternak foundation parameter on the postbuckling response of an elastically supported seven-layer graphite-epoxy shallow spherical shell

(K_b=10, K_i=5, K_f=5, K_n=0, a/h=10, H/a=0.25)

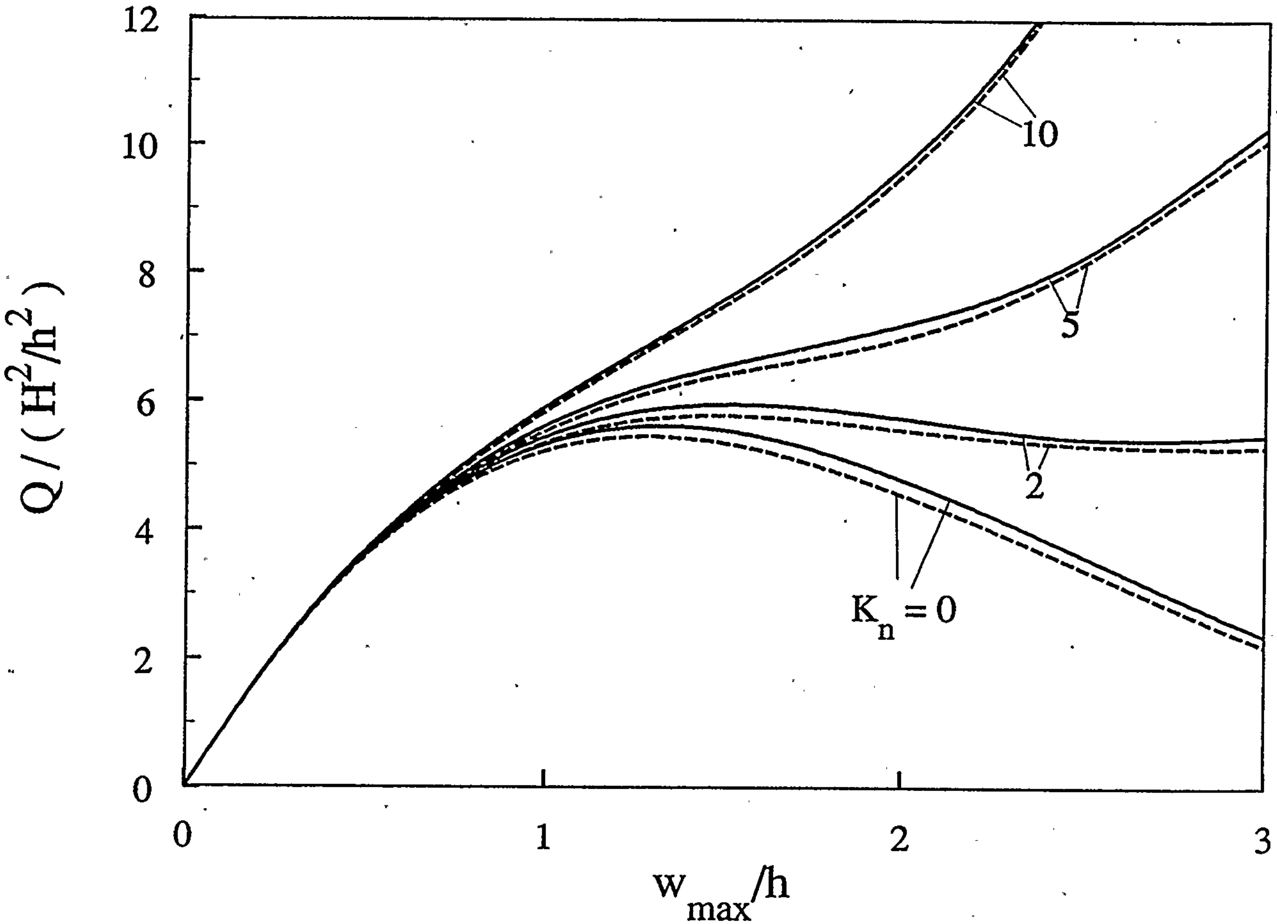

Figure 4.59: Effect of nonlinear Winkler foundation parameter on the postbuckling response of a movable simply-supported five-layer graphite-epoxy shallow spherical shell (K_f=0, G_f=0, a/h=20, H/a=0.2)

4.5.2 Symmetrically Laminated Circular Plates

In this section, the large-deflection response of symmetrically laminated circular plates is presented for various geometric and material parameters.

4.5.2.1 The Effect of the Radius-to-Thickness Ratio on the Static Large-Deflection Response

The effect of transverse shear on the large-deflection response of an immovable five-layer graphite-epoxy circular plate is shown in Fig. 4.60 for different ratios of radius-tô-thickness. This effect reduces the load compared with that excluding this effect and is pronounced for moderately thick plates. At w_{max}=3h, the load is decreased by approximate 5.4%, 11% and 17% for a/h=20, 10 and 5, respectively. As expected, this effect is weakened for the thin plate, for instance in this figure, a/h=50.

4.5.2.2 The Effect of the Number of Layers on the Static Large-Deflection Response

Figure 4.61 shows the effect of the number of layers on the large-deflection response of a movable simply-supported glass-epoxy circular plate. The load decreases with an increase in the number except for N=1. The transverse shear effect(not shown herein) is not remarkable as the low material ratio, i.e., GL composite.

4.5.2.3 The Effect of Material Properties on the Static Large-Deflection Response

The load-deflection response of an elastically supported circular plate with different materials is demonstrated in Fig. 4.62 The load in the figure increases as the modulus ratio, E_L / E_T, increases. The effect of transverse shear reduces the load by 1.6%, 1.8%, 10.5% and 13.3% for materials of isotropic, glass-epoxy, boron-epoxy and graphite-epoxy, respectively, at $w_{max} = 3h$.

4.5.2.4 The Effect of Boundary Conditions on the Static Large-Deflection Response

The effect of edge stiffnesses on the large-deflection response is presented in Figs. 4.63 and 4.64. The large deflection response of an elastically supported seven-layer boron-epoxy circular plate is shown in Fig. 4.63 for different edge rotational stiffness, K_b. The load increases with increasing K_b and the effect of K_b is pronounced. At w_{max}=3h, the load for $K_b=\infty$(clamped edge) is increased by 63% compared with that for K_b=0(simply -supported edge). The load response including the effect of transverse shear is similar that shown in this figure, but not presented here. Similarly, the load increases with increasing K_i, which is demonstrated in Fig. 4.64 for a clamped five-layer graphite-epoxy circular plate. At w_{max}=3h, the load for $K_i=\infty$(immovable edge) is increased by approximately 133% compared with that for $K_i=0$(movable edge). The effect of transverse shear reduces the load by about 10%. It is noted from these figures that the effect of inplane edge stiffness is more pronounced than rotational one.

4.5.2.5 The Effect of Geometrically Initial Imperfections on the Static Large-Deflection Response

The load increases with an increase in the value of the initial deflection, $\bar{W}_1$, which is shown in Fig. 4.65 for a movable clamped five-layer glass-epoxy circular plate. This is resulted from the change of midplane curvature due to the imperfection.

4.5.2.6 The Effect of Elastic Foundations on the Static Large-Deflection Response

The load-deflection curves for an immovable clamped five-layer boron-epoxy imperfect circular plate on elastic foundations are plotted in Fig. 4.66 for various values of elastic foundation parameters. It is found that the load increases with an increase of the values of foundation parameters K_f and/or K_n. The effect of transverse shear reduces the load by about 6% at $w_{max} = 3h$.

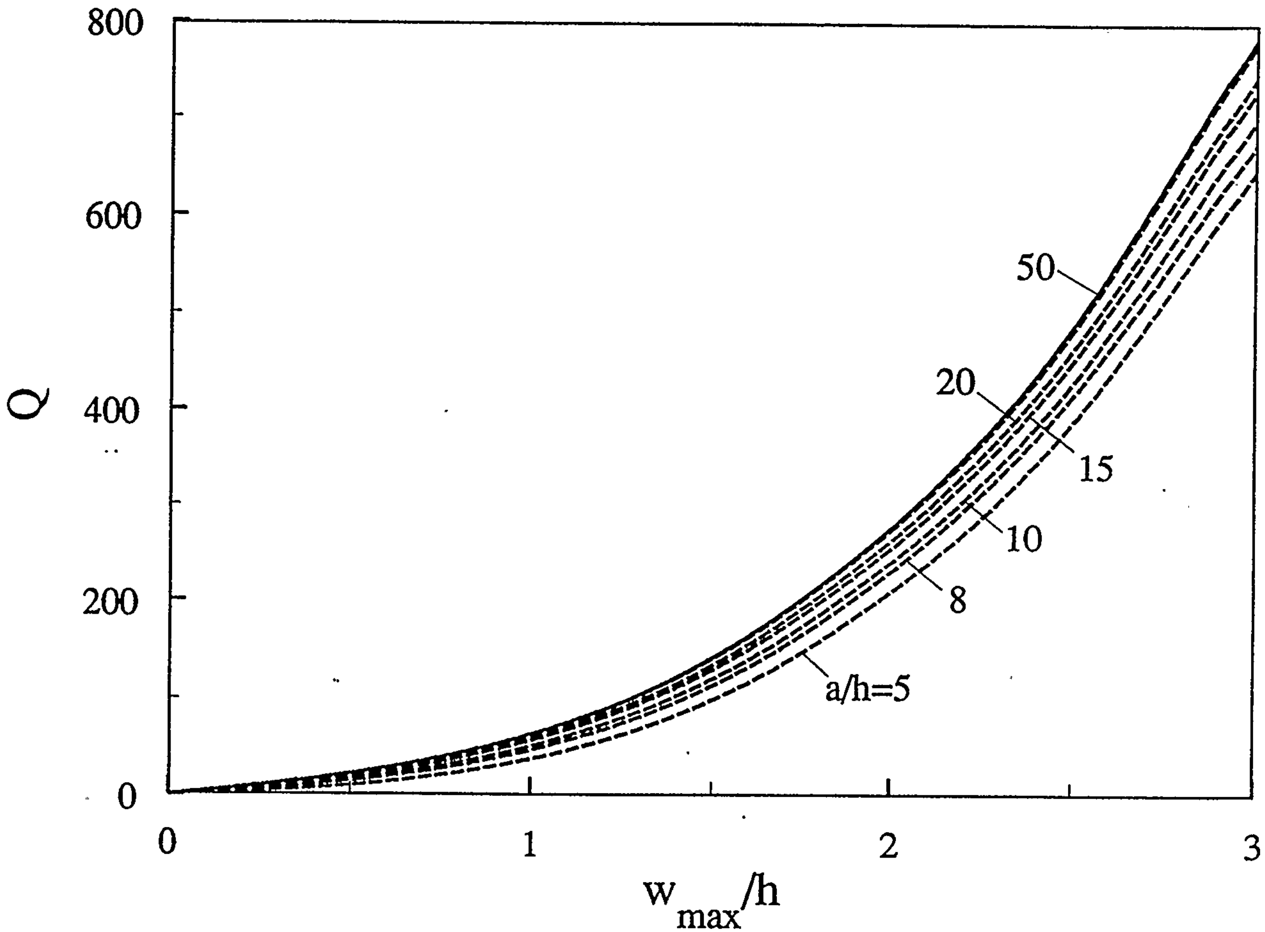

Figure 4.60: Effect of the base radius-to-thickness ratio on the static large-deflection response of an immovable clamped five-layer graphite-epoxy circular plate

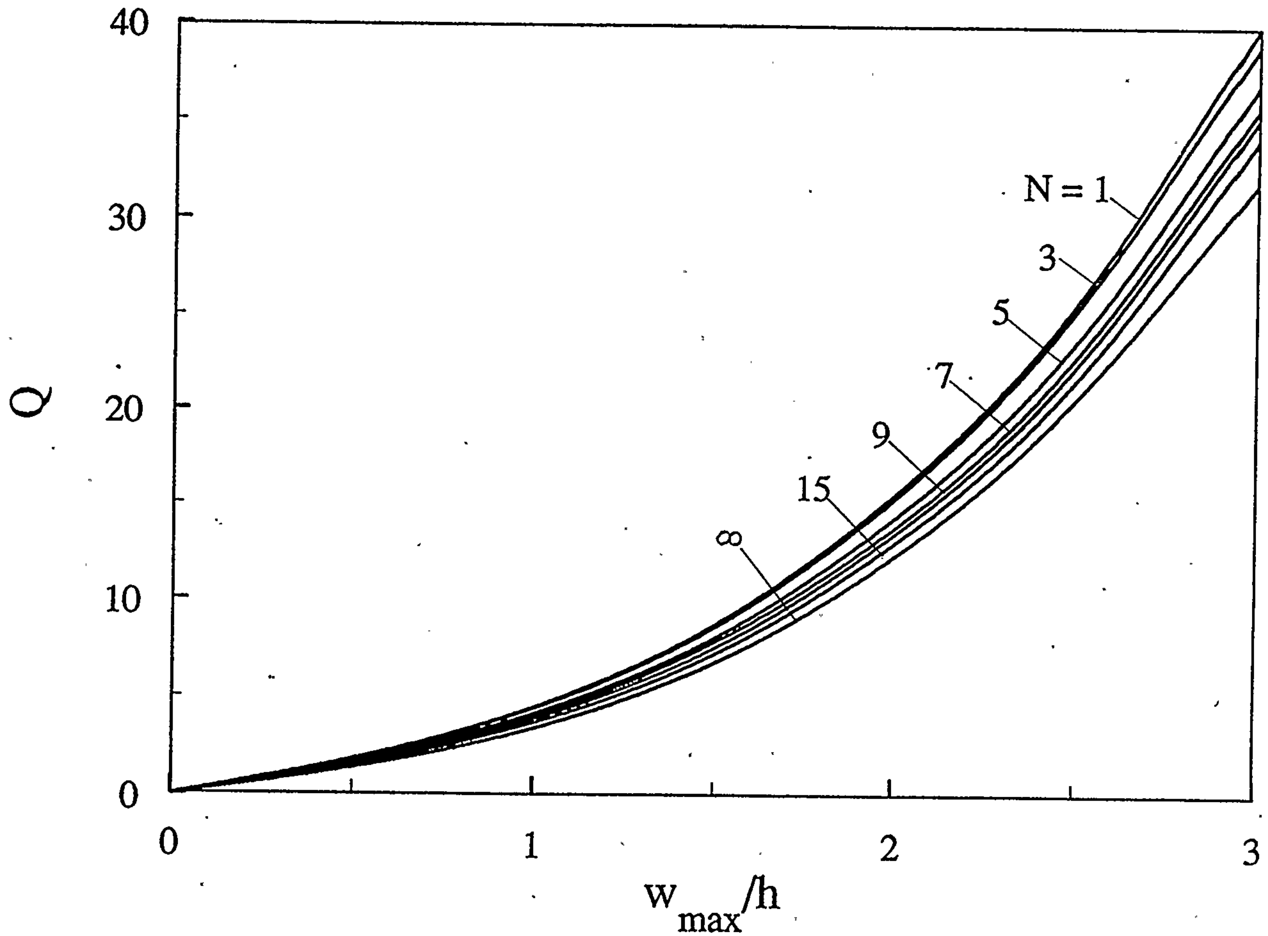

Figure 4.61: Effect of the number of layers on the static large-deflection response of a movable simply-supported glass-epoxy circular plate (a/h=12)

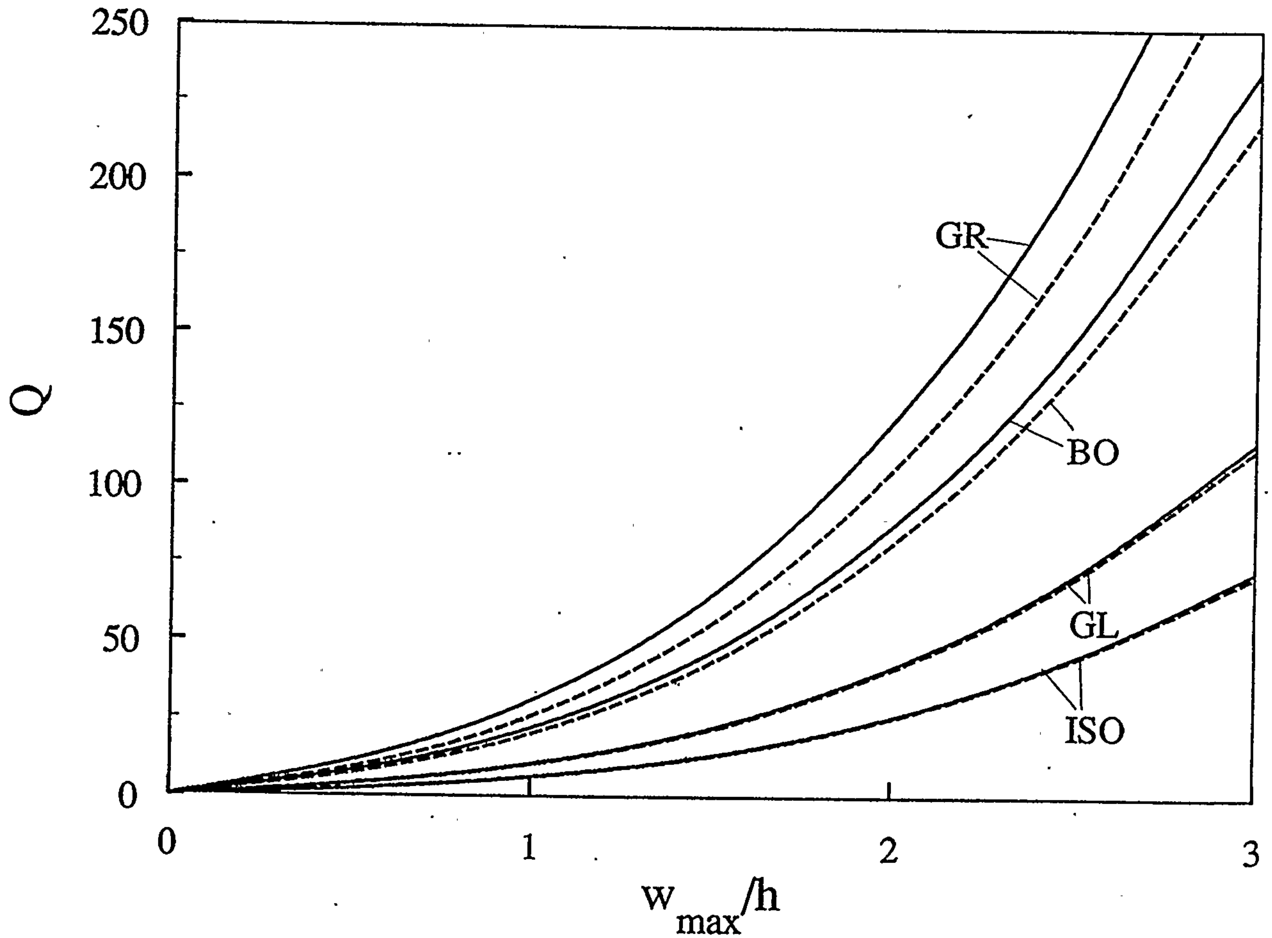

Figure 4.62: Effect of material properties on the static large-deflection response of an elastically supported three-layer circular plate (K_b=1, K_i=2, a/h=10)

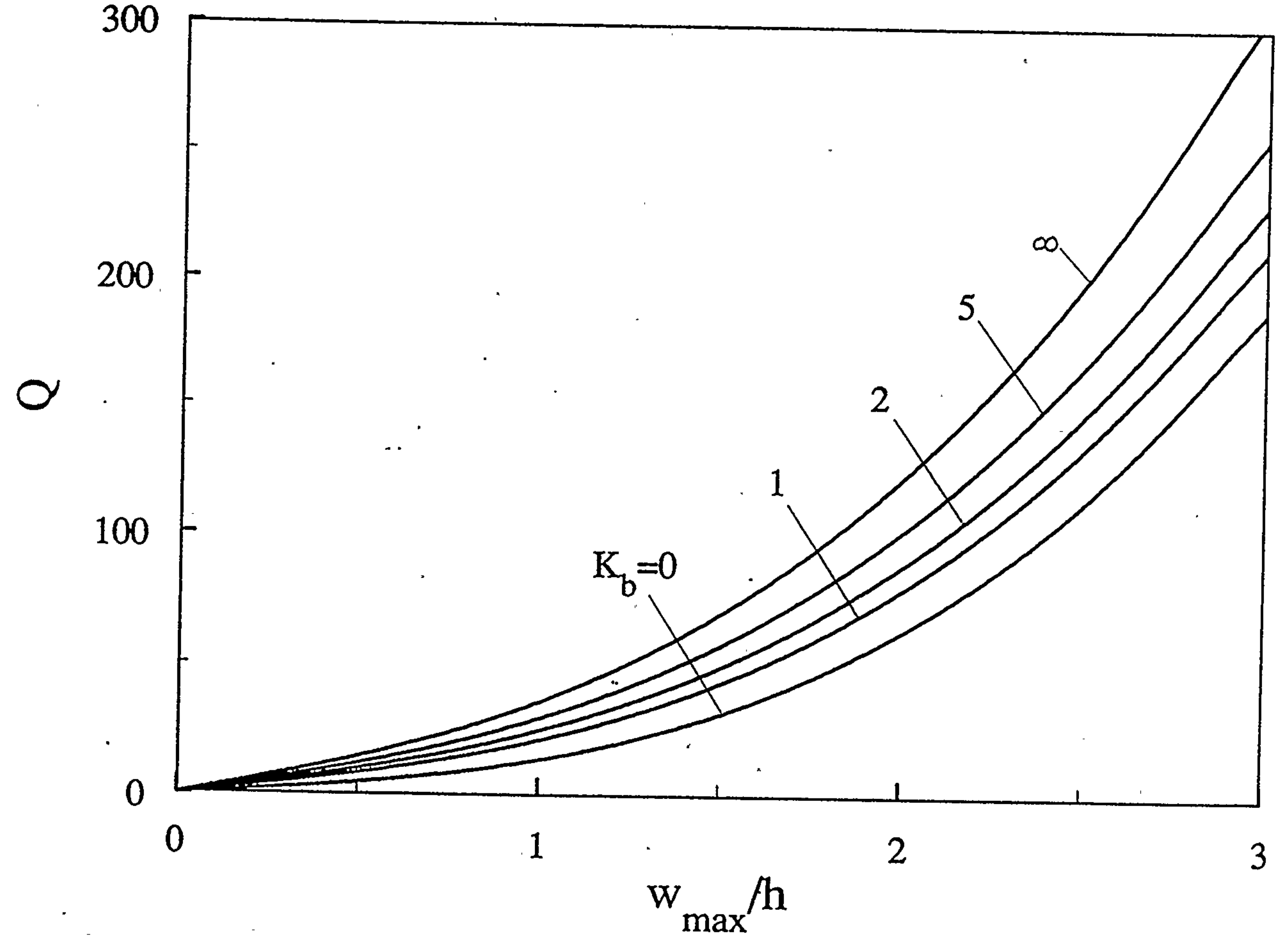

Figure 4.63: Effect of rotational edge stiffness on the static large-deflection response of an elastically supported seven-layer boron-epoxy circualr plate (K_i=2, a/h=10)

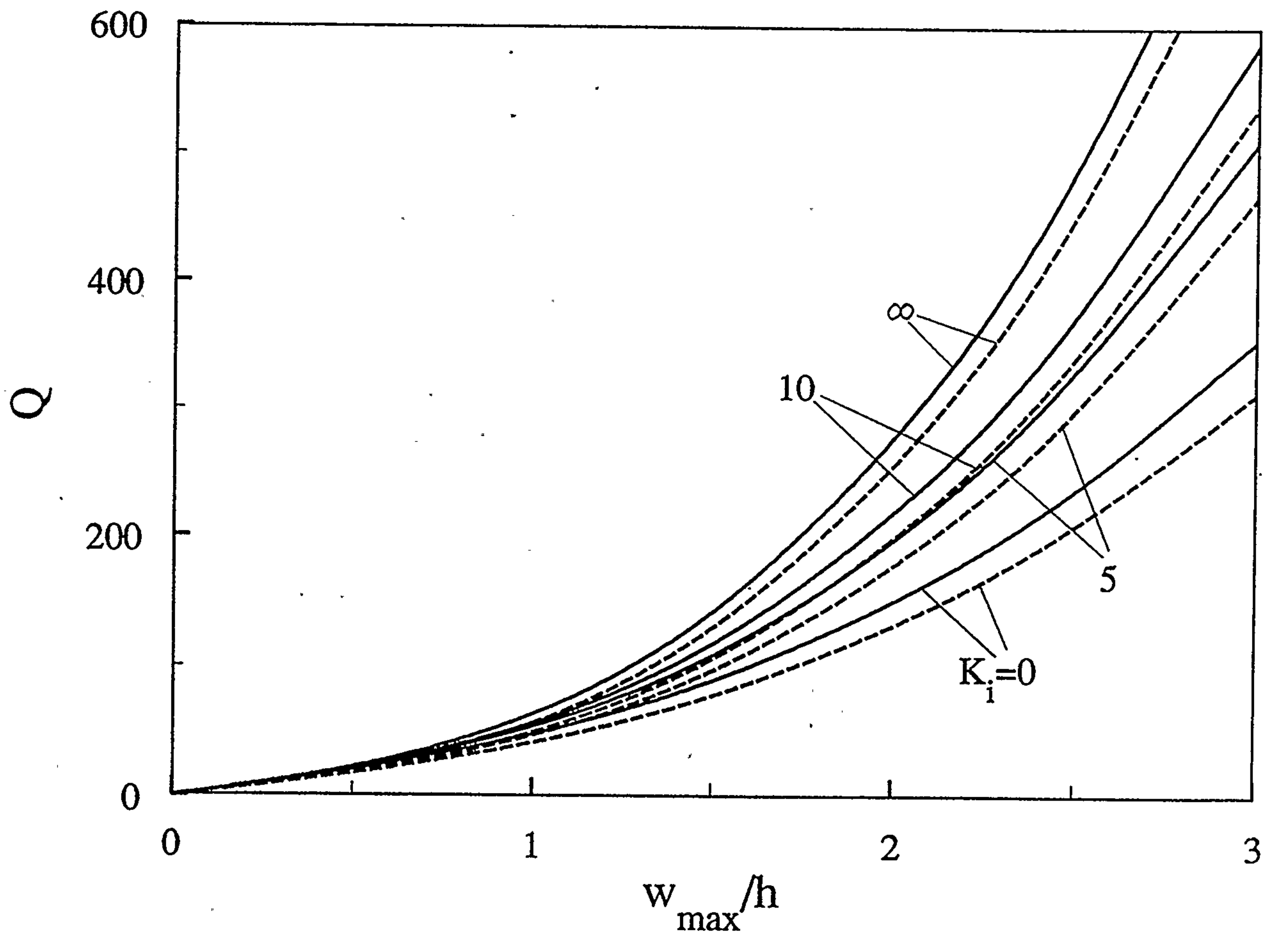

Figure 4.64: Effect of inplane edge stiffness on the static large-deflection response of a five-layer graphite-epoxy circular plate with a clamped edge (a/h=15)

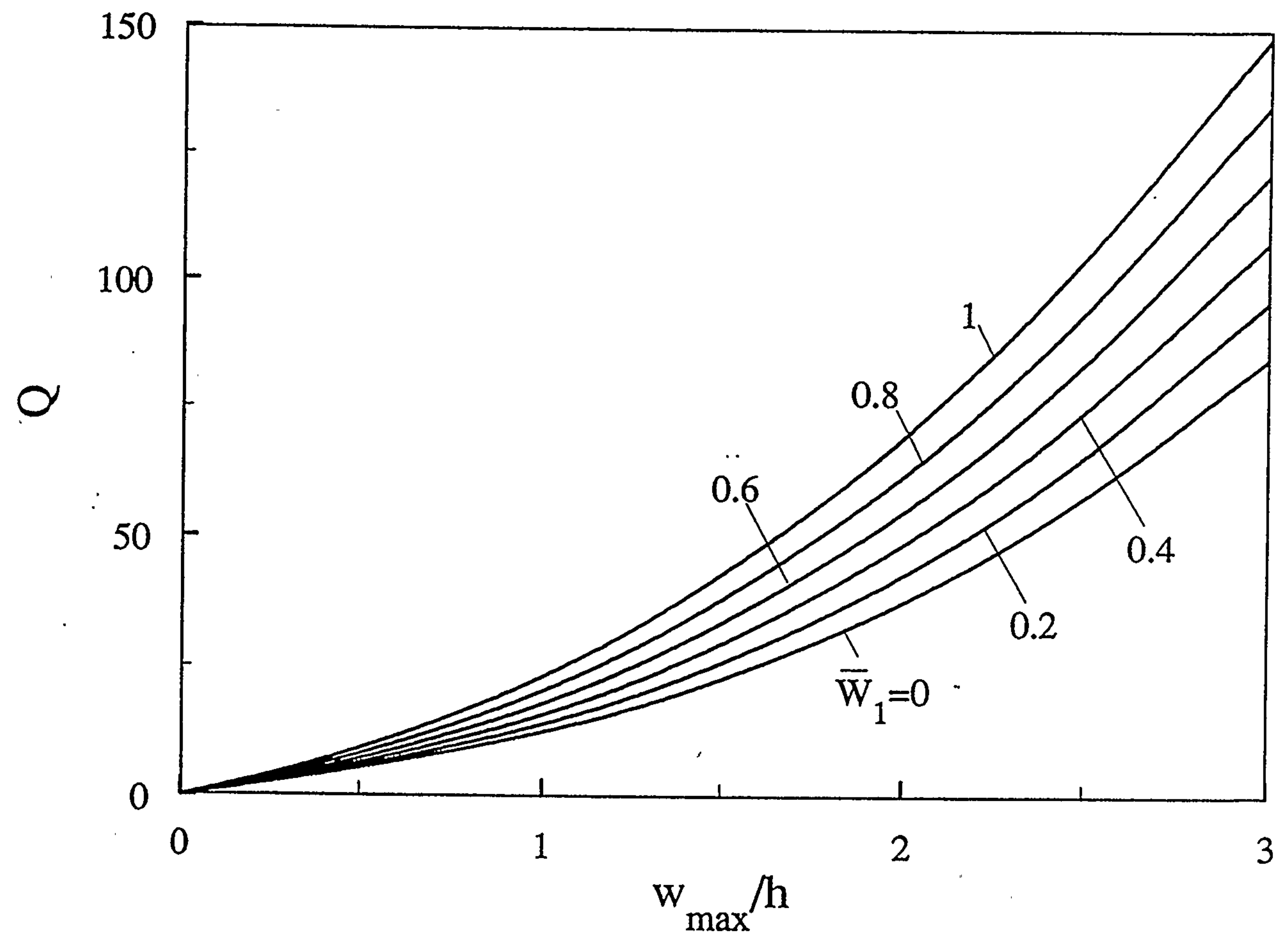

Figure 4.65: Effect of geometrically initial imperfections on static the large-deflection response of a movable clamped five-layer glass-epoxy circular plate (a/h=20)

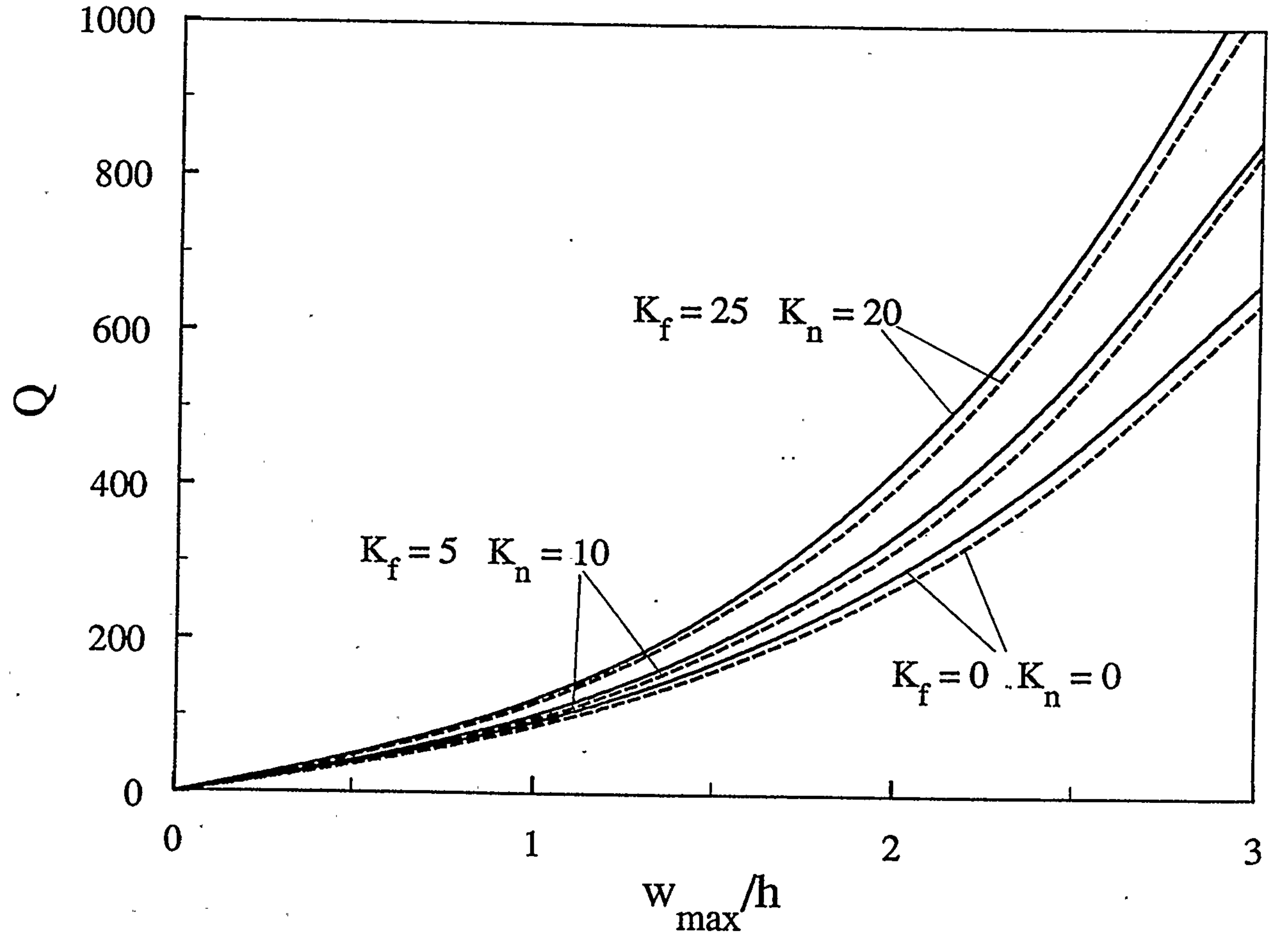

Figure 4.66: Effect of elastic foundations on the static large-deflection response of an immovable clamped five-layer glass-epoxy imperfect circular plate ($\overline{W}_1$=0.1, G_f=10 a/h=10)

4.5.3 Unsymmetrically Laminated Shallow Spherical Shells and Circular Plates

The buckling, postbuckling response for unsymmetrically laminated shallow spherical shells and large-deflection response for unsymmetrically laminated circular plates are presented in this section for various geometric and material parameters.

4.5.3.1 The Effect of Material Properties on the Buckling Load

The buckling response of a movable clamped two-layer shallow spherical shell is given in Fig. 4.67. The values of $(H/a)_{cr}$ and the associated buckling load Q_{cr} which are defined in section 4.5.1.1 are listed in Table 4.22. It is observed that once the critical value $(H/a)_{cr}$ occurs, the buckling load Q_{cr} initially decreases and then increases with increasing the value of H/a. The buckling load Q_{cr} increases but the critical value $(H/a)_{cr}$ decreases as the material ratio, E_L/E_T, increases. The effect of transverse shear increases with increasing the modulus ratio, E_L/E_T and reduces the buckling load.

Table 4.22 Values of $(H/a)_{cr}$ and $[Q/(H^2/h^2)]_{cr}$ in Fig. 4.67

	Mat.	N	a/h	$T_S=0$		$T_S=1$	
				$(H/a)_{cr}$	$[Q/(H^2/h^2)]_{cr}$	$(H/a)_{cr}$	$[Q/(H^2/h^2)]_{cr}$
Fig. 4.67	GL	2	20	0.1498	2.7637	0.1476	2.7894
	BO	2	20	0.1323	6.1895	0.1279	6.1153
	GR	2	20	0.1257	8.9412	0.1214	8.5880

4.5.3.2 The Effect of the Radius-to-Thickness Ratio on the Postbuckling Response

The postbuckling response of a movable clamped four-layer graphite-epoxy shallow spherical shell with dimensionless initial rise, H/h, equal to 3 is demonstrated in Fig. 4.68 for different ratios of base radius-to-thickness, a/h. The buckling load increases with the ratio, a/h. The effect of transverse shear reduces the buckling load by 29% for a/h=12 compared with that excluding this effect. As expected, this effect is not significant for large values of a/h. The load has a reduction after buckling and then a little increase at large value of deflection.

4.5.3.3 The Effect of the Number of Layers on the Postbuckling Response

The response curves for the number, N, larger than 4 are very close that for $N=\infty$, which can be seen in Fig. 4.69 for a movable clamped boron-epoxy shallow spherical shell. The buckling load is reduced by 23% for N=2 than for N=4. This reduction is considerably significant for the load-carrying capacity. The effect of transverse shear reduces the buckling load and postbuckling carrying capacity which is not shown herein.

4.5.3.4 The Effect of Material Properties on the Static Large-Deflection Response

It is observed from Fig. 4.70 that the effect of transverse shear on the large-deflection response is much pronounced for the boron-epoxy and graphite-epoxy materials. For an elastically supported six-layer circular plate, this effect reduce the load by 12% and 18% at w_{max}=3h for material of BO and GR, respectively. The load increases with an increase in the modulus ratio, E_L/E_T.

4.5.3.5 The Effect of Rotational Edge Stiffness on the Static Large-Deflection Response

The large-deflection response curves excluding the effect of transverse shear for a movable two-layer glass-epoxy circular plate are plotted in Fig. 4.71 for different rotational stiffness of edge, K_b. The K_b=0 and $K_b=\infty$ correspond the simply-supported and clamped edges, respectively. The load for given deflection increases with an increases in K_b. The effect of K_b on the load is not much pronounced for the value, K_b>5 compared with that for $K_b=\infty$.

4.5.3.6 The Effect of the Shell Rise on the Postbuckling Response

Figure 4.72 shows the load-deflection response of a movable clamped two-layer graphite-epoxy shallow spherical shell with different initial rise, H/h. The shell with H/h=3 and 4 undergo snap-through buckling and has a reduction in the load after buckling. The load for given deflection decreases as the value of H/h increases. The effect of transverse shear reduces the load and increases at large value of deflection.

4.5.3.7 The Effect of Geometrically Initial Imperfections on the Static Large-Deflection Response

The Effect of initial imperfection, $\overline{W}_1$, increases the load, which can be seen in Fig. 4.73 for a movable clamped four-layer glass-epoxy circular plate. This is due to the change of midplane to midsurface. The load for a given deflection is increased when the initial imperfection, $\overline{W}_1$, increases. The effect of transverse shear (not shown herein) is small as the GL with low modulus ratio.

4.5.3.8 The Effect of Elastic Foundations on the Static Large-Deflection Response

In Fig. 4.74, the load-deflection of a movable clamped four-layer graphite-epoxy imperfect shallow spherical shell resting on elastic foundations is presented for different values of nonlinear Winkler foundation parameter, K_n. The effect of K_n is pronounced for larger deflection. The load increases with an increase in the value of K_n. The effect of transverse shear increases with decreasing the value of K_n and reduces load at w_{max}=3h by 10.5%, 8.5%, 6.5% and 4% for K_n=5, 10, 15 and 20, respectively.

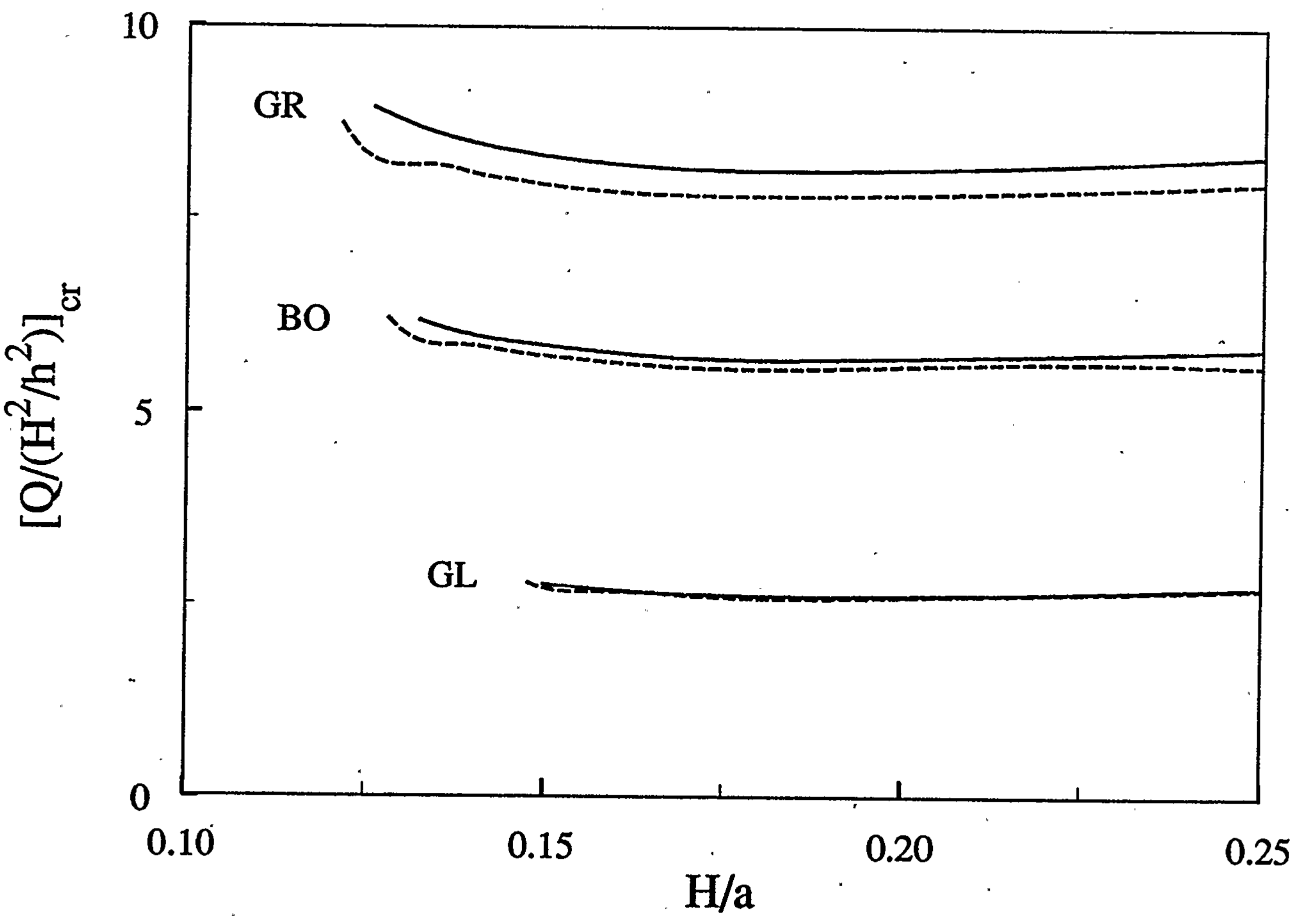

Figure 4.67: Effect of material properties on buckling load of a movable clamped two-layer shallow spherical shell (a/h=20)

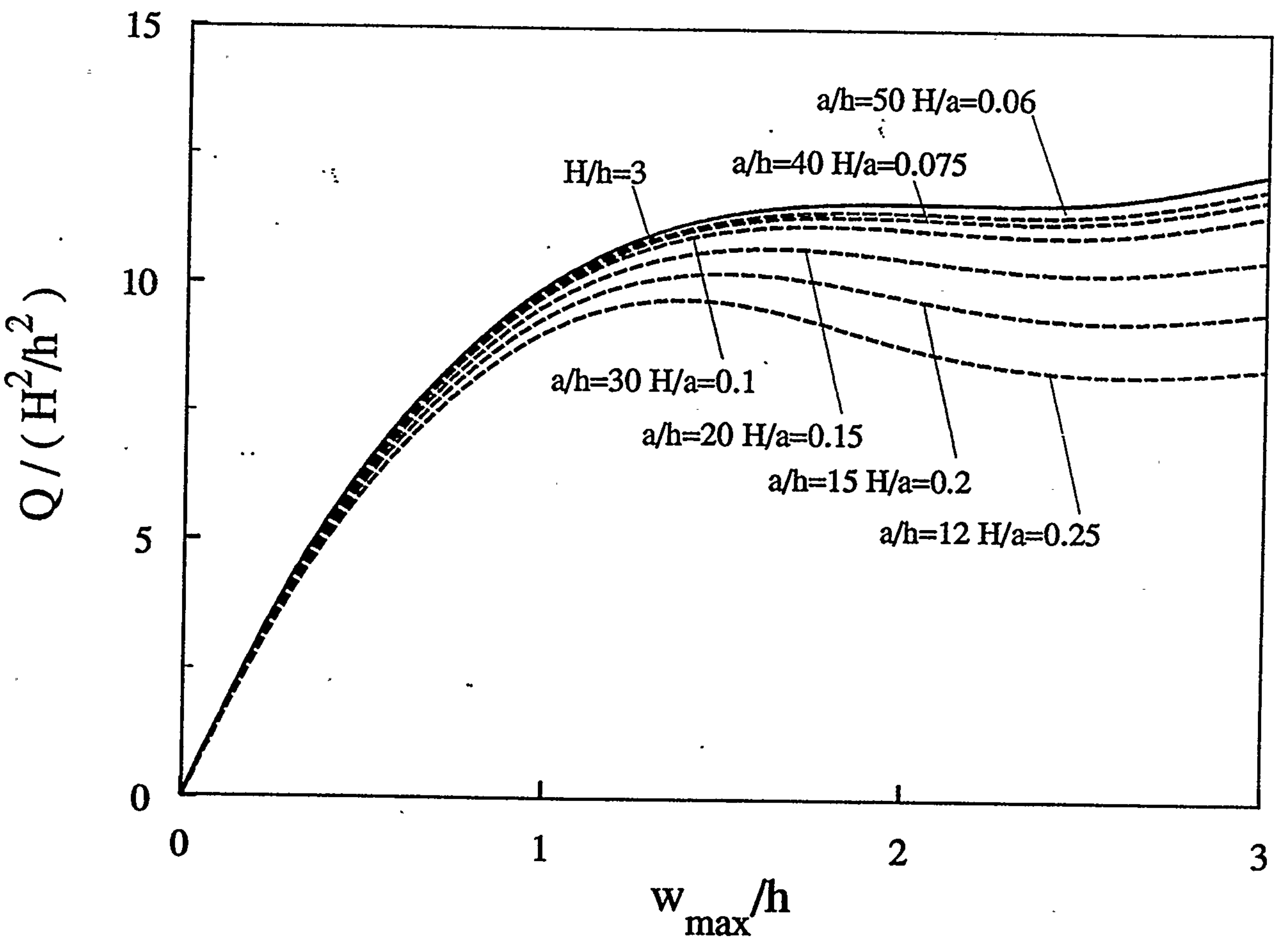

Figure 4.68: Effect of the base radius-to-thickness ratio on the postbuckling response of a movable clamped four-layer graphite-epoxy shallow spherical shell

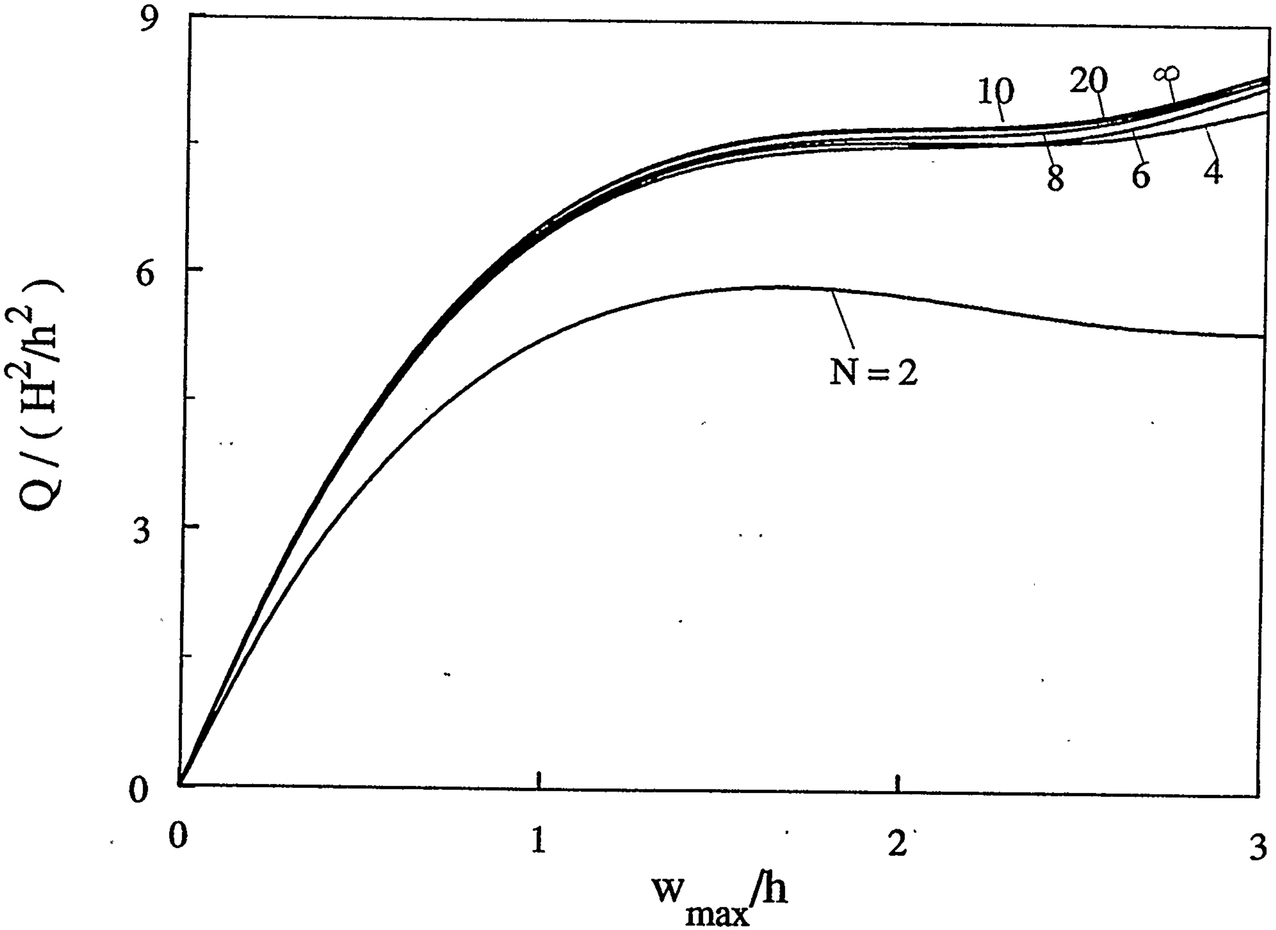

Figure 4.69: Effect of the number of layers on the postbuckling response of a movable clamped boron-epoxy shallow spherical shell (a/h=50, H/a=0.06)

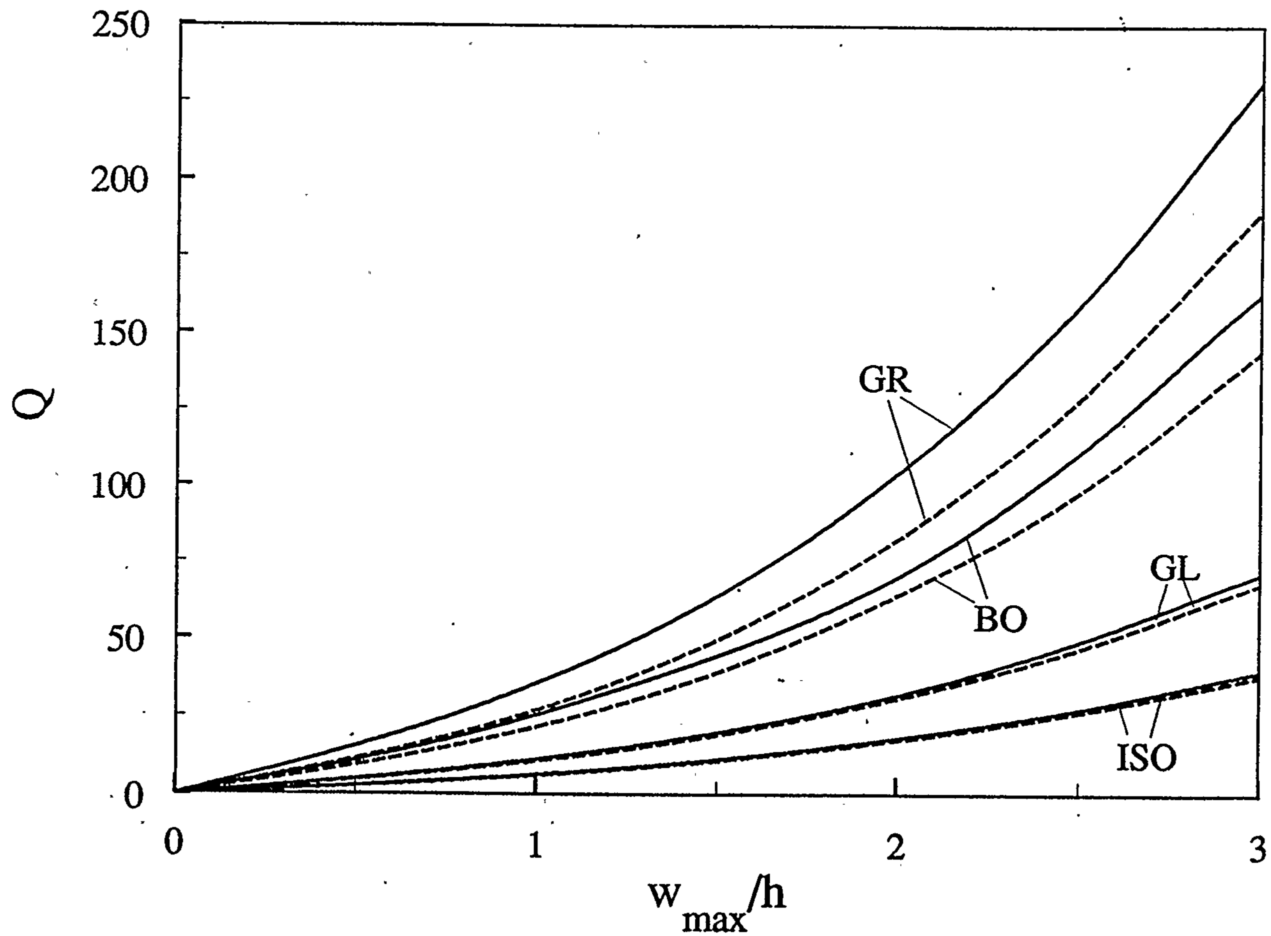

Figure 4.70: Effect of material properties on the static large-deflection response of an elastically supported six-layer circular plate (K_b=3, a/h=10)

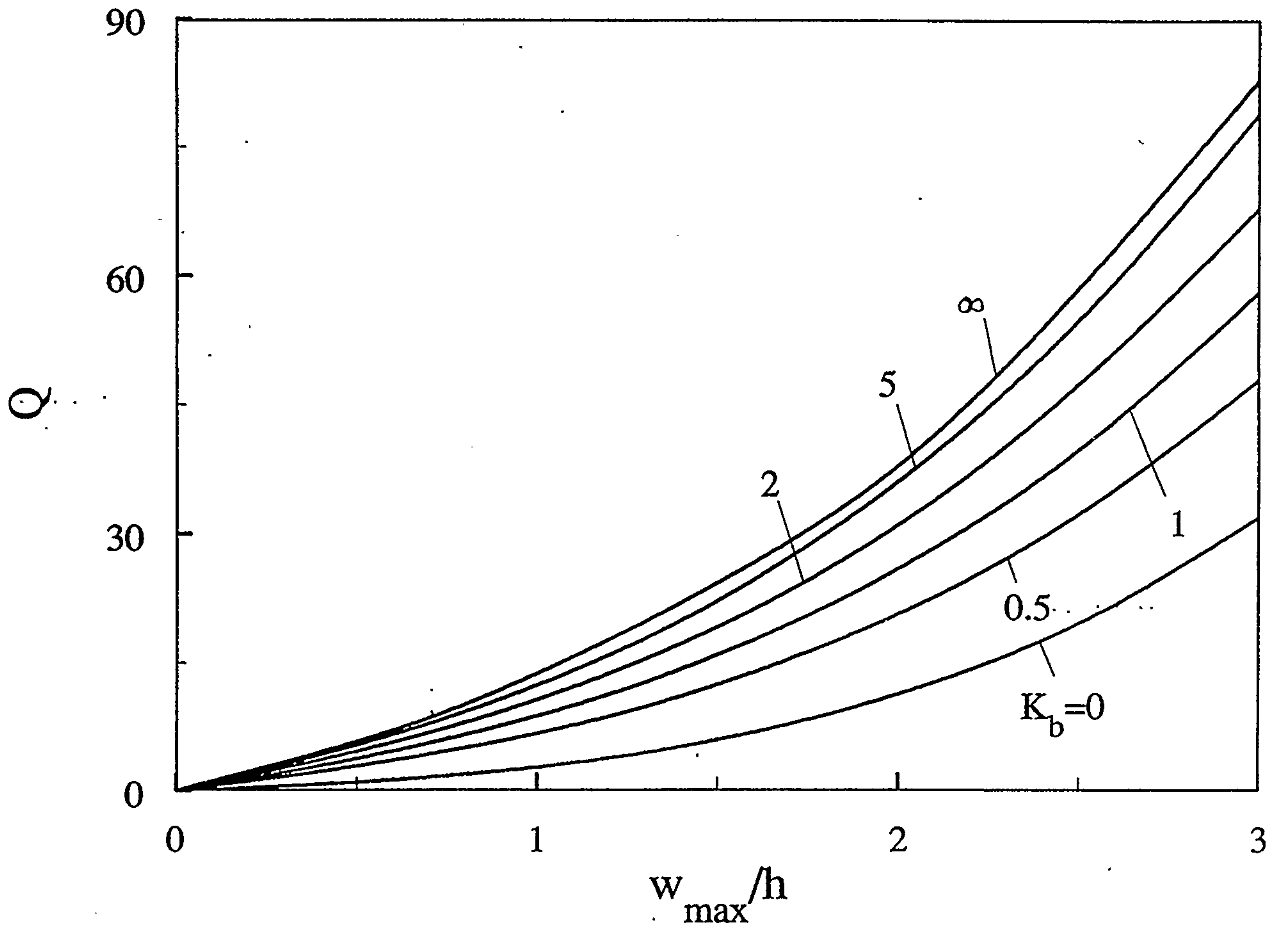

Figure 4.71: Effect of rotational edge stiffness on the static large-deflection response of a two-layer glass-epoxy circular plate with a movable edge (a/h=20)

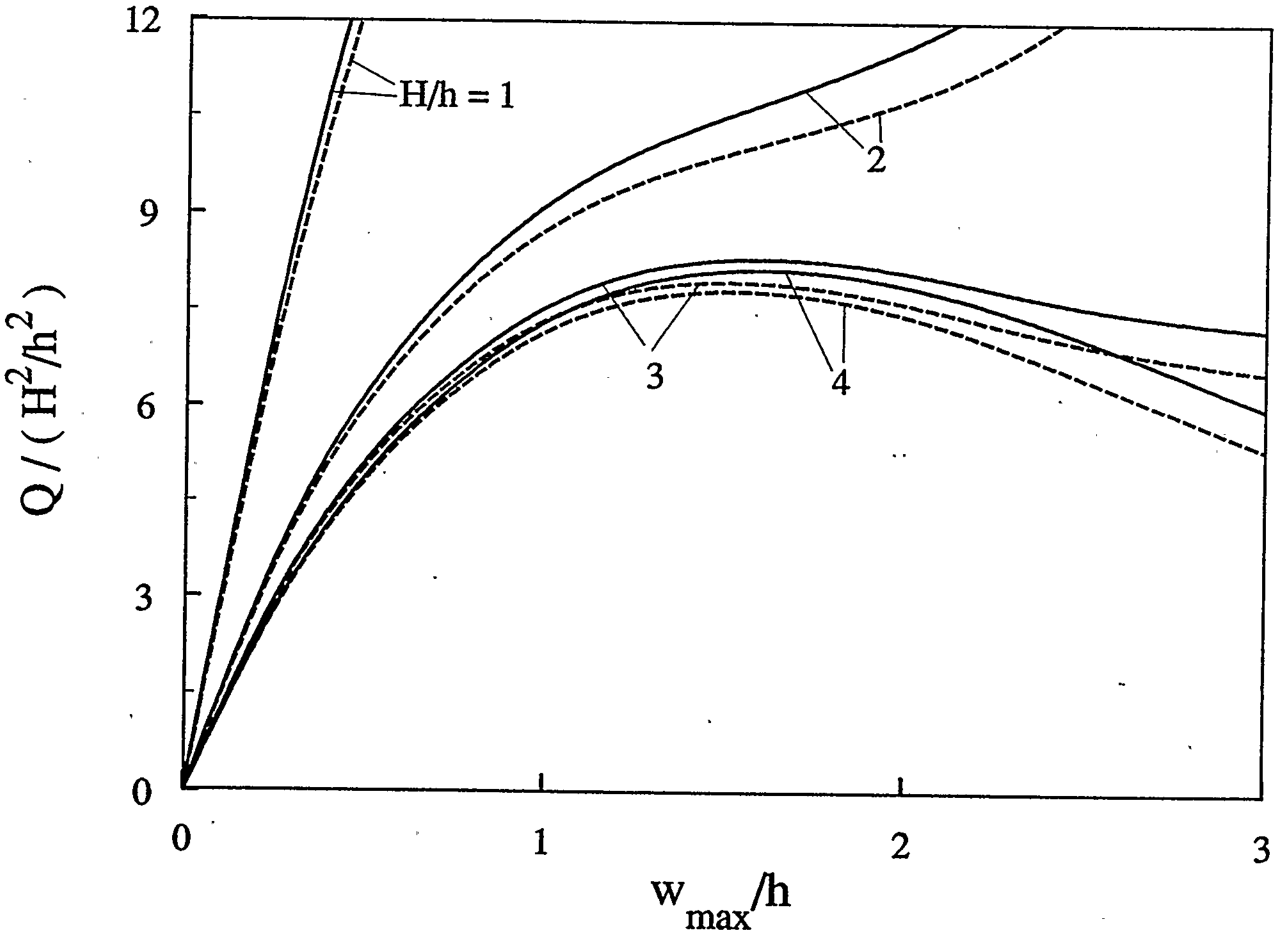

Figure 4.72: Effect of the shell rise on the postbuckling response of a movable clamped two-layer graphite-epoxy shallow spherical shell (a/h=20)

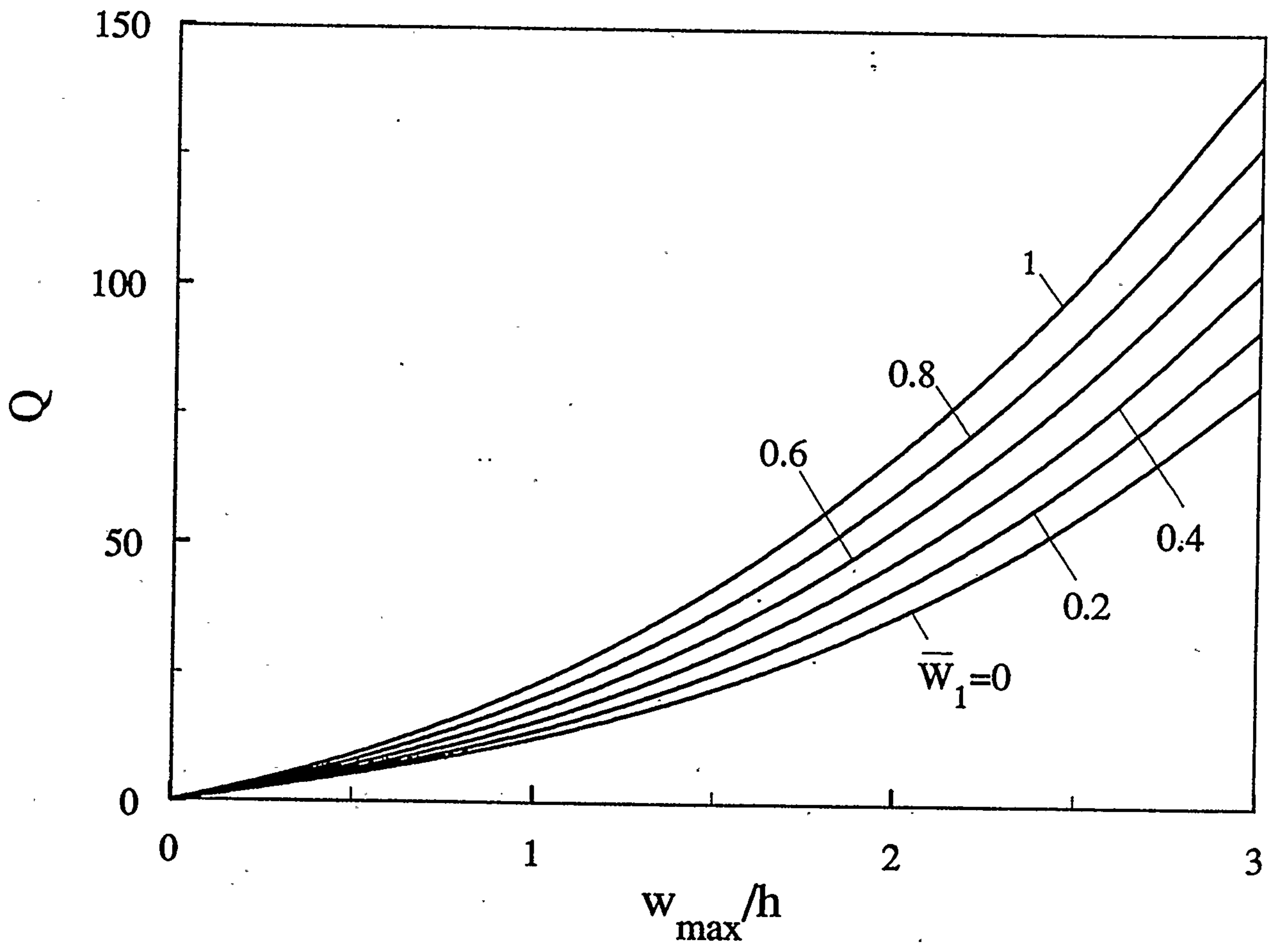

Figure 4.73: Effect of geometrically initial imperfections on the static large-deflection response of a movable clamped four-layer glass-epoxy circular plate (a/h=15)

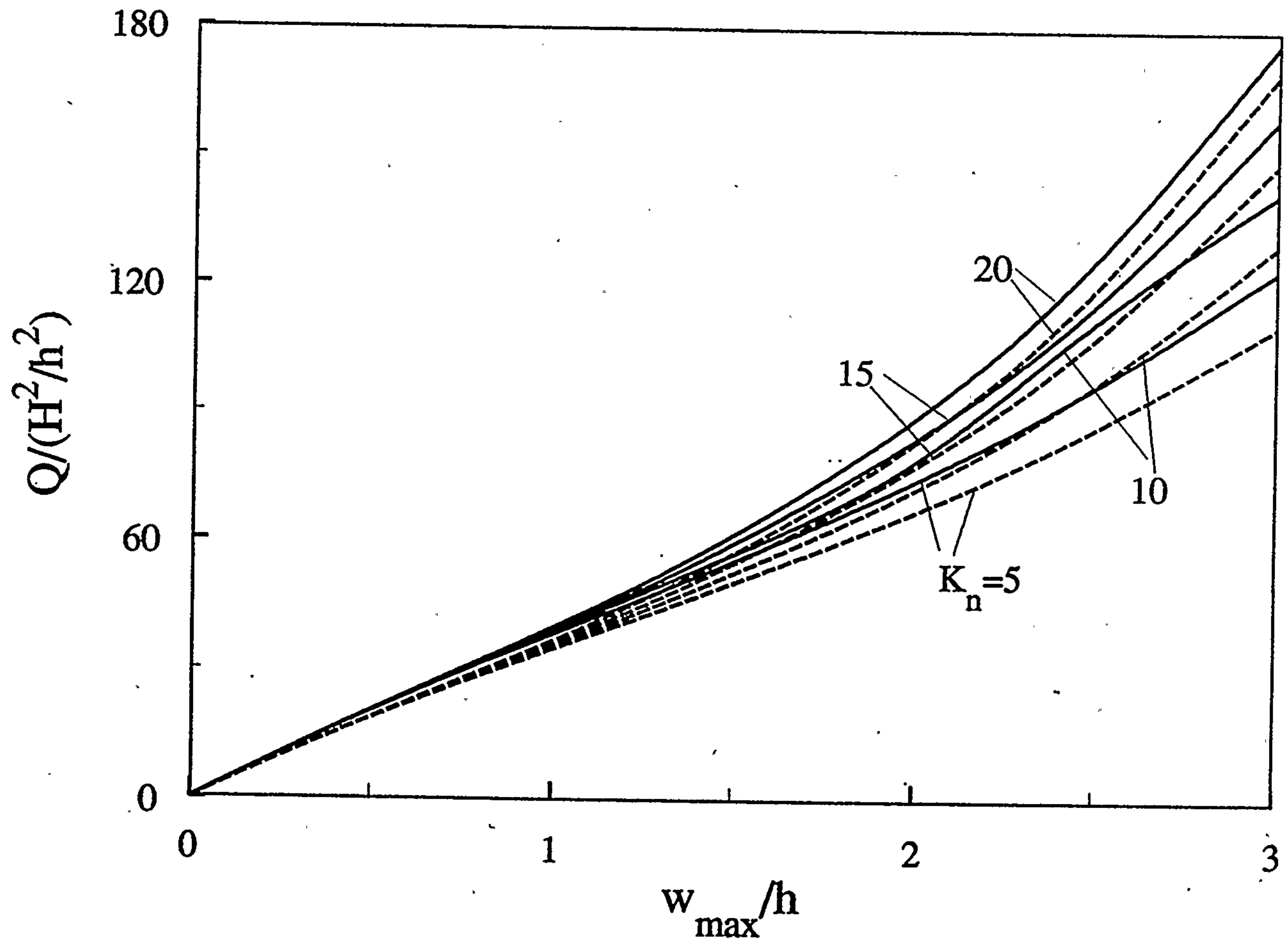

Figure 4.74: Effect of elastic foundation parameters on the postbuckling response of a movable four-layer graphite-epoxy imperfect shallow spherical shell ($\bar{W}_1$=0.2, K_f=10, G_f=20, a/h=10, H/a=0.2)

4.6 SUMMARY

In this chapter, the numerical results are presented for nonlinear free vibration, buckling, postbuckling and large-deflection of symmetrically and unsymmetrically shallow spherical shells and circular plates with various geometric, material and mechanical parameters. Some available previous results are also given for comparison. The effects of ratio of base radius-to-thickness, the modulus ratio, E_L/E_T, the number of layers, boundary conditions, geometric imperfection and elastic foundations on the elastic response of these shells and plates are analyzed. The effects of transverse shear and rotatory inertia are investigated in some detail. Some significant results are obtained.

CHAPTER 5

CONCLUSIONS AND RECOMMENDATIONS

5.1 CONCLUSIONS

In this thesis, a generally dynamic nonlinear theory is developed for the axisymmetric deformation of moderately thick shallow spherical shells and circular plates composed of laminated cylindrically (or polar) orthotropic layers with flexible supports. The effects of transverse shear, rotatory inertia, geometrically initial imperfection and linear, nonlinear extension Winkler and shear Pasternak elastic foundations are taken into account in the theory.

In Chapter 2, the constitutive relations for a moderately thick laminated shallow spherical shell are established on the basis of the generalized Hooke's law. The transverse shear stiffness is given by employing a parabolic shear stress distribution across the shell thickness and the principle of complementary energy. The governing equations and the associated set of boundary conditions are presented by use of the dynamic principle of virtual work, stress function and condition of compatibility. These nonlinear equations of transverse motion are coupled in terms of transverse displacement, rotation of a normal to mid-surface and stress function. For specific cases, the governing equations can be simplified to those given in the earlier theories, such as Marguerre-type equations and Mindlin-von Karman equations, etc. The present theory is more general and accurate for studying the elastic behaviour of laminated shallow spherical shells in comparison with previous theories.

In Chapter 3, a solution of the Fourier-Bessel series satisfying the prescribed boundary conditions is formulated for the governing equations of laminated shallow spherical shells. These equations are reduced to a set of nonlinear ordinary differential equations by making use of the Galerkin method. For undamped nonlinear free vibration, the time dependent coefficients of Fourier-Bessel series are expanded as Fourier cosine series and a system of simultaneous nonlinear algebraic equations obtained by the principle of harmonic balance. For the static response, the nonlinear ordinary differentail equations become the nonlinear algebraic equations by treating the time functions as constants and deleting the inertia terms. The Newton-Raphson method is used for solving the system of simultaneous nonlinear equations. The eigenvalues of Bessel functions are listed in Tables for some typical cases. The technique of replacing the edge moments by an equivalent pressure near the edge is adopted for unsymmetrically laminated shells with rotational restrained edges. The outline of computer program NALSSS is introduced for implementing the numerical calculations.

In Chapter 4, the numerical results and discussions have been presented in graphs and tables for nonlinear free vibration, buckling and postbuckling or static large deflection response of symmetrically and unsymmetrically laminated shallow spherical shells and circular plates with various geometric, material and mechanical parameters. Based on this study, some conclusions may be drawn.

5.1.1 Nonlinear Free Vibration

Generally, the frequency-amplitude response curves exhibit the softening type of nonlinearity for the shells with high dimensionless rise, H/h, and hardening one for the shells with low value of H/h and the plates.

5.1.1.1 The Effect of Transverse Shear and Rotatory Inertia

The Effect of transverse shear plays an important role. The effect of rotatory inertia can be neglected in an analysis. The effects of transverse shear and rotatory inertia reduce the linear frequency and the frequency ratio at any amplitude of vibration. These effects are quite significant for both shells and plates with the low ratio of base radius to thickness, a/h, and high modulus ratio, E_L/E_T. These effects are intensified with the increase in an values of rotational and inplane stiffnesses for symmetrically laminated shells and plates and with increasing the value of rotational stiffness for unsymmetrical shells and plates. The higher the number of layers of the shell or plate, the stronger the effects of transverse shear and rotatory inertia. The variation of these effects with the number of layers, however, is not quite noticeable. These effects in any cases do not change the general behaviour of the response.

5.1.1.2 The Effect of the Number of Layers

The frequency ratio increases with the number of layers, N, for a given amplitude of vibration. The effect of the number of layers larger than 7 for symmetrically laminated shells and plates and larger than 6 for unsymmetrically laminated shells and plates is not prominent.

5.1.1.3 The Effect of Boundary Conditions

The frequency ratio decreases with an increase in the value of the inplane edge stiffness, K_i, for symmetrically laminated shells. This ratio increases for symmetrically laminated shells but generally decreases for laminated plates as the value of the rotational edge stiffness, K_b, increases. The effect of K_b is not quite noticeable for symmetrically laminated shells. The nonlinear frequency increases more quickly for immovable edges than movable edges for symmetrically laminated plates.

5.1.1.4 The Effect of Geometrically Initial Imperfection

The frequency ratio increases for the shells but decreases for the plates with increasing the amplitude of initial imperfections.

5.1.1.5 The Effect of Elastic Foundation

The nonlinear frequency increases with an increase in the values of parameters of elastic foundations K_f, K_n and G_f for all cases.

5.1.2 Static Response

The shells undergo snap-through buckling and have a reduction in the load after the first maxima for high dimensionless rise, H/h. For some cases, the load after reduction inverts to increase with an increase in the deflection.

5.1.2.1 Buckling Response

The buckling load, Q_{cr}, increases but the critical value, $(H/a)_{cr}$, decreases with an increase in the modulus ratio, E_L/E_T, for the shells. Once the critical value occurs, the buckling load initially decreases and then increases with an increase in the ratio of H/a. For symmetrically laminated shallow spherical shells, the effect of the inplane edge condition on the buckling load is quite remarkable.

5.1.2.2 The Effect of Transverse Shear

The effect of transverse shear reduces the buckling load and postbuckling load carrying capacity for shells and plates at any value of the deflection. This effect is more pronounced for the shells and plates that are moderately thick and have the high modulus ratio. This effect increases at large values of the deflection of shells and plates.

5.1.2.3 The Effect of the Number of Layers

The load increases with the number of layers except for N=1 for symmetrically laminated plates and for N>10 for unsymmetrically laminated shells. This effect is quite noticeable for the number equal to 3 and 5 for symmetrically laminated shells and plates, and 2 and 4 for unsymmetrically laminated shells and plates, respectively.

5.1.2.4 The Effect of Material Properties

The load in postbuckling and large-deflection response increases with increasing the value of the modulus ratio.

5.1.2.5 The Effect of Boundary Conditions

The load increases with an increase in the values of K_b and K_i for symmetrically laminated shells and plates and of K_b for unsymmetrically laminated shells and plates.

5.1.2.6 The Effect of Geometrically Initial Imperfections

The buckling load decreases as the amplitude of initial imperfections, $\bar{W}_1$, increases. The postbuckling load initially decreases and then increases in the large value of the deflection for symmetrically laminated shells. This load increases with an increase in $\bar{W}_1$ for symmetrically and unsymmetrically laminated plates.

5.1.2.7 The Effect of Elastic Foundations

The buckling load and the load in postbuckling or large-deflection response increase as the values of parameters of an elastic foundation K_f, K_n and G_f increase.

5.2 RECOMMENDATIONS FOR FURTHER RESEARCH

This research is concerned with the nonlinear free vibration, buckling, postbuckling and static large-deflection (or nonlinear bending) response of symmetrically and unsymmetrically laminated shallow spherical shells and circular plates. Since the present formulation is general in nature, further work can be done:

(1) to analyze stress resultants and couples or stresses;

(2) to study the nonlinear dynamic response of laminated shallow spherical shells and circular plates subject to a time-dependent transverse load;

(3) to apply the present theory established in this study to the laminated shallow spherical shells with circular opening at the apex and annular plates;

(4) to establish a comprehensive analytical system to incorporate systematic analysis of laminated shallow spherical shells and circular plates both with and without a hole.

REFERENCES

Alwar, R. S. and Reddy, B. S., (1979a), "Dynamic buckling of isotropic and orthotropic shallow spherical cap with circular hole", Int. J. Mech Sci., Vol. **21**, pp. 681-688.

Alwar, R. S. and Reddy, B. S., (1979b), "Large deflection static and dynamic analysis of isotropic and orthotropic annular plates", Int. J. Nonlinear Mech., Vol. **14**, pp. 347-359.

Ambartsumyan, S. A., (1964), "Theory of anisotropic", NASA TTF-118

Berger, H. M., (1955), "A new approach to the analysis of large deflection of plates", J. Appl. Mech., Vol. **22**, pp. 465-472.

Bhattacharya, A. P., (1984), "Large amplitude vibrations of imperfect cross-ply laminated cylindrical shell panels with elastically restrained edges and resting on elastic foundation", Fib. Sci. Technol., Vol. **12**, pp. 205-221.

Biricikoglu, V. and Kalnins, A., (1971), "Large elastic deformation of shells with the inclusion of transverse normal strain", Int. J. Solids Struct., Vol. **7**, pp. 431-444.

Budiansky, B., (1959), "Buckling of clamped shallow spherical shells", Proceedings of the Symposium on the theory of thin elastic shells, Delft, Holland, pp. 64-94.

Chia, C. Y., (1980), "Nonlinear Analysis of Plates", McGraw-Hill, New York

Chia, C. Y., (1985), "Nonlinear oscillation of unsymmetric angle-ply plate on elastic foundation having nonuniform edge supports", Composite Struct., Vol. **4**, pp. 161-178.

Chia, C. Y., (1987a), "Nonlinear vibration and postbuckling of unsymmetrically laminated imperfect shallow cylindrical panels with mixed boundary conditions resting on elastic foundation", Int. J. Eng. Sci., Vol. **25**, pp. 427-441.

Chia, C. Y., (1987b), "Non-linear free vibration and postbuckling of symmetrically laminated orthotropic imperfect shallow cylindrical panels with two adjacent edges simply supported and other edges clamped", Int. J. Solids Struct., Vol. **23**, pp. 1123-1132.

Chia, C. Y., (1988a), "Geometrically nonlinear behaviour of composite plates: a review", Appl. Mech. Rev., Vol. **41**, pp. 439-451.

Chia, C. Y., (1988b), "Nonlinear analysis of doubly curved symmetrically laminated shallow shells with rectangular planform", Ingenieur-Archiv, Vol. **58**, pp. 252-264.

Chia, C. Y. and Sathamoorthy, M., (1981), "Nonlinear vibration of circular plates with transverse shear and rotatory inertia", J. Sound Vib., Vol. **78**, pp. 131-137.

Chien, W. Z. and Yeh, K. Y., (1954), " On the large deflection of circular plates", Sci. Sin., Vol. **3**, pp. 405-436.

Donnell, L. H., (1933), "Stability of thin-walled tubes under torsion", NACA Rep., pp. 479-.

Donnell, L. H., (1976), "Beams, Plates and Shells", McGraw-Hill, New York

Dong, S. B., (1972), "Studies relating to the structural dynamic behaviour of laminated plates and shells", UCLA-ENG-7236, School of Engineering and Applied Science, University of California, Los Angeles, CA

Dong, S. B., Pister, K. S., and Tayler, R. L., (1962), "On the theory of laminated anisotropic shells and plates", J. Aeronaut Sci., Vol. **29**, pp. 969-975.

Dong, S. B. and Tso, F. K. W., (1972), "On a laminated orthotropic shell theory including transverse shear deformation", J. Appl. Mech., Vol. **39**, pp. 1091-1097.

Dumir, P. C., (1985), "Nonlinear axisymmetric response of orthotropic thin spherical caps on elastic foundation", Int. J. Mech. Sci., Vol. **27**, pp. 751-760.

Dumir, P. C., (1986), "Nonlinear axisymmetric response of orthotropic thin truncated conical and spherical caps", Acta Mech., Vol. **30**, pp. 121-132.

Dumir, P. C., Gandhi, M. L., and Nath, Y., (1984a), "Axisymmetric static and dynamic buckling of orthotropic shallow spherical cap with circular hole", Comput. Struct., Vol. **19**, pp. 725-736.

Dumir, P. C., Gandhi, M. L., and Nath, Y., (1984b), "Axisymmetric static and dynamic buckling of orthotropic shallow spherical caps with flexible supports", Acta Mech., Vol. **52**, pp. 93-106.

Fu, Y. M. and Chia, C. Y., (1989a), "Multi-mode non-linear vibration and postbuckling of antisymmetric imperfect angle-ply cylindrical thick panels", Int. J. Non-linear Mech., Vol. **24**, pp. 365-381.

Fu, Y. M. and Chia, C. Y., (1989b), "Nonlinear analysis of unsymmetrically laminated imperfect thick panels on elastic foundation", Composit Struct., Vol. **13**, pp. 289-314.

Galerkin, B. G., (1915), Vestn. Inzh. Tekh., Vol. **1**, pp. 879-903.

Ganapathi, M. and Varadan, T. K., (1982), "Dynamic buckling of orthotropic shallow spherical shells", Comput. Struct., Vol. **15**, pp. 517-520.

Grossman, P. L., Koplik, B. and Yu, Y. Y., (1969), "Nonlinear vibrations of shallow spherical shells", J. Appl. Mech., Vol. **36**, pp. 451-458.

Hartree, D. R., (1958), "Numerical Analysis, 2nd Edition", Clarendon Press, Oxford

Hayashi, C., (1964), "Nonlinear Oscillations in Physical Systems", McGraw-Hill, New York

Herrmann, G. and Mirsky, I., (1956), "Three-dimensional and shell-theory analysis of axially symmetric motions of cylinders.", J. Appl. Mech., Vol. **23**, pp. 563-578.

Hildebrand, F. B., Reissner, E., and Thomas, G. B., (1949), "Notes on the foundations of the theory of small displacements of orthotropic shells", National Advisory Comm. Aero. Tech. Notes. No. 1833, Washington DC.

Hirano, Y., (1979), "Buckling of angle-ply laminated circular cylindrical shells", J. Appl. Mech., Vol. **46**, pp. 233-234.

Hsu, N. Z., Xu, C. S., and Chia, C. Y., (1991), "Multi-mode nonlinear vibration and postbuckling of antisymmetrically laminated imperfect angle-ply cylindrical panel with free straight edges", Archive of Appl. Mech., Vol. **61**, pp. 295-304.

Hsu, T. M. and Wang, J. T. S., (1970), "A theory of laminated cylindrical shells consisting of layers of orthotropic laminae", AIAA J., Vol. **8**, pp. 2141-

2146.

Huang, C. L. and Sandman, B. E., (1971), "Large amplitude vibrations of a rigidly clamped circular plate", Int. J. Non-linear Mech., Vol. **3**, pp. 451-468.

Hui, D, (1983a), "Large-amplitude vibrations of geometrically imperfect shallow spherical shells with structural damping", AIAA J. , Vol. **21**, pp. 1736-1741.

Hui, D. , (1983b), "Large amplitude axisymmetric vibrations of geometrically imperfect circular plates.", J. Sound Vib., Vol. **91**, pp. 239-246.

Hui, D., (1985), "Asymmetric postbuckling of symmetrically laminated cross-ply, short cylindrical panels under compression", J. compos. Struct., Vol. **3**, pp. 81-95.

Hyman, B. I., (1971), "Snap-through of shallow clamped spherical caps under uniform pressure", Int. J. Nonlinear Mech., **6**, pp. 55-67.

Iu, V. P. and Chia, C. Y., (1988a), "Non-linear vibration and postbuckling of unsymmetric cross-ply circular cylindrical shells", Int. J. Solid Stuct., Vol. **24**, pp. 195-210.

Iu, V. P. and Chia, C. Y., (1988b), "Effect of transverse shear on nonlinear vibration and postbuckling of anti-symmetric cross-ply imperfect cylindrical shells", Int. J. Mech. Sci., Vol. **30**, pp. 705-718.

Jain, R. K. and Nath, Y., (1986), "Effect of foundation nonlinearity on the nonlinear transient response of orthotropic shallow spherical shells", Ingenieur-Arch, Vol. **56**, pp. 295-300.

Jones, R. M., (1975), "Mechanics of composite materials", McGraw-Hill, New York

Kaplan, A. and Fung, Y. C., (1954), "A nonlinear theory of bending and buckling of thin elastic shallow spherical shells", NACA TN 3212, Washington, D. C.

Kerr, A. D., (1964), "Elastic and viscoelastic foundation models", J. Appl. Mech., Vol. **31**, pp. 491-498.

Khot, N. S., (1970), "Postbuckling behaviour of geometrically imperfect composite cylindrical shells under axial compression", AIAA J., Vol. **8**, pp. 579-581.

Kirchhoff, G., (1850), "Uber das Glaichgewicht und Bewegung einer Elastischen Scheibe", Crelle's Journal of Math., Vol. **40**

Koiter, W. T., (1959), "A consistent first approximation in the general theory of thin elastic shells", Proceedings of the Symposium on The Theory of Thin Elastic Shells, Delft, Holland, pp. 12-33.

Kunukkaseril, V. X. and Venkateshan, S., (1979), "Axisymmetric non-linear oscillations of isotropic layered circular plates", J. Sound Vib., Vol. **64**, pp. 295-302.

Levison, M. and Bharatha, S., (1978), "Elastic foundation models -- a new approach", Proceedings of the 4th Symposium on Engineering Applications of Solid Mechanics, Sheridan Park Research Community, Canada, pp. 177-189.

Love, A. E. H., (1888), "The small free vibration and deformation of thin elastic shells", Philosophical Transaction of the Royal Society, Series A, vol. **79**.

Librescu, L., (1987), "Refined geometrically nonlinear theories of anisotropic laminated shells", Q. Appl. Math., pp. 1-27.

Librescu, L., (1988), "Geometrically non-linear theory of shear deformable anisotropic laminated composite shallow shells", Proceedings ASCE Engineering Mechanics Specially Conference, Blacksburg, VA, pp. 283-.

Marguerre, K., (1938), "Zur theorie der gekrummten platte grosser formanderung", Proceeding 5th Int. Cong. Appl. Mech., John Wiley & Sons, Inc., New York, pp. 93-101.

Mclachlan, N. W., (1955), "Bessel Functions for Engineers", Clarendon Press, Oxford

Mindlin, R. D., (1951), "Influence of rotatory inertia and shear on flexural motions of isotropic, elastic plates", J. Appl. Mech., Vol. **18**, pp. 31-38.
Mirsky, I. and Herrmann, G., (1957), "Nonaxially symmetric motion of cylindrical shells", J. Acoust. Soc. Am., Vol. **29**, pp. 1116-1123.

Naghdi, P. M. and Cooper, R. M., (1956), "Propagation of elastic waves in cylindrical shells including effects of transverse shear and rotatory inertia", J. Acoust. Soc. Am., Vol. **28**, pp. 56-63.

Nath, Y. and Alwar, R. S., (1980), "Nonlinear dynamic analysis of orthotropic circular plates", Int. J. Solids Struct., Vol. **16**, pp. 433-443.

Nath, Y. and Jain, R. K., (1985a), "Orthotropic annular shells on elastic foundation", J. Eng. Mech., Vol. **111**, pp. 1242-1256.

Nath, Y. and Jain, R. K., (1985b), "Influence of foundation mass on the nonlinear damped response of orthotropic shallow spherical shells", Int. J. Mech. Sci., Vol. **27**, pp. 471-479.

Nath, Y. and Jain, R. K., (1986), "Non-linear studies of orthotropic shallow spherical shells on elastic foundation", Int. J. Non-linear Mech., Vol. **21**, pp. 447-458.

Nath, Y. and Jain, R.K., (1989), "Static buckling of orthotropic spherical shells on elastic foundations", J. Eng. Mech., Vol. **115**, pp. 2621-2634.

Nath, Y., Jain, R. K., and Mahrenholtz, O., (1987), "Orthotropic circular plates and spherical shells on elastic subgrade", Arch. Mech., Vol. **39**, pp. 275-281.

Noor, A. K. and Burton, W. S., (1990), "Assessment of computational models for multilayered composite shells", Appl. Mech. Rev., Vol. **43**, 67-97.

Nowinski, S. L., (1963), "Nonlinear vibrations of elastic circular plates exhibiting rectilinear orthotropy", Zeitschrift fur Angewandte Mathematik und Physik (ZAMP), Vol. **14**, pp. 113-124.

Nowinski, S. L. and Ismail, I. A., (1965), "Application of a multi-parameter perturbation method to elastostatics", Dev. Theor. Appl. Mech., Vol. **2**, pp. 35-45.

Pasternak, P. L., (1954), "On a new method of an elastic foundation by means of two foundation constants (in Russian)", Gosudarstvennoe Izdatelstvo Literaturi Po Stritelstou i Arkhitekture, Moscow, USSR

Poincare, H., (1892), "New methods in celestial mechanics", Gauthier-Villars

Ramachadran, J., (1976), "Large amplitude vibration of shallow spherical shells with concertrated mass", J. Appl. Mech., Vol. **43**, pp.363-365.

Rath, B. K. and Das, Y. C., (1973), "Vibration of layered shells", J. Sound Vib., Vol. **28**, pp. 737-751.

Reddy, J. N. and Chandrashekhara, K., (1985a), "Nonlinear analysis of laminated shells including transverse shear strains", AIAA J., Vol. **23**, pp. 440-441.

Reddy, J. N. and Chandrashekhara, K., (1985b), "Geometrically non-linear transient analysis of laminated, doubly curved shells", Int. J. Nonlinear Mech., Vol. **20**, pp. 79-90.

Reddy, J. N. and Liu, C. F., (1985), "A higher-order shear deformation theory of laminated elastic shells", Int. J. Eng. Sci., Vol. **23**, pp. 319-330.

Reissner, E., (1945), "The effect of transverse shear deformation on the bending of elastic plates", J. Appl. Mech., Vol. **12**, pp. a60-a77.

Reissner, E., (1946), "Stress and small displacements of shallow spherical shells:I",J. Math. Phys., Vol. **25**, pp. 80-85.

Reissner, E., (1950), "On a variational theorem in elasticity", J. Math. Phys., Vol. **29**, pp. 90-97.

Reissner, E., (1955), " on axisymmetric buckling of shallow spherical shells", Q. Appl. Math., Vol. **13**, pp.279-290.

Reissner, E., (1958), "A note on deflections of plates on visco-elastic foundation", J. Appl. Mech., Vol. **25**, pp. 144-145.

Reissner, E. and Stavsky, Y., (1961), "Bending and stretching of certain types of heterogeneous anisotropic elastic plates", J. Appl. Mech., Vol. **28**, pp. 402-408.

Ritz, W., (1908), "Uber eine neue methode zur losung gewissen variations-problems der mathematischen physik", J. Reine u. Angew. Math., Vol. **135**, pp. 1-61.

Ruei, K. H., Jiang, C., and Chia, C. Y., (1984), "Dynamic and static nonlinear analysis of cylindrically circular plates with nonuniform edge constraints", J. Appl. Math. Phys., Vol. **35**, pp. 387-400.

Sathyamoorthy, M. and Chia, C. Y., (1979), "Nonlinear vibration of orthotropic circular plates including transverse shear and rotatory inertia", In: ASME Modern developments in compos. mat. struct., pp. 357-372.

Sathyamoorthy, M. and Chia, C. Y., (1982), "Nonlinear flexural vibration of moderately thick orthotropic circular plates", Ingenieur-Archiv., Vol. **52**, pp. 237-243.

Sinha, P. K. and Rath, A. K., (1975), "Vibration and buckling of cross-ply laminated circular cylindrical panels", Aeronaut Q., Vol. **26**, pp. 221-228.

Sinha, S. N., (1963), "large deflection of plates on elastic foundations", J. Engg. Mech. Div. ASCE, Vol. **89**, pp. 1-24.

Sinharay, G. C. and Banerjee, B., (1985), "Large amplitude free vibrations of shallow spherical and cylindrical shell--a new approach", Int. J. Non-linear Mech., Vol. **20**, pp.69-78.

Sivakumaran, K. S., (1983), "A refined of generally laminated plates", Thesis submitted to the Faculty of Graduate Studies, The University of Calgary, in partial fulfilment of the requirement for the degree of Doctor of Philosophy, Vol. **January 1983**

Solsatos, K. P., (1986), "On thickness shear deformation theories for the dynamic analysis of non-circular cylindrical shells", Int. J. Solids Struct., Vol. **22**, pp. 625-641.

Soldatos, K. P., (1987), "Influence of thickness shear deformation on free vibrations of rectangular plates, cylindrical panels and cylinders of antisymmetric angle-ply construction", J. Sound Vib., Vol. **119**, pp. 111-137.

Srinivasamurthy, K. and Chia, C. Y., (1987), "Nonlinear vibration and bending of laminated anisotropic circular plates", Proc. 4th Int. Conf. Compos. Struct., pp. 1436-1446.

Srinivasamurthy, K. and Chia, C. Y., (1990), "Nonlinear dynamic and static analysis of laminated anisotropic thick circular plates", Acta Mech., Vol. **82**, pp. 135-150.

Stein, M., (1986), "Nonlinear theory for plates and shells including the effects of transverse shearing ", AIAA J., Vol. **24**, pp. 1537-1544.

Stephens, W. B. and Fulton, R, E., (1969), "Axisymmetric static and dynamic buckling of spherical caps due to centrally distributed pressure", AIAA. J., **7**, pp. 2120-2126.

Turvey, G. J., (1982), "Axisymmetric elastic large deflection analysis of composite circular plates", Fibre Sci. Tech., Vol. **16**, pp. 191-217.

Varadan, T. K., (1978), "Snap-buckling of orthotropic shallow spherical shells", J. Appl. Mech., Vol. **45**, pp. 445-447.

Varadan, T. K. and Pandalai, K. A. V., (1978), "Nonlinear flexural oscillations of orthotropic shallow spherical shells", Computer Struct., Vol. **9**, pp. 417-425.

Vinson, J. R. and Chou, J. W., (1975), "Composite materials and their use in structures", Applied Science Publishing LTD., London

von Karman, T., (1910), "Festigkeits probleme im mashinenbau", Encykl Math. Wiss., Vol. **4**, pp. 348-352.

von Karman, T. and Tsien, H. S., (1939), "The buckling of spherical shells by external pressure", J. Aeronaut. Sci. , **7**, pp. 43-50.

Washizhu, K., (1968), "Variational methods in elasticity and plasticity", Pergamon Press

Way, S., (1934), "Bending of circular plate with large deflection",Trans. ASME., Vol. **56**, pp. 627-636.

Weichert, D., (1988), "Anisotropic elastic-plastic shells at moderate rotations", Proceedings, 7th ASCE Engineering Mechanics Specialty Conference, Blackburg, VA, pp. 282-.

Weinitschke, H. J., (1960), " On the stability problem for shallow spherical shells", J. Math. Phys., **38**, pp. 209-231.

Whitney, J. M. and Sun, C. T., (1973), "A refined theory for extensional motion of laminated anisotropic shells and plates", J. Sound Vib., Vol. **30**, pp. 85-96.

Whitney, J. M. and Sun, C. T., (1974), "A refined theory for laminated anisotropic, cylindrical shells", J. Appl. Mech., Vol. **41**, pp. 471-476.

Winkler, E., (1867), "Die lehre von der elasticitaet und festigkeit", Prag. Dominicus

Xu, C. S., (1991), "Buckling and postbuckling of symmetrically laminated moderately thick spherical caps", Int. J. Solids Struct., Vol. **28**, pp. 1171-1184.

Xu, C. S., (1992a), "Multi-mode nonlinear vibration and large deflection of symmetrically laminated imperfect spherical caps on elastic foundations", Int. J. Mech. Sci. (in press).

Xu, C. S., (1992b), "Nonlinear static and dynamic response of symmetrically laminated imperfect thick circular plates on elastic foundations", accepted for presentation to the annual OMAE (Offshore Mechanics & Arctic Engineering) Conference, Calgary, June 1992 for presentation

Xu, C. S. and Chia, C. Y., (1991a), "Nonlinear vibration of symmetrically laminated thin spherical caps with flexible supports", Acta Mech. (in press)

Xu, C. S. and Chia, C. Y., (1991b), "Nonlinear analysis of symmetrically laminated moderately thick circular plates", Proc. 1st Canadian International Composite Conference and Exhibition, Montreal, Sept. 1991 (Edited by S. V. Hoa), pp. 1E8.1-1E8.8.

Xu, C. S. and Chia, C. Y., (1992a), "Nonlinear analysis of unsymmetrically laminated moderately thick shallow spherical shells", to be submitted to Nonlinear Mech. for publication.

Xu, C. S. and Chia, C. Y. (1992b), "Large amplitude vibration of unsymmetrically laminated moderately thick circular plates on elastic foundation", accepted for presentation to 1992 ASME Summer Mechanics and Materials Meeting, Tempe, Arizona, April, 1992.

Zhang, Y. and Matthews, F. L., (1985), "Large deflection behaviour of simply supported laminated panels under in-plane loading", J. Appl. Mech., Vol. **52**, pp. 553-557.

Zhang, Y. and Matthews, F. L., (1983), "Postbuckling behaviour of curved panels of generally layered composite materials", J. Compos. Struct., Vol. **1**, pp. 115-135.

APPENDIX A

PROPERTIES OF BESSEL FUNCTIONS

(1) Properties for first kind of Bessel functions

$$J_{-n}(z) = (-1)^n J_n(z)$$

$$J_n(-z) = (-1)^n J_n(z)$$

$$J_{-n}(z) = J_n(-z)$$

$$zJ_n'(z) = nJ_n(z) - zJ_{n+1}(z)$$

$$zJ_n'(z) = -nJ_n(z) + zJ_{n-1}(z)$$

$$2J_n'(z) = J_{n-1}(z) - J_{n+1}(z)$$

$$\frac{2n}{z} J_n(z) = J_{n+1}(z) + J_{n-1}(z)$$

$$J_0'(z) = -J_1(z)$$

$$\int_0^z z^{-n} J_{n+1}(z)\, dz = -z^{-n} J_n(z)$$

$$\int_0^z z^n J_{n-1}(z)\, dz = z^n J_n(z)$$

$$\left(\frac{1}{z}\frac{d}{dz}\right)^r \{z_n J_n(z)\} = z^{n-r} J_{n-r}(z)$$

$$J_n'(kz) = \frac{d\{J_n(kz)\}}{d(kz)}$$

(2) Properties for first kind of modified Bessel function

$$I_{-n}(z) = I_n(z)$$

$$I_n(-z) = (-1)^n I_n(z)$$

$$zI_n'(z) = nI_n(z) + zJ_{n+1}(z)$$

$$zI_n'(z) = -nI_n(z) + zI_{n-1}(z)$$

$$2I_n'(z) = I_{n-1}(z) + I_{n+1}(z)$$

$$\frac{2n}{z} I_n(z) = I_{n-1}(z) - I_{n+1}(z)$$

$$I_0'(z) = I_1(z)$$

$$\int_0^z z^{-n} I_{n+1}(z)\, dz = z^{-n} I_n(z)$$

$$\int_0^z z^n I_{n-1}(z)\, dz = z^n I_n(z)$$

$$\left(\frac{1}{z}\frac{d}{dz}\right)^r \{z_n I_n(z)\} = z^{n-r} I_{n-r}(z)$$

$$I_n'(kz) = \frac{d\{I_n(kz)\}}{d(kz)}$$

APPENDIX B

INTEGRATION CONSTANTS

(1) The coefficients in eqn. (3.26) are:

$$a_{1s}^{r}=\int_0^1 (\bar{A}_{22}\rho Z_s Z_r'' + \bar{A}_{22} Z_s Z_r' - \bar{A}_{11} Z_s Z_r/\rho)\,d\rho$$

$$a_{2s}^{m}=\frac{1}{\lambda_1}\int_0^1 [\bar{B}_{21}\rho Z_s Y_m'' + (\bar{B}_{21}+\bar{B}_{22}-\bar{B}_{11}) Z_s Y_m' - \bar{B}_{12} Z_s Y_m/\rho]\,d\rho$$

$$a_{3s}^{m}=2\lambda_2\int_0^1 \rho Z_s X_m'\,d\rho$$

$$a_{4s}^{m}=\frac{1}{\lambda_1}\sum_{p=1}^{\infty}\bar{W}_p\int_0^1 Z_s X_m' X_p'\,d\rho$$

$$a_{5s}^{mk}=\frac{1}{2\lambda_1}\int_0^1 Z_s X_m X_k\,d\rho$$

$$a_{6n}^{r}=\lambda_1 T_s\int_0^1 [\bar{B}_{21}\rho Y_n Z_r'' + (\bar{B}_{21}+\bar{B}_{22}-\bar{B}_{11}) Y_n Z_r' - \bar{B}_{12} Y_n Z_r/\rho]\,d\rho$$

$$a_{7n}^{m}=T_s\int_0^1 (\bar{D}_{11}Y_nY_m' + \bar{D}_{11}\rho Y_nY_m'' - \bar{D}_{22}Y_nY_m/\rho)\,d\rho - \lambda_1^2\bar{G}\int_0^1 \rho Y_nY_m\,d\rho$$

$$a_{8n}^{m}=-\lambda_1^2\bar{G}\int_0^1 \rho Y_nX_m'\,d\rho$$

$$a_{9n}^{m}=-\frac{T_sR_I}{12\lambda_1^2}\int_0^1 \rho Y_n Y_m\,d\rho$$

$$a_{10n}^{r}=\lambda_1\int_0^1 [\bar{B}_{21}\rho X_n Z_r'' + (\bar{B}_{21}+\bar{B}_{22}-\bar{B}_{11}) X_n Z_r' - \bar{B}_{12} X_n Z_r/\rho]\,d\rho$$

$$a_{11n}^{r}=2\lambda_1^2\lambda_2\int_0^1 \rho X_n Z_r\,d\rho$$

$$a_{12n}^{r}=\lambda_1\sum_{p=1}^{\infty}\bar{W}_p\int_0^1 X_p' X_n Z_r\,d\rho$$

$$a_{13n}^{m}=\int_0^1 (\bar{D}_{11} X_n Y_m' + \bar{D}_{11}\rho X_n Y_m'' - \bar{D}_{22} X_n Y_m/\rho)\,d\rho$$

$$a_{14n}^{m}=2K_b Y_m(\alpha_m)\sum_{i=1}^{\infty}\frac{(-1)^i}{i}\int_0^1 X_n\rho\left[-\rho\cos(i\pi\rho)+\frac{1}{i\pi}\sin(i\pi\rho)\right]d\rho$$

$$a_{15n}^{mr} = \lambda_1 \int_0^1 X_n X_m' Z_r \, d\rho$$

$$a_{16n}^{m} = -K_f \int_0^1 X_n \left(\int_0^\rho \eta X_m d\eta \right) d\rho + G_f \int_0^1 X_n \left[\int_0^\rho (\eta X_m'' + X_m') \, d\eta \right] d\rho$$

$$a_{17n}^{mkj} = -K_n \int_0^1 X_n \left(\int_0^\rho \eta X_m X_k X_j \, d\eta \right) d\rho$$

$$a_{18n}^{m} = -\frac{R_I}{12 \lambda_1^2} \int_0^1 \rho X_n Y_m \, d\rho$$

$$a_{19n}^{m} = \int_0^1 X_n \left(\int_0^\rho \eta X_m d\eta \right) d\rho$$

$$Q_n = \int_0^1 \rho X_n \left(\int_0^\rho \eta Q d\eta \right) d\rho$$

(2) The coefficients in eqn. (3.28) are:

$$a_{20n}^{m} = -a_{6n}^{r} [a_{1s}^{r}]^{-1} a_{2s}^{m} + a_{7n}^{m}$$

$$a_{21n}^{m} = -a_{6n}^{r} [a_{1s}^{r}]^{-1} (a_{3s}^{m} + a_{4s}^{m}) + a_{8n}^{m}$$

$$a_{22n}^{mk} = -a_{6n}^{r} [a_{1s}^{r}]^{-1} a_{5s}^{mk}$$

$$a_{23n}^{m} = -(a_{10n}^{r} + a_{11n}^{r} + a_{12n}^{r}) [a_{1s}^{r}]^{-1} a_{2s}^{m} + a_{13n}^{m} + a_{14n}^{m}$$

$$a_{24n}^{mk} = -a_{15n}^{mr} [a_{1s}^{r}]^{-1} a_{2s}^{k}$$

$$a_{25n}^{m} = -(a_{10n}^{r} + a_{11n}^{r} + a_{12n}^{r}) [a_{1s}^{r}]^{-1} (a_{3s}^{m} + a_{4s}^{m}) + a_{16n}^{m}$$

$$a_{26n}^{mk} = -(a_{10n}^{r} + a_{11n}^{r} + a_{12n}^{r}) [a_{1s}^{r}]^{-1} a_{5s}^{mk} - a_{15n}^{mr} [a_{1s}^{r}]^{-1} (a_{3s}^{k} + a_{4s}^{k})$$

$$a_{27n}^{mkj} = -a_{15n}^{mr} [a_{1s}^{r}]^{-1} a_{5s}^{kj} + a_{17n}^{mkj}$$

(3) The coefficients in eqns. (3.31) are:

$$\begin{Bmatrix} b_{1r}^{m} \\ b_{3j}^{m} \end{Bmatrix} = -\begin{bmatrix} a_{1s}^{r} & a_{2s}^{j} \\ a_{6n}^{r} & a_{7n}^{j} \end{bmatrix}^{-1} \begin{Bmatrix} a_{3s}^{m} + a_{4s}^{m} \\ a_{8n}^{m} \end{Bmatrix}$$

$$\begin{Bmatrix} b^{mk}_{2r} \\ b^{mk}_{4j} \end{Bmatrix} = - \begin{bmatrix} a^{r}_{1s} & a^{j}_{2s} \\ a^{r}_{6n} & a^{j}_{7n} \end{bmatrix}^{-1} \begin{Bmatrix} a^{mk}_{5s} \\ 0 \end{Bmatrix}$$

(4) The coefficients in eqn. (3.32) are:

$$c^{m}_{1n} = (a^{r}_{10n} + a^{r}_{11n} + a^{r}_{12n}) \, b^{m}_{1r} + (a^{j}_{13n} + a^{j}_{14n}) \, b^{m}_{3j} + a^{m}_{16n}$$

$$c^{mk}_{2n} = (a^{r}_{10n} + a^{r}_{11n} + a^{r}_{12n}) \, b^{mk}_{2r} + (a^{j}_{13n} + a^{j}_{14n}) \, b^{mk}_{4j} + a^{mr}_{15n} b^{k}_{1r}$$

$$c^{mkj}_{3n} = a^{mr}_{15n} b^{kj}_{2r} + a^{mkj}_{17n}$$

in which primes denote differentiation with respect to the corresponding coordinate.

APPENDIX C

PROGRAM FOR NONLINEAR ANALYSIS OF LAMANATED SHALLOW SPHERICAL SHELLS

```
C=================================================================
C
C                           PROGRAM NALSSS
C
C    NONLINEAR ANALYSIS OF LAMINATED SHALLOW SPHERICAL SHELLS
C
C                         ON NOVEMBER 1, 1991
C
C                           BY CHANGSHI XU
C
C=================================================================

C
C    THIS PROGRAM IS DESIGNED TO ANALYSIS BUCKLING, POSTBUCKLING
C    AND VIBRATION OF SYMMETRICALLY AND ANTISYMMETRICALLY LAMINATED
C    MODERATELY THICK SPHERICAL SHELLS AND CIRCULAR PLATES WITH INITIAL
C    IMPERFECTION, LINEAR, NONLINEAR, AND SHEAR ELASTIC FOUNDATIONS
C
C
C    THIS VERSION IS REVISED ON APRIL 3, 1991
C           (1)-------MINOR REVISION ON AUGUST 9,1991
C           (2)-------MINOR REVISION ON AUGUST 20,1991
C           (3)-------MINOR REVISION ON SEPTEMBER 18,1991
C           (4)-------MINOR REVISION ON OCTOBER 2,1991
C

      PROGRAM NALSSS(INPUT,OUTPUT,XMAT,XGEM,XDYN,XINT,XOUT,XPCR,
     #        TAPE3=XMAT,TAPE4=INPUT,TAPE5=XGEM,TAPE6=XOUT,
     #        TAPE7=XDYN,TAPE8=XINT,TAPE9=XPCR)
      DIMENSION Z11(10,10),Z12(10,10),Z21(10,10),Z31(10,10,10),
     #     Y11(10,10),Y12(10,10),Y13(10,10),Y21(10,10),X11(10,10),
     #     X21(10,10,10),X31(10,10),X32(10,10),
     #     Z1(10,10),Z2(10,10),Z3(10,10,10),Y1(10,10),
     #     Y2(10,10),X1(10,10),X2(10,10,10),X3(10,10),X4(10,10),
     #     Z1V(10,10),Y1V(10,10),Z1T(10,10),Z2T(10,10,10),
     #     Y1S(10,10),X1W1(10,10),X1W2(10,10,10),X2W1(10,10,10),
     #     X2W2(10,10,10,10),X3W1(10,10),X3W2(10,10,10),
     #     Y(60),SS(10),TT(10),WK(6000),FVEC(60),
     #     BSI(5),BSJ(5),OK1(10,10),OK2(10,10),WA(20),
     #     AD(10,10),S(2),RS(60,3),EIG(10),BETA1(10),
     #     PQ(0:300),PCR(0:100),PWM(300),PWMA(300),
     #     OW(300),OO(300),PQ0(0:300),X11W0(10,10)
      DIMENSION Y1TS1(10,10),Y1VTS1(10,10),Y1STS1(10,10),X3WTS1(10,10),
     #     ATS1(10,10),
     #     XB1(10,10),XB2(10,10),XB3(10,10),YB1(10,10),YB2(10,10),
     #     YB3(10,10),ZB1(10,10),ZB2(10,10),ZB3(10,10),XKF(10,10),
     #     XGF(10,10),QE(10),XB(10,10),YB(10,10),ZB(10,10),
     #     ZW0(10,10),XKN(10,10,10,10),
     #     YZBL(20,20),BV(20,20),YZBST1(20,20),YZBST2(20,20,20),
     #     Y2S(10,10,10),YZBLTS1(20,20),BVTS1(20,20),
     #     YZBST1TS(20,20),Z1TTS1(10,10),X1WTS1(10,10)
      DIMENSION ZKBA(12),ZKIA(12),NA(12),IMATA(12),RM1A(12),RM2A(12),
     #     W0A(12),ZKFA(12),ZKNA(12),ZGFA(12),ZMAT(3)
      DIMENSION DX(10,10),DY(10,10),ZDV(10,10),XD1(10,10),XD2(10,10,10),
     #     XD3(10,10,10,10),XDY1(10,10),XDY(10,10,10),YDX1(10,10),
     #     YDX2(10,10,10),YD1(10,10),XRI(10,10),YD1TS1(10,10)
      COMMON/DYNA/ NTOT,KXM,NT,KX1,X(60),OMEGA0,ICOS(10),
     #          ITBLA(10,10,2),ITBLB(10,10,10,4),ITER
      COMMON/POS/ IPOS
```